

University of Strathclyde
Department of Electronic and Electrical Engineering

**FACTS and HVDC systems for enhancing tie-line power transfer
capability**

Abdussalam S. Elansari

B.Sc., M.Sc.

A thesis presented in fulfilment of the requirement for the degree of Doctor of
Philosophy

April 2016

The copyright of this thesis belongs to the author under terms of United Kingdom copyright acts as qualified by University of Strathclyde Regulation 3.51. Due acknowledgement must always be made of the use of any material in, or, derived form of this thesis.

Abdussalam Elansari

12/05/2016

Acknowledgements

I would like to express my thanks to Allah, who helped me to complete this thesis, and gives me the reasons to succeed.

I would also like to express my sincerest thanks to my supervisors Prof. Stephen Finney and Prof. Keith Bell for their guidance, patience, keen interest and effort, at all times.

Also, I would like to thank Dr. Grain Philip Adam for his technical and moral support during my Ph.D. study, including proofreading the thesis. Special thanks go to Prof. Barry Williams for his helpful comments. I want to thank all the staff and students in the PEDEC group.

I would like to thank the General Electricity Company of Libya and Ministry of Higher Education in Libya for financing my Ph.D. study.

Finally, I express my sincere appreciation to my family for their prayers and support.

Dedication

To my parents and my wife and my daughters and my brother and sisters

Table of Contents

	Page	
	No.	
Copyright	II	
Acknowledgment	III	
Dedication	IV	
Table of Contents	V	
Abstract	XIII	
List of Symbols and Abbreviations	XIV	
List of Figures and Tables	XVII	
Chapter One: Introduction		
1.1	Background	1
1.2	Applications of FACTS devices in interconnected power systems	2
1.3	Applications of HVDC links in interconnected of power systems	4
1.4	Research Motivation	5
1.5	Research objectives	7
1.6	Thesis organization	7
1.7	Research contribution	9
1.8	List of publications	11
Chapter Two: Fundamentals of Power Flow in the Interconnected Power Systems		
2.1	Introduction	14
2.2	Active and reactive power flow in AC power system	15
	2.2.1 Effect of transmission line resistance on power flow	16
	2.2.2 Effect of long line charging on power flow	17
	2.2.3 Effect of shunt admittance on power flow	18
	2.2.4 Generic power flow equation.	19
2.3	Load-ability of transmission line	21
	2.3.1 Thermal limit	22
	2.3.2 Voltage stability limit (VSL)	23
	2.3.3 Angular stability limit (ASL)	27
2.4	Power transfer capability of transmission tie-line	30
	2.4.1 Total transfer capability of a tie-line (TTC)	31

2.4.2	Available transfer capability of a tie-line (ATC)	33
2.5	Power transfer capability calculation (case study)	33
2.5.1	TTC of a weak interconnection link	34
2.5.2	TTC of a strong interconnection link	37
2.6	Summary	39
Chapter Three: Shunt connected FACTS devices		
3.1	Introduction	41
3.2	Variable impedance shunt FACTS devices	42
3.2.1	Thyristor controlled reactor (TCR)	43
3.2.2	Thyristor switched capacitor (TSC)	45
3.2.3	Inclusion of variable impedance FACTS in power flow equation	46
3.2.4	Static VAr Compensator (SVC)	48
3.2.5	Dynamic response of the SVC	50
3.3	Converter based shunt FACTS (STATCOM)	53
3.3.1	Inclusion of converter based FACTS in power flow equation	54
3.3.2	STATCOM operation principles	56
3.3.3	Basic control of the STATCOM	57
3.4	Control requirements of shunt FACTS	59
3.5	Effect of midpoint shunt compensation on tie-line load-ability	61
3.6	Allocating of shunt VAr generators for system load-ability improvement	64
3.6.1	Total voltage change index for FACTS allocating (TVCI)	64
3.7	Sizing of shunt FACTS for system load-ability improvement	66
3.7.1	Maximum allowable reactive power injection at a given node	66
3.7.2	Security criteria for shunt FACTS sizing	68
3.7.3	Sizing of variable impedance shunt FACTS	68
3.7.4	Sizing of converter based shunt FACTS	70
3.7.5	Generic sizing method based on P-V curve analysis	72
3.8	Comparison between variable impedance and converter based FACTS	72
3.8.1	Steady state performance comparison	73
3.8.2	Dynamic performance comparison	74

3.9	Summary	76
Chapter Four: Series connected FACTS devices		
4.1	Introduction	79
4.2	Series compensation principles	80
4.3	Power transfer capability improvement with series compensation	82
	4.3.1 Voltage stability limit improvement with series FACTS	82
	4.3.2 Impact of series compensation factor on angular stability limit	85
4.4	Subsynchronous resonance	86
	4.4.1 Calculation of natural resonance frequency for series compensated tie-line	87
	4.4.2 Sub-synchronous resonance damping	89
4.5	Allocating and sizing of series FACTS	91
	4.5.1 Sizing of series FACTS considering SSR	91
	4.5.2 Series FACTS allocation on the basis of two identical line segments	92
4.6	Thyristor controlled series compensator (TCSC)	95
	4.6.1 Operating principle of the TCSC	95
	4.6.2 V-I characteristics of the TCSC	97
	4.6.3 Natural resonance frequency with TCSC	99
	4.6.4 TCSC control principles	99
4.7	Static synchronous series compensator (SSSC)	102
	4.7.1 SSSC operation principles	102
	4.7.2 Power flow equation for an SSSC series compensated tie-line	104
	4.7.3 V-I characteristics of an SSSC	105
	4.7.4 SSSC control principles	106
4.8	Performance comparison between TCSC and SSSC	107
4.9	Summary	109
Chapter Five: Voltage source converter based HVDC transmission systems		
5.1	Introduction	112
5.2	HVDC Transmission System Configurations	116
	5.2.1 Monopolar HVDC configuration	116
	5.2.2 Bipolar HVDC configuration	116

5.2.3	Back-to-back (BTB) HVDC configuration	117
5.2.4	Multi-terminal HVDC configuration	117
5.3	VSC-HVDC transmission system components	119
5.3.1	Voltage source converter	120
5.3.2	Coupling transformers	122
5.3.3	Phase reactors	122
5.3.4	AC filters	122
5.3.5	DC link capacitor	122
5.3.6	DC line	123
5.4	VSC-HVDC operating principle	123
5.5	Power flow equation for a VSC-HVDC transmission system	125
5.5.1	Calculation of the power angle at the converter side	127
5.5.2	Power flow calculations at the sending end VSC-HVDC	128
5.5.3	Power flow equations in the dc link	130
5.5.4	Power flow calculations at the receiving end VSC-HVDC	130
5.5.5	Validation of power flow equations	131
5.6	VSC capability chart	132
5.6.1	Current limiter	134
5.7	VSC-HVDC control	135
5.7.1	d-q transformation	135
5.7.2	Vector control	136
5.7.3	Inner current controller	137
5.7.4	DC voltage outer controller	140
5.7.5	Active and reactive power outer controllers	142
5.8	Total transfer capability of VSC-HVDC transmission system	143
5.9	Black start capability of VSC-HVDC	143
5.10	Frequency control capability of VSC-HVDC	144
5.10.1	Dynamics of system frequency in AC systems	145
5.10.2	Fixed frequency control strategy	146
5.10.3	DC voltage based frequency control strategy in VSC-HVDC	146
5.10.4	Active Power based frequency control strategy	147
5.11	Summary	148

**Chapter Six: Strengthening the Libyan internal tie-line
with FACTS technologies**

6.1	Introduction	152
6.2	Present performance of WEST-EAST Libyan internal tie-line	153
6.2.1	Present load-ability of East and West Libyan tie-line	154
6.2.2	Reduced model of the west-east tie-line	154
6.2.3	Validation of reduced model of the west-east tie-line	155
6.2.4	Voltage stability limit (VSL) of west-east Libyan tie-line	156
6.2.5	Angular stability limit (ASL) of west-east Libyan tie-line	158
6.2.6	Summary of West-East tie-line performance and requirements	159
6.3	Discussion of the proposed solutions to improve west-east tie-line performance	161
6.4	Allocating and sizing of shunt FACTS to maximize TTC in the Libyan internal tie-line	162
6.4.1	Allocating shunt FACTS on the basis of TVCI	162
6.4.2	Technical constraints for shunt FACTS sizing	163
6.4.3	Sizing of shunt FACTS on the basis of device terminal voltage	165
6.5	Libyan internal tie-line with midpoint SVC	167
6.5.1	Dynamic performance of the SVC during TSC switching	168
6.5.2	Dynamic behavior of the tie-line during three phase short circuit	168
6.6	Libyan internal tie-line with midpoint STATCOM	170
6.6.1	Dynamic behavior of the tie-line during a three phase short circuit	171
6.7	Libyan internal tie-line with series compensation	173
6.7.1	Potential subsynchronous resonance around the Libyan internal tie-line	173
6.7.2	Allocating series compensation to maximize TTC of the Libyan tie-line	174
6.7.3	Technical considerations for series compensation sizing in the Libyan tie-line	175

6.8	Thyristor controlled series compensation (TCSC) in the Libyan tie-line	177
6.8.1	TCSC operating ranges	177
6.8.2	Total transfer capability of the Libyan internal tie-line with TCSC	178
6.8.3	Dynamic performance of the TCSC during a severe fault	180
6.9	Summary	182

Chapter Seven: Strengthening the Libyan internal tie-line with VSC-HVDC Transmission

7.1	Introduction	184
7.2	Rationale for converting an existing AC line to a DC transmission systems	184
7.3	Sizing of the VSC-HVDC links based on ASL	186
7.4	Sizing of VSC-HVDC converter base on terminal voltage	186
7.5	Power transfer capability of the strengthened west-east Libyan tie-line	190
7.5.1	Existing configuration of the tie-line (no HVDC link)	190
7.5.2	Steady state transfer capability of the reinforced west-east Libyan tie-line	191
7.6	Dynamic performance of the VSC-HVDC link	192
7.6.1	Step response of the dc Power controller	193
7.6.2	Step response of reactive Power and AC voltage controllers	195
7.6.3	System response to a 3-phase short circuit at the receiving end terminal	196
7.7	DC power ramping in the hybrid AC/DC Libyan internal tie-line	198
7.7.1	AC system time constant (inertia) and its influence on dc power ramping	198
7.7.2	Simulation of DC power ramping during load demand increase	199
7.7.3	Operating strategy of the hybrid AC/DC tie-line during N-1 scenario	201
7.8	STATCOM operation	204

7.9	Frequency control capability of the reinforced Libyan internal tie-line	205
7.10	Comparison between shunt FACTS, series FACTS, and VSC-HVDC in the Libyan internal tie-line	207
7.11	Summary	209

Chapter Eight: Conclusions and Recommendations

8.1	General conclusions	211
8.2	Suggestions for future research	214

Appendix A: Long mathematical formulas

A-1	Angular stability limit (ASL) derivation	215
A-2	Active power formula at the PCC of receiving end in VSC-HVDC link	216

Appendix B: Matlab script codes

B-1	P-V and P- δ curves for detailed and lossless tie-lines (Fig 2-5 and Fig 2-8)	217
B-2	Impact of the midpoint compensation on TTC (Fig 3-18)	217
B-3	level of shunt compensation versus critical voltage (Fig 3-25)	218
B-4	Series compensation (k) versus VSL and ASL (Fig 4-4 and Fig 4-6)	218
B-5	sizing of series compensation on the bases of the SSR (Fig 4-10)	219
B-6	Firing delay angle-VS-effective TCSC impedance (Fig 4-13)	219
B-7	P-V curve and compensated voltage with 25% compensation factor SSSC (Fig 4-20 a -b)	219
B-8	VSC-HVDC power flow calculation and sizing	220

Appendix C: Two areas Kundur test system technical data

C-1	Single line diagram of two areas Kundur test system	221
C-2	Network data	221
C-3	Generator excitation control system	223

Appendix D: Single line diagram of the Libyan national grid

D-1	Single line diagram of the Libyan national grid	224
-----	---	-----

Appendix E: NEPLAN detailed power flow

E-1	Reduced model of the Libyan internal tie-line Power flow results	225
E-2	Detailed model of the Libyan internal tie-line Power flow results	226

Abstract

This thesis investigates the use of flexible AC transmission systems (FACTS) and voltage source converter (VSC) high-voltage direct current (HVDC) transmission systems for improving the power transfer capability of the Libyan internal tie-line between east and west, for a secure, reliable and efficient operation of this power corridor. Mathematical-based analysis supported by numerical-based analysis, which employs NEPLAN power system analysis tool, are carried out to investigate the steady state and dynamic behaviour of the power system.

Different FACTS technologies, including variable impedance based and converter-based shunt and series FACTS devices, are studied during steady-state and transient operating conditions to evaluate the capabilities, control systems and weaknesses in these technologies. The investigations focus on the common types of shunt and series FACTS including: the static VAR compensator, static synchronous compensator, and thyristor controlled series compensator. A challenge in this thesis is to find an efficient method to allocate and size FACTS devices, to ensure maximum utilization of the tie-line considering technical constraints including: voltage rise at a point of voltage collapse, equipment terminal voltage and subsynchronous resonance risk.

For the VSC-HVDC system, a mathematical model that calculates power flow throughout the HVDC link and at both AC sides is confirmed as an efficient steady-state model facilitating estimation of reactive power requirements at the converter terminal and at the point of common coupling. This model can be used to estimate the optimal converter rating based on the system strengths at both sides. Further modelling and analysis investigates the operation of a hybrid AC/DC system. Multi-tasking control systems for voltage source converter HVDC systems are used to facilitate operation of the hybrid AC/DC system during normal and emergency operating conditions. The controllers include: frequency control in the case of an unsynchronized connection and power management control necessary to balance the power flow during an emergency, in addition to the primary control of the AC and DC voltages, and active and reactive powers.

Well-known and referenced two areas Kundur test system with a weak tie-line, which suffers from a limited power transfer capability between the operating areas, is used throughout the analysis. The tie-line between two regions in the Kundur test system is investigated when incorporating different FACTS technologies and a VSC-HVDC system. Based on the introduced approaches and models the benefits and challenges of these technologies in the Libyan internal tie-line are explored. The research shows that the power transfer capability of the tie-line can be improved by shunt and to a lesser extent, by series compensation. Comparison between FACTS devices and VSC-HVDC indicates, apart from the cost, VSC-HVDC transmission may be the better option for Libyan internal tie-line improvement, especially in the near future, when secure and reliable interconnected power system is required.

List of symbols and abbreviations

List of symbols

B	Line susceptance
$B_{(\alpha)}$	Shunt admittance of the TCR
B_{Cmax}	Maximum capacitive susceptance of variable impedance FACTS
B_{Lmax}	Maximum inductive susceptance of variable impedance FACTS
F_C	Ferranti effect constant
E_{CRT}	Critical voltage
I	Mean average current
I_{Cmax}	Maximum capacitive current of the STATCOM
I_{Lmax}	Maximum inductive current of the STATCOM
i_{cd}, i_{cq}	Direct and quadrature axis currents at converter ac side
i_{sd}, i_{sq}	Direct and quadrature axis currents at grid ac side
I_{dc}	dc link current
$I_{L(\alpha)}$	Amplitude of the fundamental reactor current
G	Line conductance
k_{pi}, k_{ii}	Proportional and integral gain of the current controller
k_{pac}, k_{iac}	Proportional and integral gain of the ac voltage controller
k_{dcp}, k_{dci}	Proportional and integral gain of the dc voltage controller
k_{fp}, k_{fi}	Proportional and integral gain of the frequency controller
P_{dc}	dc link power
P	ac active power
P_{ref}	Active power reference of the active power controller
pf	Power factor
Q	ac reactive power
Q_{ref}	Reactive power reference of the active power controller
Q_{satu}	Reactive power output of variable impedance FCATS device
$Q_{TCR(\alpha)}$	Reactive power output of the TCR
Q_{STAT}	Reactive power output of converter based FCATS device
R	Line resistance
\tilde{S}_R	Complex power
v_{sd}, v_{sq}	Direct and quadrature axis voltages at point of common coupling
v_{cd}, v_{cq}	Direct and quadrature axis voltages at converter ac side terminal

V_{pu}	ac voltage magnitude in per unit
V_{dc}	dc link voltage
V_L	Ac voltage amplitude of the applied voltage in the TCR
V_C	Ac voltage across the capacitor in TSC
V_{ac}^*	ac voltage reference point of the ac voltage controller
V_{dc}^*	dc voltage reference point of the dc voltage controller
X	Line reactance
Z	Line impedance
Z_C	Surge impedance
α	Firing delay angle
λ	Eigenvalue
δ	Power angle
ω	Angular frequency
β	Line phase constant
ΔP_{dc}	the change on the dc transmitted power
ΔP_L	the load change
τ	Time constant

List of abbreviations

ASL	Angular Stability Limit
ATC	Available Transfer Capability
FACTS	Flexible AC Transmission System
HVAC	High Voltage Alternating Current
HVDC	High Voltage Direct Current
IEEE	Institute of Electrical and Electronics Engineers
IGBT	Insulated gate bipolar transistor
LCC	Line Commutated Converter
MTDC	Multi-Terminal Dc System
NPC	Neutral-Point-Clamped
PCC	Point of Common Coupling
PWM	Pulse-Width Modulation
RoCoF	Rate of Change of Frequency
SCR	Short-Circuit Ratio

SIL	Surge Impedance Loading
SSSC	Static Synchronous Series Compensator
SSDC	Subsynchronous Damping Controller
STATCOM	Static Synchronous Compensator
SVC	Static VAr Compensator
TCR	Thyristor Controlled Reactor
TSC	Thyristor Switched Capacitor
TCSC	Thyristor-Controlled Series Compensation
TSSC	Thyristor-Switched Series Compensation
TTC	Total Transfer Capability
TVCI	Total Voltage Change Index
ULTC	Under-Load Tap Changer
UPFC	Unified Power Flow Controller
VSC	Voltage Source Converter
VSL	Voltage Stability Limit
VSC	Voltage Source Converter
XLPE	Cross-Linked Polyethylene

List of Figures and Tables

List of Figures

Figure 1-1	Geographical distribution of the Libyan generation and load demand	5
Figure 1-2	Real measurements of Power oscillation on the internal tie-line (20-06-2012)	6
Figure 2-1	Basic 2-bus AC system	15
Figure 2-2	Transmission line load-ability curve	22
Figure 2-3	Voltage and active power at the receiving as a function of load demand	25
Figure 2-4	Power versus voltage curve (P-V curve or nose curve)	26
Figure 2-5	P-V curves for detailed and lossless the tie-line in Table 2-1	27
Figure 2-6	Power versus load angle curve	28
Figure 2-7	Phasor diagram representation of the two AC systems	28
Figure 2-8	P- δ curves for detailed and lossless the tie-line	30
Figure 2-9	Change of TTC restricted limit with time	31
Figure 2-10	Total transfer capability (TTC) calculation based on P-V curve	33
Figure 2-11	Two interconnected power systems (Kundur test system)	34
Figure 2-12	P-V curves at Bus-3 for normal and emergency cases (weak interconnection link)	35
Figure 2-13	Load flow results at maximum loadability - weak interconnected power systems	36
Figure 2-14	Time domain simulation of 200ms fault at the middle of line-3 for C0 operating case (weak interconnected power systems)	36
Figure 2-15	P-V curves at Bus-2 for normal and emergency cases (strong interconnection link)	37
Figure 2-16	Load flow results at maximum load-ability- strong interconnected power systems	38
Figure 2-17	Time domain simulation of 200ms fault at the middle of line-3 during transmission of 375MW from Area 1 to Area 2	38
Figure 2-18	Time domain simulation of 200ms fault at the middle of line-3 during transmission of 450MW from Area 1 to Area 2	39
Figure 3-1	TCR voltage and current operating waves for firing delay angle α	43
Figure 3-2	Change of TCR current with the firing angle α	44
Figure 3-3	TCR V-I characteristics	44
Figure 3-4	Thyristor switched capacitor topology	45
Figure 3-5	Transient free switching conditions for the TSC	46

Figure 3-6	Effect of variable impedance shunt connected FACTS on system load-ability	48
Figure 3-7	Static VAr Compensation (SVC) topology	48
Figure 3-8	V-I operating characteristic of SVC with three TSCs and TCR	49
Figure 3-9	VSC basic control scheme	50
Figure 3-10	Kundur two areas test system with (-180, +63 MVar) SVC	51
Figure 3-11	Response of the SVC for the change in the system voltage	52
Figure 3-12	Switching on/off instants of TSC-1	53
Figure 3-13	Commonly used voltage source converter structures in converter based VAr generators	54
Figure 3-14	V-I characteristic of STATCOM	55
Figure 3-15	Static Synchronous Compensation (STATCOM) topology	56
Figure 3-16	Basic control structure of converter based VAr compensator	58
Figure 3-17	Basic transfer function for SVC and STATCOM control	59
Figure 3-18	V-I characteristics of SVC and STACTCOM during steady state and dynamic operation	60
Figure 3-19	Simple two interconnected AC power systems with shunt VAr compensation	62
Figure 3-20	Impact of midpoint compensation on the power angle and system impedance	62
Figure 3-21	Impact of the midpoint compensation on the transfer capability of the tie-line in the Kundur test system	63
Figure 3-22	Effect of improved system load-ability on overall system performance	64
Figure 3-23	Effect of shunt compensation on load-ability and voltage stability	67
Figure 3-24	Sizing of variable impedance FACTS devices on the basis of PoC security criteria	69
Figure 3-25	Level of shunt compensation versus critical voltage	70
Figure 3-26	Sizing of static VAr compensation using a generic P-V curve method where PoC high is taken as sizing criteria ($V_{critical}$ should be less than 85%)	73
Figure 3-27	Dynamic comparison between SVC and STATCOM	75
Figure 4-1	Two interconnected power systems with series compensated tie-line	80
Figure 4-2	Phasor representation of two interconnected power systems with series compensation	81
Figure 4-3	Kundur test system technical data	83
Figure 4-4	Voltage stability limit versus series compensation factor (VSL-k curve)	84
Figure 4-5	P-V curves with different series compensation factor values	85

Figure 4-6	Degree of series compensation k versus angular stability limit ASL	86
Figure 4-7	Effective series reactance between two interconnected power systems with a series compensated tie-line	87
Figure 4-8	Natural resonance frequency versus compensation factor k	89
Figure 4-9	Shift of capacitor voltage by NGH Damper at SSR to be in-line with the line current	90
Figure 4-10	Sizing of series compensation on the basis of SSR	92
Figure 4-11	Two identical line segments approach for Series FACTS sizing and allocating	93
Figure 4-12	Thyristor controlled series compensation (TCSC) topology	95
Figure 4-13	TCSC reactance versus firing angle delay α [FC=40 μ F, L=22.8mH]	97
Figure 4-14	V-I characteristics of TCSC	98
Figure 4-15	Reactance versus current characteristic of TCSC	98
Figure 4-16	Ideal TCSC compensating voltage waveform ($V_c(\alpha)$)	100
Figure 4-17	Simple control structure of the TCSC	101
Figure 4-18	Two interconnected power systems with an SSSC compensated tie-line	102
Figure 4-19	Phasor diagram for converter based series compensation (SSSC)	103
Figure 4-20	P-V curve at the receiving end in the case 25% SSSC compensated tie-line, and the compensating voltage provided by an SSSC at different line currents	105
Figure 4-21	V-I Characteristic of SSSC	106
Figure 4-22	Control structure of the SSSC	107
Figure 5-1	HVAC and HVDC transmission cost versus link distance	113
Figure 5-2	Monopolar HVDC configuration	116
Figure 5-3	Bipolar HVDC configurations	117
Figure 5-4	Back-to-back HVDC configuration	117
Figure 5-5	Multi-terminals HVDC configurations	119
Figure 5-6	Typical voltage source converter based HVDC transmission system[11]	119
Figure 5-7	VSC-HVDC configurations	121
Figure 5-8	Generic multilevel converter	121
Figure 5-9	Simplified circuit diagram for VSC-HVDC terminal	124
Figure 5-10	Equivalent circuit of a two power systems with a VSC-HVDC link	126
Figure 5-11	Angle relationship between the voltage at the PCC and at the converter terminal	127

Figure 5-12	Typical P-Q capability characteristics of VSC-HVDC	133
Figure 5-13	Current limiting strategies	134
Figure 5-14	Axis transformation between three stationary coordinates to d-q rotating coordinates	136
Figure 5-15	Block diagram of inner control loop in dq axes	138
Figure 5-16	Block diagram of the inner controller	140
Figure 5-17	DC voltage control loop in d-q axis	140
Figure 5-18	Active power control loop in d-q axes	142
Figure 5-19	Reactive power control loop in d-q axes	142
Figure 5-20	DC voltage based control strategy	147
Figure 5-21	Active power based frequency control structure	148
Figure 6-1	West-East internal Libyan tie-line	153
Figure 6-2	Impedance representation of the Libyan internal west-east tie-line	155
Figure 6-3	Power versus voltage at 400kV stations along the west-east Libyan tie-line	157
Figure 6-4	Calculation of ASL for west-east Libyan internal tie line using time domain simulation	159
Figure 6-5	Summary performance of west-east Libyan internal tie-line	160
Figure 6-6	Single line diagram of West-East Libyan internal tie line of about 510 km long	162
Figure 6-7	Acceptable operational voltage levels for temporary operation	166
Figure 6-8	Sizing of shunt VAr sources on the basis of terminal voltage	167
Figure 6-9	Dynamic of SVC during TSC switching	168
Figure 6-10	Proposed NEPLAN control model for a (-200,+72)MVar SVC installed in Ras-Lanouf	169
Figure 6-11	SVC response for a 3-ph fault on the middle of 400kV line	170
Figure 6-12	Proposed NEPLAN control model for a 200 MVA STATCOM installed in Ras-Lanouf	171
Figure 6-13	STATCOM response for a 3-ph fault on the middle of 400kV line	172
Figure 6-14	Effective series impedance around the internal tie-line	174
Figure 6-15	Natural resonance frequency versus the tie-line compensation factor	176
Figure 6-16	Effective impedance versus firing delay angle for the TCSC in the Libyan internal tie-line	178
Figure 6-17	Tie-line load-ability at different series compensation factors (P-V curves)	179
Figure 6-18	Pre and post -fault configuration around the compensated tie-line	180

Figure 6-19	Dynamic performance for compensated tie-line during 3-phase fault	181
Figure 7-1	Impedance representation of the Libyan internal tie-line	185
Figure 7-2	West-east internal tie-line after VSC-HVDC reinforcement	185
Figure 7-3	Sizing of HVDC converters on the basis of the AC voltage at the converter terminals	188
Figure 7-4	P-Q curve for Ras-Lanuf and Khalij converter stations	189
Figure 7-5	Definition of step response	193
Figure 7-6	Simulation results for a step change of 100MW in the dc power	194
Figure 7-7	Simulation for a step change of -123MVar in the reactive power output at the Khalij converter station	195
Figure 7-8	Results for 3-phase short circuit at the receiving terminal	197
Figure 7-9	Change of the dc voltage with dc power ramp rate at the Ras-Lanufe converter station	199
Figure 7-10	Steady state dc power change	201
Figure 7-11	Power flow control strategy in the HVDC link and the AC parallel path	202
Figure 7-12	Libyan internal tie-line with power flow control strategy	203
Figure 7-13	STATCOM operation mode during dc line disconnection	205
Figure 7-14	Performance of tie-line with and without frequency control at the eastern terminal	206

List of Tables

Table 1-1	Summary of investment cost and main features of FCATS devices	3
Table 2-1	Typical parameters of a 230KV transmission line	20
Table 2-2	Effect of line resistance and line charging on tie-line power flow	21
Table 2-3	Equivalent system impedances for normal operating conditions	34
Table 2-4	Equivalent system impedances for emergency operating conditions (line-3 out of service)	34
Table 3-1	VAR source allocating, on the basis of TVCI, in a weak power systems (Figure 2-13)	65
Table 3-2	VAR source allocating, on the basis of TVCI, in a strong power systems (Figure 2-16)	66
Table 3-3	Main technical differences between variable impedance and converter based shunt FACTS	73
Table 3-4	Steady state comparison between SVC and STATCOM	74
Table 5-1	Summary of worldwide VSC-HVDC projects	114

Table 5-2	Technical comparison between VSC and LCC HVDC technologies	115
Table 5-3	Summary of power flow comparison between NEPLAN and mathematical approach	132
Table 6-1	Equivalent of east and west system impedances at the terminals of the tie-line	155
Table 6-2	Validation of west-east tie-line reduced model (buses voltages)	156
Table 6-3	Validation of west-east tie-line reduced model (active and reactive powers)	156
Table 6-4	Power transfer limitation of west-east Libyan internal tie-line	160
Table 6-5	TVCI calculation for shunt VAR source allocation amongst the substations in Figure 6-6	163
Table 6-6	Torsional oscillatory modes of the generating units around the internal tie-line	174
Table 6-7	summary of tie-line performance with TCST with different compensation factors	179
Table 7-1	Branch participation factor analysis	185
Table 7-2	System impedances at the AC terminals of the proposed HVDC link	187
Table 7-3	Summary of existing west-east Libyan tie-line (without HVDC reinforcement)	191
Table 7-4	performance Summary of strengthened west-east Libyan internal tie-line	191
Table 7-5	Comparison between the mathematical equation and time domain analysis using NEPLAN	200
Table 7-6	Technical performance comparison between FACTS and VSC-HVDC	208

Chapter One

Introduction

1.1 Background

For decades, the electrical power industry worldwide has been expanding to accommodate an industrial renaissance. In recent years, security of the power supply, environmental constraints, electricity markets, climate change, and renewable energy commitments are the main drivers of new trends in the network expansion. Accommodation of these drivers requires new network planning that, without sacrificing the stability of the systems, is able to cope with new operational trends. These new operational tendencies lead to additional challenges for interconnected power systems as they lead to a steady rise of inter-area power exchange, and consequently, more congestions in the existing ageing stressed AC systems [1]. For this reason, investment in power interconnectors links has become one of the pillars in advanced interconnected power systems, where the efficient exchange of bulk energy over long distances is required. Accordingly, the tie-lines in the interconnected power systems should be designed to operate reliably and securely during normal and emergency conditions. This leads to acceptance of maximizing the available transfer capability (ATC) of existing AC tie-lines, without violating system security, which represents one of the important challenges of interconnected power systems [2-5].

Many studies have established that efficient utilization of a tie-line is restricted either by a thermal limit, voltage stability limit, or transient stability limit. However, it is well-known that steady state voltage instability is the main concern for efficient utilization of medium and long tie-lines[6, 7].

Voltage instability is a slow dynamic phenomenon, which is exuberated as power loading level increases, approaching the point of collapse (*PoC*). Technically, this point defines the voltage stability limit (*VSL*) of the transmission line and accordingly it normally defines the total transfer capability (TTC) of medium and long transmission lines. Therefore, secure operation of the power system interconnectors must respect the TTC so that maximum power exchanges over the tie-line should be a reasonable distance from the *VSL*. Otherwise, the maximum load-ability point becomes unreachable [7-9].

Insufficient reactive power support along a tie-line can be reflected as a mid-point voltage sag during heavy loading, and can develop to voltage collapse should the line loading continue to increase[10]. Therefore, reactive power manipulation is frequently used to mitigate voltage instability problems by compensating the reactive power consumption by the line passive parameters; thus, keeping the node voltages close to their nominal values[6]. This improves the total and available transfer capabilities (*TTC* and *ATC*) of the power corridors in interconnected power systems [11, 12].

Flexible AC Transmission Systems (FACTS) devices and High Voltage Direct Current (HVDC) transmission systems are effective technologies for inductive and capacitive reactive power manipulation for improving the VSL of AC tie-lines, and consequently their power transfer capacities [6, 13-16].

Based on this background, the main theme of this research focuses on the use of these technologies to improve the power transfer capacity of critical power corridors in interconnected power systems.

1.2 Applications of FACTS devices in interconnected power systems

There is a large body of research presented in the literature covering FACTS devices and their application in power transmission systems. FACTS devices are fast acting controllers that provide a means to control more than one system parameter simultaneously, such as voltage magnitude and angle, line series impedance, line current, and shunt admittance. As a result, they provide a wide range of functions such as power flow control and power oscillation damping; extension of voltage and power stability limits; angular and transient stability improvement; and voltage profile improvement, including tie line power transfer capacity[1, 6, 11]. According to reference[1], FACTS devices allow power transfer capacity of the transmission line to be improved by about 40% to 50 % without violating its thermal capacity limit, depending on the rating and type of the FACTS device employed.

Generally, FACTS devices can be classified into the variable impedance type (also known as line commutating type that employs thyristors, inductors and capacitors), and the converter type that uses self-commutated devices such as the Gate Turn-Off (GTO) thyristor or Insulated Gate Bipolar Transistor (IGBT) [13]. These devices can also be classified based on their connections into:

- Shunt type controllers such as the Static VAR compensator (SVC) and Static synchronous compensator (STATCOM), which inject compensating current into the system.
- Series type controllers such as the Thyristor Controlled Series Capacitor (TCSC) and Static Synchronous Series Compensator (SSSC), which interpose a series compensating voltage into the system.
- Combined controllers that employ shunt and series technologies such as the Thyristor Controlled Phase Shifting Transformer (TCPST) and the Unified Power Flow Controller (UPFC).

The SVC is the most common and widespread FACTS device, with worldwide total installation capacity of about 90 GVA. The STATCOM and then the TCSC come after the SVC in terms of number of projects and in terms of worldwide installed capacity. About 20 STATCOM projects are installed worldwide with total capacity of 3GVA compared with 2GVA TCSC rated capacity installed in 10 places. The UPFC is the least common type and only three UPCF projects have been installed worldwide with only 0.25 GVA[6].

The cost and the complexity are the main drawbacks that slowed the spread of FACTS devices compared with mechanically-switched VAR sources. However, the necessity for these technologies encourages the researchers to find ways to reduce their costs. Table 1-2 summarise investments cost range and main key features of selected FACTS[1].

Table 1-2: summary of investment cost and main features of FCATS devices [1]

Cost and installation	SVC	STATCOM	TCSC	SSSC	UPFC
Rating rang (MVar)	100-850	100-400	25-600	100-400	100-325
Operational experience	> 30 years	> 20 years	> 15 years	new	> 10 years
Lifetime	40 years	30 years	30 years	30 years	30 years
losses	1-1.5%	1-2.5	0.5-1%	-	2-3%
investment cost (400 kV) (K-Euro/MVAR)	30-50	50-75	35-50	50-80	90-130
System improvement					
TTC	limited	limited	strong	strong	strong
Power flow control	limited	limited	good	strong	strong
Transient stability	limited	good	strong	strong	strong
Power oscillation damping	good	good	good	good	strong

1.3 Applications of HVDC links in interconnected of power systems

The high loss of the long distance AC transmission systems was the main motivation for the development of the HVDC transmission technology. However, the overall efficiency cost effectiveness of DC transmission systems compared with AC systems are a function of the line length when conversion losses and equipment cost are considered [13, 17]. In modern power systems, security of power supply, integration of renewable energy, and the electricity markets require transmission network operators to improve transfer capacity of their transmission systems, and this encourages increased use of HVDC links, even at relatively short distances.

The first generation of HVDC transmission systems use the line-commuted converter (LCC) that controls the power flow by controlling the firing delay angle of the thyristors [13]. The performance of HVDC systems has been continually improving since the emergence of the second generation of HVDC systems that employ voltage source converter (VSC) technology. Being independently able to control active and reactive power at ac both sides, voltage and frequency control has become achievable with VSC-HVDC.

From a power system point of view, there are a number of challenges that can affect efficient utilization of a HVDC-link. For example, in a hybrid AC/DC tie-line, $N-1$ contingency in the AC system can affect the performance of the DC system and vice versa. From a reliability perspective, transfer capacity of the hybrid AC/DC system has to be limited to the level that keeps the system operational during an $N-1$ condition. Pessimistic opinions impose the HVDC link to transfer only the power capacity of the AC parallel path as a precaution against losing the HVDC link, which may force the power to flow on the AC path and the other way around [18]. However, this challenge can be faced by fast-acting measures that reduce the loading of the tie-line [19], or by a special HVDC controller that changes the power order of the dc power in response to the AC system requirements, as will be addressed in this thesis. Another challenge that can affect HVDC system efficacy is the strength of the AC systems on both sides which in the case of weak transmission systems, can increase the reactive power output at the expenses of active power in the dc link.

1.4 Research motivation

The Libyan transmission grid is divided into four geographical areas: East, West, South-West and South-East. The east and west transmission networks are connected via a 510km tie line that includes a 220kV double circuit overhead transmission line (OHTL) and a single circuit 400kV OHTL [20, 21].

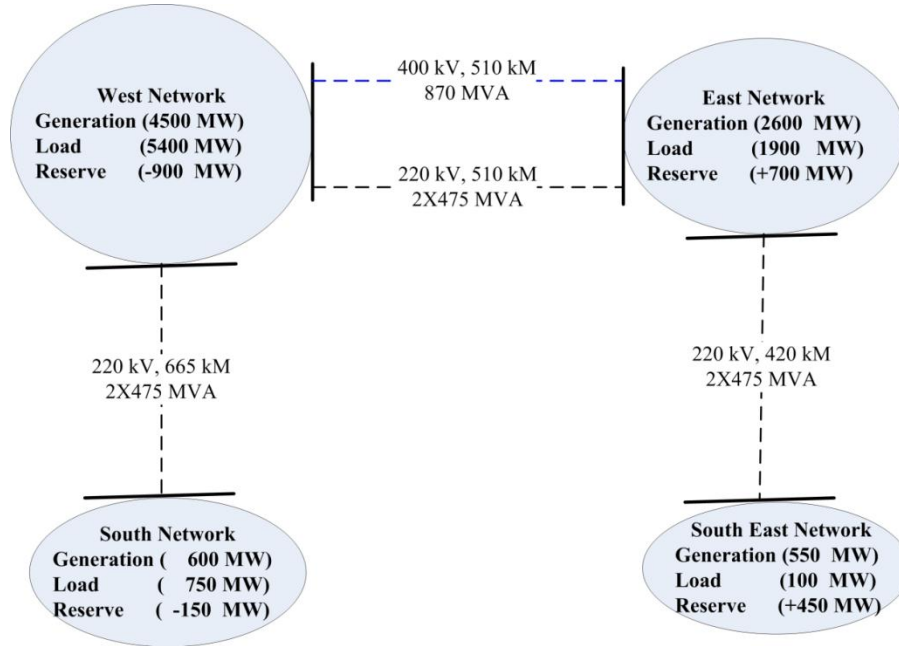


Figure 1-1: Geographical distribution of the Libyan generation and load demand

Normal power flow is from the eastern side of the country, where 40% of the generation capacity is installed to the western network, where about 75% of the total Libyan load resides [22]. Distribution of Libyan generation and demand in addition to the lack of reactive power support along the transmission corridor, have stressed the internal tie-line despite being continuously operated far below its design load-ability limits. The main economic and technical challenges facing the operation of the Libyan internal tie-line are:

- The limited transfer capability of the West-East tie-line increases network operational costs. The congestion in the tie-line leads to generation reduction on the eastern side which reduces its efficiency, and consequently increases production costs.
- Power exchanges with neighbouring countries have also been affected as a result of a bottleneck in the internal tie-lines. As a consequence, power wheeling through the Libyan transmission, from Egypt to Tunisia and vice versa, is reduced to cope with the Libyan internal tie-line capability.

- Security of power supply is also affected by the weakness of the internal tie-line. The necessity to operate the tie-line close to its current critical load-ability (which is much lower than the design value) causes voltage instability, even with normal load-demand change. Voltage quality around the tie-line is also affected during tie-line loading, where the voltage level sometimes drops below the acceptable limits.
- A power oscillation phenomenon is also exacerbated by the weakness of the Libyan internal tie-line. Despite the rarity of this electromechanical phenomenon, the weakness of the tie-line increases the impact of this phenomenon on the system security. Figure 1-2 shows real measurements of an inter-area un-damped power oscillation on the internal tie-line that causes tripping of the internal tie-line. This figure confirms that the poor performance of the Libyan internal tie-line complicates the situation, and as the tie-line is tripped, the system regains its stability.

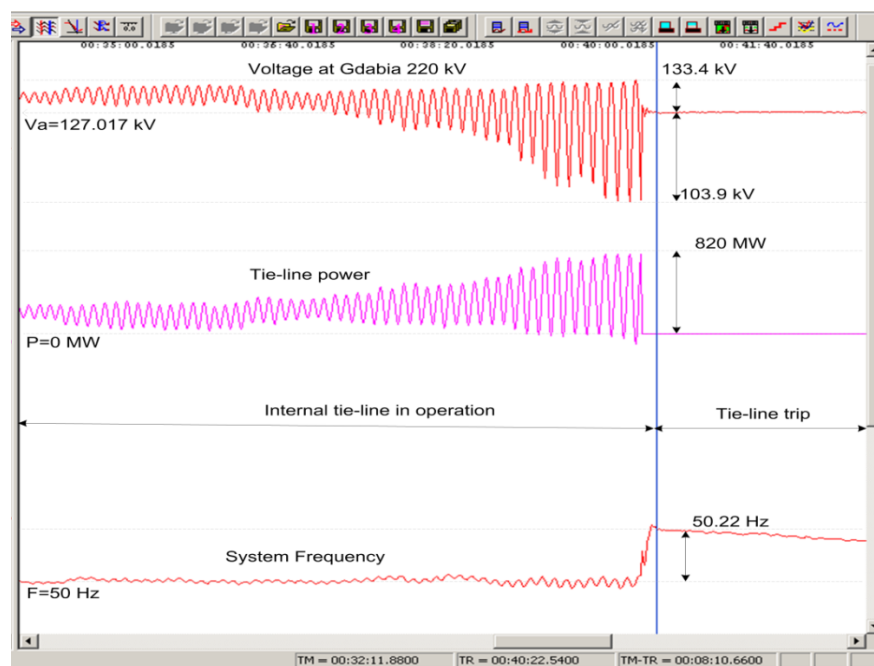


Figure 1-2: Real measurements of Power oscillation on the internal tie-line (20-06-2012)

Improvement of the Libyan internal tie-line in terms of power transfer capability by using advanced features that can be provided by FACTS devices and HVDC links is the main motivation of this research. Therefore, this thesis intends to exploit sophisticated features of these technologies to improve the performance of the main internal tie-lines of the Libyan power network, and its economic and security prospects.

1.5 Research objectives

This research investigates the use of FACTS and VSC-HVDC as possible solutions to improve power transfer capacity of the main Libyan internal tie-line between its east and west regions. The main objectives are:

- To provide a comprehensive review of the state of the art research on the impact of FACTS devices and HVDC links on the performance of power transmission systems.
- To provide a systematic analytical approach for determination of power transfer capacity of the Libyan internal tie-line, considering its present and future configurations.
- Determination of the optimal location and size for each FACTS device and HVDC link to be deployed that ensures maximum power transfer over the East-West tie-line.
- Build valid steady-state and dynamic models for FACTS (SVC, STATCOM, TCSC and SSSC) and VSC-HVDC to be used for sizing and estimation of their optimal locations.
- Investigate to what extent FACTS devices and HVDC links could improve the Libyan tie-line in terms of utilization, operational flexibility, and voltage and power stability.

1.6 Thesis organization

The thesis is organized in the logical sequence of the scientific research to include eight chapters that cover the lecturer review and the computer simulations required to achieve the research objectives of the thesis. Starting from the fundamental theories of active and reactive power flow in the AC system in chapter two, causes and challenges affecting efficient utilization of power transmission lines are discussed. The rules of power electronic-based technologies, including shunt and series FACTS and VSC-HVDC transmission systems, to improve power transfer capability of the tie-line in the interconnected power systems are addressed in chapters three, four and five. The findings of these chapters are used in subsequent chapters to study the applications of FACTS and VSC-HVDC system for enhancing the Libyan internal tie-line power transfer capability. The chapters in the thesis are organized as follows:

- Chapter One presents a brief background of the challenges of interconnected power systems and outlines the main motivation and objectives of the thesis.
- Chapter Two presents power flow fundamentals applied to interconnected power systems, including the challenges that hamper utilization of tie-lines in a cost effective and technical desirable manner. The chapter considers active and reactive power flow at given node and the main factors that limit power transfer capacity of transmission lines.
- Chapter Three presents the theory of variable impedance and converter based shunt FACTS devices. It presents systematic methods for allocating and sizing of shunt FACTS devices to improve voltage stability and angular stability, and tie line total transfer capacity. Also discussed is SVC and STATCOM steady state and dynamic modelling.
- Chapter Four focuses on series FACTS devices, namely, TCSC and SSSC, and highlights the superiority of series compensator over shunt compensation in term of improvement in the power transfer capacity of a tie line. Also, it highlights the relationship between series compensation factor and risk of subsynchronous resonance. This chapter proposes methods for allocation and sizing of series FACTS, considering voltage and angular stability limits and improvement of tie line total transfer capacity.
- Chapter Five presents analytical formulations that can be used to assess the steady-state power flow performance of VSC-HVDC links. It discusses allocation and sizing methods of VSC-HVDC to improve the utilization of existing AC transmission system. STATCOM operation, frequency control and black start capabilities of the VSC-HVDC are investigated. Also, the chapter examines the dynamic response of a VSC-HVDC link during power step changes and three-phase faults.
- Chapter Six focuses on the use of FACTS technologies to improve the performance of the critical power corridor that links the eastern and western parts of the current Libyan power system. From this scenario, the performance of the east-west tie-line is evaluated by calculating voltage and power stability limits and its maximum power transfer capacity. Optimal allocation and sizing of shunt and series FACTS devices to improve tie-line performance are obtained. Steady state and dynamic performance of the Libyan power systems are studied, which incorporate SVC, STATCOM and TCSC.

- Chapter Seven focuses on the use of VSC-HVDC to improve the performance of the main power corridor (tie-line) that links the eastern and western parts of the Libyan power system. In this scenario, the proposed VSC-HVDC link is sized and allocated using optimal allocation and sizing method developed in Chapter Five in order to improve the power transfer capacity of the existing west-east AC tie-line. Steady state and dynamic performance of the resultant hybrid system is evaluated, considering severe AC network disturbances, ramping of the dc power, and STATCOM operation. DC power management in the hybrid AC/DC tie-line is also investigated during loss of one of the parallel AC lines.
- Chapter Eight summarises the main conclusions of this thesis, the author's contribution, and presents suggestions for future research.

1.7 Research contribution

Since the main objective of the thesis was to investigate the potential of FACTS devices and VSC-HVDC links for the performance improvement of the main tie-line between east and west Libya, the following points highlight the main contribution of this thesis:

1. A new generic power flow equation is developed in chapter 2 that account for the effects of line resistance, charging current and inductance. This equation allows derivation of analytical formulas for calculation of voltage and angular stability limits, and accurate calculation of the total transfer capability of a given power corridor. These formulas is validated against BCP commercial software NEPLAN.
2. The generic power flow equation developed in chapter two is modified to include $V-I$ characteristics of variable impedances and converter based series and shunt type FACTS devices (SVC, STATCOM, TCSC and SSSC). This modification facilitates plotting of $P-V$ and $P-Q$ curves at the PCC, reactive power output of the FACTS device during linear and nonlinear operation; sizing of FACTS devices based on reactive power requirements at the PCC; the extent of TTC improvement in a tie line; and FACTS device utilization factor.
3. New algorithms for allocation and sizing of FACTS is introduced. These algorithms employ total voltage change index ($TVCI$), which is introduced in chapter 3 as an efficient effective way to allocate FACTS devices. Also, in the

case of series compensation, new algorithms are introduced to estimate a suitable compensation factor and the FACTS location along the tie line in order to achieve maximum power transfer, while avoiding the risk of subsynchronous resonance; ensuring minimum short circuit current flow in the FACTS devices during ac faults.

4. Analytical equations that describe steady state behaviour of a VSC-HVDC that can be used for power flow calculations are introduced in chapter 5. Validations of these equations against NEPLAN established that these equations can accurately estimate both AC and DC voltages and powers.
5. Chapter 5 also introduces a new method for VSC-HVDC link converter sizing on the basis of their terminal voltage during changes of dc power, taking into account the network strength at the PCC.
6. The proposed methods for allocating and sizing of the FACTS devices (SVC, STATCOM, TCSC) and a VSC-HVDC link are tested on a full-scale model of Libyan internal tie-line, considering steady state and dynamic conditions.
7. Multi-task control for a VSC-HVDC link is proposed to facilitate dc power management during $N-1$ contingency in the AC/DC hybrid tie-line; frequency support at the eastern network during unsynchronized operation, and provision of independent voltage/reactive power control at the PCC.
8. A technical comparison between shunt FACTS, series FACTS and VSC-HVDC system in terms of overall performance improvement of the Libyan internal tie-line, is an effective overall outcome of the research.

1.8 List of publications

- 1) **A. Elansari**, S. Finney, J. Burr and M. Edrah, "Frequency control capability of VSC-HVDC transmission system," in AC and DC Power Transmission, 11th IET International Conference on, 2015, pp. 1-6.
- 2) **A. Elansari**, S. Finney, J. Burr and M. Edrah, "Optimal location for shunt connected reactive power compensation," in Power Engineering Conference (UPEC), 2014 49th International Universities, 2014, pp. 1-6.
- 3) M. Edrah, , O. Anaya-Lara, K. L. Lo, **A. Elansari** "Impact of DFIG Based Offshore Wind Farms Connected Through VSC-HVDC Link on Power System Stability," in AC and DC Power Transmission, 11th IET International Conference on, 2015, pp. 1-7.
- 4) M. Edrah, O. Anaya-Lara, K. L. Lo, **A. Elansari**, "Power oscillation damping capabilities of doubly fed wind generators," in Power Engineering Conference (UPEC), 2014 49th International Universities, 2014, pp. 1-6.
- 5) **A. Elansari**, Musa, A. ; Alssnoui, A , "Impact of new wind farms on power distribution networks (Derna Wind project case study)," in Renewable Energies for Developing Countries (REDEC), 2012 International Conference on, 2012, pp. 1-6.
- 6) **A. Elansari**, G. P. Adam S. Finney, J., "Optimal Sizing of Shunt VAR Compensation to Maximize Power Transfer Capability" Submitted to the IEEE Transactions on Power Systems delivery.
- 7) **A. Elansari**, S. Finney, J. "steady state mathematical model for power flow calculation at the VSC-HVDC link" to be submitted to IET journal.
- 8) **A. Elansari**, S. Finney, J."sizing of the VSC-HVDC link on the basis of the converter terminal voltage" to be submitted to IEEE Transactions on Power delivery.

References

- [1] A. L'Abbate, *et al.*, "The role of facts and HVDC in the future paneuropean transmission system development," in *AC and DC Power Transmission, 2010. ACDC. 9th IET International Conference on*, 2010, pp. 1-8.
- [2] F. Alvarado and S. Oren, "Transmission system operation and interconnection," *National transmission grid study–Issue papers*, 2002.
- [3] X. Ying, *et al.*, "Available transfer capability enhancement using FACTS devices," *Power Systems, IEEE Transactions on*, vol. 18, pp. 305-312, 2003.
- [4] Y. Xiao, *et al.*, "Application of unified power flow controller to available transfer capability enhancement," *IEEE Power Engineering Review*, vol. 21, pp. 66-68, 2001.
- [5] K.R.Padiyar, *HVDC power transmission systems: technology and system interactions*. New Delhi: New Age International (P) Limited, Publishers, 2005.
- [6] X.-P. Zhang, *et al.*, *Flexible AC transmission systems: modelling and control*: Springer Science & Business Media, 2012.
- [7] P. Kundur, *Power system stability and control*: Tata McGraw-Hill Education, 1994.
- [8] J. J. Grainger and W. D. Stevenson, *Power system analysis* vol. 621: McGraw-Hill New York, 1994.
- [9] T. Van Cutsem and C. Vournas, *Voltage stability of electric power systems* vol. 441: Springer, 1998.
- [10] N. A. E. R. Council, "Available Transfer Capability Definitions and Determination," ed, 1996.
- [11] F. M. Albatsh, *et al.*, "Enhancing power transfer capability through flexible AC transmission system devices: a review," *Frontiers of Information Technology & Electronic Engineering*, vol. 16, pp. 658-678, 2015.
- [12] L. Zhang, *et al.*, "Power System Reliability and Transfer Capability Improvement by VSC-HVDC (HVDC Light®)," *Cigré, Security and Reliability of Electric Power Systems*, 2007.
- [13] N. G. Hingorani and L. Gyugyi, *Understanding FACTS: Concepts and Technology of Flexible AC Transmission Systems*: Wiley, 2000.
- [14] E. Ghahremani and I. Kamwa, "Optimal placement of multiple-type FACTS devices to maximize power system loadability using a generic graphical user interface," *Power Systems, IEEE Transactions on*, vol. 28, pp. 764-778, 2013.
- [15] X.-P. Zhang, *et al.*, *Flexible AC transmission systems: modelling and control*: Springer, 2006.
- [16] C. Ya-Chin, *et al.*, "Transmission System Loadability Enhancement Study by Ordinal Optimization Method," *Power Systems, IEEE Transactions on*, vol. 26, pp. 451-459, 2011.
- [17] J. Arrillaga, *et al.*, *Flexible power transmission: the HVDC options*: John Wiley & Sons, 2007.
- [18] J. Beerten, *et al.*, "Modeling and control of HVDC grids: a key challenge for the future power system," in *Power Systems Computation Conference (PSCC), 2014*, 2014, pp. 1-21.
- [19] M. Vargončík and M. Kolcun, "SPECIAL PROTECTION SCHEMES IN ELECTRIC POWER SYSTEMS," *Acta Electrotechnica et Informatica No*, vol. 7, p. 4, 2007.

- [20] C. E. a. A. S. G.Vukojevic "CONSULTANCY FOR UPDATING LIBYAN TRANSMISSION NETWORK EXPANSION STUDIES 2010-2030 " 15.00/PP01:63713A/151010., 2010.
- [21] A. S. Elansari, *et al.*, "Improve transient frequency response by adjusting generators' over frequency relays," in *Power and Energy (PECon), 2012 IEEE International Conference on*, 2012, pp. 458-463.
- [22] G. C. C. Bruno, "Consultancy services about Optimal Operation Schemes for the Libyan 400 kV and 220 kV Networks " CESI, Milan, Italy2011.

Chapter two

Fundamentals of Power Flow in the Interconnected Power Systems

2.1 Introduction

This chapter provides a detailed explanation of the basic concepts of power flow in interconnected power systems. Basic equations that govern active and reactive power flow over a tie-line in the interconnected power systems are addressed. Well-Known Kundur test system with a weak tie-line is used throughout this chapter to provide an understanding of the issues that affect transmission efficiency of tie-lines [1].

Starting from the standard power flow equation, a new generic power flow equation is introduced in this chapter. The equation accounts for the effects of network losses and charging effects of long transmission lines.

As the main objective of this research is to improve transfer capability of tie-lines, the most important definitions related to transmission line capabilities and power transfer limitations are introduced. This includes discussion of line load-ability concept introduced by H.P. St. Clair in 1953, upon which transmission lines are classified based on their lengths into; short, medium and long transmission lines [1]. Depending on the tie-line length, thermal, voltage or transient stability limits can all affect the utilization of the tie-line which results in overall poor performance of the transmission system [2]. In the course of these definitions, the North American Electric Reliability Corporation (NERC) has established a set of definitions that defines the rules and limits of power transfer between interconnected power systems. Among the relevant NERC definitions which are addressed in this chapter are; Total Transfer Capability (TTC) and Available Transfer Capability (ATC) of a power transmission corridor [3].

The voltage instability phenomenon is a concern in weak interconnected AC power systems, as it can dramatically affect the power transfer capability of tie-lines. For this reason, voltage stability proximity and mechanisms are addressed in this chapter. In this regards, a mathematical equation that determines voltage stability limit (*VSL*) for power transfer in a given tie-line is introduced.

In a relatively strong interconnection where the voltage is maintained at the two terminals of the tie-line, power transfer capability can be restricted by the steady

state angular stability limit (*ASL*) that defines a synchronism boundary of the interconnected power systems. The introduced power flow equation is used to establish a formula that determines the steady state angular stability limit. This equation allows the derivation of power versus load angle curve, which facilitates estimation of maximum power that can be transmitted by AC transmission systems.

Outcomes of this chapter include assessment of tie-line performance in terms of; power transfer capability, utilization factor, power transfer limitation, and the proposed technologies and solution for efficient tie-line utilization.

As the main cause of poor tie-line utilization is the lack of reactive power support along the tie-line, reactive power manipulation is proposed as an effective approach to mitigating voltage instability and to improve tie-line performance. Therefore, following chapters will address the potential of Flexible AC Transmission Systems (FACTS) and HVDC transmission systems to improve tie-line performance.

2.2 Active and reactive power flow in AC power system

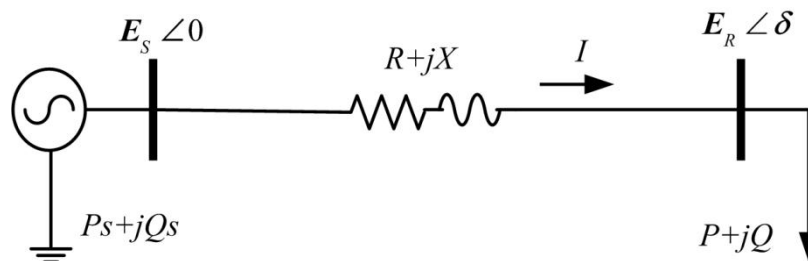


Figure 2-1: Basic 2-bus AC system

Figure 2-1 illustrates a two-bus AC system, where the power flow is from bus 1 (sending and reference end) to bus 2 (receiving end). Tie-line series impedance is $R+jX$, and the load demand at the receiving end is expressed by active and reactive power $P+jQ$.

When line resistance is considered negligible compared to line reactance in Figure 2-1, the complex power at the receiving end (\tilde{S}_R) is given by (2-1) [1].

$$\tilde{S}_R = P_R + jQ_R = \tilde{E}_R \tilde{I}^* \quad (2-1)$$

Accordingly, active and reactive power equations at each end for the case of a lossless network are:

$$P_s = P_R = \frac{E_S E_R \sin \delta}{X} \quad (2-2)$$

$$Q_S = \frac{E_S^2 - E_S E_R \cos \delta}{X} \quad (2-3)$$

$$Q_R = \frac{E_S E_R \cos \delta - E_R^2}{X} \quad (2-4)$$

As the series impedance of a given tie-line is constant and the voltages E_S and E_R have to be within a certain range, equation (2-2) implies that active power flow is mainly determined by the power angle δ at the receiving end with respect to the sending end. But equations (2-3) and (2-4) indicate that reactive power flows from the highest to the lowest nodal voltages. This fact leads to the conclusion that reactive power cannot be transmitted over long distances because it will be consumed in the line's inductive reactance. Moreover, transmission of reactive power over long distances requires a large voltage gradient between the sending and receiving voltages which is not possible due to the need to respect the limits of permissible operating voltage in real power systems.

Practically, the receiving end can represent a capacitive or inductive source with respect to the network. This can be explained by rewritten equation (2-4) as:

$$Q_R = \frac{E_R}{X} (E_S \cos \delta - E_R) \quad (2-5)$$

The reactive power direction is defined by the change of E_R with the change of power angle δ , if

$$E_S \cos \delta > E_R, Q_R \text{ is capacitive}$$

$$E_S \cos \delta < E_R, Q_R \text{ is inductive}$$

$$E_S \cos \delta = E_R, P_R \text{ is at unity power factor (} pf \text{) at the receiving end.}$$

2.2.1 Effect of transmission line resistance on power flow

The transmission line resistance can have a considerable effect on the voltage behaviour in typical transmission systems. From the system in Figure 2-1, the tie-line impedance causes voltage difference between the sending and receiving ends, that is given by [4, 5].

$$\tilde{E}_S - \tilde{E}_R = \tilde{Z} \tilde{I} \quad (2-6)$$

where \sim refers to complex quantities. Multiplying both sides of (2-6) by the receiving end voltage conjugate \tilde{E}_R^* yields:

$$\tilde{E}_S \cdot \tilde{E}_R^* - E_R^2 = \tilde{Z} \tilde{I} \tilde{E}_R^* \quad (2-7)$$

As $\tilde{S}^* = \tilde{I} \cdot \tilde{E}_R^*$, equation (2-7) can be rewritten as

$$\tilde{E}_S \cdot \tilde{E}_R^* = E_R^2 + \tilde{Z} \cdot \tilde{S}^* \quad (2-8)$$

When equation (2-8) is multiplied by its conjugate:

$$\begin{aligned} \left(\tilde{E}_S \cdot \tilde{E}_R^* \right) \cdot \left(\tilde{E}_S \cdot \tilde{E}_R^* \right) &= \left(E_R^2 + \tilde{Z} \cdot \tilde{S}^* \right) \cdot \left(E_R^2 + \tilde{Z} \cdot \tilde{S}^* \right) \\ E_S^2 \cdot E_R^2 &= \left(E_R^2 + \tilde{Z} \cdot \tilde{S}^* \right) \cdot \left(E_R^2 + \tilde{Z} \cdot \tilde{S}^* \right) \end{aligned} \quad (2-9)$$

Substituting the series impedance Z and the apparent power S in equation (2-9) by $(R+JX)$ and $(P+JQ)$ respectively gives the following quadratic equation that considers the effect of the resistive part in the AC power flow at a receiving end.

$$E_R^4 + (2(RP + XQ) - E_S^2)E_R^2 + (R^2 + X^2)(P^2 + Q^2) = 0 \quad (2-10)$$

Equation (2-11) is one of the positive solutions of the above power flow equation, and it gives the receiving end voltage $V_{(pu)}$ in per unit for a given P and Q in MW and MVar.

$$V_{(pu)} = \frac{1}{2} \sqrt{2 \left(1 - \frac{2(RP + XQ)}{E_S^2} \right) + \sqrt{1 - \frac{4(RP + XQ)}{E_S^2} - \frac{4(XP - RQ)^2}{E_S^4}}} \quad (2-11)$$

2.2.2 Effect of long Line charging on Power flow

Generally in typical power systems, the impedance of overhead transmission lines and power cables behave differently from lumped impedance representation. This can affect the power flow calculation, especially in the long transmission lines. Therefore, the stray capacitance should be considered in power flow calculations because of its boosting effect in long transmission lines and cables[1].

In order to consider the line charging in the power flow equation, R and X in (2-11) are replaced by R_{ln} and X_{ln} , to include the impact of; line length l , line susceptance B_l , and conductance G_l .

The new resistance and reactance R_{ln} and X_{ln} can be calculated as[1];

$$\begin{aligned} R_{ln} &= \frac{1}{2}(R_C \sinh 2\alpha l + X_C \sin 2\beta l) \\ X_{ln} &= \frac{1}{2}(R_C \sin 2\beta l + X_C \sinh 2\alpha l) \end{aligned} \quad (2-12)$$

where R_C and X_C are the real and imaginary parts of the surge impedance Z_C in (2-13), α and β are attenuation and the phase constants obtained from the line propagation constant γ .

$$Z_C = \sqrt{\frac{(R + jX)}{(G + jB)}} \quad (2-13)$$

In addition to the affect the long line susceptance and conductance, the power flow equation is also influenced by the Ferranti effect, specifically caused by the stray capacitance of long lines especially in lightly loaded lines. The voltage tends to be higher at the receiving end due to voltage boosting effect coefficient of the line F_C that is given by:

$$F_C = \frac{1}{2}(\cosh(2\alpha l) + \cos(2\beta l)) \quad (2-14)$$

Therefore, load flow equation (2-11) can be rewritten to include the long line charging effect:

$$V_{(pu)} = \sqrt{\frac{1 - \frac{2(R_{ln} \cdot P + X_{ln} \cdot Q)}{E_s^2} + \sqrt{1 - \frac{4(R_{ln} \cdot P + X_{ln} \cdot Q)}{E_s^2} - \frac{4(X_{ln} \cdot P - R_{ln} \cdot Q)^2}{E_s^4}}}{2 \cdot F_C}} \quad (2-15)$$

2.2.3 Effect of shunt admittance on power flow

Power flow equation (2-15) is derived when considering a constant power load at the receiving end. However, this equation is not valid if the system includes passive reactive power components with constant impedance and voltage dependency characteristics. The reactive power consumption of such loads changes with the voltage square.

The effect of shunt susceptance (b) and conductance (g) of the passive reactive power components can change the series impedance of the transmission line as indicated in equation(2-16):

$$\begin{aligned} R_{sh} &= R + (R^2 + X^2) p_{sh} \\ X_{sh} &= X + (R^2 + X^2) q_{sh} \end{aligned} \quad (2-16)$$

where p_{sh} and q_{sh} are active and reactive power admittances given by $P_{sh} = g.E_R^2$ and $Q_{sh} = -b.E_R^2$ respectively [1, 5].

Equation (2-16) reveals the importance of including the effect of shunt admittance in power flow equation (2-15) for the systems that include shunt reactive compensation such as shunt reactors, capacitors banks and FACTS devices (SVCs). The effect of shunt admittance components on power flow will be incorporated in the mathematical model of the SVC that will be addressed in the coming chapter.

2.2.4 Generic power flow equation

To establish a generic load flow equations, the tie-line parameters R_{eqv} , X_{eqv} and F_{Ceqv} in that equation are defined to incorporate simultaneously the effects of line length and passive shunt components (p_{sh} and q_{sh}), described in subsections 2.2.2 and 2.2.3. R_{eqv} , X_{eqv} and F_{Ceqv} can be calculated as (detailed in [5]):

$$\begin{aligned} R_{eqv} &= R_{ln} + (R_{ln}^2 + X_{ln}^2) p_{sh} / F_C \\ X_{eqv} &= X_{ln} + (R_{ln}^2 + X_{ln}^2) q_{sh} / F_C \\ F_{Ceqv} &= F_C + 2(R_{ln} \cdot p_{sh} + X_{ln} \cdot q_{sh}) + (R_{ln}^2 + X_{ln}^2)(p_{sh}^2 + q_{sh}^2) / F_C \end{aligned} \quad (2-17)$$

For clarity assume $r = R_{eqv}/E_S^2$, $x = X_{eqv}/E_S^2$ and $a = (r^2 + x^2)/F_{Ceqv}$. Also, assume p_{sh} of the passive shunt is negligible, hence $R_{eqv} = R_{ln}$ in(2-17). Then the generic power flow equation, which considers effects of shunt passive reactive components q_{sh} and line length and its associated Ferranti phenomena, is given by equation(2-18):

$$V_{(pu)} = \sqrt{\frac{(1 - A + \sqrt{1 - 2A - B})}{C}} \quad (2-18)$$

where

$$\begin{aligned} A &= 2 \left[r \cdot P + (a \cdot q_{sh} + x) P \cdot \tan \left(\left[\cos^{-1} pf \right] \right) \right] \\ B &= 4 \left(P (a \cdot q_{sh} + x) - r \cdot P \cdot \tan \left(\left[\cos^{-1} pf \right] \right) \right)^2 \\ C &= 2 \left[q_{sh} (a \cdot q_{sh} + 2x) + F_{Ceqv} \right] \end{aligned}$$

The reactive power in equation (2-18) is represented by its power factor $Q=P.tan(cos^{-1}(pf))$, assuming the load at the receiving end changes with a constant power factor pf .

Although the calculations behind this equation assume a radial system with a remote load, it is also valid for power flow calculations at the borders of interconnected power systems. The net exchanged active and reactive powers at the receiving end represent the active and reactive power P and Q in equation(2-18). Hence, the positive sign represents the demand situation, and a negative sign represents the generation case.

For a simple lossless power flow calculation the resistive part can be neglected ($r=0$), and line charging effect in short lines can be also neglected ($F_C=1$). Neglecting the effects of shunt passive reactive components q_{sh} , the generic power flow equation (2-18) is simplified to

$$V_{(pu)} = \frac{1}{\sqrt{2}} \sqrt{1-2.x.Q + \sqrt{1-4(P^2x^2 - Qx)}} \quad (2-19)$$

If the resistive part of the network is considered, equation (2-19) can be rewritten as

$$V_{(pu)} = \frac{1}{\sqrt{2}} \sqrt{1-2(r.P-x.Q) + \sqrt{1-4(rP-x.Q-(P.x-Q.r)^2)}} \quad (2-20)$$

This equation is valid for power flow calculation in short and medium transmission line length. A typical 230kV, a 100km length transmission line with the parameters in Table 2-1 [1] is used to produce power flow results with and without considering the effect of line resistance and the voltage boosting associated with the Ferranti phenomenon. The tie-line in Figure 2-1 feeds a 100MW load demand with 0.95 lagging power factor. Power flow compression of the three cases is illustrated in Table 2-2.

Table 2-1: Typical parameters of a 230KV transmission line

$R (\Omega)/km$	$X (\Omega)/km$	$B (\mu\bar{C})/km$	r	x	FC
0.05	0.488	3.371	9.400e-5	9.148e-4	9.837e-1

Table 2-2: Effect of line resistance and line charging on tie-line power flow

Case	Equation	V_R (p.u)	P losses (MW)	Q losses (MVA _r)	Charging (MVA _r)
full model	(2-18)	0.9622	1.082	10.53	-17.9
lossless model	(2-19)	0.964	-	11	-
no line charging	(2-20)	0.953	1.15	11.23	-

Table 2-2 indicates that the approximation in equations (2-19) and (2-20) are acceptable for power flow calculations in light loading, and in a short and medium tie-line.

The significant of the generic power flow equation (2-18) is that it allows derivation of analytical formulas for calculation of voltage and angular stability limits, and accurate calculation of the total transfer capability of a given power corridor. Furthermore, it can be used to incorporate the V-I characteristics of power electronic-based technologies which facilitate steady-state analysis of the power systems with FACTS and HVDC systems at a given node. Although, the accuracy of the introduced equation in the steady-state calculation of a radial power system, this equation may not be valid for a very complicated meshed network especially in the presence of nearby voltage regulates such as under-load tap changers transformers (ULTC).

2.3 Load-ability of a transmission line

The relation between line length and line load-ability was introduced in 1953 by H.P. St.Clair and was developed based on practical considerations and experience; see the St. Clair curve shown in Figure 2-2. According to H.P. St. Clair, line load-ability is defined as the degree of the line loading, as a percentage of its Surge Impedance Loading (*SIL*), to the permissible loading of the restrictive limit (thermal, voltage stability or transient stability). The St Clair curve is analytically extended to cover long transmission lines up to 960km with high transmission voltage levels up to 1500kV[1].

The St Clair curve in Figure 2-2 illustrates that, regardless of the voltage transmission level, the restrictive limit of the line load-ability varies with line length. Up to 80km the restrictive limit is the thermal capacity of the line conductor which can be up to 3 times the *SIL*. For medium tie-lines, line load-ability is considerably affected by voltage drop and can be as lower as 1.3 the *SIL* for a 320km line length.

As the line length exceeds 320km, load-ability is often restricted by steady state voltage instability and can be less than the SIL of the transmission line.

It is appreciated to mention that reactive power manipulation can have considerable rule for the medium and long transmission lines as it shifts the region of steady-state and angular stability up closer to the thermal limit[2].

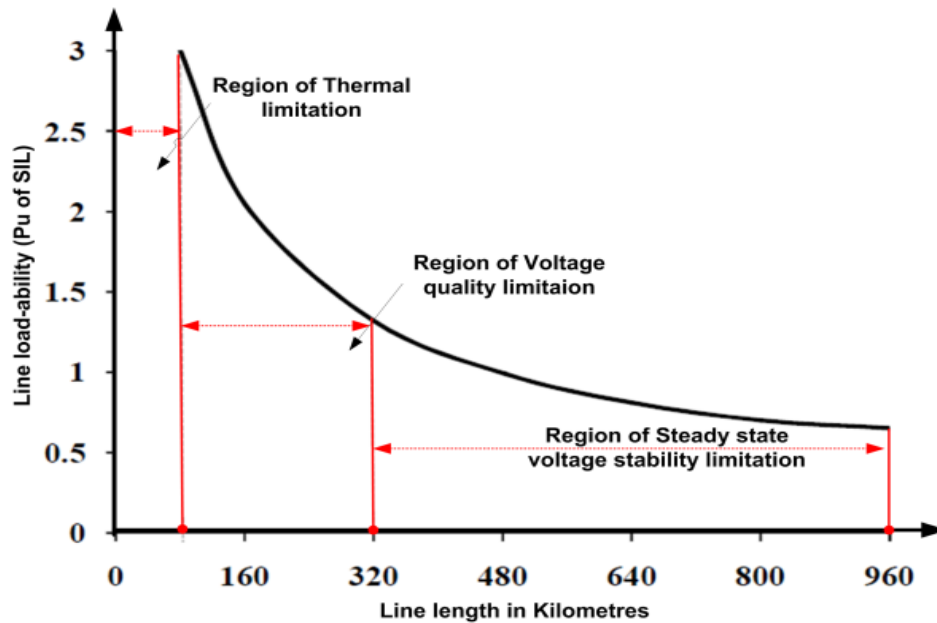


Figure 2-2: Transmission line load-ability curve

2.3.1 Thermal Limit

The thermal capacity of a power conductor is determined by its physical characteristics which specify the maximum current flow in the conductor. If the current flow in the conductor exceeds the thermal limit for a specific duration, the heat which is produced due to current flow can permanently damage the electrical facility. Additionally, exceeding the maximum allowable temperature affects the mechanical strength characteristics of the aluminium conductors of power transmission lines. Furthermore, conductor overheating increases conductor sag reducing the clearance distance between the conductor and ground which is the main thermal limiting concern for overhead lines. Figure 2-2 indicates that power transfer capability in a short tie-line up to 80km is normally restricted by thermal violation[3].

2.3.2 Voltage Stability limit (VSL)

IEEE and CIGRE Task Forces have defined voltage stability as the ability of a power system to maintain steady voltages at all buses in the system after being subjected to a disturbance, from a given initial operating condition[6]. According to this definition, a system is considered voltage unstable when a nodal voltage decreases with the injection of the reactive power at that node or vice versa.

Steady-state voltage instability is a slow dynamic phenomenon, with a time-scale ranging from a few seconds to several minutes or even hours. It develops slowly over time as the system loading is increased when operating in close proximity to the voltage stability limit. Thus, any further increase in system loading may cause a sudden, large drop in nodal voltages beyond the permissible limit. At this instant, the system operating point could be shifted towards the point of collapse (PoC) should the system loading continued to increase, and at this point the Jacobian of the power flow equation becomes singular (as all gradients with respect to voltage vanish), which indicates voltage instability [1, 7, 8].

Numerous voltage stability analysis approaches are proposed to determine the secure level of power exchange over interconnection links. These types of studies include evaluation of voltage instability proximity and analysis of the voltage instability mechanism. The proximity gives an approximation of the gap between the operating point and the voltage instability point. Understanding the mechanism of voltage instability allows the prediction of voltage instability occurrence, the causes, the weak points and the preventive actions[9].

The main cause of voltage instability is the lack of reactive power support at a given node which causes a voltage drop as the active and reactive power demand increases, which can dramatically limit the transfer capability of the transmission corridor[3, 10]. Therefore, reactive power manipulation can be used to mitigate voltage instability problems and to improve load-ability of the interconnection links between power systems.

i. Mechanism of voltage instability

Mechanism of voltage instability can be established as a relation between the change in the load demand impedance and the equivalent impedance at the load bus. From

the AC system in Figure 2-1, the phasor current \tilde{I} can be written as a function of the voltage source and the total network impedance \tilde{Z}_{total} as:

$$\tilde{I} = \frac{\tilde{E}_s}{\tilde{Z}_{total}} \quad (2-21)$$

The total impedance \tilde{Z}_{total} includes the line impedance phasor \tilde{Z}_{line} and the load impedance phasor \tilde{Z}_{load} , and it is given by

$$\tilde{Z}_{total} = Z_{line} \angle \theta + Z_{load} \angle \Phi \quad (2-22)$$

The current magnitude can be obtained from equations (2-21) and (2-22) is:

$$I = \frac{E_s}{\sqrt{(Z_{line} \cdot \cos \theta + Z_{load} \cdot \cos \Phi)^2 + (Z_{line} \cdot \sin \theta + Z_{load} \cdot \sin \Phi)^2}} \quad (2-23)$$

The denominator of the equation (2-23) can be simplified to

$$\sqrt{R} \cdot Z_{line} \quad (2-24)$$

where

$$R = 1 + \left(\frac{Z_{load}}{Z_{line}} \right)^2 + 2 \left(\frac{Z_{load}}{Z_{line}} \right) \cos(\theta - \Phi)$$

Using equation(2-24), current flow in equation (2-23) can be rewritten as:

$$I = \left(\frac{E_s}{Z_{line} \cdot \sqrt{R}} \right) \quad (2-25)$$

Hence, the receiving end voltage E_R , which results from the current flow I through the load impedance Z_{load} , can be calculated from (2-24) and (2-25) as:

$$E_R = \left(\frac{Z_{load}}{Z_{line}} \right) \cdot \left(\frac{E_s}{\sqrt{R}} \right) \quad (2-26)$$

Active power at the receiving end can be estimated from (2-25) and (2-26) as:

$$P_R = \left(\frac{Z_{load}}{R} \right) \cdot \left(\frac{E_s}{Z_{line}} \right)^2 \cos \Phi \quad (2-27)$$

As the load at a given node changes (increases or decreases), the ratio between Z_{line} and Z_{load} in equation (2-27) also changes. A change of the Z_{load} / Z_{line} ratio can be used to evaluate system performance during light and peak load conditions which facilitates analysis of voltage stability.

The load demand P_R changes inversely with load impedance Z_{load} . Equation (2-27) indicates that at the light loading conditions, the increase in load demand (Z_{load} decrease), starts rapidly then slows as the load-ability increases as it can be seen in Figure 2-3. The maximum load-ability at a given node corresponds to the loading point where Z_{load} equals Z_{line} ($Z_{load} / Z_{line} = 1$) in the (2-27) as indicated by the black curve in Figure 2-3. This loading condition is known as the voltage stability limit, where voltage decreases with decreasing Z_{load} dominates over the current increase as shown by the red dashed voltage curve in Figure 2-3. Theoretically, the voltage drop across the line impedance is approximately equal to the receiving voltage end E_R at the voltage stability limit.

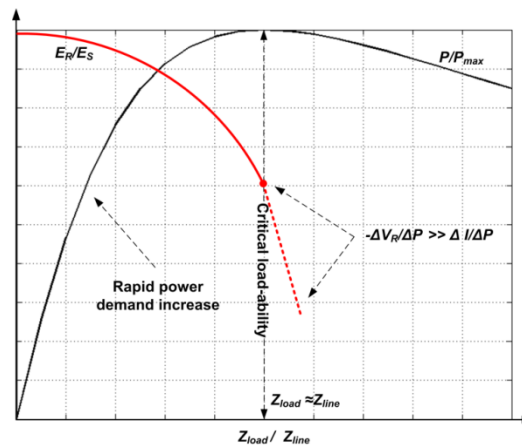


Figure 2-3: Voltage and active power at the receiving as a function of Z_{load} / Z_{line} ratio

ii. Determination of voltage stability limit (VSL) using P-V curve technique

Voltage instability proximity can be assessed using $P-V$ and $Q-V$ curve analysis, model analysis or time domain simulation. These techniques allow determination of the point of voltage collapse (PoC) on the $P-V$ curve in Figure 2-4 upon which the voltage stability limit (VSL) is determined. Beyond this point, any further increase in system loading shifts the system towards instability conditions as illustrated in Figure 2-4. However, system security imposes working with sufficient voltage stability margin (VSM) from the VSL to avoid slipping into voltage instability during post-fault conditions.

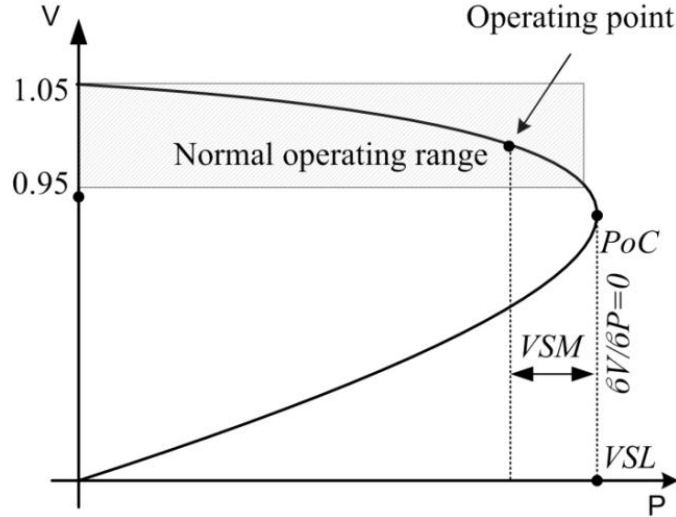


Figure 2-4: Power versus voltage curve (P-V curve or nose curve)

Mathematically, the voltage stability limit at a given node can be determined from the generic power flow equation (2-18) at the loading condition when the discriminant $1-2A-B$ in (2-18) is zero. That is

$$\sqrt{1-2A-B}=0 \quad (2-28)$$

At this operating condition, voltage change with respect to active power change is zero ($dv/dp=0$) and $Z_{load}/Z_{line}=1$.

Equation (2-29) is the positive solution of equation (2-28), and gives the voltage stability limit in MW at the node with the given system parameters (r , x and F_C).

$$VSL \text{ (MW)} = \frac{pf \left(x F_C \sqrt{1-pf^2} + F_C \cdot pf \cdot r - \sqrt{F_C^2 (r^2 + x^2)} \right)}{2 \left(F_C \left(2 pf \cdot x \cdot r \sqrt{1-pf^2} + pf^2 r^2 - pf^2 x^2 - r^2 \right) \right)} \quad (2-29)$$

Assume line charging is neglected ($F_C=1$), a lossless network ($r=0$), and unity power factor ($pf=1$), then the voltage stability limit is given by

$$VSL \text{ (MW)} = \frac{1}{2 \cdot x} \quad (2-30)$$

In equation(2-30), $x=X/E_S^2$ indicates that the voltage stability limit at a given node is half the steady state angular stability calculated by equation(2-2). This point represents the knee point of the P-V curve (known as the nose curve) shown in Figure 2-4. The voltage at the tip of the nose curve in Figure 2-4 is known as critical voltage E_{CRT} , and can be established from (2-18) assuming ($1-2A-B=0$):

$$E_{CRT} = \sqrt{\frac{1-A}{C}} \quad (2-31)$$

For two interconnected power systems with tie-line's parameters in Table 2-1, equations (2-29) and (2-30) indicate that the voltage stability limit for a lossless (396MW) tie-line is slightly different from that limit when the line resistance is considered (367MW). This finding is validated from the $P-V$ curves in Figure 2-5 that are established from equations (2-18) and(2-19).

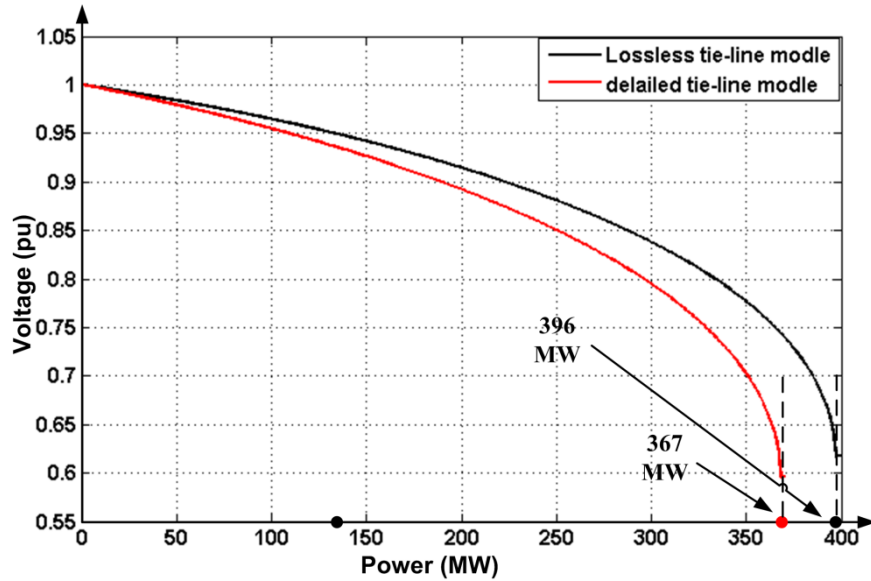


Figure 2-5: $P-V$ curves for detailed and lossless the tie-line in Table 2-1

2.3.3 Angular stability limit (ASL)

The steady-state stability limit represents a stable operating point at which any arbitrarily small change in system operating quantities in an unfavourable direction can cause the power system to lose stability. This is also known as the Small Disturbance Stability Limit[11].

From this definition, the angular stability limit of the tie-line, in interconnected power systems, is determined by the maximum power transfer level that maintains synchronism of the interconnected power systems after being subjected to disturbance.

Assuming a lossless network and maintained receiving end voltage, in Figure 2-1, the steady state angular stability limit (ASL) is calculated from equation(2-2). This equation indicates that active power transfer depends mainly on the power angle δ as depicted in the power versus load angle curve in Figure 2-6. Equation (2-32)

indicates that the maximum power transfer across the series inductive reactance in Figure 2-1 is achieved at $\delta=90^\circ$ which represents the angular stability limit for the power transfer between the two areas.

$$ASL = \frac{E_s E_R}{X} \sin \delta \quad \text{when } \delta=90^\circ \quad (2-32)$$

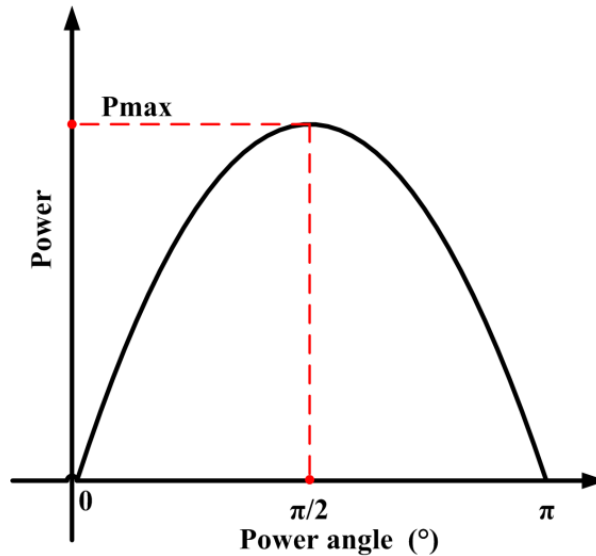


Figure 2-6: Power versus load angle curve

The angular stability limit that is calculated using equation (2-32) is an optimistic approximation. However, accurate calculation of *ASL* should also include network losses and the Ferranti effect in the long lines.

The relation between load angle δ and load demand at the receiving end of the simple two AC power systems in Figure 2-1 can be illustrated by the phasor representation in Figure 2-7.

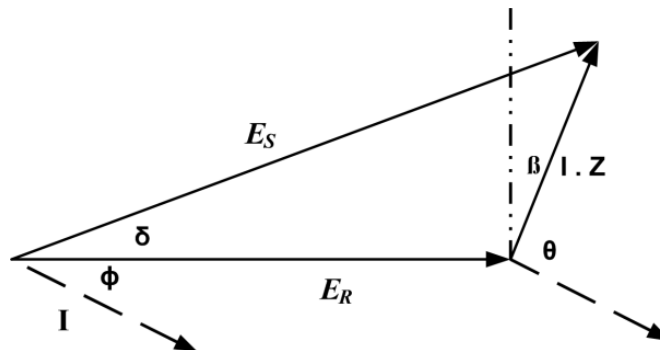


Figure 2-7: Phasor diagram representation of the two AC systems in Figure 2-1

From Figure 2-7, load angle changes with current flow in the series impedance of the tie-line. As line resistance is included in the series impedance Z , the voltage drop in the tie-line ($I.Z$) is tilted by angle β from the Y axis. The maximum power consumption, which represents the angular steady state stability limit, is achieved when the vector $I.Z$ in Figure 2-7, displaces the sending end voltage E_S by 90° from the receiving end voltage E_R , as addressed in section 2.2.

In attempt to include the current (I) in the generic load flow equation (2-18) to estimate the change of power angle (δ) with the current flow through the line impedance, reactive power in the generic load flow equation is expressed as a constant current load given by:

$$Q = \sqrt{3} I V \sin[\cos^{-1}(pf)] \quad (2-33)$$

The modified power flow equation that calculates the voltage change with current is established in appendix-A-1.

The angular steady state stability limit is determined at the maximum current that corresponds to the load-ability level that fulfils the following equation.

$$\sqrt{3} \left[(pf^2 - 1) (F_c r V^2 (F_c r V^2 + 2P r^2 + 2P x^2 - r) + P^2 (2 + r^4 + r^2 x^2 + x^4) - F_c V^2 x^2) \right] = 0 \quad (2-34)$$

Equation (2-35) is one of the positive solutions of this equation that estimate the steady state angular stability limit in (MW) which displaces the load angle at that node by 90° .

$$ASL = \left[\frac{(\sqrt{F_c (r^2 + x^2)} - F_c r V) V}{r^2 + x^2} \right] \sin \delta \quad \text{when } \delta = 90^\circ \quad (2-35)$$

If line charging is neglected in a lossless network, equation (2-35) gives the same ASL as that calculated by equation(2-32).

Considering the same tie-line parameters in Table 2-1 the P - δ curves in Figure 2-8 are established from equations (2-32) and (2-35) for a lossless and detailed tie-line model.

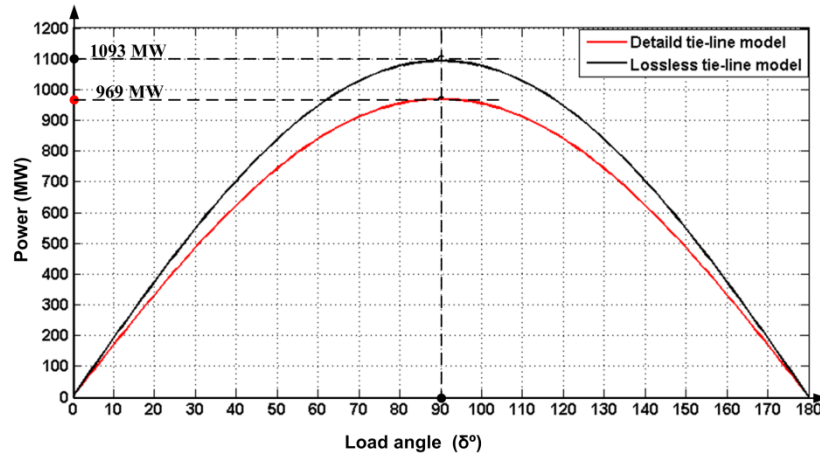


Figure 2-8: $P-\delta$ curves for detailed and lossless the tie-line in Table 2-1

Equation (2-35) indicates that the angular stability limit for power transfer is a function of the receiving end voltage and the series impedance of the transmission line. This means that improvement of ASL can be achieved either by maintaining the receiving end voltage or by reducing the tie-line series impedance. Therefore, both shunt and series FACTS devices can improve the stability limit which allows further load-ability of the transmission line. Shunt connected FACTS are able to maintain the voltage at a pilot point along the line while series connected FACTS reduces the series impedance of the line.

2.4 Power transfer capabilities in transmission tie-lines

Generally, interconnected power systems are designed to operate reliably and securely during normal and emergency conditions. In strong interconnected power systems with reliable tie-lines and well-distributed generation regions or areas, a generation deficit in one area is easily compensated by other areas; thus, it has a higher chance to survive a major disturbance than a weak power system with overloaded tie lines and depressed bus voltages. With the growing demand for electric power, transmission of large power efficiently over ageing and highly interconnected power systems with a large number of tie-lines has become technically challenging, and this must be taken into consideration during planning and operation of such power systems. According to the North American Electric Reliability Corporation (NERC) 1996 definition [3], interconnected power systems are judged to be appropriate for the purpose of power exchange if the following reliability requirements are fulfilled:

- 1- During normal operation, all nodal or bus voltages and loading of every individual line or equipment of the power system should be maintained within permissible limits.
- 2- Following a loss of a single element due to network disturbance, the power system should remain stable, with line loading and nodal voltages maintained within the permissible emergency limits.

2.4.1 Total transfer capability of a tie-line (TTC)

According to the NERC definition, TTC is defined as the amount of electric power that can be transferred over the interconnected transmission network in a reliable manner while meeting all of a specific set of defined pre- and post-contingency system requirements [3]. On other words, the total transfer capability (TTC) for a given corridor is determined at the loading conditions where the first security violation (thermal limit, voltage limit or stability limits) is encountered. This means that, TTC is determined by the most restrictive limit (TCC= minimum of thermal limit, voltage limit or stability limit). However, due to the changeable nature of the load demand and consequently the power flow in the network, TTC can vary with time to be defended either by thermal, voltage stability or transient stability limits as shown in Figure 2-9.

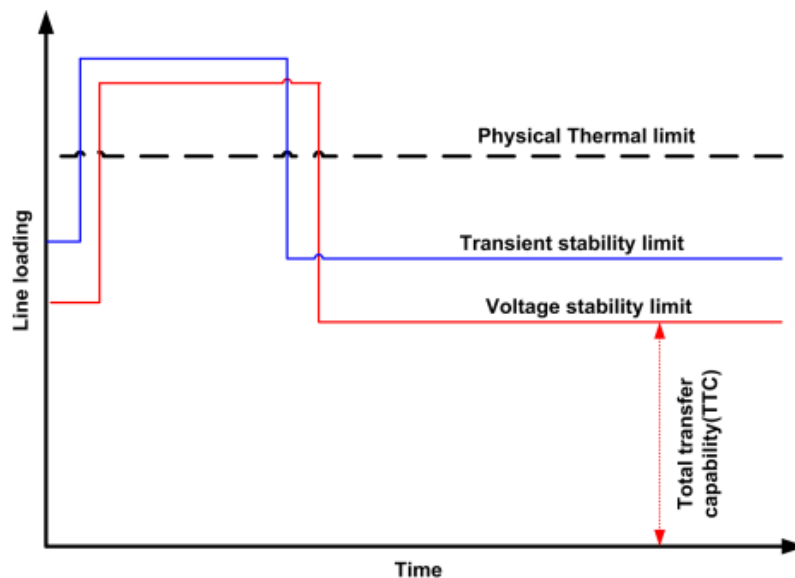


Figure 2-9: Change of TTC restricted limit with time

A TTC calculation is normally performed offline where the power system is modelled to include generation dispatch, load demand and the network configuration for the period being considered. TTC is considerably affected by the severity of the contingency which can change the equivalent system impedance causing considerable power flow change in the system. Therefore, several credible contingencies ($N-1$) are evaluated to identify the most severe contingency which upon total transfer capability of the tie-line (TTC) should be determined. Generally, $N-1$ security precautions are essential for TTC calculation regardless of cost, because achieving this level of security is in the same category as balancing of generation and load [12].

Based this discussion, voltage levels during normal and emergency operating conditions must be maintained within acceptable predefined levels. Accordingly, total transfer capability of a tie-line should respect these operational rules under a worst $N-1$ contingency.

In this approach, total transfer capability of a tie-line is calculated based on VSL because it is normally the restricted limitation in medium and long tie-lines. TTC is calculated using two $P-V$ curves for N and $N-1$ conditions, as depicted in Figure 2-10. O_{11} , O_{21} and O_{22} are operating points on the N and $N-1$ $P-V$ curves. Total transfer capability of the tie-line can be estimated, to satisfy predefined voltage levels during emergency conditions (90%), using power flow equation (2-18) or using $P-V$ algorithms within power system analysis tools.

During a transition from the steady-state pre-fault operating point (O_{11} on N curve) to the other steady-state post-fault operating point (O_{21} on $N-1$ curve), the new operating point established along the $N-1$ $P-V$ curve may temporarily oscillate before settling. During the oscillation, the operating point may temporary enter an unstable region. Therefore, reliability requirements impose availability of reasonable voltage stability margin VSM that is represented by the horizon distance from the settled operating point O_{21} on the $N-1$ $P-V$ curve to the voltage stability limit at point B in Figure 2-10.

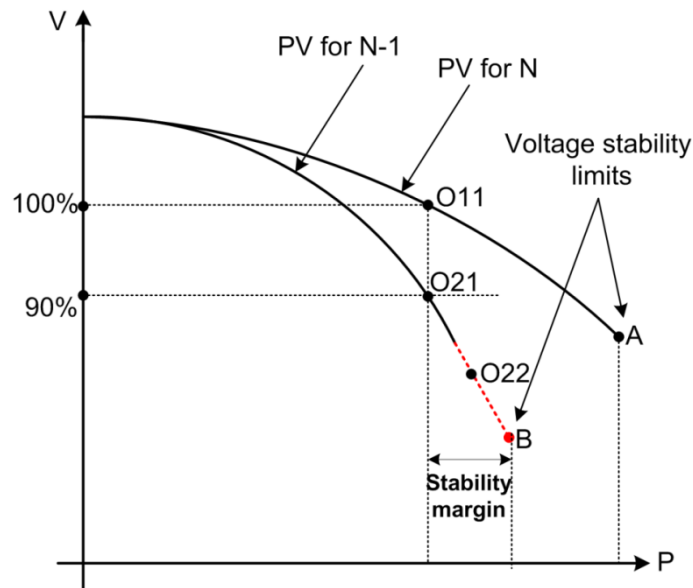


Figure 2-10: Total transfer capability (TTC) calculation based on P-V curve

2.4.2 Available transfer capabilities of a tie-line (ATC)

NERC define Available Transfer Capability (ATC) of a tie-line as [A measure of the transfer capability remaining in the physical transmission network for further commercial activity over and above already committed uses]. Based on this definition the ATC in transmission corridor should be determined based on total transfer capability that determines the amount by which the exchanged power in the interconnected systems can be securely increased, for further commercial activities and for specific operating conditions during a certain period of time. Under deregulation, it is important to determine ATC because it affects both security and energy markets where the market participants may have conflicting interests in different levels of ATC [3].

2.5 Power transfer capability calculation (cases study)

TTC calculation for a tie-line in an interconnected power system is systematically performed offline for a specific time and system configuration. Although performance improvement of Libyan tie-lines is the main object of this thesis, it is appropriate to investigate these issues using well-known and referenced test system models that are similar and suffer from a limited tie-line power transfer capability before proceeding to the more complicated Libyan system. For this reason, a two area Kundur test system with a 220km tie-line length shown in Figure 2-11, is used to determine the total transfer capability of the tie-line, and the most restrictive limit.

The synchronous machine G1 represent the stronger sending end area-A while G2 is a local generation at the receiving end, Area-B. Technical data of the described test system, which is required to carry out steady-state and time-demine based analysis's, are in the Appendix C. It has been confirmed that general conclusion drawn from this system can be applied to large real power systems [13].

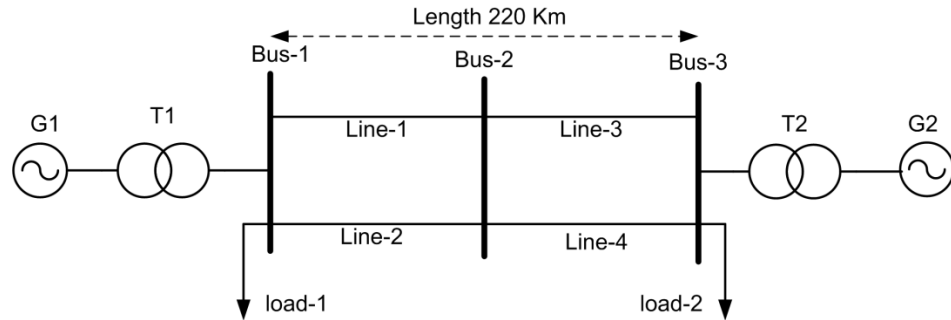


Figure 2-11: Two interconnected power systems (Kundur test system)

Since the TTC of the tie-line depends on system strength, two different scenarios, for weak and strong interconnection tie-lines, are investigated. The equivalent system impedances for the proposed study scenarios are given in Table 2-3 and Table 2-4 for normal and emergency operating conditions where *Line-3* is put out of service.

Table 2-3: Equivalent system impedances for normal operating conditions

Node	$r (R/E_s^2)$	$x (X/E_s^2)$	FC
Bus-2 (middle)	5.300e-5	6.270e-4	9.672e-1
Bus-3 (receiving)	1.060e-4	1.097e-3	8.873e-1

Table 2-4: Equivalent system impedances for emergency operating conditions (line-3 out of service)

Node	$r (R/E_s^2)$	$x (X/E_s^2)$	FC
Bus-2 (middle)	5.300e-5	6.270e-4	9.672e-1
Bus-3 (receiving)	1.590e-4	1.631e-3	9.148e-1

2.5.1 TTC of a weak interconnection link.

System strength at the receiving end is one of the influencing factors which determine the transmission efficiency of the tie-line. Therefore, voltage behaviour in a weak (limited reactive power support) remote end is similar to the voltage behaviour of a radial connected power system. Voltage drop is degraded along the tie-line reaching its lowest value at the receiving end bus, forcing the reactive power to flow towards the receiving end node. Since a reliable and high-quality power

supply is important during normal and emergency operating conditions, the TTC should be determined upon $N-1$ conditions [14].

Based on the system parameters in Table 2-3 and

Table 2-4, the $P-V$ curves at Bus-3 are plotted for normal and emergency operating conditions, using equation(2-18).

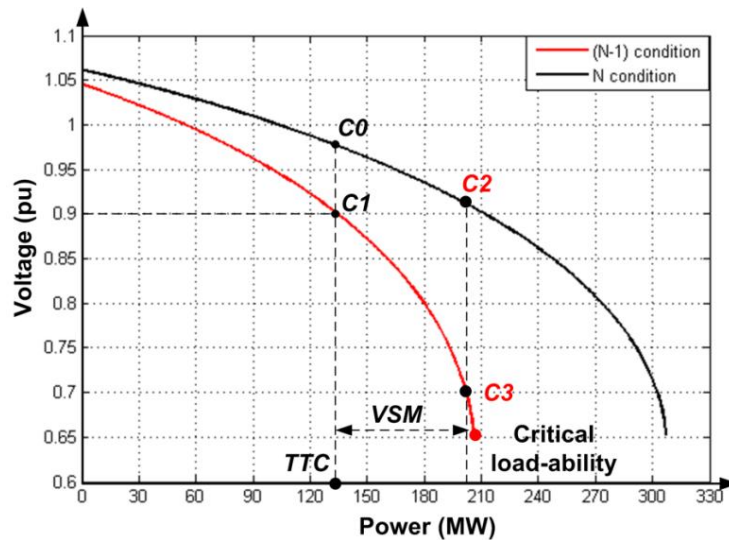


Figure 2-12: $P-V$ curves at Bus-3 for normal and emergency cases (week interconnection link)

Figure 2-12 illustrates that during a transition from normal to emergency operating conditions (from $C0$ to $C1$), the new operating point established along the $N-1$ $P-V$ curve may temporarily oscillate before settling at the new equilibrium point $C1$. The point $C0$ in Figure 2-12 represents the total transfer capability (135MW) of the tie-line that is determined to satisfy emergency voltage requirements ($V > 90\%$).

From a voltage stability point of view, during the transition from pre-fault to post-fault conditions, it is stable to transmit as high power as voltage stability limit of 192MW ($C3$). In contrast, working beyond $C2$ is critical as the voltage stability limit would be violated during the transition from N to $N-1$.

Further analysis for this particular case is performed using the commercial power system analysis tool (NEPLAN) to evaluate system behaviour at different load-ability levels represented by $C0$ and $C2$.

Figure 2-13 demonstrates load flow results for the post-fault operating condition where the operating point has changed from $C0$ to $C1$ as a result of system disturbance that puts line-3 in Figure 2-11 out-of-service. This case represents an

acceptable load-ability level at the receiving end (node-3) because the emergency voltage levels and instability limits are not violated during the post-fault condition. This result validates the TTC calculation in Figure 2-12 which is obtained analytically from the generic load flow equation(2-18).

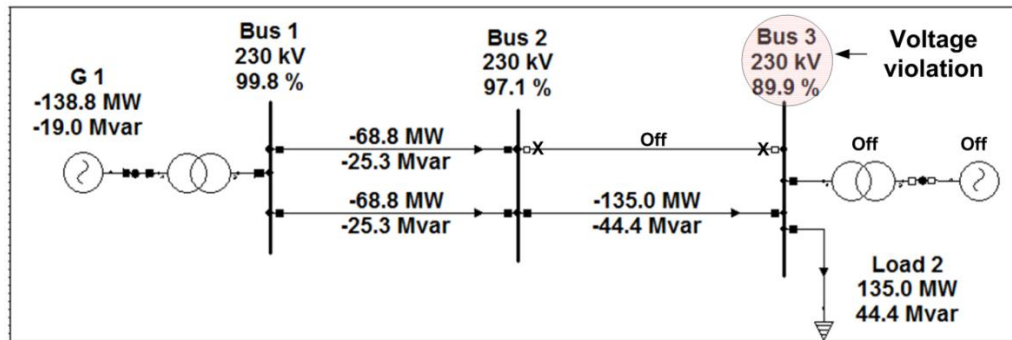


Figure 2-13: Load flow results at maximum loadability (weak interconnected power systems)

Time domain simulation is performed to evaluate system performance during system transition from $C0$ to $C1$, where line-3 is tripped due to a 200ms 3-phase short circuit fault at the middle of line-3. Figure 2-14 (a and b) depict the receiving end voltage at bus-3 and active and reactive power on line-4 which continues feeding the load after fault clearance. From Figure 2-14-(b), as expected for a radial configuration, active and reactive power flow towards the receiving end as the voltage drop is degraded from the sending end to receiving end. Therefore, tie-line load-ability improvement requires reactive power to be supported at the receiving end.

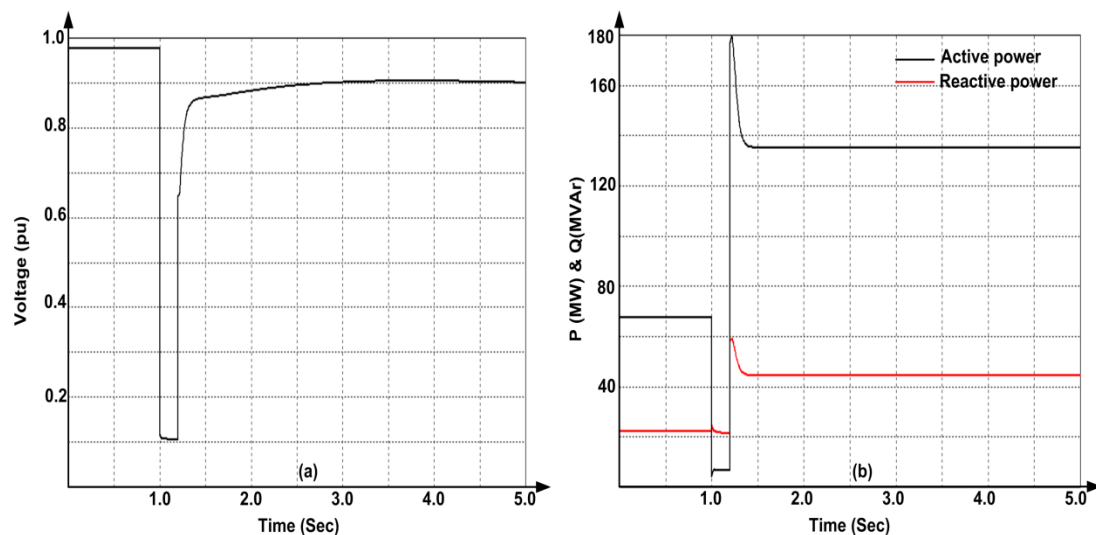


Figure 2-14 : Time domain simulation of 200ms fault at the middle of line-3 for $C0$ operating case (weak interconnected power systems)

2.5.2 TTC of a strong interconnection link

Since voltage is supposed to be maintained at the both ends of the strong interconnection, the reactive power is consequently forced to flow towards the lowest voltage sag, at the middle of the transmission corridor.

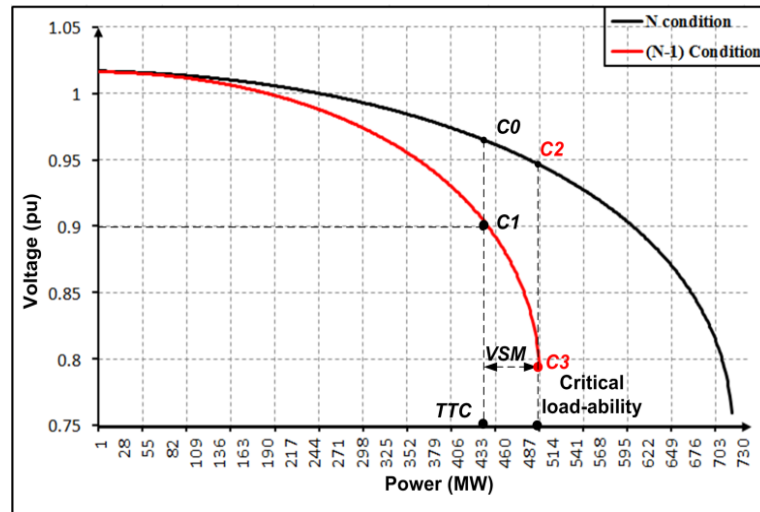


Figure 2-15: P - V curves at Bus-2 for normal and emergency cases (strong interconnection link)

Figure 2-15 depicts P - V curves at the middle of the tie-line (bus-2) for N and $N-1$ conditions plotted from equation (2-18) with the system parameters in Table 2-3 and Table 2-4. From the steady state point of view, the TTC for the system is considerably improved, from 135MW to about 440MW ($C0$), because of the reactive power support at the receiving end. However, the presence of considerable power generation at both sides may give rise to long electromechanical oscillations that can further fatigue the voltage, especially at the middle. For this reason, further steady state and dynamic numerical based analysis should be performed to determine the secure level of power transfer. Figure 2-16 shows power flow analysis results for the $C0$ load-ability condition which refers to the maximum acceptable load-ability in the case of two strong interconnected systems (point $C0$ in Figure 2-15).

Active and reactive power behaviour during the transient and post-fault operating conditions is evaluated with time domain simulation where a 200ms 3-phase short circuit fault at the middle of line-3 is simulated for $C0$ and $C2$ load-ability conditions (440MW and 490MW).

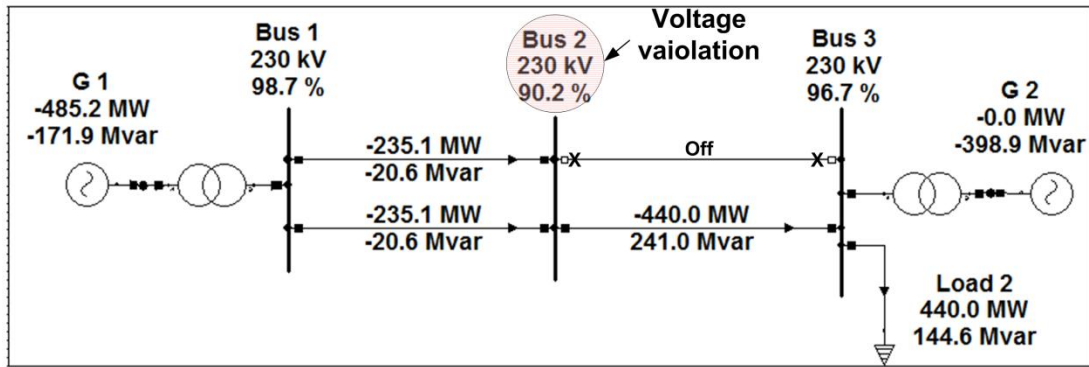


Figure 2-16: Load flow results at maximum load-ability (strong interconnected power systems)

Simulation results in Figure 2-17 confirm that the system is relatively stable with about 440MW of power transfer. From Figure 2-17-(a), the voltage at the middle is lower than that of the receiving end which forces reactive power to flow from the supported ends to the middle, as indicated in Figure 2-17-(b).

Time domain analysis shows that the system may not survive, with a C2 load-ability level of 490MW, when it is subjected to the same disturbance. In Figure 2-18, loss of synchronism occurs after fault clearance. Figure 2-18-(b) shows that significant reactive power flows towards the middle of the line where the voltage collapse is established due to acceding the VSL .

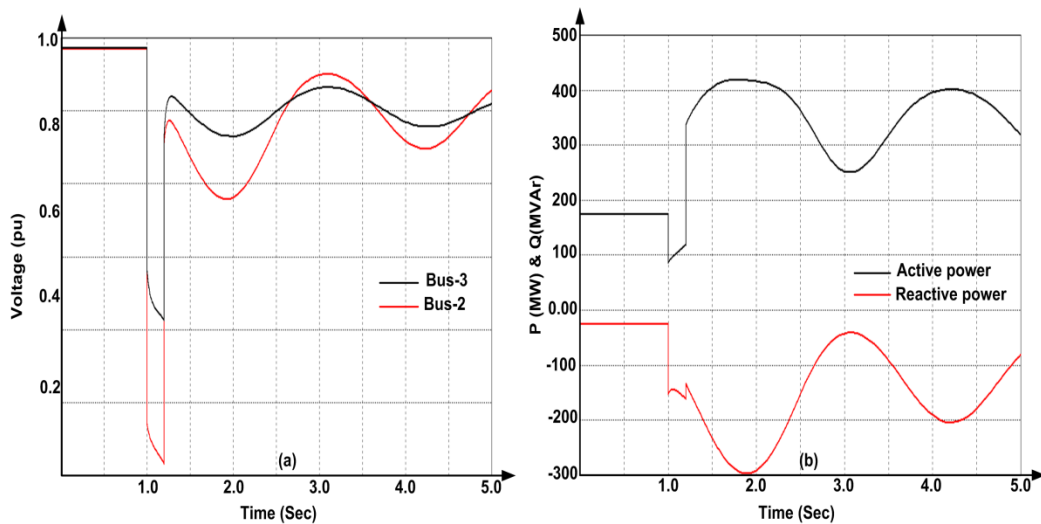


Figure 2-17: Time domain simulation of 200ms fault at the middle of line-3 during transmission of 440MW from Area 1 to Area 2

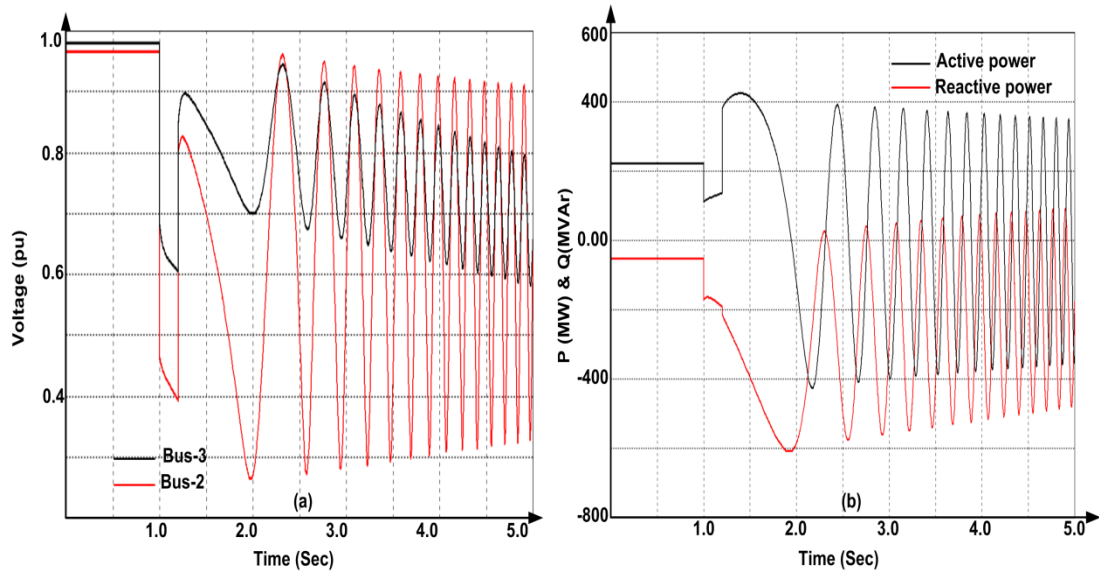


Figure 2-18: Time domain simulation of 200ms fault at the middle of line-3 during transmission of 490MW from Area 1 to Area 2

This discussion shows that total transfer capability of the tie-line improves with the presence of reactive power support at both sides of the interconnection link. As the middle of the line is the weakest link point, tie-line load-ability can be efficiently improved by midpoint reactive power support by the means of a FACTS device.

2.6 Summary

System impedance or system strength at a given node determines the voltage behaviour during pre and post-fault operation, and consequently, the power flow in an AC power system.

Lack of reactive power support is the main reason for limited power transfer in the interconnected power systems. Therefore, reactive power manipulation can be used to mitigate voltage instability problems, and to improve transmission load-ability of the tie-lines in the interconnected power systems. In weak interconnected power systems, the voltage drop is progressively degraded from the sending end to the receiving end. Therefore, improve tie-line performance requires reactive power measures at the receiving end. On the other hand, the midpoint of a tie-line in a strong interconnection link is the weakest point in the link, and it represents the optimal place for reactive power support.

The proposed analytical equation (2-18) allows accurate plotting of a $P-V$ curve and facilitates calculation of voltage stability limit (VSL), angular stability limit (ASL), total transfer capability (TCC), and voltage stability margin. Hence, this equation

will be used in subsequent chapters to facilitate system analysis with FACTS and HVDC technologies.

References

- [1] P. Kundur, *Power system stability and control*: Tata McGraw-Hill Education, 1994.
- [2] X.-P. Zhang, *et al.*, *Flexible AC transmission systems: modelling and control*: Springer Science & Business Media, 2012.
- [3] N. A. E. R. Council, "Available Transfer Capability Definitions and Determination," ed, 1996.
- [4] V. Ajjarapu, *Computational techniques for voltage stability assessment and control*: Springer, 2007.
- [5] A. B. Morton, "A Guide to 'Steady-State' Voltage Stability Analysis," November 2007 ed: Senergy/Econnect, 2007, pp. 1-23.
- [6] P. Kundur, *et al.*, "Definition and classification of power system stability IEEE/CIGRE joint task force on stability terms and definitions," *Power Systems, IEEE Transactions on*, vol. 19, pp. 1387-1401, 2004.
- [7] J. J. Grainger and W. D. Stevenson, *Power system analysis* vol. 621: McGraw-Hill New York, 1994.
- [8] T. Van Cutsem and C. Vournas, *Voltage stability of electric power systems* vol. 441: Springer, 1998.
- [9] B. Gao and P. Kundur, "Voltage Stability Evaluation Using Modal Analysis," *Power Engineering Review, IEEE*, vol. 12, p. 41, 1992.
- [10] J. B. M. Begovic, T. Domin, S. Easterday-McPadden, A. Girgis, W., *et al.*, "Voltage Collapse Mitigation," IEEE Power System Relaying Committee 1996.
- [11] "Proposed Terms & Definitions for Power System Stability," *Power Apparatus and Systems, IEEE Transactions on*, vol. PAS-101, pp. 1894-1898, 1982.
- [12] F. Alvarado and S. Oren, "Transmission system operation and interconnection," *National transmission grid study–Issue papers*, 2002.
- [13] M. Klein, *et al.*, "A fundamental study of inter-area oscillations in power systems," *Power Systems, IEEE Transactions on*, vol. 6, pp. 914-921, 1991.
- [14] P. W. Sauer, "Technical challenges of computing available transfer capability (ATC) in electric power systems," in *System Sciences, 1997, Proceedings of the Thirtieth Hawaii International Conference on*, 1997, pp. 589-593.

Chapter three

Shunt connected FACTS devices

3.1 Introduction

It was established in Chapter 2 that lack of reactive power support is the primary reason for the under-utilization and poor efficiency of many AC transmission systems. Shunt reactive compensation is effective in improving AC transmission systems utilization and efficiency as it provides the reactive power consumption of the line's passive components (inductors and stray capacitors); thus, maintains the system nodal voltage profiles within tolerable limits, increases steady-state load ability of transmission lines, and improves system stability [1-3].

Shunt connected static reactive power generators can be classified based on their physical components and operation theory, into two types [3-5]:

- Variable impedance VAR compensators
- Converter based VAR compensators.

Both types exhibit similar characteristics in the linear operating region when nodal voltages are close to the nominal voltage. But each type has its own $V-I$ characteristics during operation in the nonlinear region when the nodal voltages have drifted significantly from the nominal voltage. In the nonlinear region, the output reactive power from impedance type VAR generators deteriorates rapidly with voltage (due to increased dependency of their reactive power output on the terminal voltage). In contrast, the reactive power output of converter based VAR generators deteriorates slowly with voltage and linearly until their current controllers saturate, injecting constant reactive current into the affected ac bus. Therefore, the mathematical inclusion of these factors when modeling impedance and converter based FACTS devices in power flow equations is essential for accurate and realistic results. Therefore, the generic power flow equation 2-18, which was introduced in Chapter 2, is modified in this chapter to account for these considerations and their linear and nonlinear regions, for both FACTS device types.

There are a number of optimization methods presented in the literature for allocation and sizing of FACTS devices. Allocation and sizing of FACTS are formulated as

critical components of reactive power planning (RPP) as their effectiveness greatly depends on location and size of these devices [6-8]. These methods vary in complexity depending on the number of objective functions and constraints to be satisfied and the detail of mathematical models employed. A review of some of these optimization techniques can be found in [7-9].

Heuristic optimization algorithms are used to find the optimal solution for predefined objective functions. Practical swarm optimization (PSO) [10-12], genetic algorithm (GA) [13-15] and harmony search algorithm (HSA) [16, 17] are the most used heuristic algorithms for FACTS allocating [7, 9]. Other types of approaches use analytical optimization techniques such as Power flow Jacobian matrix [18, 19] and line flow index (LFI) [20, 21] for allocating and sizing of FACTS. Since the emergence of voltage instability and its associated load-ability problems, additional voltage security constraints have been added to FACTS allocation and sizing optimization problems. As an example, security and voltage stability constraints have been added to the conventional optimal power flow (OPF) to form what are called, security constrained OPF model (SCOPF) and SCOPF with voltage stability constraints model (SCOPF-VS) [8].

This chapter proposes new methods for the allocation and sizing of shunt FACTS devices that aim to maximize tie-line load-ability. The proposed methods introduce total voltage change index (*TVCI*) for a FACTS device allocation and take into account the risk of higher *PoC* when sizing a shunt FACTS device. Applications of these methods for typical and large power systems will be tested in subsequent chapters, considering the Libyan National Transmission System.

3.2 Variable impedance shunt FACTS devices

Capacitor and reactor banks represent two passive sources of reactive power which are commonly integrated with thyristor valves to realize variable impedance VAR generators, with controllable reactive power output. Manipulation of the on and off times of the thyristors that connect shunt admittance (inductance or capacitance) to the ac bus are used to realize fast and smooth variation of reactive power, from maximum capacitive to maximum inductive; hence, voltage control.

The thyristor-controlled reactor TCR and the thyristor-switched capacitor TSC are the major building blocks of variable impedance shunt FACTS devices. Steady state

and dynamic performance of variable impedance shunt FACTS is determined by the voltage and current (V - I) characteristics of TCR and TSC. The static VAR compensator, SVC, is a widely used variable impedance shunt FACTS device due to its flexibility, dynamic response and often cost-effective compared with other technologies [3, 13].

3.2.1 Thyristor controlled reactor (TCR)

Current in each phase of the thyristor controlled reactor (TCR) $I_{l(\alpha)}$ can be regulated by varying the thyristor on and off times or duty cycles, which is achieved by adjustment of the firing angle α relative to the current zero or peak of the applied phase voltage, as shown in Figure 3-1.

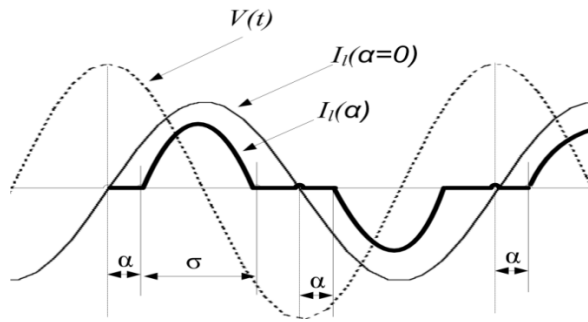


Figure 3-1: TCR voltage and current operating waves for firing delay angle α

When the firing delay angle is zero ($\alpha=0$) TCR bidirectional thyristor is turned on at the peak of the applied voltage ($v(t)$) and the same steady state current will flow in the reactor as represented by the curve $I_l(\alpha=0)$. When a firing angle delay is applied to the gating of the valve, the current flow in the reactor is represented by the bold curve in Figure 3-1. The amplitude of the fundamental reactor current $i_l(\alpha)$ as a function the firing delay angle is given by;

$$I_L(\alpha) = \frac{V_L}{\omega L} \left(1 - \frac{2}{\pi} \alpha - \frac{2}{\pi} \sin 2\alpha \right) \quad (3-1)$$

where V_L is the amplitude of the applied voltage with angular frequency ω . This equation is used to plot TCR current versus firing delay angle α , shown in Figure 3-2. The figure shows that the current $I_l(\alpha)$ can be controlled at a maximum of $V_L/\omega L$ when the thyristor is turned on at firing angle $\alpha=0$, and at zero when it is turned off at $\alpha=1/2\pi$, where α is measured from the zero crossing of the phase current or peak of

the applied voltage. This means that the TCR behaves as a variable inductor, where admittance changes with the firing angle according to:

$$B(\alpha) = \frac{1}{\omega L} \left[1 - \frac{2}{\pi} \alpha - \frac{2}{\pi} \sin 2\alpha \right] \quad (3-2)$$

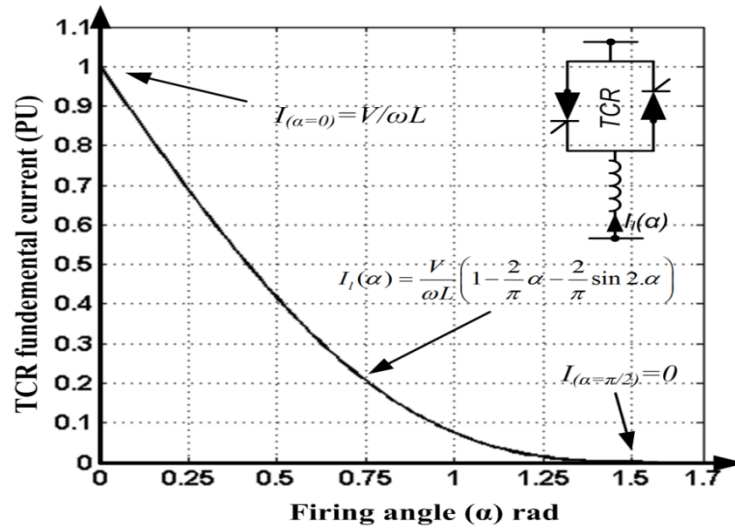


Figure 3-2: Change of TCR current with the firing angle α

Equation (3-2) indicates the relationship between effective admittance $B(\alpha)$ of the TCR and firing delay angle α . Fundamental reactive current is determined based on the effective admittance $B(\alpha)$ and the magnitude of the applied AC voltage V_L as $I_L = B_L(\alpha) \cdot V_L$.

The reactive power absorbed by the TCR at firing delay angle α is expressed by:

$$Q_{TCR}(\alpha) = \frac{V_L^2}{\omega L} \left[1 - \frac{2}{\pi} \alpha - \frac{2}{\pi} \sin 2\alpha \right] \quad (3-3)$$

This discussion reveals that the reactive power rating of the TCR is determined by the maximum current ratings of the thyristor valve and the reactor which defines, along with the AC applied voltage, the TCR V - I characteristics shown in Figure 3-3.

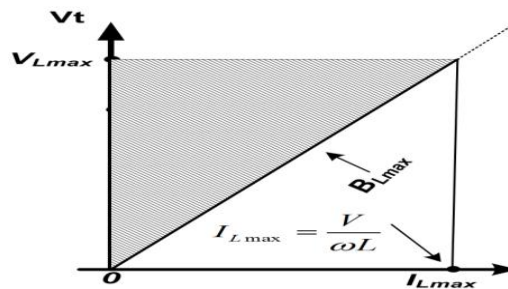


Figure 3-3: TCR V - I characteristics

3.2.2 Thyristor-switched capacitor (TSC)

Figure 3-4 shows the structure of the thyristor-switched capacitor that includes a capacitor, bidirectional thyristor valves, and a small current limiting reactor L [4].

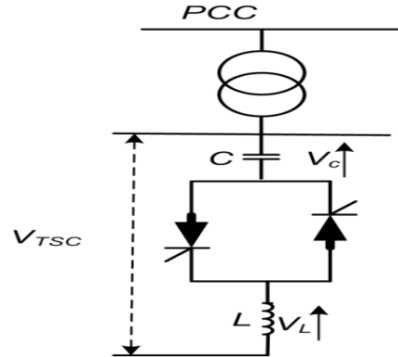


Figure 3-4: Thyristor switched capacitor topology

When a steady state sinusoidal voltage $v(t) = V_m \sin(\omega t)$ is applied to one phase of the TSC in Figure 3-4, current flow and the voltage amplitude V_C across the capacitor are given by (3-4) and (3-5):

$$i(\omega t) = V_m \omega C \cdot \left(\frac{n^2}{n^2 - 1} \right) \cos \omega t \quad \text{where } n = \sqrt{\frac{X_C}{X_L}} \quad (3-4)$$

$$V_C = V_m \frac{n^2}{n^2 - 1} \quad (3-5)$$

The TSC capacitor banks are disconnected at current zeros. The disconnected capacitors stay charged at their corresponding voltages pre-disconnection, say V_C , and, as a result, the voltage across the non-conducting thyristor valve varies between zero and the peak-to-peak of the applied voltage.

When the voltage across each capacitor bank remains unchanged, the TSC capacitor bank can be switched in again at the appropriate peak of the applied ac voltage without any significant transient. However, practically the TSC capacitor is normally discharged after disconnection, and consequently, the connection of the capacitor bank has to be executed at any residual capacitor voltage between zero and V_C . For this reason, switch-in of the capacitor bank should be when the peak of the applied voltage is close to V_C , and in this manner, transient free switching can be achieved.

In order to minimize any transient switching disturbance, the switching conditions of the TSC has to be according to the following guidelines:

- 1- If the peak of the applied voltage V_m is greater than the residual capacitor voltage V_C ($V_m > V_C$), the switching should take place at the instance when the instantaneous ac voltage $v(t)$ applied to the TSC equal the capacitor voltage V_C , as shown in Figure 3-5a.
- 2- When the residual capacitor voltage is equal to or greater than the peak of the applied ac voltage ($V_m \leq V_C$), the proper switching instant should be at the peak of the ac voltage as shown in Figure 3-5b.

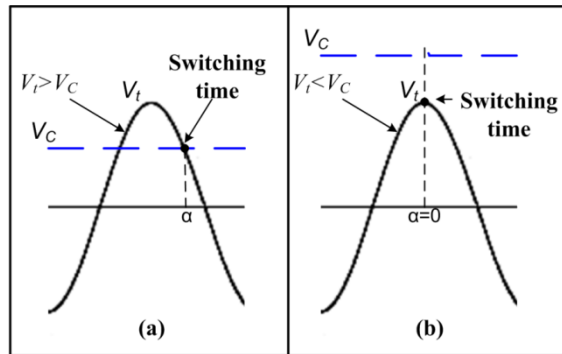


Figure 3-5: Transient free switching conditions for the TSC

From these TSC switching guidelines, the maximum possible switching delay for the capacitor bank is a full cycle (the interval from one peak to the next peak) of the applied AC voltage. Therefore, the capacitor bank has to be switched at a specific instant in each cycle, at $\alpha=0$, which means that TSC firing delay angle control is not applicable. Therefore, TSC switching is a step-like change in the reactive admittance. In a typical SVC, the TSC step-like change is smoothed by the proper lagging reactive power provided by TCR firing angle control.

3.2.3 Inclusion of variable impedance shunt FACTS in Power flow equation

The reactive power of a TSC and TCR is determined by their $V-I$ characteristics, which are classified as constant impedance passive loads with voltage dependent characteristics. Therefore, the inclusion of this type of FACTS in power flow calculations should be on the basis of the generic power flow equation 2-18 derived in Chapter 2, which accounts for the effects of shunt components with constant impedance.

i. **Linear operation of variable impedance shunt FACTS**

Variable impedance shunt FACTS device changes its susceptance B according to equation (3-6), to provide the reactive current I_q required to regulate the voltage in response to system loading change.

$$I_q = \frac{B \cdot V_{ref}}{\sqrt{3}} \quad (3-6)$$

Therefore, the generic power flow equation 2-18 is extended to include the $V-I$ characteristic of variable impedance shunt FACTS during linear operation. Thus, the amount of reactive power Q_{ref} required to maintain the voltage of a receiving end at a predefined voltage value V_{ref} at any loading level P can be extracted from the generic power flow equation as:

$$Q_{ref} = \frac{\zeta - F_C \cdot V_{ref}^2 \cdot x - \left(\frac{\sqrt{1 - pf^2 P \cdot z^2}}{pf} \right)}{V_{ref}^2 \cdot z^2} \quad (3-7)$$

where $z = \sqrt{r^2 + x^2}$ and $\zeta = \sqrt{-F_C^2 r^2 V_{ref}^4 - 2 z (P \cdot r - 1/2) V_{ref}^2 F_C - P^2 z^4}$

Notice that the term $(P \cdot r - 1/2)$ is usually less than zero, as r is very small (R/VB^2) .

ii. **Non-linear operation of variable impedance shunt FACTS**

When the voltage exceeds linear operation of the variable impedance VAR generator during stressed operating conditions, the VAR generator (TSC or TCR) behaves as a fixed capacitor or inductor bank with maximum susceptance (B_{cmax} or B_{lmax}). In this saturated operating condition, the $V-I$ characteristics of the variable impedance VAR generator forces the reactive power output (Q_{satu}) to change with voltage square, based on equation(3-8).

$$Q_{satu} = B_{max} \cdot V^2 \quad (3-8)$$

Figure 3-6 depicts the load-ability versus voltage $P-V$ curve at a given node during linear and nonlinear operation of a variable impedance shunt FACTS device. The voltage is kept at V_{ref} up to maximum capacitive rating Q_{Cmax} ; beyond this point, the node voltage declines as the loading increases.

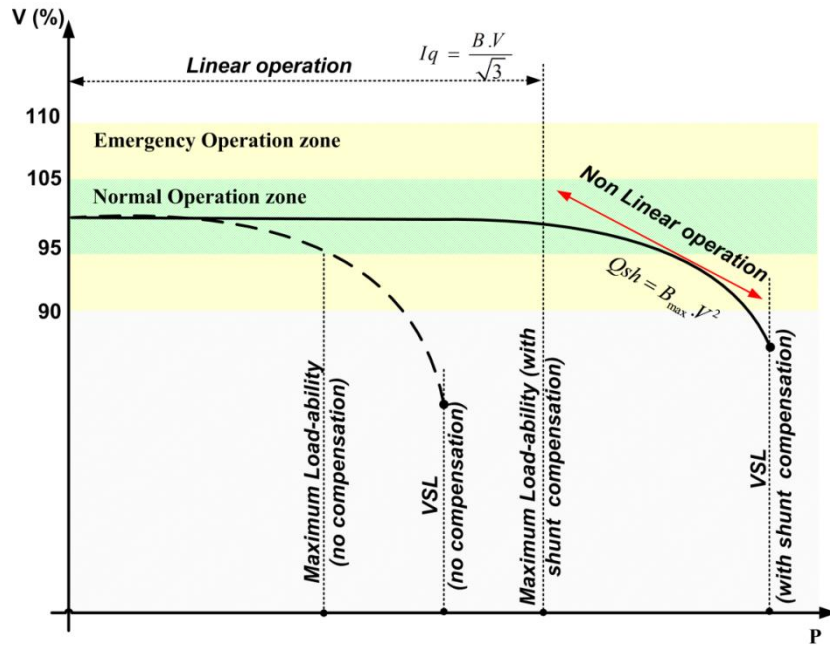


Figure 3-6: Effect of variable impedance shunt connected FACTS on system load-ability

3.2.4 Static VAR Compensators (SVC)

A static VAR compensator (SVC) is a variable impedance shunt FACTS device and is widely used for autonomous voltage control [4]. The SVC is shown in Figure 3-7 typically includes several TSCs and one TCR. The TSC allows fast switching in of the capacitor banks, which gives coarse step control of reactive power generation. The TCR allows smooth reactive power variation. The combination of the TSC and TSR allows fine variation of both leading and lagging reactive power [22].

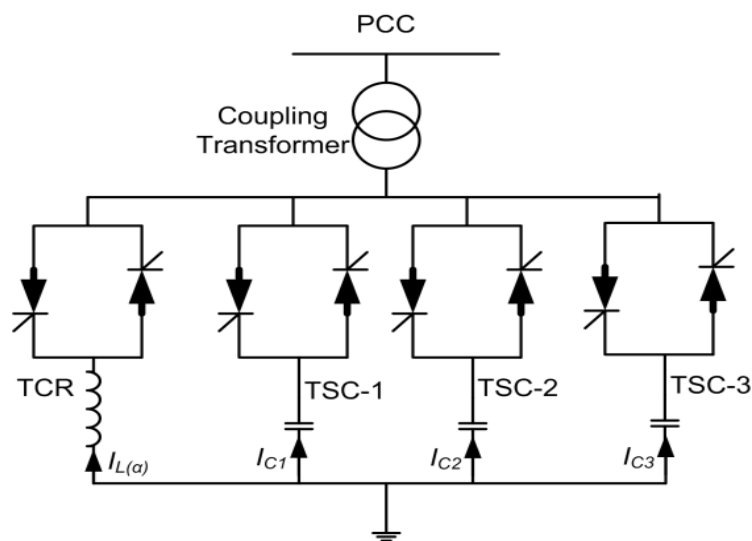


Figure 3-7: Static VAR Compensation (SVC) topology

i. **Operation principles**

The total capacitive rating of the SVC (Q_{Cmax}) is determined by the number of parallel connected TSCs, n , with a reactive power rating of each TSC being Q_{Cmax}/n . When the capacitive reactive power required (Q_{ref}) to support node voltage is less than the rating of a single TSC, one TSC will be switched on, and TCR will be controlled to absorb the surplus reactive power generated by the TSC $[(Q_{Cmax}/n) - Q_{ref}]$; allowing the SVC to source Q_{ref} .

When the capacitive reactive power required (Q_{ref}) is greater than the rating of a single TSC, an additional TSC is switched on, increasing the capacitive output; and in this manner, the SVC capacitive reactive power is increased to Q_{Cmax} , with sequential switching in the TSC until all available TSCs are switched on.

For inductive reactive power, only TCR is switched on, with all TSCs remain off.

The $V-I$ operating area of the SVC is formed from a combination of TCR and TSCs as shown in Figure 3-8.

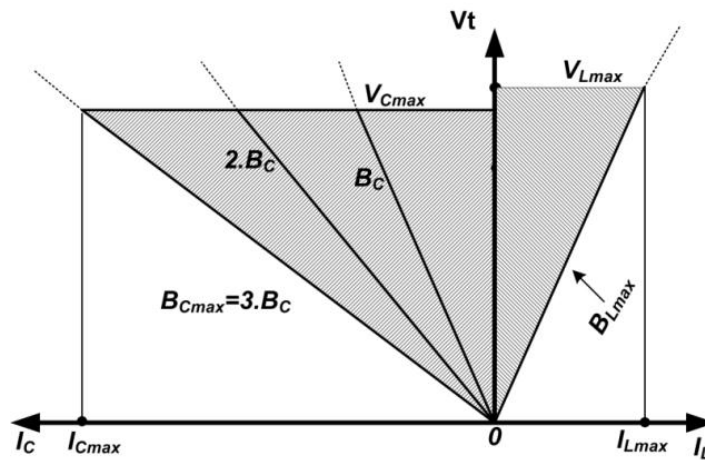


Figure 3-8: $V-I$ operating characteristic of SVC with three TSCs and TCR

As the capacitor banks are switched in and out within one full cycle in a step-like change, the TCR theoretically should have the same or slightly greater rating of a TSC (Q_{Cmax}/n) in order to absorb smoothly surplus reactive power output caused by the step-like change of a TSC. However, there is still a transient since the TCR cannot react instantaneously to the reactive step change of the TSC.

ii. SVC control principles

Reactive power control of the SVC requires coordinated operation of both TSCs and TCR. The basic control scheme of the SVC is shown in Figure 3-9, where reactive power output control is performed by three major functions:

- 1- Determination of the required number of TSC branches from the reference reactive power reference (Q_{ref}). The number of required capacitor branches N is the next higher integer that results from the division of the desired reactive power Q_{ref} by the capacitive reactive power of a single switched capacitor bank. Accordingly, the required inductive reactance from the TCR (Q_{TCR}) is calculated as the difference between the sum of switched on TSCs capacitive reactance and the desired reactive power reference (Q_{ref}) as follows:

$$Q_{TCR} = Q_{ref} - \sum_{j=0}^N Q_{TSCj} \quad (3-9)$$

- 2- Switching control of the TSCs is performed through a logic circuit which controls switching of the TSCs in and out in a transient free manner as described in 3.2.2 (see Figure 3-5).
- 3- The inductive reactive power needed to make the SVC output continuous in order to avoid over-voltages due to reactive power mismatch as described in equation (3-9) is translated into lagging reactive current $I_{l(\alpha)}$ which is controlled by manipulation of firing delay angle α .

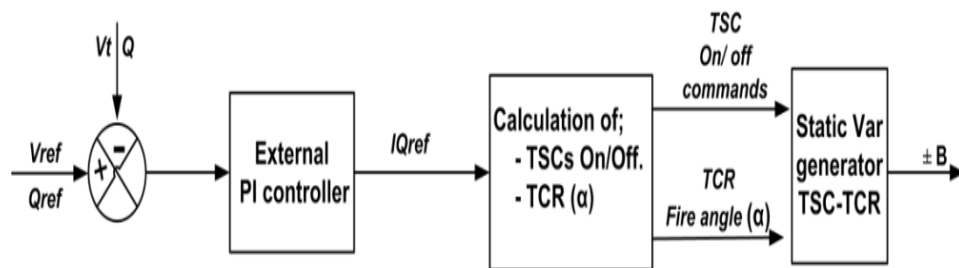


Figure 3-9: VSC basic control scheme

3.2.5 Dynamic response of the SVC

Time domain simulation is used to investigate the system response during switching of the TSCs banks of the SVC. Static VAR compensator with a rating of (-180, +63 MVAR) is installed at the receiving end (Bus-3) in Figure 3-10. Technical data and

the generators controllers of the test system are in Appendix C. based on the switching rules discussed in section 3.2.2, and to illustrate the smoothing effect of the TCR. In this simulation, the voltage reference of the synchronous machine G_1 is stepped down by 5% at $t=0.5s$ before it is brought back to its normal value after 1 second at $t=1.5s$.

Figure 3-11c indicates that the first TSC-1 is switched on at $t=1.1s$ in an attempt to maintain the voltage at the PCC (bus-3). This figure also shows that TSC-1 is switched off (to initial condition) at $t=1.653s$ in response to the system voltage change in Figure 3-11a. The leading reactive phase current i_a that flows in TSC-1 during its switching on is shown in Figure 3-11d. The initial reactive power output of the SVC in Figure 3-11b indicates that the SVC is in an inductive mode as the TCR consumes about 25 MVar to maintain the voltage at 1pu. The importance of the TCR is reflected in the smoothed accommodation of the step-like change caused by the switching of TSC-1 in Figure 3-11b.

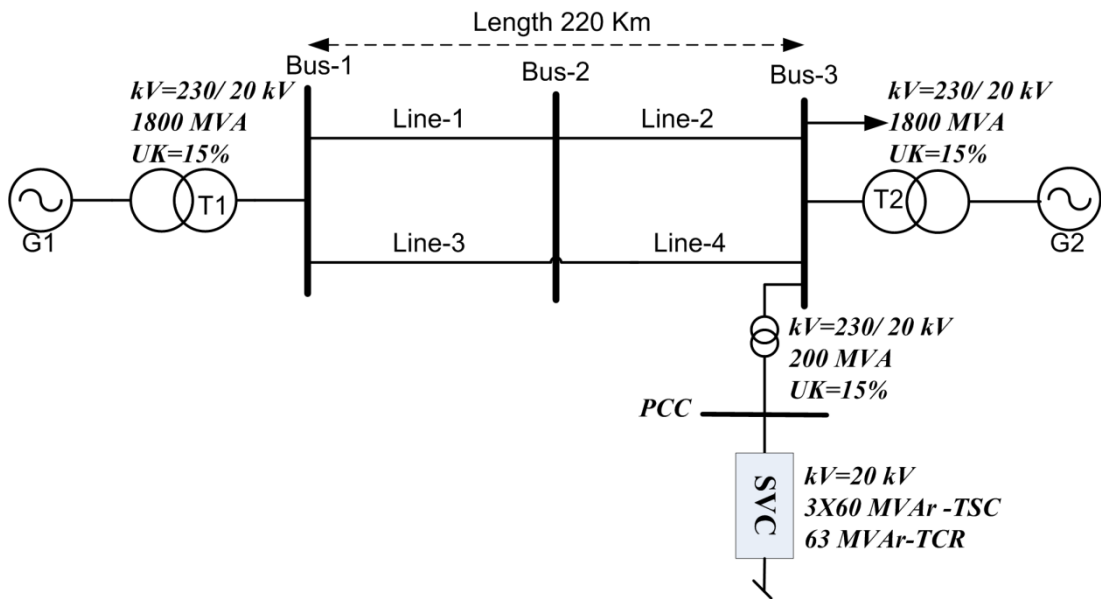


Figure 3-10: Kundur two areas test system with (-180, +63 MVar) SVC

Figure 3-12 demonstrates that switching timing of TSC-1 is in accordance with the transient free switching rules discussed in section 3.2.2. In Figure 3-12a, the switching-on of TSC-1 coincides with the zero crossing of the voltage v_a . In contrast, TSC-1 is switched off at the peak of the voltage phase v_a as indicated in Figure 3-12b.

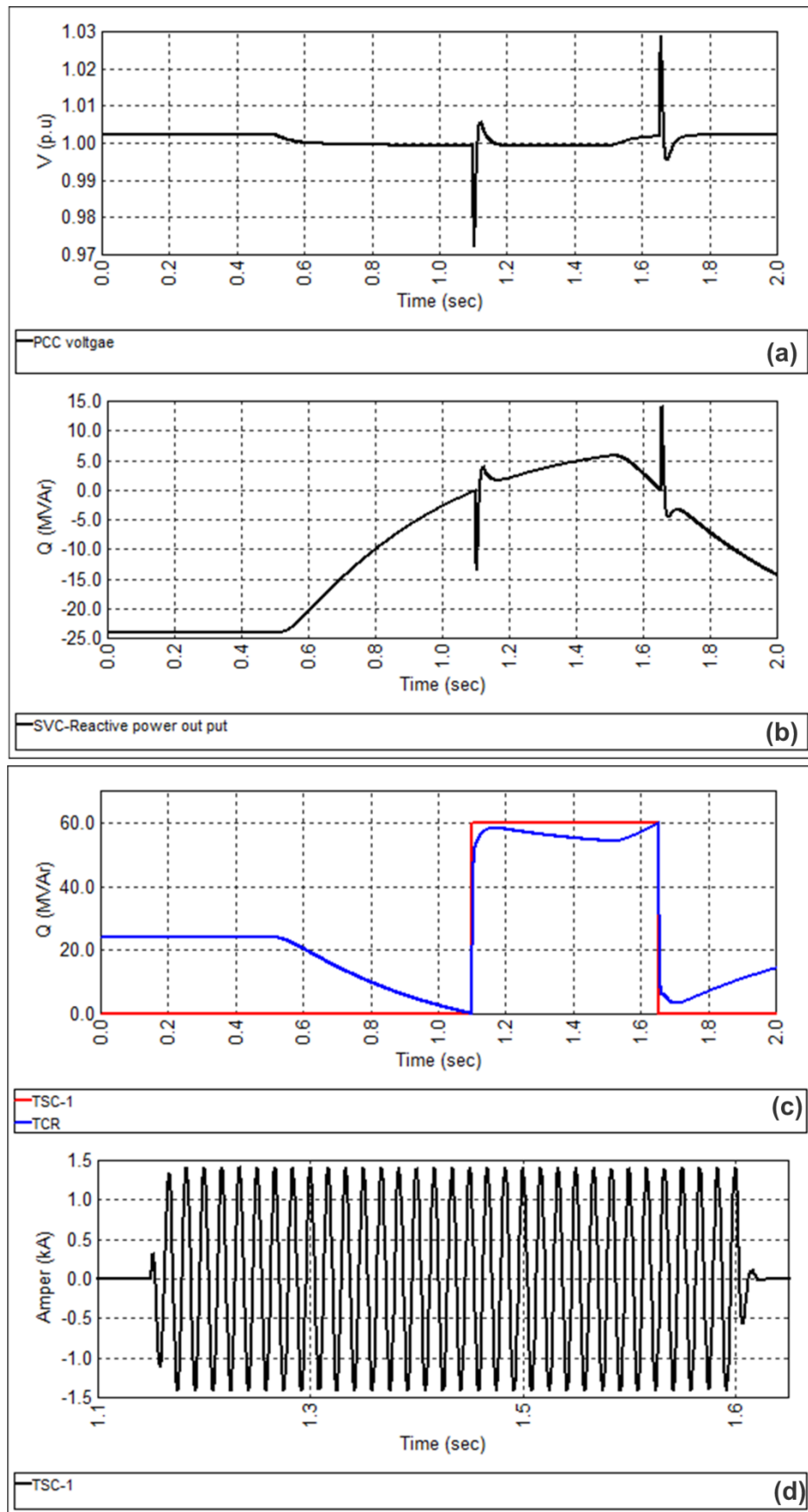


Figure 3-11: Response of the SVC for the change in the system voltage

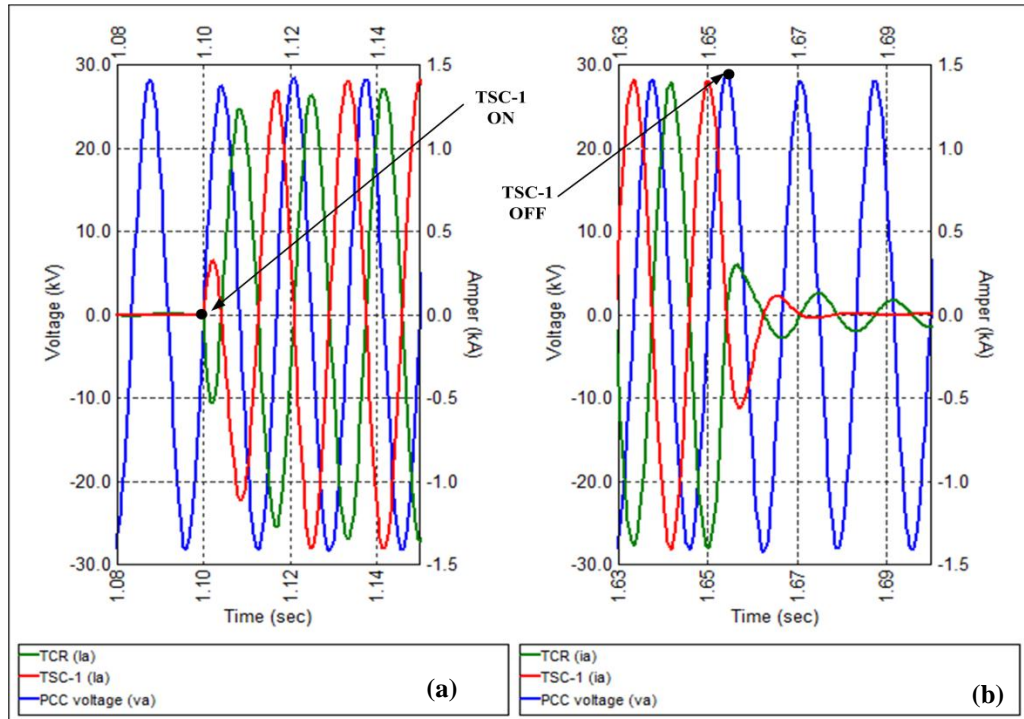


Figure 3-12: Switching on/off instants of TSC-1

3.3 Converter based shunt FACTS (STATCOM)

Unlike variable impedance VAR compensators that require passive elements such as capacitor and inductor banks to control their reactive power output, a converter based VAR compensator employs voltage or current source converters to provide a controllable reactive power. This type of VAR generator is able to provide controllable reactive power by manipulating the phase and magnitude of the converter ac voltage and current relative to grid voltage at the PCC [4]. A shunt converter based VAR generator is termed a static synchronous compensator (STATCOM). From a power system point of view, it is similar to the rotating synchronous condenser that provides a controllable reactive power by the means of their excitation system [5]. Examples of converters frequently used in this type of VAR generator are; single phase H-bridges, single phase full bridge, three-phase two-level six-pulse bridge, and three-phase three-level 12-pulse-bridge, all shown in Figure 3-13, and their extensions in multilevel converter structures. These converter types employ a number of series conducting devices such as an insulated gate bipolar transistor (IGBT), gate turn on (GTO) thyristor, and integrated gate commutated thyristor (IGCT) with anti-parallel diodes [4, 23].

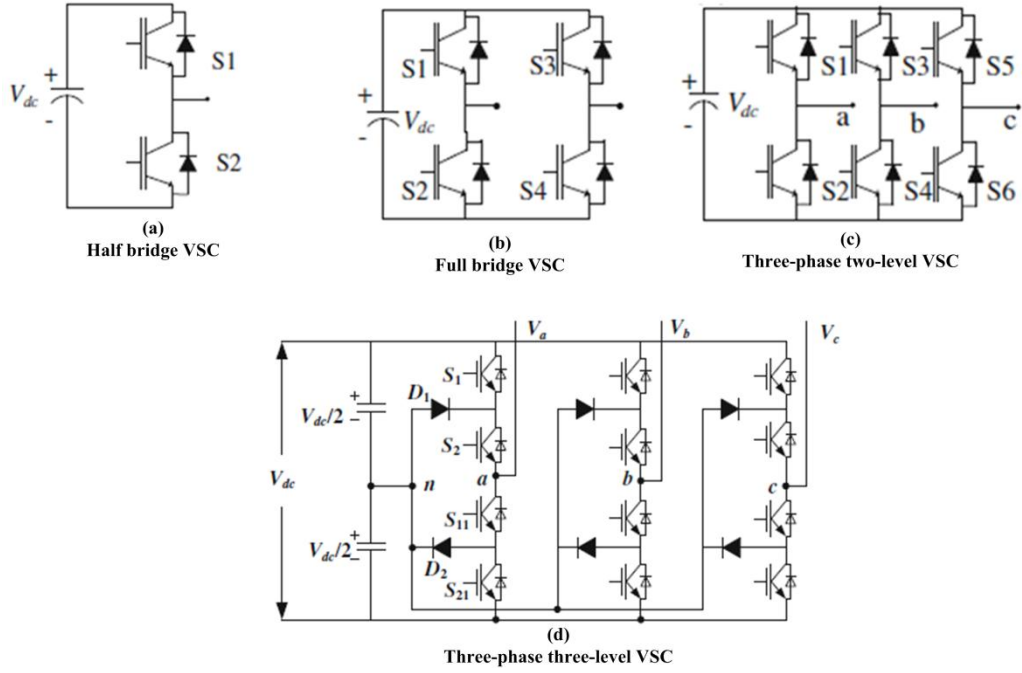


Figure 3-13: Commonly used voltage source converter structures in converter based VAR generators[23]

3.3.1 Inclusion of converter based FACTS characteristics in Power flow equation

A number of approaches have been introduced to model the converter based FACTS devices. Different methods have been put in place to model single and multi-converter FACTS devices in power flow analysis considering inclusion of the internal and external power flow constraints in the Newton-Raphson power flow [3]. As with the variable impedance shunt FACTS in section 3.2.3, converter based shunt FACTS should be included in the Power flow equation (2-18), as a reactive power source with constant current characteristic.

i. Linear operation of converter based shunt FACTS

During linear operation, converter based FACTS can be represented as a controllable output reactive power source that controls its reactive power output:

$$Q_{STAT} = \sqrt{3} V_{ref} I_q \quad (3-10)$$

The linear operation characteristic of the converter based shunt FACTS in equation (3-10) can be included into the generic power flow equation (2-18). Hence, the amount of reactive current I_{ref} required to maintain the voltage at a predefined value V_{ref} (pu) at any loading level P is given by:

$$I_{ref} = \frac{1}{3} \frac{\eta - \sqrt{3} \left(P \cdot z \cdot \sqrt{1 - pf^2} + V_{ref}^2 \cdot x \cdot F_C \cdot pf \right)}{V_{ref} \cdot pf \cdot z \cdot VB} \quad (3-11)$$

where $\eta = pf \cdot \sqrt{-3F_C^2 r^2 V_{ref}^4 - 6V_{ref}^2 \cdot z \cdot F_C (P \cdot r - 1/2) - 3P^2 \cdot z^2}$

Hence the desired reactive power to maintain the voltage V_{ref} at any loading condition can be calculated from equations (3-10) and(3-11):

$$Q_{ref} = \frac{1}{\sqrt{3}} \frac{\eta - \sqrt{3} \cdot \left(P \cdot z \cdot \sqrt{1 - pf^2} + V_{ref}^2 \cdot x \cdot F_C \cdot pf \right)}{pf \cdot z} \quad (3-12)$$

ii. Non-linear operation of converter based shunt FACTS

During current saturation (nonlinear operation), the $V-I$ characteristics of the converter based shunt FACTS determine the reactive power output of FACTS devices. As the current is maintained at its maximum current output I_{qmax} , the reactive power is changed linearly with the applied AC voltage. The output current of the converter-based FACTS is maintained at its maximum reactive current I_{qmax} regardless the voltage level (as less as 0.2 pu is required to feed converter losses) as illustrated in Figure 3-14 [4].

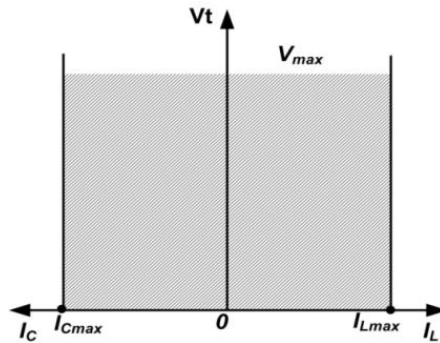


Figure 3-14: $V-I$ characteristic of STATCOM

The reactive power output during nonlinear operation is

$$Q_{STAT} = \sqrt{3} V I_{qmax} \quad (3-13)$$

As the reactive current output reaches its maximum (I_{qmax}), the voltage begins to decline with increasing load demand. The generic power flow equation that includes converter based shunt FACTS characteristics during saturated operating conditions is given by equation(3-14).

$$V_{(p,u)} = \sqrt{\frac{1 + \gamma - 2r.P - 2x(\sigma.P + \sqrt{3}I_{qmax}.v.VB)}{2F_C}} \quad (3-14)$$

where $\sigma = \frac{\sqrt{1-pf^2}}{pf}$ and $\gamma = \sqrt{1+x.P - 4(r.P + x - r(P.\sigma + \sqrt{3}.I_{qmax}.v.VB))^2}$

3.3.2 STATCOM operating principles

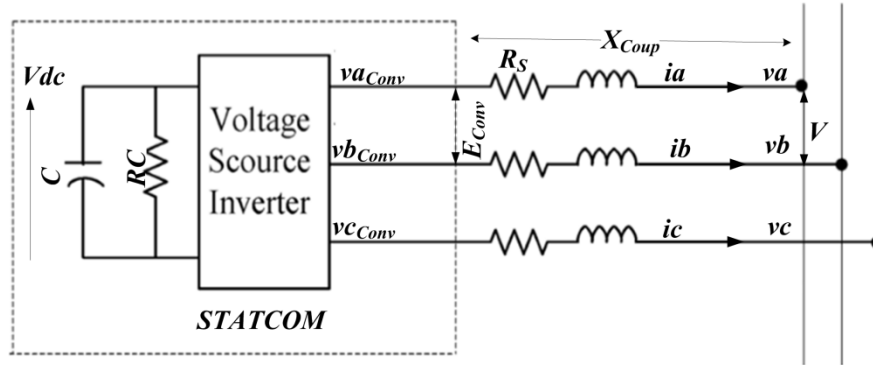


Figure 3-15: Static Synchronous Compensation (STATCOM) topology

The schematic diagram of an STATCOM is shown in Figure 3-15. The inverter conduction losses and the coupling transformer resistance losses are represented by resistance R_s in the ac side. The losses on the DC side (R_c) are the sum of the converter switching losses and the DC capacitor power losses.

STATCOM reactive current, as a function of line to line RMS voltages on both sides of the coupling transformer (V and E_{Conv}), in the Figure 3-15 is governed by:

$$I_{Stat} = \frac{V - E_{Conv}}{X_{Coup}} \quad (3-15)$$

where E_{Conv} and V are the ac voltage amplitudes at the converter terminal and network side of the coupling transformer, and X_{Coup} is the total circuit reactance, which includes coupling transformer leakage inductance. The difference between the converter and the system voltage amplitudes determine the amount and direction of reactive power exchange between the STATCOM and the system:

$$Q_{Stat} = \frac{V^2}{X_{Coup}} \left[1 - \frac{E_{Conv}}{V} \right] \quad (3-16)$$

The three-phase ac voltage at the converter side is generated by the dc-ac converter. The charged capacitor of the STATCOM provides a sustained DC voltage which is

converted by the means of pulse-width modulation, PWM, to a set of controllable three-phase output voltages synchronized and coupled to the ac voltage through the coupling transformer leakage inductance.

The idea of the producing voltage at the STATCOM ac terminal can be explained by the fact that the net instantaneous powers at both terminals (AC and DC) of the STATCOM are the same (neglecting the losses). Although the DC capacitor in the STATCOM is important to sustain the DC voltage, it does not play any role in the active or reactive power exchange between the STATCOM and the ac system. This can be justified from two points of view:

- 1- The active power from the DC capacitor is zero because the net instantaneous power at both terminals (AC and DC) of the STATCOM is the same and is assumed to be zero (neglecting the losses).
- 2- Zero frequency in the DC part prevents reactive power generation from the DC capacitor.

Therefore, the controllable ac three-phase voltage E_{conv} is established from the circulating current flow between the phases with zero instantaneous active power exchange with the system[24].

3.3.3 Basic Control of the STATCOM

Since the STATCOM does not exchange active power with the AC system, apart from very little to keep the DC capacitor charged, DC source in the STATCOM can be replaced by passive sources such as a capacitor in the voltage source based STATCOM and the inductor in the current source STATCOM. In the STATCOM, the voltage across the dc capacitor must be maintained constant; and the peak ac voltage at the STATCOM terminals ($E_{m_{conv}}$) can be expressed as a function of modulation index M by:

$$E_{m_{conv}} = \frac{1}{2} M V_{dc} \quad (3-17)$$

Being able to control the magnitude of E_{conv} in equation(3-16), means that the STATCOM reactive power output can be controlled in both directions. The reactive power flows towards the ac network provided the amplitude of the converter terminal voltage E_{conv} is greater than the amplitude of network voltage V at the PCC,

and this represents a capacitive mode operation of the STATCOM. But if the amplitude of the ac voltage V at PCC is greater than the amplitude of the converter terminal voltage (E_{conv}), reactive power flows from the ac network to the STATCOM, and this represents an inductive operation mode of the STATCOM.

Figure 3-16 illustrates the basic STATCOM control structure. It includes; an external voltage regulation controller, internal current controller, and converter gate pattern logic. The required current reference I_{Qref} is determined in the external PI controller in response to the error signal which can be a voltage or reactive power deviation from the reference set-point. Then the current reference I_{Qref} is passed to the fast inner current controller which operates the converter switches with a defined turn on/off period, which in turns generates gating commands in the response to the required reference currents I_d and I_q . Current I_d is required to maintain the DC voltage across the DC capacitor.

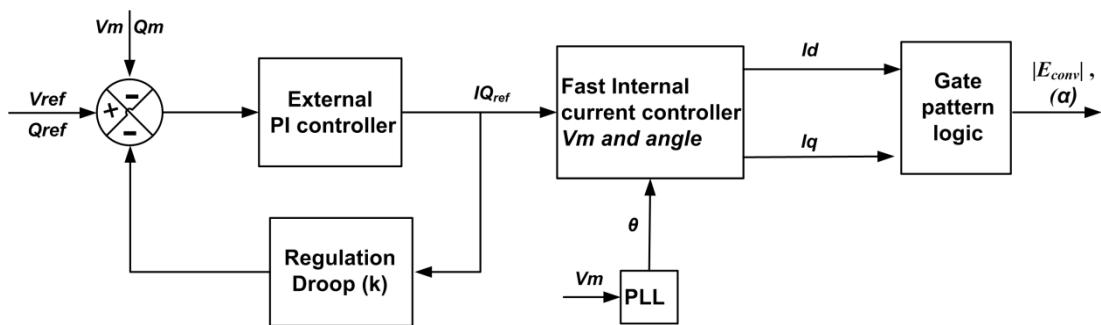


Figure 3-16: Basic control structure of converter based VAR compensator

The converter based VAR source can be seen, from the ac grid, as a synchronous voltage source that provides a controllable reactive current in response to the system reactive power requirements. The STATCOM reactive current can change within a pre-defined range from the maximum capacitive current I_{Cmax} to the maximum inductive current I_{Lmax} , regardless of the operating ac voltage, as shown in Figure 3-14. However, a minimum ac voltage of about 0.2 pu is required to provide the necessary active power to feed the STATCOM internal losses [4]. The STATCOM $V-I$ characteristics are defined by the maximum current and voltage ratings of the IGBT voltage source converter.

3.4 Control requirements of shunt FACTS

The control strategy of shunt-connected static VAR generators depends on the application and on the task to be performed in the power system. Some control strategies require maintained voltage at specific nodes to improve: system loadability, voltage stability, and first swing transient stability. On the other hand, coordinated variation of the terminal voltage in interconnected power systems can be targeted by other control strategies to improve power oscillation damping (POD) in the interconnected power systems. That is, the voltage at the PCC can be maintained or vary depending on the desired function. When a shunt compensator requires, an additional task such as POD, an auxiliary controller can be incorporated into the general outer control scheme[4].

Despite the different structures, operating principles, power losses, response times, and $V-I$ characteristics of variable impedance and converter based shunt VAR generators, their behavior in the linear region is similar. This means that both types of static VAR generators provide the same amount of reactive power in response to the ac voltage change. As the external controllers of both shunt FACTS types define the same reference current input I_{Qref} to be passed to the static VAR generators, the same general transfer function is established for the basic control of the SVC and STATCOM shown in Figure 3-17. Consequently, the same reactive power output will be drawn for the same regulation droop.

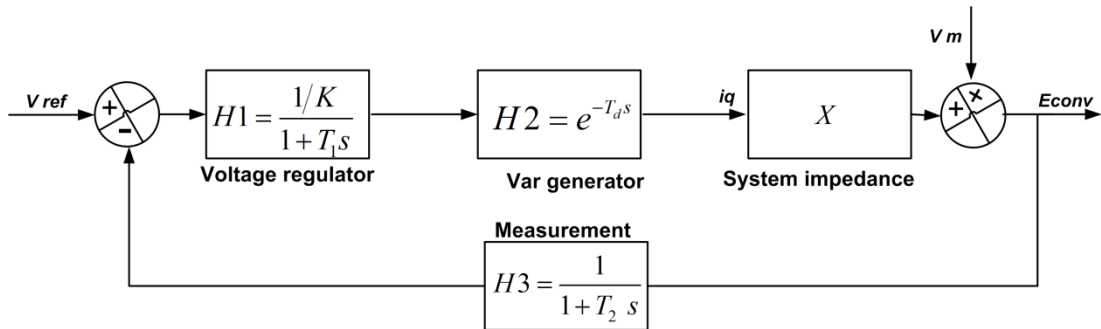


Figure 3-17: Basic transfer function for SVC and STATCOM control

This basic control system of shunt FACTS devices reflects the $V-I$ characteristics of SVC and STATCOM during steady state and dynamic operation, as shown in Figure 3-18.

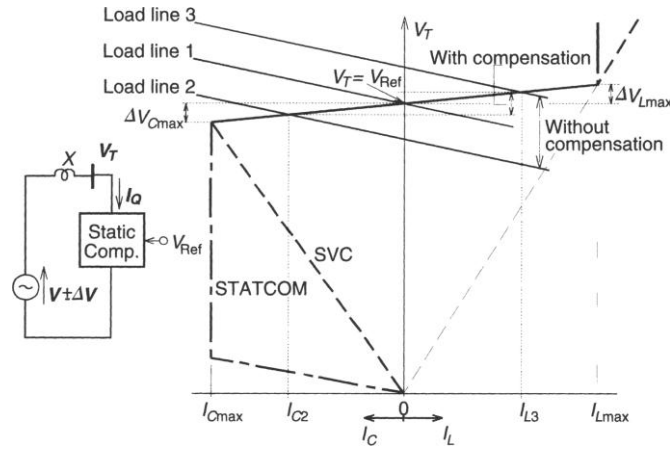


Figure 3-18: V - I characteristics of SVC and STATCOM during steady state and dynamic operation[4]

During the linear operation region, the voltage V and reactive current I_q of shunt VAR generator varies linearly based on the regulation droop K that can be calculated from:

$$K = \frac{\Delta V_{Cmax}}{I_{Cmax}} = \frac{\Delta V_{Lmax}}{I_{Lmax}} \quad (3-18)$$

where I_{Cmax} and I_{Lmax} are the maximum capacitive and inductive output currents respectively, and ΔV_{Cmax} and ΔV_{Lmax} are the deviations (decrease and increase) of the terminal voltage V from the reference voltage V_{ref} . As the voltage diverges from its nominal value, the required leading or lagging reactive current I_{Qref} is calculated in the voltage regulator in Figure 3-17.

If the voltage drifts beyond the linear control range of the VAR compensator, the output current is governed by the non-linear V - I characteristic of the compensator. In nonlinear operation, a variable impedance shunt FACTS behaves as a fixed capacitor or inductor with a voltage dependency characteristic, where the reactive current output changes linearly with voltage squared. But the reactive current stays at its maximum capacitive or inductive current rating in the case of a converter based VAR compensator (STATCOM).

Figure 3-17 shows a high-level representation of an SVC or STATCOM as a transfer function that includes three main parts:

- 1- The external PI voltage regulator with time constant T_l (typically 10-50 ms) and regulation droop k (typically 1-5%)[4]. The general transfer function of voltage regulator is:

$$H_1 = \frac{1/K}{1+T_1s} \quad (3-19)$$

- 2- The VAR generator part can be variable impedance or converter based, and both can be represented by transport delay T_d . The value of T_d can be set depending on the type of VAR generator, 0.2-0.3ms for converter base and 2.5-5ms for a variable impedance VAR compensator[4].

$$H_2 = e^{-T_d s} \quad (3-20)$$

- 3- Time constant for the circuit measurements T_2 (typically 8-16ms) [4] which is given by:

$$M = \frac{1}{1+T_2s} \quad (3-21)$$

Figure 3-17 indicates that the amplitude of the terminal voltage of the VAR compensator (E_{conv}) can be expressed in terms of the ac voltage V_m and the reference voltage V_{ref} as:

$$E_{conv} = V_m \frac{1}{1+H_1H_2MX} + V_{ref} \frac{H_1H_2X}{1+H_1H_2MX} \quad (3-22)$$

The system impedance X is included in the integral feedback loop in the equation (3-22) which means that the dynamic behavior and the time response of the shunt VAR generator are a function of system impedance.

3.5 Effect of midpoint shunt compensation on the tie-line load-ability

One of the most important roles of the shunt VAR generators is to improve load-ability of the tie-lines in interconnected power systems. This could be achieved with SVC or STATCOM, which changes the system impedance characteristics smoothly to accommodate any change in the operating conditions.

Figure 3-19 illustrates a simplified model of two interconnected AC transmission systems with a controllable capacitor bank C installed in the middle of the transmission line. This midpoint compensation divides the line into two identical segments, each of $j\frac{1}{2}X_L$ series impedance.

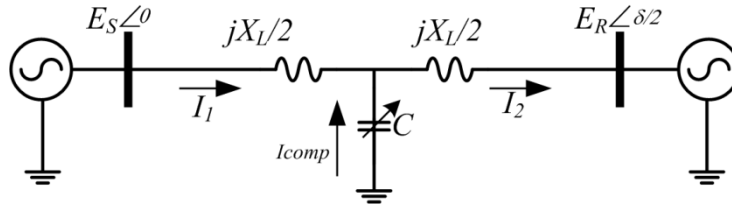


Figure 3-19: Simple two interconnected AC power systems with shunt VAR compensation

For simplicity; the tie line is modeled as pure inductive reactance X , and the midpoint voltage V_C is assumed to be maintained at the nominal voltage ($E_S = V_{mid} = E_R = V$).

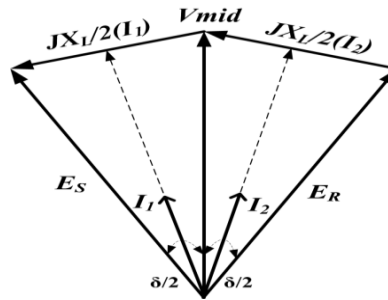


Figure 3-20: Impact of midpoint compensation on the power angle and system impedance

Figure 3-20 shows a phasor representation of the simple circuit in Figure 3-19. This figure indicates that the ideal midpoint compensation reduces the effective system impedance to $jX_L/2$ and the power angle to $\delta/2$. Consequentially, it doubles the transfer capability of the tie-line as indicated by the equation (3-23) compared with that obtained in section 2.2 for the same lossless network [25].

$$P_1 = P_2 = \frac{2V^2}{X_L} \sin\left(\frac{\delta}{2}\right) \quad (3-23)$$

From Figure 3-19, the reactive current absorbed or injected at the midpoint is;

$$I_2 = I_1 \pm I_{comp} \quad (3-24)$$

From equations (2-3) and (2-4), and assuming that the voltage is maintained at the middle point of a lossless tie-line in Figure 3-19, the currents at the two segments of the line are given by:

$$I_1 = \frac{E_S \angle 0 - V_{mid} \angle \delta/2}{\frac{1}{2}X_L} \quad \text{and} \quad I_2 = \frac{V_{mid} \angle \delta/2 - E_R \angle \delta}{\frac{1}{2}X_L} \quad (3-25)$$

Hence, the reactive current injected by the midpoint compensation to maintain the voltages such as ($E_S=V_C=E_R=V$) is calculated from equations (3-24) and (3-25) as:

$$I_{comp} = \pm \frac{4V_{mid}}{X_L} (1 - \cos \frac{1}{2}\delta) \quad (3-26)$$

The above equation allows calculation of the reactive power injected or absorbed by the shunt compensation at maintained midpoint voltage (V_{mid}) (the negative sign represents a capacitive operation mode):

$$Q_{comp} = \pm \frac{4V_{mid}^2}{X_L} (1 - \cos \frac{1}{2}\delta) \quad (3-27)$$

Figure 3-21 shows the impact of ideal midpoint compensation on the transfer capability of the tie-line in the assumed lossless Kundur two areas test system described in section 2.5. Power versus angle curves ($P-\delta$ curve) are obtained from equations (2-3) for non-compensated tie-lines, and from equation (3-23) for an ideally compensated tie-line's midpoint.

From steady state angular stability points of view, Figure 3-21 depicts that the transfer capability of the tie-line (58Ω reactance) is doubled (from 577 to 1154 MW).

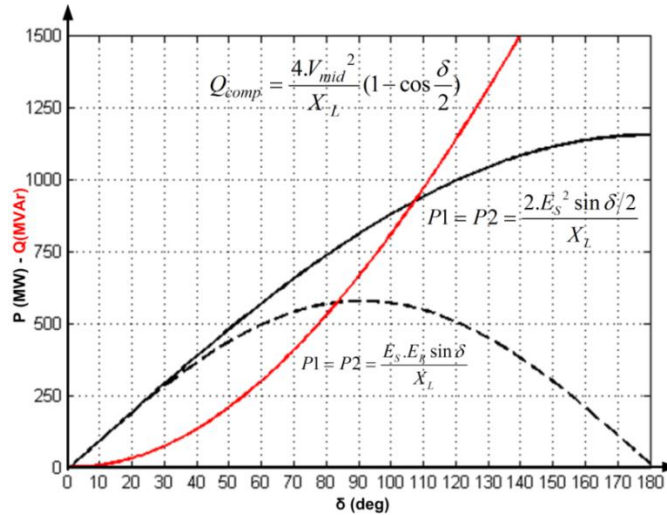


Figure 3-21: Impact of the midpoint compensation on the transfer capability of the tie-line in the Kundur test system

This figure establishes that the transfer capability of a tie-line is doubled because of reactive power support provided by ideal midpoint compensation. However, this increase in active power may be at the expense of dramatic consumption of reactive

power at the midpoint as shown in the figure, which can outweigh the achieved load-ability improvement.

3.6 Allocating of shunt VAR generators for system load-ability improvement

A number of optimization approaches have been introduced for allocation and sizing of shunt reactive power generators. These allocation methods vary in complexity depending on the application, objective functions, constraints and mathematical models. A review of different optimization techniques is given in [7-9, 13].

Nodal voltage during normal and emergency operating conditions is one of the indicators used to assess the quality and performance of power systems. Voltage profile improvement in specific key nodes in the network can dramatically improve system load-ability, which reflects on the system performance in many ways as it provides: reduced operation cost, network operation flexibility, and enhance system security, as shown in the Figure 3-22.

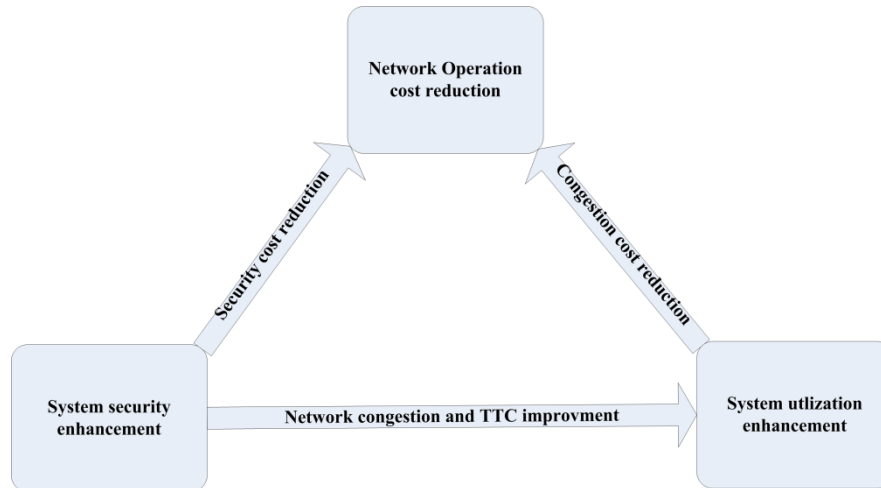


Figure 3-22: Effect of improved system load-ability on overall system performance [26]

3.6.1 Total voltage change index (TVCI) for FACTS allocation

The relation between voltage change and reactive power change at a given node (self-sensitivity BS_{ii}) can be estimated from $V-Q$ sensitivity analysis. This relation can be given by;

$$BS_{ii} = \frac{\Delta V_{BUS(i)}}{\Delta Q_{BUS(i)}} = J_R^{-1} \quad (3-28)$$

Where; J_R^{-1} is the reduced Jacobian matrix at the bus (i), $\Delta V_{BUS(i)}$ and, $\Delta Q_{BUS(i)}$ are the incremental change in voltage magnitude and in the reactive power magnitude at the bus(i).

In the same context, mutual-sensitivity, which defines the impact of reactive power change in bus i on the voltage in the bus j , can be calculated from the reduced Jacobian matrix. The elements of the inverse of reduced Jacobian matrix are the V - Q sensitivity. The diagonal components of this matrix are self-sensitivities ($\partial V_i / \partial Q_i$), whereas non-diagonal components in the matrix represent the mutual sensitivity ($\partial V_i / \partial Q_j$) which can be calculated as [25];

$$BM_{ij} = \frac{\Delta V_{BUS(i)}}{\Delta Q_{BUS(j)}} = J_R^{-1} \quad (3-29)$$

Self and mutual sensitivities, obtained from equations (3-28) and(3-29), are used to calculate the total voltage change index ($TVCI$) in equation (3-30) that is proposed for shunt FACTS allocating. The optimal allocation for the shunt VAr sources can be defined by the node with higher $TVCI$, which upon the candidate buses are descending ranked.

$$TVCI_{BUS(i)} = \sum_{i=1}^j BS_{ii} \dots \dots BS_{ij} \quad (3-30)$$

Table 3-1 shows results of $TVCI$ calculation for allocating of shunt FACTS to maximize tie-line load-ability in weak interconnected power systems in figure 3-10. Bus-3 at the remote end of the radial system has the highest $TVCI$ of 0.2424 ($V\%/MVAR$) which nominates it as a suitable place to install static VAr generation.

Table 3-1: VAr source allocating, on the basis of $TVCI$, in weak power systems

Candidate bus	Self and mutual sensitivity $\Delta V(\%)/\Delta Q(MVAR)$		
	Bus-1	Bus-2	Bus-3
Bus-1	0.0083	0.0083	0.0083
Bus-2	0.0086	0.0633	0.0633
Bus-3	0.0087	0.0641	0.1708
TVCI	0.0256	0.1357	0.2424

In contrast, $TVCI$ result in Table 3-2 indicates that the midpoint compensation at bus-2 in figure 3-10, assuming that both systems are strong, is the optimal location for VAr source installation in a strongly connected power systems (highest $TVCI$ of 0.0495 $V\%/MVAR$).

Table 3-2: VAr source allocating, on the basis of *TVCI*, in strong power systems

Candidate bus	Self and mutual sensitivity $\Delta V(\%)/\Delta Q(\text{MVar})$		
	Bus-1	Bus-2	Bus-3
Bus-1	0.0079	0.0054	0.0004
Bus-2	0.0055	0.0412	0.0029
Bus-3	0.0004	0.0029	0.0079
TVCI	0.0138	0.0495	0.0112

The above results indicate that the introduced *TVCI* is an effective approach to allocating shunt VAr compensation in the case of weak and strongly interconnected power systems.

3.7 Sizing of shunt FACTS for system load-ability improvement

Sizing of FACTS is formulated as a critical aspect of reactive power planning (RPP) because its effectiveness in improving the power system performance mainly depends on their size and where installed. System load-ability improvement is amongst the important FACTS sizing objectives in reactive power planning, and this objective is achieved efficiently if adequate reactive power is injected at a suitable location. The amount of reactive power required to improve system load-ability depends on system strength and the type of FACTS device.

3.7.1 Maximum allowable reactive power injection at a given node

Figure 3-23(a) shows power versus voltage ($P-V$) curves at a given bus with different levels of shunt compensation. As discussed in Chapter 2, Figure 3-23(b) indicates that total transfer capability (*TTC*), voltage stability limit (*VSL*), critical voltage (E_{CRT}) and voltage stability margin *VSM* vary as the knee point (*PoC*) moves with the level of shunt compensation.

In certain operational conditions, the noticeable improvement in the tie-line load-ability, by the means of shunt FACTS, is achieved at the expense of system security in two ways;

- i. Higher *PoC* 'C2' tends to fall inside the secondary voltage regulators remedy zone; thus, the system may end up being unstable as a consequence of the normal functionality of secondary voltage regulators such as *ULTC* as reported in [27]. Although most modern power systems have adopted new remedies to this problem, such as *ULTC* blocking, voltage stability assessment (*VSA*), and

special protection schemes (*SPS*) to avoid voltage instability; uncoordinated action of these strategies may conflict with functionality of other automated correction measures which can have severe consequences in the case of insufficient *VSM* (high *PoC*) [28].

- ii. The impact of shunt compensation on the system security can easily be understood from the term $(a.q_{sh}+x)$ in equation (2-18) which shrinks with an increase of q_{sh} (negative sign). Equations (2-28) and (2-31) indicates that the load-ability and critical voltage increase with capacitive reactive power injection, reaching a theoretically maximum value when $a.q_{sh}$ equals $-x$. As the reactive power injected is increased, the *PoC* rises and the gap between the maximum load-ability curve (*TTC*) and voltage stability limit curve (*VSL*), which represents the voltage stability margin *VSM*, decreases. With continued increase in reactive power injection, the two curves converge to the same value when the voltage stability margin approaches zero. Reactive power at this point can be calculated from equation (3-31), and represents the maximum reactive power that can be injected at a given node. Beyond this level of injected reactive power, any additional reactive power increases the term $a.q_{sh}+x$ in the equation (2-18) and consequently decreases the voltage, as shown in Figure 3-23(b).

$$Q_{stb} = -x F_C / (r^2 + x^2) \quad (3-31)$$

Equation (3-31) can be used for estimation of the maximum permissible shunt capacitive rating of the variable impedance VAR source (Q_{stb}) which equals $1/x$ ($x = X/E_S^2$).

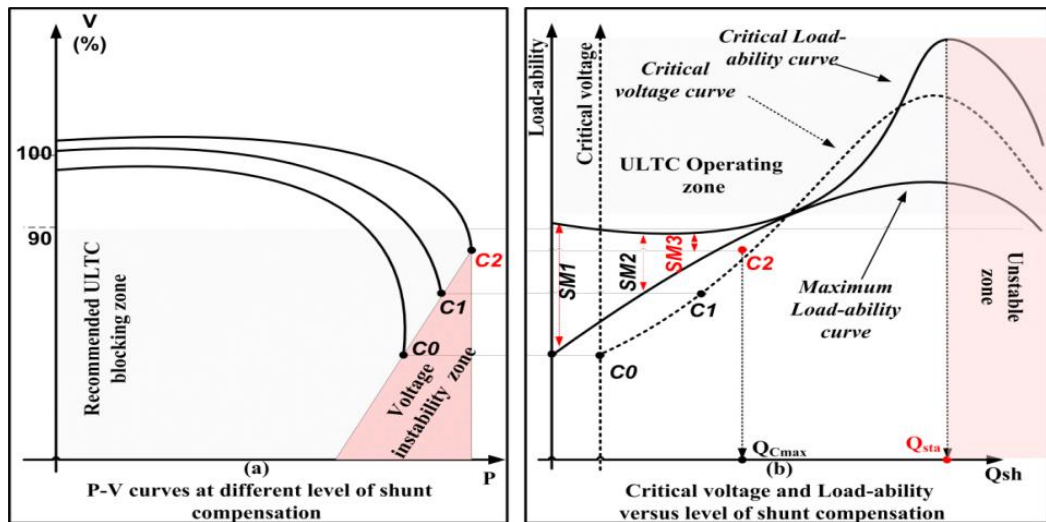


Figure 3-23: Effect of shunt compensation on load-ability and voltage stability

From this discussion, the upper curve in Figure 3-23(a) represents the case where the PoC ' C_2 ' is exaggeratedly pushed higher, which results in a reduced safety margin SM_3 , where PoC is likely to be extremely close to the acceptable operating voltage level. In contrast, C_1 represents a suitable compensation level with an improved load-ability and reasonable stability margin SM_2 , where activation of $ULTC$ blocking may help maintain voltage stability [25, 29].

3.7.2 Security criteria for shunt FACTS sizing

System security during normal and emergency operating conditions is given high priority in reactive power planning. For this reason, security constraints are higher rank compared with other quality or economic considerations in FACTS allocating and sizing optimization problems.

As discussed, sizing of FACTS devices has to satisfy post-fault ($N-1$) security requirements. This is because a weak system is influenced more by reactive power change than a strong system because of its higher voltage sensitivity as evidenced in section 3.6.1 (see Table 3-1 and Table 3-2).

The second important security aspect in shunt FACTS sizing is the risk of higher PoC on system stability, addressed in section 3.7.1, which has to be taken as an additional constraint in shunt FACTS sizing.

Therefore, sizing methodology should aim to maximize system load-ability during post-fault operating conditions (higher voltage sensitivity) while considering violation of any of the following listed security criteria to define the maximum VAR generator size:

- 1- Maintaining a reasonable voltage stability margin (VSM) to face any credible contingency or
- 2- Keeping the knee point (PoC) reasonable high, for instance blocking zone of the secondary voltage regulation ($ULTC$) to avoid their undesired automatic action that can exacerbate voltage instability[27]

3.7.3 Sizing of variable impedance shunt FACTS

Maximum capacitive size for a shunt connected FACTS that ensures maximum load-ability at a given remote node, while considering the mentioned security constraints

in 3.7, can be analytically calculated for a radial system or whenever reasonable equivalent system impedance is available (R , X , and B).

Calculation of the maximum size of a variable impedance shunt FACTS device (Q_{Cmax}) which is required to maximize tie-line load-ability, while stressing the need to consider the mentioned security constraints, can be calculated by equation 2-18.

Q_{Cmax} can be estimated straight forwards, on the basis of the stability margin VSM security criteria, by substituting the power P in the equation (3-7) by the total transfer capability (TTC) of the tie-line which is calculated considering, at least, the minimum required stability margin VSM , as discussed in section 2.4.5.

In relatively weak systems where voltage instability can be exacerbated by some actions of secondary voltage regulation measures, sizing of shunt FACTS devices should be on the basis of security criteria that considers PoC height. On this basis, the maximum size of the VAR source (Q_{Cmax}) can be determined from the $E_{CRT}-q_{sh}$ curve (equation (2-31)). The maximum shunt capacitive rating (Q_{Cmax}) that ensures maximum tie-line utilization while maintaining the PoC reasonably-high ($ULTC$ blocking zone) is obtained from the intersection of the $E_{CRT}-q_{sh}$ curve with the predefined E_{CRT} (defined in the network operation rules) line as shown in Figure 3-24.

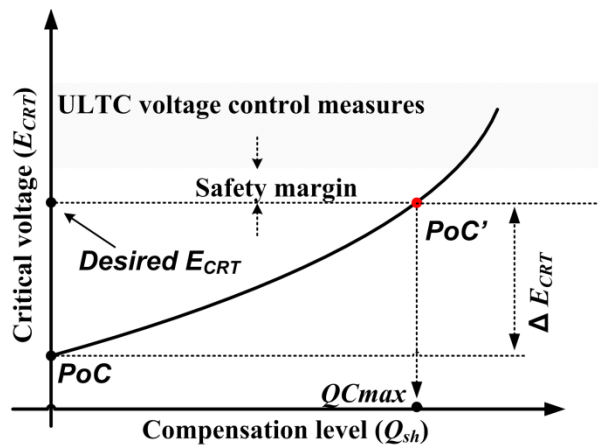


Figure 3-24: Sizing of variable impedance FACTS devices on the basis of PoC security criteria

To illustrate the sizing approach with an example, consider the tie-line with limited transfer capability (134 MW) in the test system in Figure 3-10.

The proposed sizing approach is used to determine the optimal size of VAR compensation that securely improves system load-ability at the remote end (Bus-3).

Assuming that 85% is the highest accepted critical voltage (as represented by C1 in Figure 3-23-a), simultaneous solution of equations 2-29, 2-31 and (3-7) indicates that installation of an SVC with 180 MVar capacitive rating improves total transfer capability of the tie-line by 98%, to reach about 256 MW.

Figure 3-25 shows the shunt compensation level of a variable impedance shunt FACTS device versus the critical voltage at the receiving end ($Q_{sh}-E_{CRT}$ curve). About 180MVar is required to raise the collapse point (PoC) from 0.63 to 0.85, along the Y axis.

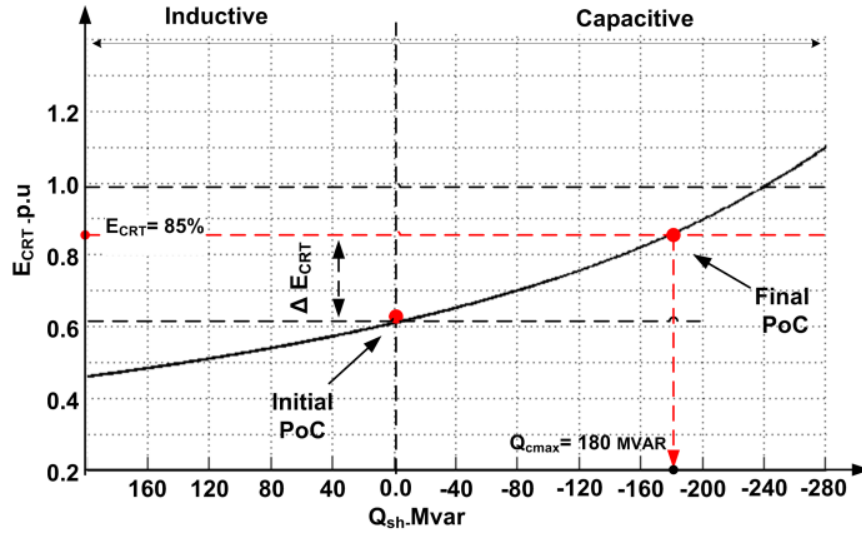


Figure 3-25: Level of shunt compensation versus critical voltage at Bus-3 of Figure 3-10

3.7.4 Sizing of converter based shunt FACTS

Theoretically, converter based shunt FACTS is able to maintain the nominal voltage up to the angular stability limit (ASL) given by equation (2-35) in Chapter 2. It follows that maximum current rating of the converter based FACTS device, which is required to maintain the voltage at its reference during maximum loadability, which corresponds to the angular stability limit (ASL), is given by the equation (3-32). This equation is established by substituting the power P in equation (3-11) by the ASL value established from equation (2-35) at $\delta=90^\circ$.

$$IQ_{CRT} = \frac{F_C \cdot V_{ref} \cdot (r \cdot \sqrt{1 - pf^2} - pf \cdot x) - \sqrt{F_C \cdot z^2 \cdot \sqrt{1 - pf^2}}}{\sqrt{3} (pf \cdot z^2 \cdot VB)} \quad (3-32)$$

However, working at this reactive current level (IQ_{CRT}) is not desired because:

- Sufficient stability margin is not available at this loading level, as the system is running almost at the critical collapse point (high PoC). Although the nominal voltage is maintained, any small disturbance can lead to system instability (see section 2.3.1-I for further detail).
- The reactive power requirement at such a load-ability level is high as established in equation (3-27). Therefore, the load-ability improvement may not be economically comparable to the high reactive power required rating capacity of the FACTS device.

Based on this discussion, reasonable stability margin (VSM), as a percentage of ASL is included in equation(3-11). That is, the power (P) in equation(3-11) is calculated as;

$$P = VSL - VSM \quad (3-33)$$

Where; VSL is voltage stability limit calculated from equation (2-29), and VSM is voltage stability margin defined based on the grid requirements as discussed in 3.7.1. Equations (2-29) and (3-33) are used to establish the sizing equation that defines the maximum current rating of the STATCOM considering safety margin as portion from voltage stability limit:

$$IQ_{max} = \frac{(b-c)}{3 pf (r^2 + x^2) VB} \quad (3-34)$$

$$b = \sqrt{VSM \left[(F_c \cdot r^2 \cdot V_{ref}^2 + r^2 + x^2) - 3F_c \left(-2r \cdot V_{ref} (VSM - 1) \sqrt{F_c (r^2 + x^2)} - 2r^2 - 2x^2 \right) \right] pf}$$

$$c = \sqrt{3} \left(F_c \cdot V_{ref} \left(r (VSM - 1) \sqrt{(1 - pf^2)} + x \cdot pf \right) - \sqrt{(1 - pf^2)} (VSM - 1) \sqrt{F_c (r^2 + x^2)} \right)$$

In order to evaluate the load-ability improvement of the tie-line in Figure 3-10, with the STATCOM, the same SVC sizing criteria in the previous section is used. That is, assuming $E_{CRT}=85\%$, the sizing equation (3-34) shows that a 225 MVar STATCOM rating improves the transfer capability of the tie-line in the test system by 147 %, reaching about 331 MW. For a typical STATCOM $V-I$ characteristic, this current rating provides a maintained voltage up to maximum STATCOM current rating, and then the voltage declines sharply with loading increase before collapsing just after a critical load-ability of 340 MW.

3.7.5 Generic sizing method based on P - V curve analysis

This generic sizing approach can be used for both shunt FACTS types and regardless the system configuration complexity. This is because most commercial power system analysis tools are equipped with algorithms that allow P - V and P - Q analysis with a detailed network representation.

The proposed approach in this section aims to maximize system load-ability while considering the security constraints mentioned in section 3.7.

Reactive power required to move the PoC from $C0$ to $C1$, shown Figure 3-23a, can be obtained by the means of repeated P - V curve calculation. The knee point (PoC) of a P - V curve is monitored as the capacitive size of the VAR compensator (SVC or STATCOM) gradually increases.

Maximum capacitive size (Q_{Cmax}) of the shunt connected FACTS corresponds to the receiving end load-ability where the first of the mentioned security constraints (PoC high or VSM) is violated.

3.8 Comparison between variable impedance and converter based shunt FACTS

The previous discussions have shown that variable impedance and converter based shunt FACTS have a similar behavior during linear operation, inspite of the different in the basic operating principles. Converter based shunt FACTS is seen as a shunt connected voltage source while variable impedance shunt FACTS is a shunt connected controllable admittance. Dynamic performance during the disturbance, non-linear V - I characteristics, time response and control flexibility indicate a preference for converter based FACTS. In addition to the physically small size of the converter based shunt FACTS (30- 40 % smaller) compared with large sizes of the variable impedance shunt FACTS that includes reactive power energy storage (capacitor and inductor banks) and their associated switchgear and filters.

A summary of a technical comparison between variable impedance and converter based shunt FACTS is presented in Table 3-3.

Table 3-3: Main technical differences between variable impedance and converter based shunt FACTS

	Variable impedance shunt FACTS	Converter based shunt FACTS
FACTS device	SVC	STATCOM
V-I characteristics	I_{Qmax} changes Proportional to V	I_{Qmax} is independent of V
Q-V characteristics	Q_{max} changes linearly with V^2	Q_{max} changes linearly with V
IQ Output change	A step-like for TSC, smooth change for TCR	Smooth change for both capacitor and inductive mode
Maximum delay	One cycle	Negligible
Installation land and size	A large landscape is required because of huge capacitor and inductor banks and filters	30-40% smaller

3.8.1 Steady state performance comparison

Generic sizing approach ($P-V$ curve) is used in this comparison. PoC rise is taken as the sizing constraint where $V=85\%$ is taken as the maximum acceptable high for the PoC as addressed in subsection 3.7.1. Figure 3-26 depicts that a shunt FACTS dramatically increase the transfer capability of a tie-line but with varying levels of load-ability improvement. This disparity is due to the difference in $V-I$ characteristics during nonlinear operation between variable impedance and converter based shunt FACTS as previously mentioned. Previous results show that higher load-ability improvement, achieved by a STATCOM, is reflected in the overall steady state system performance and on the utilization index of the installed FACTS devices as shown in Table 3-4.

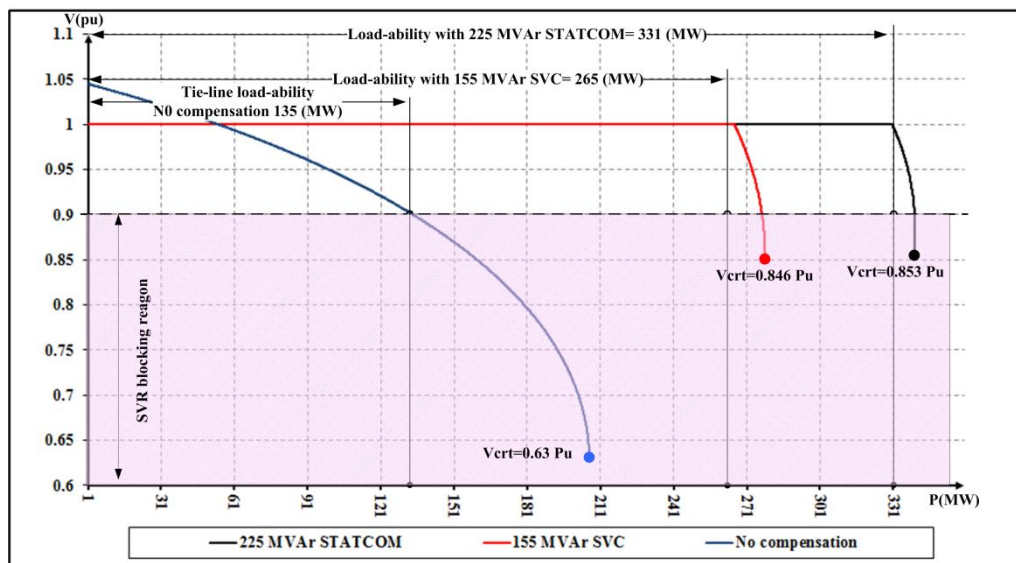


Figure 3-26: Sizing of static VAr compensation using a generic P-V curve method where PoC high is taken as sizing criteria (E_{CRT} should be less than 85%)

Table 3-4: Steady state comparison between SVC and STATCOM

	Base case	Variable impedance shunt FACTS	Converter based shunt FACTS
Optimal rating on the basis of PoC high (MVA _r)	-	155	225
Max- load-ability (TTC) MW	134	265	331
VSL (MW)	206	278	340
ASL (MW)	346	457	457
TTC improvement (%)	0	98	147
VSM (%)	53	5	3
$\frac{P_{l_{max}} \text{ increas}}{\text{FACTS size}} \left(\frac{\text{MW}}{\text{MVA}_r} \right)$	0	0.85	0.88

3.8.2 Dynamic performance comparison

The transfer function for the basic control of the shunt FACTS in Figure 3-17 determines the dynamic performance of the FACTS device during a disturbance. The transport lag time delay of the converter based device is considerably smaller than that of the variable impedance device, which provides better frequency bandwidth, smaller voltage regulator time constant, and better overall dynamic performance.

In order to compare the dynamic performance of the two FACTS types each type is evaluated under a stressed operating condition. Time domain analysis is performed to assess the response of both FACTS types with the same reactive power rating of 225 MVA_r, installed at the receiving end in the Kundur test system in Figure 3-10 when a 150ms 3-phase fault is applied at the middle of line-3.

The red curves in Figure 3-27a and Figure 3-27b show that in the case of the uncompensated tie-line with 500 MW (250 MW on each circuit) of power transfer, loss of any of the parallel lines causes a loss of synchronism between the interconnected systems because of a lack of reactive power support. On the other hand, the green and blue curves that refer to SVC and STATCOM midpoint shunt compensation, indicate that both shunt devices manage to maintain system stability as they provide sufficient reactive power support during the first swing following the disturbance.

Since the installed SVC and STATCOM have the same rated, both provide almost the same reactive power output, with the STATCOM exhibiting slightly better power oscillation damping.

The reactive currents and reactive power outputs during and after fault clearance are shown in Figure 3-27c and Figure 3-27d respectively. In Figure 3-27c, the STATCOM (blue curve) is able to provide full current rating during the fault which provides better voltage recovery during the fault compared with that provided by the SVC. Furthermore, the disparity between the two FACTS types is shown Figure 3-27d which represents the reactive power outputs of both FACTS devices. The figure indicates that reactive power output of the variable impedance types (SVC) further dropped during and just after the fault.

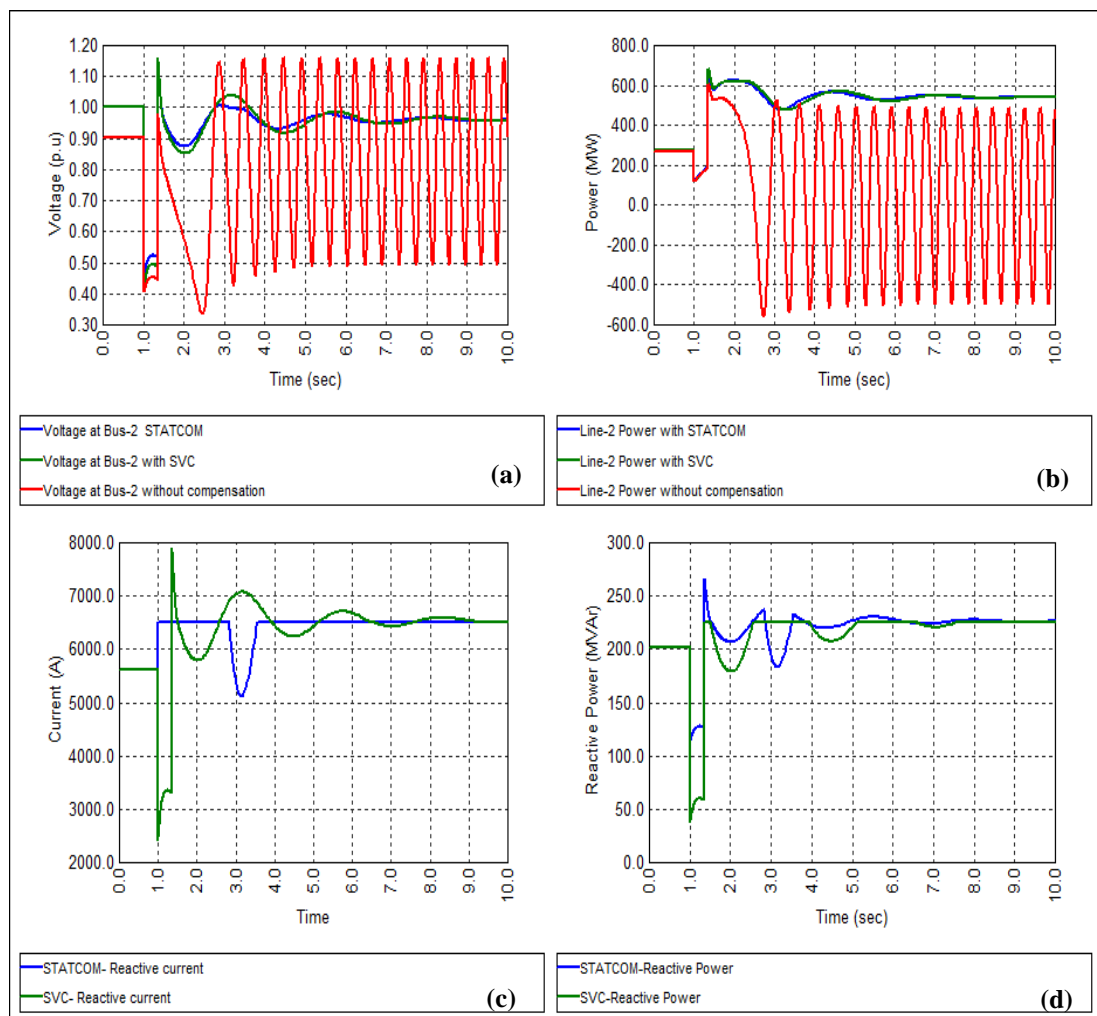


Figure 3-27: Dynamic comparison between SVC and STATCOM (installed at Bus-2 in Figure 3-10)

3.9 Summary

Despite a big difference in structure, operation principles, power loss, response time, and $V-I$ characteristics between variable impedance and converter based VAR generators; during linear operation both types are similar. Both reactive shunt compensation types can efficiently improve system utilization as they provide reactive power support which maintains the voltage profile, increases steady-state transmissible power, and improves system stability. However, converter based shunt FACTS show better dynamic performance.

The generic power flow equation (2-18) was modified to incorporate the linear and nonlinear effects of variable impedance and converter based shunt FACTS devices (equations 3-7 and 3-14). These equations are used for accurate power flow calculation with SVC and STATCOM, allocation and sizing of shunt FACTS, improvement of TTC with shunt FACTS, and can also be used to calculate FACTS utilization factor.

It was established that FACTS sizing should include PoC and VSM as additional sizing constraints. Regarding the allocation of shunt FACTS, the total voltage change index (TVCI) can be used efficiently to allocate a shunt FACTS device. In the same context, it is confirmed that midpoint compensation is the optimal place for shunt compensation in the case of strong terminals of the tie-line. On the other hand, the receiving end is the optimal position for shunt compensation in radial and weak interconnected power systems.

The proposed analytical equations, in addition to the sizing and allocating methodologies, will be used for steady state assessment of the Libyan internal tie-line, and to obtain optimal shunt FACTS size and location in different weak interconnection corridors in the Libyan network.

References

- [1] A. Lashkar Ara, *et al.*, "Multiobjective Optimal Location of FACTS Shunt-Series Controllers for Power System Operation Planning," *Power Delivery, IEEE Transactions on*, vol. 27, pp. 481-490, 2012.
- [2] Milanovic, *et al.*, "Modeling of FACTS Devices for Voltage Sag Mitigation Studies in Large Power Systems," *Power Delivery, IEEE Transactions on*, vol. 25, pp. 3044-3052, 2010.
- [3] X.-P. Zhang, *et al.*, *Flexible AC transmission systems: modelling and control*: Springer Science & Business Media, 2012.
- [4] N. G. Hingorani and L. Gyugyi, *Understanding FACTS: Concepts and Technology of Flexible AC Transmission Systems*: Wiley, 2000.
- [5] E. Acha, *et al.*, *FACTS: modelling and simulation in power networks*: John Wiley & Sons, 2004.
- [6] J. C. Carlisle, *et al.*, "A review of capacitor placement techniques on distribution feeders," in *System Theory, 1997., Proceedings of the Twenty-Ninth Southeastern Symposium on*, 1997, pp. 359-365.
- [7] R. Sirjani, *et al.*, "Optimal Placement and Sizing of Shunt FACTS Devices in Power Systems Using Heuristic Optimization Techniques: a Comprehensive Survey," *Przeegl±d Elektrotechniczny Selected full texts*, vol. 88, pp. 335-341, 2012.
- [8] Z. Wenjuan, *et al.*, "Review of Reactive Power Planning: Objectives, Constraints, and Algorithms," *Power Systems, IEEE Transactions on*, vol. 22, pp. 2177-2186, 2007.
- [9] E. Ghahremani and I. Kamwa, "Optimal placement of multiple-type FACTS devices to maximize power system loadability using a generic graphical user interface," *Power Systems, IEEE Transactions on*, vol. 28, pp. 764-778, 2013.
- [10] E. N. Azadani, *et al.*, "Optimal placement of multiple STATCOM," in *Power System Conference, 2008. MEPCON 2008. 12th International Middle-East, 2008*, pp. 523-528.
- [11] M. Saravanan, *et al.*, "Application of PSO technique for optimal location of FACTS devices considering system loadability and cost of installation," in *Power Engineering Conference, 2005. IPEC 2005. The 7th International, 2005*, pp. 716-721 Vol. 2.
- [12] R. Benabid, *et al.*, "Optimal placement of FACTS devices for multi-objective voltage stability problem," in *Power Systems Conference and Exposition, 2009. PSCE '09. IEEE/PES, 2009*, pp. 1-11.
- [13] S. Gerbex, *et al.*, "Optimal location of multi-type FACTS devices in a power system by means of genetic algorithms," *Power Systems, IEEE Transactions on*, vol. 16, pp. 537-544, 2001.
- [14] M. Behshad, *et al.*, "Optimal location of UPFC device considering system loadability, total fuel cost, power losses and cost of installation," in *Power Electronics and Intelligent Transportation System (PEITS), 2009 2nd International Conference on*, 2009, pp. 231-237.
- [15] A. Kazemi, *et al.*, "Optimal Location of UPFC in Power Systems for Increasing Loadability by Genetic Algorithm," in *Universities Power Engineering Conference, 2006. UPEC '06. Proceedings of the 41st International, 2006*, pp. 774-779.
- [16] R. Sirjani and A. Mohamed, "Improved Harmony Search Algorithm for Optimal Placement and Sizing of Static Var Compensators in Power

- Systems," in *Informatics and Computational Intelligence (ICI), 2011 First International Conference on*, 2011, pp. 295-300.
- [17] A. Kazemi, *et al.*, "On the use of harmony search algorithm in optimal placement of facts devices to improve power system security," in *EUROCON 2009, EUROCON '09. IEEE*, 2009, pp. 570-576.
- [18] A. D. Shakib and G. Balzer, "Optimal location and control of shunt FACTS for transmission of renewable energy in large power systems," in *MELECON 2010 - 2010 15th IEEE Mediterranean Electrotechnical Conference*, 2010, pp. 890-895.
- [19] A. Z. Gamm and I. I. Golub, "Determination of locations for FACTS and energy storage by the singular analysis," in *Power System Technology, 1998. Proceedings. POWERCON '98. 1998 International Conference on*, 1998, pp. 411-414 vol.1.
- [20] S. N. Singh and I. Erlich, "Locating unified power flow controller for enhancing power system loadability," in *Future Power Systems, 2005 International Conference on*, 2005, pp. 5 pp.-5.
- [21] V. P. Rajderkar and V. K. Chandrakar, "Comparison of Series FACTS Devices Via Optimal Location in a Power System for Congestion Management," in *Power and Energy Engineering Conference, 2009. APPEEC 2009. Asia-Pacific*, 2009, pp. 1-5.
- [22] P. Chopade, *et al.*, "Reactive power management and voltage control of large Transmission System using SVC (Static VAR Compensator)," in *Southeastcon, 2011 Proceedings of IEEE*, 2011, pp. 85-90.
- [23] F. Shahnian, *et al.*, *Static Compensators (STATCOMs) in Power Systems*: Springer, 2014.
- [24] S. Gupta, *et al.*, "Voltage stability improvement in power systems using facts controllers: State-of-the-art review," in *Power, Control and Embedded Systems (ICPCES), 2010 International Conference on*, 2010, pp. 1-8.
- [25] P. Kundur, *Power system stability and control*: Tata McGraw-Hill Education, 1994.
- [26] A. Elansari, *et al.*, "Optimal location for shunt connected reactive power compensation," in *Power Engineering Conference (UPEC), 2014 49th International Universities*, 2014, pp. 1-6.
- [27] Z. Gajic and S. Aganovic, "Advanced tapchanger control to counteract power system voltage instability," *ABB AB, Substation Automation Products*, 2006.
- [28] C. H. Hartmann, *et al.*, "Voltage Collapse Mitigation Report to IEEE Power System Relaying Committee."
- [29] B. Sapkota and V. Vittal, "Dynamic VAR Planning in a Large Power System Using Trajectory Sensitivities," *Power Systems, IEEE Transactions on*, vol. 25, pp. 461-469, 2010.

Chapter four

Series connected FACTS devices

4.1 Introduction

Series compensation can improve load-ability of the tie-lines, and provide an effective solution for power flow imbalance problems in parallel lines. The controllable series reactance (capacitive or inductive) of series FACTS devices effectively allows cancellation of a portion of the series inductive reactance of the tie-line. Theoretically, series capacitive compensation reduces the electrical distance between the interconnected power systems; thus, allowing increased power transfers capacity of the tie-line because of the improved voltage and angular stability limits due to the reduction in the series impedance of the line. Additionally, an adequate change in series reactance of a certain line can change power flow direction, allowing re-balancing of the power flow in parallel transmission corridors [1, 2].

Like shunt connected VAr compensators, series FACTS devices are also classified based on the physical components and the operating principles into two main types: variable impedance and converter based series FACTS devices. Thyristor controlled series compensator (TCSC) is an example of the first type, and static synchronous series compensator (SSSC) is an example of the latter. Each type has its own $V-I$ characteristics that define its linear and nonlinear control or operation range [3-5].

The level of Load-ability improvement in a series compensated transmission line depends on the figure of merit, called compensation factor k . As the compensation factor increases, the transfer capability of the line is increased. However, a higher degree of series compensation is not desirable because of the subsynchronous resonance (SSR) risk.

In this chapter, mathematical models of TCSC and SSSC are incorporated into the generic power flow equation 2-18. New sizing and allocation approaches are introduced in this chapter. The objective of the sizing approach is to increase the tie-line load-ability while considering the risk of SSR. A two identical line segment approach for series FACTS allocating is introduced to place the series FACTS devices as close as possible to the electrical centre of the interconnection link between the power systems.

4.2 Series compensation principles

The transfer capability of a tie-line in interconnected power systems highly depends on the series reactance X_L of the tie-line, as was established by equation 2-2 in chapter 2. In addition to the series impedance, the equation indicates that the active power transfer depends on the power angle difference between the two ends of the interconnection link. Hence, the power exchange between two interconnected power systems can be increased either by reducing the effective series reactance of the tie-line (X_L) as in the case of a TCSC or by increasing the voltage across the series impedance of the line which increases the phase angle allowing further power exchange as in the case of a SSSC. Physically, the series capacitor (as in FC and TCSC) ‘cancels’ a portion of the total series inductive reactance of the line; thus, effectively shortening the line electrical distance. On the other hands, the converter based series compensation can be seen as a way to compensate a portion of voltage drop caused by the current flow through the line reactance [3, 6, 7].

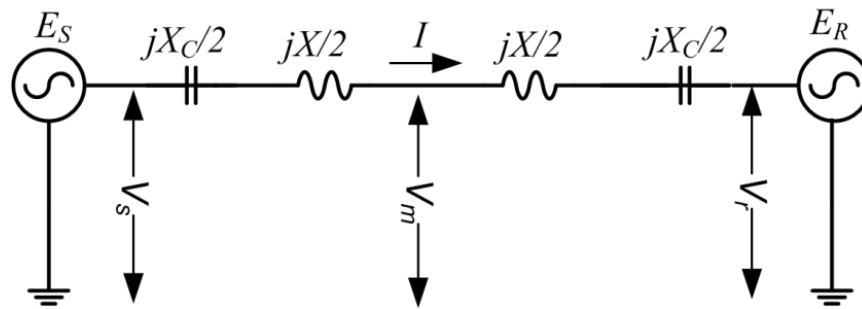


Figure 4-1: Two interconnected power systems with series compensated tie-line

Effective ways to increase the line current, and consequently increase the voltage across the series impedance of line in Figure 4-1, is to inject an opposite voltage V_C from a series compensator. For simplicity, it is assumed that the tie-line in Figure 4-1 is divided into two identical series compensated segments. The impact of the compensated tie-line on power transfer capability is illustrated by the phasor diagram representation in Figure 4-2. When the voltage magnitude at both ends of the tie-line are maintained constant, the voltage across the tie-line reactance V_x is increased by the developed voltage across the capacitor ($V_C = j\frac{1}{2}X_C I$).

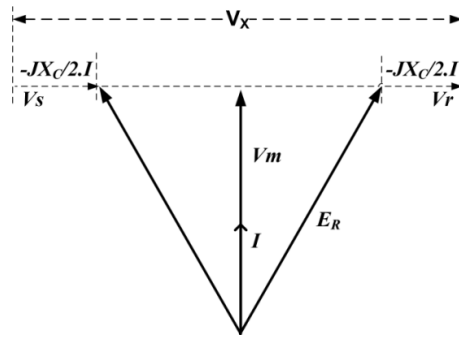


Figure 4-2: Phasor representation of two interconnected power systems with series compensation

The effective series reactance of the compensated tie-line in Figure 4-1 can be written as a function of compensation factor k as;

$$X_{total} = X_L - X_C = X_L(1 - X_C/X_L) = X_L(1 - k) \quad (4-1)$$

Where $k = X_C/X_L$ (4-2)

X_{total} is the total series reactance of the compensated tie-line after a portion of its inductive reactance X_L is cancelled by the capacitive reactance of the series compensator X_C .

Assuming the voltage along the line is maintained ($V_R = V_M = V_S$), the current in the tie-line I can be expressed, considering the total series reactance (X_{total}) as:

$$I = \frac{2 V_S}{X_{total}} \sin \frac{1}{2} \delta = \frac{2 V_S}{X_L(1 - k)} \sin \frac{1}{2} \delta \quad (4-3)$$

Hence, the active power on both sides is;

$$P_S = P_R = \frac{V_S^2}{X_{total}} \sin \delta = \frac{V_S^2}{X_L(1 - k)} \sin \delta \quad (4-4)$$

Consequently, the reactive power provided by the series capacitor is

$$Q_C = \frac{2 V_S^2 k (1 - \cos \delta)}{X(1 - k)^2} \quad (4-5)$$

Referring to the generic power flow equation 2.18 derived in chapter-2, the series inductive reactance x in the equation can be substituted by the total effective series inductive reactance of series compensated tie-line (equations(4-1)). For simplicity, the passive shunt reactive component with constant impedance q_{sh} in equation 2-18 is neglected. Hence, the power flow equation for a two interconnected power systems with k series compensated tie-line is:

$$V(pu) = \sqrt{\frac{1 - 2r.P - 2x(1-k)Q + \sqrt{1 - 4r.P - 4x(1-k)Q - 4(P.x(1-k) - Q.r)^2}}{2F_c}} \quad (4-6)$$

As the compensation factor k in equation (4-1) increases, the total series reactance of the tie-line decreases; approaching zero at $k=1$. Although a higher compensation factor allows further transfer capability, it should not exceed 75% because of: higher short circuit current during the fault and power flow imbalance in the parallel paths. Even 75% compensation is not acceptable due to the high risk of sub-synchronous resonance, and this further limits the compensation factor to less than 30%[3].

4.3 Power transfer capability improvement with series compensation

As discussed in chapter 2, voltage stability limit VSL and angular stability limit ASL are the most restrictive power transfer limits in medium and long transmission lines, where series reactance is the limiting factor for efficient power transfer. [3, 8]. Therefore, series capacitive compensation is introduced as an efficient approach to cancel a portion of the series reactance allowing more power transfer. The effect of series compensation on voltage stability limit VSL and angular stability limit ASL can be established from the generic power flow equation.

4.3.1 Voltage stability limit improvement with series compensation FACTS

A state of the art review paper on the impact of the level of series compensation on voltage stability limit is addressed in [5]. Equation (4-6) illustrates the relation between series compensation factor for a given transmission line (k), load-ability (P) and the voltage at the receiving end (V). these parameters facilitate calculation of voltage stability limit VSL as derived in section 2.3.2. In accordance with the equation (4-6), the VSL for a series compensated line (with k compensation factor) is calculated at the loading condition (P) where the expression under the square root in the equation, is equal to zero. That is;

$$\sqrt{1 - 4r.P - 4x(1-k)Q - 4(P.x(1-k) - Q.r)^2} = 0 \quad (4-7)$$

Reactive power Q in (4-7) can be represented by the its corresponds power factor (pf) as;

$$Q = P[\tan(\cos^{-1}(pf))] \quad (4-8)$$

Considering(4-8), the positive solution of the equation (4-7) represents the voltage stability limit for a series compensated tie-line is:

$$VSL = \frac{1}{2} \frac{pf}{F_c} \times \frac{\sqrt{F_c^2 [(k-1)^2 x^2 + r^2]} + F_c [(k-1)x\rho - r.pf]}{2pf(k-1)\rho rx + [(k-1)^2 x^2 - r^2] pf^2 + r^2} \quad (4-9)$$

where $\rho = \sqrt{1 - pf^2}$

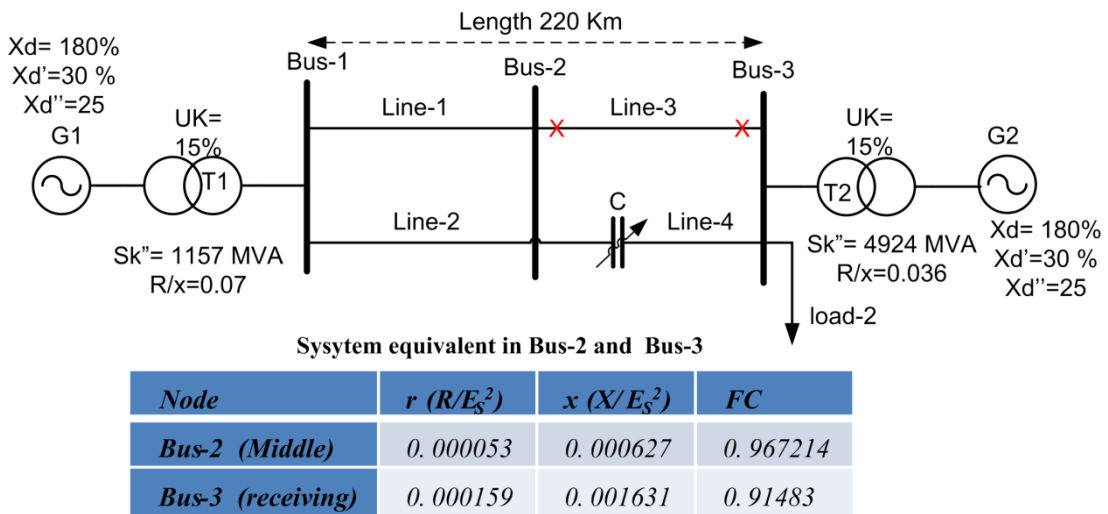


Figure 4-3: Kundur test system technical data

Figure 4-4 shows the voltage stability limit change, of the tie-line in the test system in Figure 4-3 (same test system in chapter 2), with the degree of series compensation k . VSL increases with increased capacitive series compensation reaching a maximum when theoretically the series inductive reactance is cancelled by the capacitive reactance of the series compensation ($k = 1$). However, practically exceeding a certain compensation level is not acceptable because of the LC resonance, which can be established between the capacitive inductance of the compensated line and the equivalent of the inductive reactance of the system at the PCC. The significance of this curve is that it can be used to estimate a suitable compensation factor of a series FACTS to improve the line in accordance with VSL security restrictions.

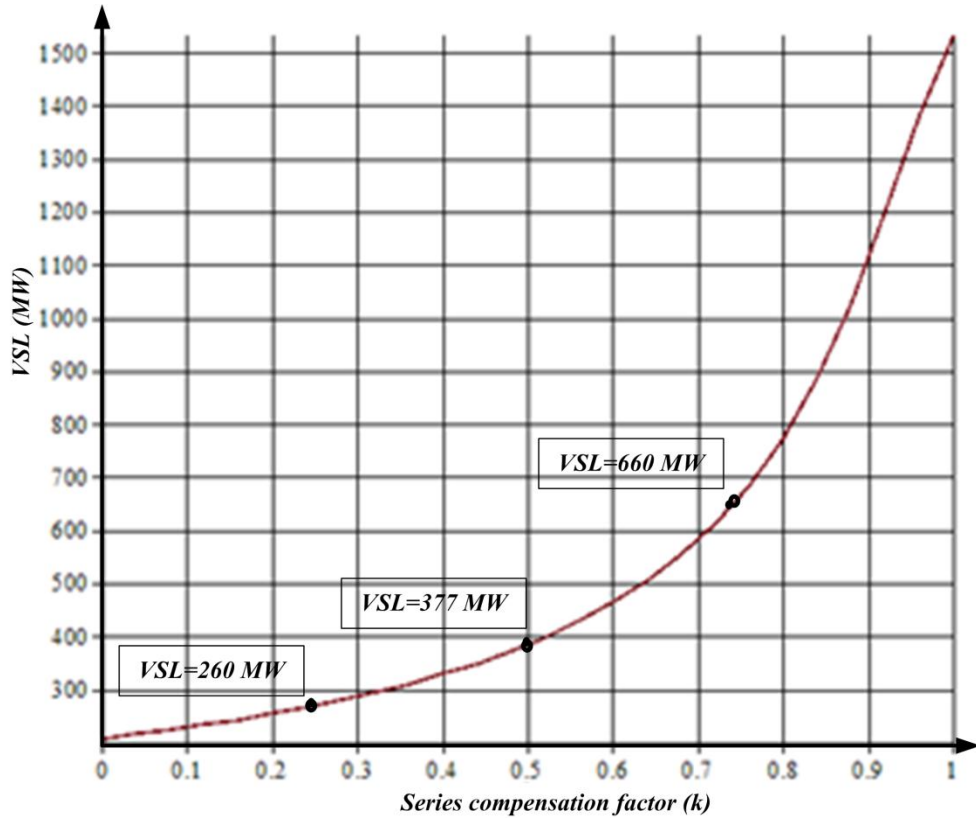


Figure 4-4: Voltage stability limit versus series compensation factor ($VSL-k$ curve)

The voltage stability limit versus compensation factor ($VSL-k$ curve) shown in Figure 4-4 corresponds to the locus of the PoC along the P axis on the $P-V$ curve. For further validation of this curve, NEPLAN software is used to establish the $P-V$ curves at different compensation factors where a variable series capacitor is used in the tie-line impedance (in series with Line-4).

Figure 4-5 shows $P-V$ curves where VSL is calculated at different series capacitive compensation levels (25%, 50% and 75%). The VSL indicated by the black points in Figure 4-4 (for 25%, 50% and 75%) correspond to the $PoCs$ of the $P-V$ curves in Figure 4-5 for the same compensating factors which validates the proposed relationship between compensation factor and voltage stability limit (equation (4-9) and Figure 4-4).

The VSL of the tie-line is dramatically improved to about 660MW with a 75% compensated tie-line. When the calculated VSL is compared with that obtained by the shunt compensation presented in section 3.8.1 of chapter 3, it can be concluded that series compensation is more effective than shunt compensation.

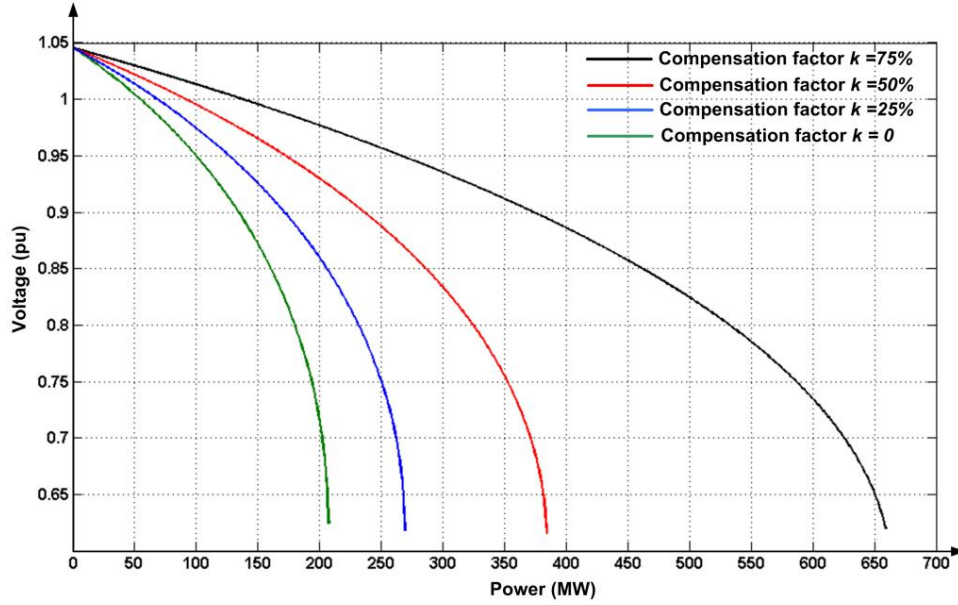


Figure 4-5: P-V curves with different series compensation factor values

4.3.2 Impact of series compensation factor on angular stability limit

The impact of a series FACTS device on angular stability limit ASL can be evaluated using equation 2-35. Based on the system parameters at a given node, this equation estimates the loading that displaces the voltage angle at that node 90° from the source. The series reactance x in 2-35 is substituted by the equivalent series reactance of the compensated line given in(4-1), which yields:

$$ASL = \left[\frac{\left(\sqrt{F_c r^2 + F_c x^2 (1-k)^2} - F_c r V \right) V}{r^2 + x^2 (1-k)^2} \right] \sin \delta; \quad \text{when } \delta=90^\circ \quad (4-10)$$

Figure 4-6 demonstrates the change of angular stability limit ASL with the level of series compensation in the test system in figure 3-4. From the figure, the ASL increases with the degree of the series compensation and reaches a maximum with slightly greater compensation factor of 80%. The steady state angular stability improvement which is achieved with a 75% series compensated tie-line in the test system in Figure 4-3 is about 1100MW, which is double that of the uncompensated tie-line.

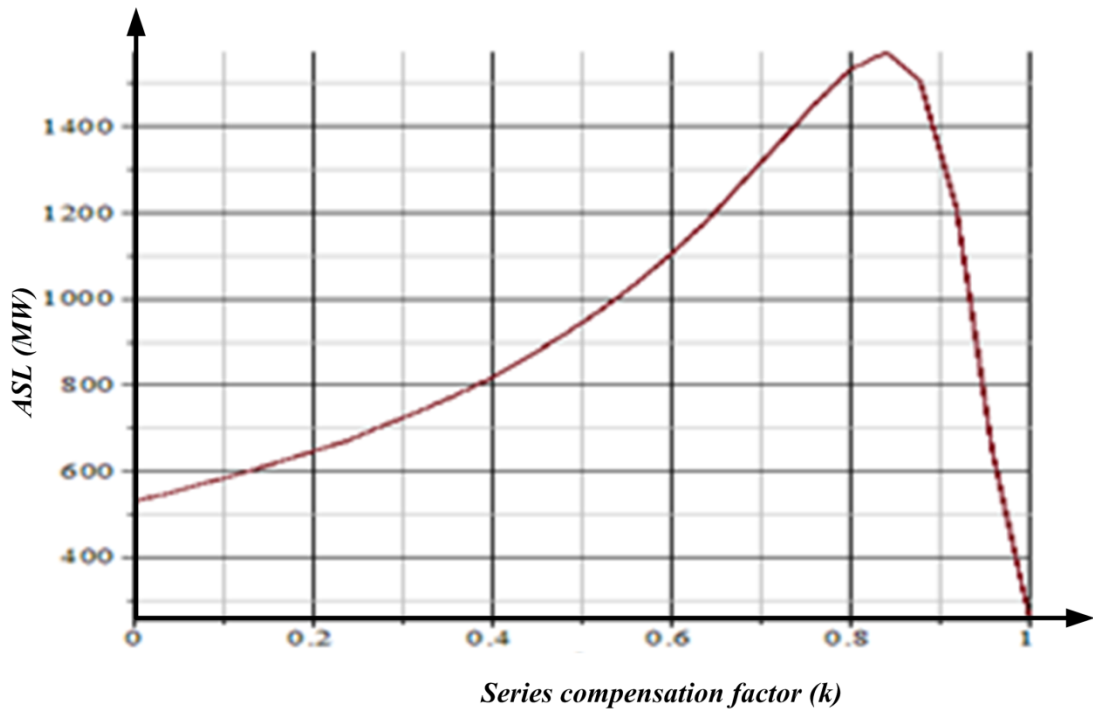


Figure 4-6: Degree of series compensation k versus angular stability limit ASL

4.4 Subsynchronous resonance

Subsynchronous resonance (SSR) phenomenon has been given an increased concern since 1970 after the Mojave generating station incidence that causes a turbine shaft failure on two generating units. SSR is an interaction between the electrical and the mechanical systems. The natural resonance frequency of the L-C circuit of a series compensated line can interact with mechanical oscillation modes generated in the rotating mechanical parts of conventional turbines.

The series capacitor of the of the compensated transmission line establishes with the series circuit inductance, including the leakage inductances of the transformers and the generating units, an L-C circuit with a natural frequency of $F_R = F_0 \sqrt{X_C / X_L}$. From the mechanical parts points of view, the rotating inertia of the mechanically coupled masses, in conventional power plants, can be represented by an equivalent electrical system that includes a series LC circuit. The capacitor C represents the system inertia that rotates with the applied AC voltage at the same rotational speed as the shaft. The inductor L represents the coupling shaft that connects all the rotating masses together[9]. Wide-ranging rotating masses in conventional turbines oscillate in a frequency range and are known as torsional oscillation. In the frequency range 10Hz

to 50Hz, the torsional oscillation can take place for individual rotors; and in conventional turbines with multiple shafts which can swing relatively to each other.

Since the compensation factor of the compensated line $k (X_c/X_L)$ ranges from 25% to 75%, F_R in the above equation indicates that the natural resonance frequency F_R is less than the synchronous power frequency F_0 . However, system disturbances can create natural resonance frequencies close to the torsional oscillation. If an oscillation is induced due to a system disturbance, some of the sub-harmonic components of the line current may create sub-harmonic fields in the machine rotor. As F_R is less than F_0 , the established sub-harmonic field rotates backwards relative to the main field creating alternating torque on the rotor at a frequency $F_0 - F_R$. If any of synchronous frequency (50 or 60 Hz) components coincide with one of the torsional frequencies (F_m) of the rotating mechanical system, the sub-synchronous resonance can be introduced into the system. This phenomenon can further excite interaction between the mechanical and electrical systems[10, 11].

4.4.1 Calculation of natural resonance frequency for series compensated tie-line

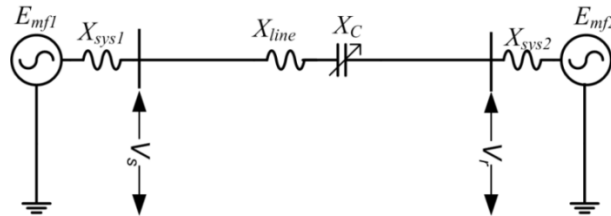


Figure 4-7: Effective series reactance between two interconnected power systems with a series compensated tie-line

The system at both ends of the interconnection link can be represented by equivalent voltage sources behind reactance X_{sys1} and X_{sys2} , as shown in Figure 4-7. These impedances determine the short circuit level and consequently the system performance at each end. Therefore, the equivalent of series inductive reactance between voltage source terminals (E_{mf1} and E_{mf2}) in Figure 4-7 is:

$$X_{system} = X_{sys1} + X_{line} + X_{sys2} \quad (4-11)$$

The natural resonance frequency of the system in Figure 4-7 occurs at conditions where

$$X_{system} = X_c \quad (4-12)$$

Therefore, the system natural frequency is given by; [12]

$$F_R = \frac{1}{2\pi\sqrt{L_{system} C_{comp}}} \quad (4-13)$$

where L_{system} is the series inductance of the system ($L_{sys1}+L_{sys2}+L_{line}$), and C_{comp} is the capacitance of the series compensation device.

The inductance and capacitance L_{system} and C_{comp} in (4-13) can be expressed by their inductive and capacitive reactance as;

$$F_R = f_0 \sqrt{\frac{X_c}{X_{L_{sys1}} + X_{L_{sys2}} + X_{line}}} \quad (4-14)$$

As discussed in section 4.2, the compensation factor k can be introduced:

$$F_R = f_0 \sqrt{\frac{k \cdot X_{line}}{X_{L_{sys1}} + X_{L_{sys2}} + X_{line}}} \quad (4-15)$$

For convenience, the equivalent system inductive reactances $X_{L_{sys1}}$ and $X_{L_{sys2}}$ in equation (4-15) can be represented by the short circuit levels S_1 and S_2 , at the sending and receiving ends of the tie-line, as follows:

$$F_R = f_0 \sqrt{\frac{k \cdot X_{line}}{VB^2 \left(\frac{1}{S_1} + \frac{1}{S_2} \right) + X_{line}}} \quad (4-16)$$

Equation (4-16) indicates that system strengths (S_1 and S_2), voltage level (VB) and the compensation factor determine the natural resonance frequency. A new line reactance weight index M that defines the percentage of compensated line reactance (X_{line}) to total reactance of the system ($X_{line} + X_{sys1} + X_{sys2}$) can be introduced. Then equation (4-16) can be written based on the line reactance weight index M as

$$F_R = f_0 \sqrt{k \cdot M} \quad (4-17)$$

where $M = X_{line} / (X_{line} + X_{sys1} + X_{sys2})$

The significance of introducing index M is that it allows prediction of the natural resonance frequency range according to system strength. This provides a preliminary assessment of the series compensation for a given line and at a given short circuit level.

Figure 4-8 shows the natural resonance frequency versus the compensation factor k for different levels of system strength ($M=25\%$, 50% , 75%) in the test system in

figure 4-3. In a strong system where M is low ($M=25\%$), the natural resonance frequency approaches the fundamental frequency f_0 as the degree of series compensation increases. This phenomenon can be noticed in a long compensated radial system with the strong sending end, where the series reactance of the compensated line can exceed the equivalent system reactance of the sending end. Therefore, it is essential to consider all the parameters in equation (4-16) when calculating the required level of series compensation.

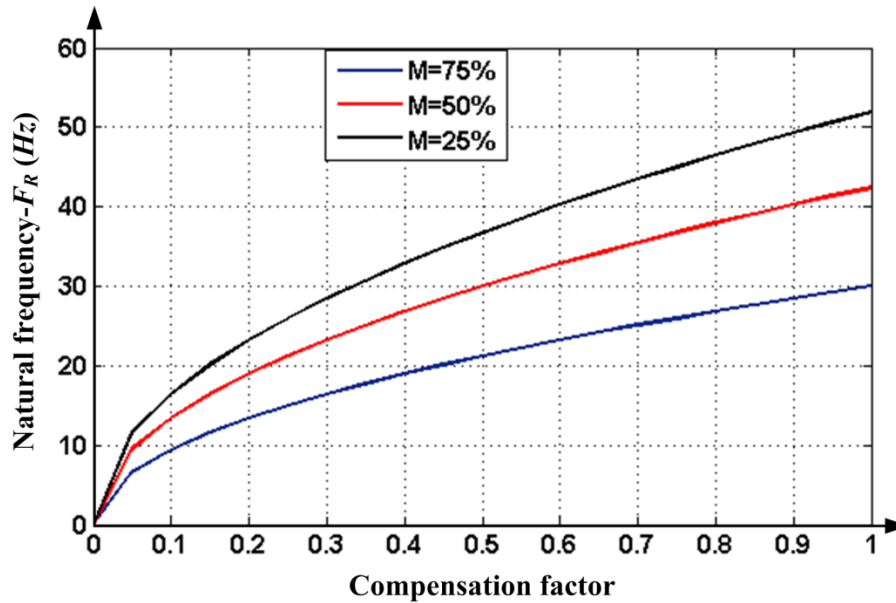


Figure 4-8: Natural resonance frequency versus compensation factor k

4.4.2 Subsynchronous resonance damping

Subsynchronous resonance is a concern, especially for variable impedance based series FACTS. A number of approaches have been suggested to introduce immunity against sub-synchronous resonance. The NGH damper approach for subsynchronous oscillations damping was introduced by N. G. Hingorani in 1981. In this approach, the compensating voltage of the series capacitor is forced to zero, at a specific instance, at the end of each half-period whenever one of the oscillatory modes of SSR is excited. This technique employs a thyristor-controlled discharge resistor in series with the limiting TCR. The discharge resistance operates synchronously with the system frequency in the region that interferes with the SSR oscillation (nearly at the end of the half cycle of the voltage capacitor). This coordinated operation of the thyristor-controlled discharge resistor, in the NGH damper, shifts the capacitor voltage at a specific SSR frequency to be almost synchronized with the line current,

as shown in Figure 4-9. This means that the NGH damper forces the series capacitor to act as a resistive rather than with a capacitive reactance characteristic at the SSR frequency [3].

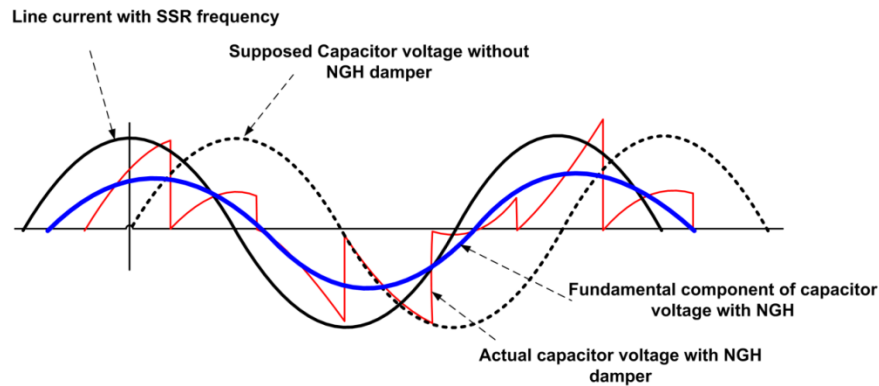


Figure 4-9: Shift of capacitor voltage by NGH Damper at SSR to be in-line with the line current [3]

From Figure 4-9, without SSR immunity, the sinusoidal line current at the SSR frequency (black curve) generates sinusoidal capacitor voltage at the SSR frequency (black dashed curve), which can be excited by the interaction of some mechanical oscillatory torsional modes or vice versa, as previously discussed. The red curve represents the actual capacitor voltage developed due to resistor discharge of the NGH damper, which acts at the end of each half-cycle interval. The fundamental of the developed voltage (blue curve) is shifted by the NGH damper to be almost in-line with the line current. This means changing the effective impedance of the TCSC from capacitive into resistive at the fundamental frequency.

With the emergence of converter based series FACTS (SSSC), different approaches have been introduced to minimize the risk of SSR.

Hybrid series compensation that consists of a passive component, such as fixed capacitor FC and VSC-based FACTS such as SSSC are used to mitigate SSR. The voltage control capability of an SSSC in hybrid series compensation allows temporary changing of the R/X ratio of the system around the SSR frequency which effectively reduces the risk of SSR [10, 13]. Some researchers claim that the TCSC with vernier operation offers adequate immunity to SSR [2, 13]. However, in the case of low line resistance, the subsynchronous damping controller (SSDC) with SSSC is preferred for damping critical torsional oscillatory modes. Many other methods, such as online estimation of sub-synchronous voltage and phase VSC based SSSC, are reported as measures of SSR immunity [13].

4.5 Allocating and sizing of series FACTS

Many approaches have been proposed for FACTS devices placement and sizing, to improve system performance. FACTS placement and sizing techniques can be classified into two main categories. The first category is a heuristic optimization technique where the FACTS allocating and sizing optimization problem is solved to find the best solution (type, number, size and location) for a given objective function. The second category adopts analytical techniques where a number of analytical indices are introduced for sizing and placement of series FACTS devices [14, 15].

Series compensation can be installed as a lumped compensation, or distributed along the tie-line. From a system security points of view, every distributed series FACTS along the compensated line has to be designed to carry 100% overload during the contingency [3]. From power transfer capability improvement points of view, lumped series compensation gives better results than a distributed compensation[16].

4.5.1 Sizing of series FACTS considering SSR

As discussed, series compensation can cause sub-synchronous resonance when the natural frequency of the established series LC resonance circuit coincides with the synchronous frequency (60/50 Hz) complement of the torsional SSR frequency. For this reason, sizing of series FACTS devices, especially when variable impedance based, should remedy the natural frequency band.

The significance of equation (4-16) is that it allows generally determination of the natural resonant frequency considering short circuit levels and the voltage levels on both sides of the compensated line.

The compensation factor k should be defined in such a way to displace the natural frequency away from the risky region of the SSR oscillatory modes. This requires knowledge of the torsional frequencies of the nearby turbines in addition to the information needed in the equation (4-16) to calculate the natural resonance frequency and its (50/60 Hz) complementary frequencies ($F_m = F_0 - F_R$).

The green curve in Figure 4-10 represents the natural resonance frequency versus compensation factor ($F_R - k$ curve) for the system in Figure 4-3, using equation (4-16). The red curve represents the complementary frequencies of 60 Hz, obtained by subtracting the resonance frequency R_F from the synchronous frequency ($F_m = 60 -$

F_R). The red points are the frequencies of some possible oscillatory modes caused by the rotational mechanical parts inside multi-mass turbine of generator 2. These mechanical oscillatory modes can be excited by the 60Hz complement of the natural resonance frequencies associated with certain compensation levels. The suitable range for series compensation for this particular system strength and configuration is from $8\% < k < 28\%$, beyond which the natural resonance frequency F_R is likely to coincide with its 60Hz complementary frequency associated with the eigenvalue $\lambda = -0.005 \pm j203$, with the oscillation of 32Hz, as shown in the figure.

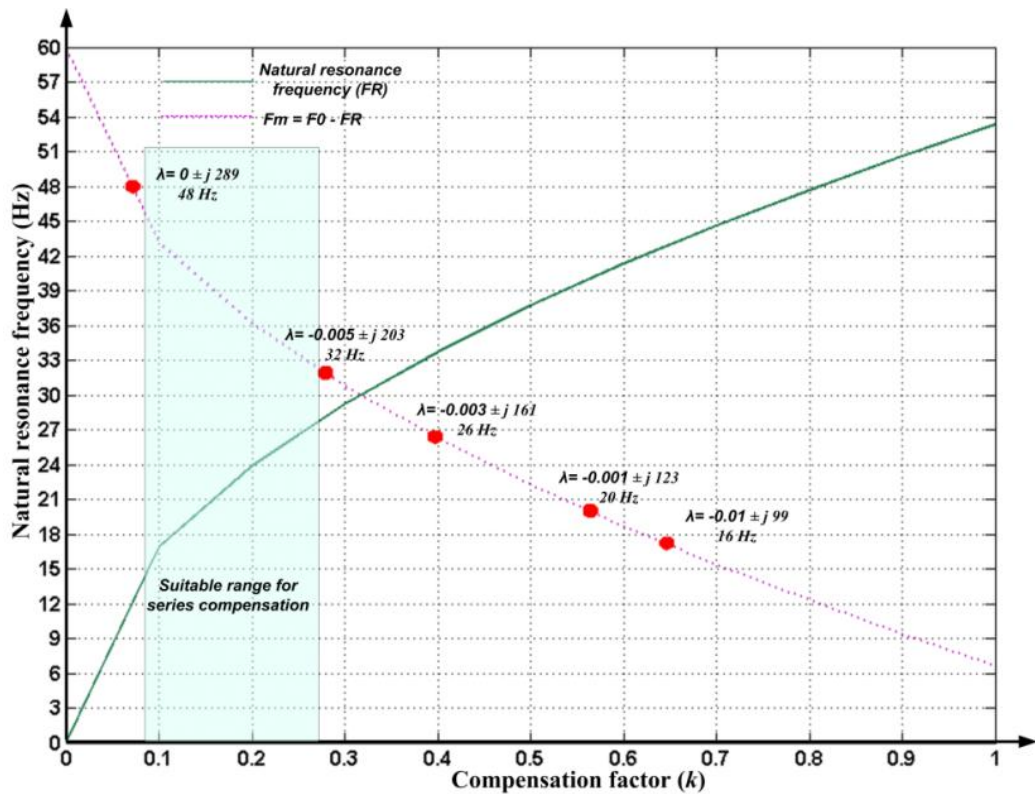


Figure 4-10: Sizing of series compensation on the basis of SSR

4.5.2 Series FACTS allocation on the basis of two identical line segments

In interconnected power systems, the tie-line mid-point normally has the largest voltage sag. The electrical centre location varies along the line based on system strengths at the sending and receiving ends, and is normally closer to the vulnerable end of the interconnection link.

Voltage support measures around the midpoint dramatically improve tie-line performance when it is composed of two identical series inductive segments, and theoretically doubles the load-ability of the tie-line as indicated by (4-4)

Lumped series compensation can displace the electrical centre of the tie-line and consequently change the impedance characteristics at the point of common coupling. If lumped series compensation is installed away from the electrical centre of interconnection link, the performance of the link may be affected during high loading conditions due to voltage sag in the middle of the weakest segment. For this reason, optimal location of the lumped series compensation has to be closer to the electrical centre of the interconnection link in order to:

- Support the voltage at the midpoint which allows further power transfer capability. Furthermore, it represents the optimal point for reactive power manipulation during disturbances as it obviously has the higher TVCI.
- Place the series compensation FACTS at the lower short circuit current along the tie-line which reduces the short-circuit current rating of the equipment.

Figure 4-11 shows a series compensated tie-line with a reactance X that connects two interconnected power systems with $MVA1$ and $MVA2$ short circuit levels. The effective series reactance of the tie-line is reduced by the compensation factor k given by(4-1).

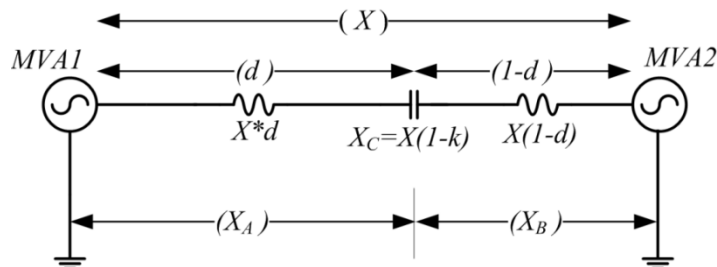


Figure 4-11: Two identical line segments approach for Series FACTS sizing and allocating

Assume that the series compensation with $X_C=X(1-k)$ is established at distance d from the power system with $MVA1$ strength as illustrated in Figure 4-11.

The series reactance of the system in Figure 4-11 can be divided into two sections. The first section (X_A) includes the lumped series compensation capacitor ($X_C=X.k$) in addition to the line inductive reactance, up to distance d . The second section (X_B) represents series reactance of the rest of the line (from d to the receiving end). Therefore, series reactance of the two sections (X_A and X_B) is given by:

$$X_A = X.d - X.k \quad 0 \leq d \leq 1 \quad (4-18)$$

Then

$$X_B = X(1-d) \quad (4-19)$$

X_A and X_B represent the fault reactances at distance d measured from the two ends of the interconnection link. Hence, these reactances can be expressed, as a function of short circuit levels at the sending end, receiving end and at distance d by equations (4-20) and (4-21) respectively:

$$X_A = \frac{V^2}{S_{M1}} - \frac{V^2}{S_1} \quad (4-20)$$

$$X_B = \frac{V^2}{S_{M2}} - \frac{V^2}{S_2} \quad (4-21)$$

where S_1 and S_2 are the short circuit levels at the interconnection ends, and S_{M1} and S_{M2} refer to the short circuit levels at distance d .

In an attempt to place lumped series compensation close to the electrical centre of a tie-line, distance (d) should be calculated to provide a balanced current contribution for a fault at the distance d . That is, S_{M1} in (4-20) has to equal S_{M2} in (4-21). This can be expressed by:

$$S_{M1} = S_{M2} \quad \text{or} \quad \frac{S_1 V^2}{S_1 X_A + V^2} = \frac{S_2 V^2}{S_2 X_B + V^2} \quad (4-22)$$

From this discussion, the optimal location for lumped series compensation is calculated from equations (4-19) and (4-22) as

$$d = \frac{S_1 S_2 (1+k)X + (S_1 - S_2)V^2}{2(S_1 S_2 X)} \quad (4-23)$$

This equation determines the electrical centre at the point that divides the series reactance of a compensated tie-line into two identical segments considering the compensation factor k in addition to the effect of system strengths at the sending and receiving ends of the tie line.

Assuming a 30% compensated tie-line in the test system in chapter 2, equation (4-23) indicates that, for the same system strengths, the optimal location for lumped series compensation lies at about 65% from the sending end side (close to bus 8).

4.6 Thyristor controlled series compensator (TCSC)

The thyristor controlled series compensator (*TCSC*) was introduced in the mid-eighties by Vithayathil [17]. It is classified as a type of variable impedance series compensator that employs a fixed series capacitor *FC* shunted by *TCR* that represents the reactive power energy storage, as shown in Figure 4-12. *TCR* provides, at the fundamental frequency, controllable inductive reactance by the means of firing delay angle α . The *TCSC* structure, with controllable inductive and capacitive reactance's from the *TCR* and the parallel fixed capacitor *FC*, provides a continuously controllable series capacitor [3, 18].

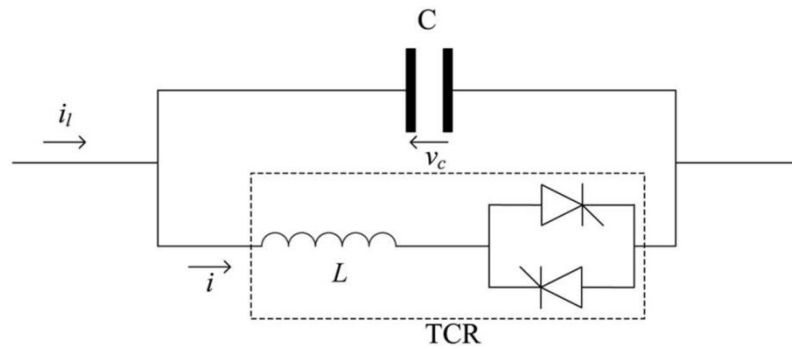


Figure 4-12: Thyristor controlled series compensation (TCSC) topology[18]

4.6.1 Operating principle of the TCSC

The total effective reactance of the *TCSC* (X_{TCSC}) is the parallel equivalent reactance of the fixed capacitor X_C , and the shunted reactance $X_{L(\alpha)}$ determined by the firing delay angle of the *TCR*, as addressed in chapter 3. Therefore, the steady state reactance of the *TCSC* is:

$$X_{TCSC} = \frac{X_C X_{L(\alpha)}}{X_{L(\alpha)} - X_C} \quad (4-24)$$

where $X_{L(\alpha)}$ is the effective inductive reactance of the TCR, given as a function of firing delay angle α as;

$$X_{L(\alpha)} = X_L \frac{\pi}{\pi - 2\alpha - \sin \alpha} \quad (4-25)$$

Substituting $X_{L(\alpha)}$ into equation (4-24) by that calculated in (4-25) allows calculation of the effective reactance of the TCSC (X_{TCSC}) at a given firing delay angle (α):

$$X_{TCSC} = - \left[\frac{2C.L.\pi^4 f^2 - \pi.\sin(2\alpha) + 2.\pi.\alpha - 4\alpha^2}{\pi.f.C(4C.L.\pi^4 f^2 - \pi^2 + 4\pi.\alpha - 4\alpha^2)} \right] \quad (4-26)$$

The Capacitor and parallel inductor of the TCSC (L and C) in equation (4-26) can be represented by their capacitive and inductive reactances at the fundamental frequency f_0 as;

$$X_{TCSC} = \frac{X_C(2\alpha(\pi - 2\alpha)X_C + \pi^2 X_{L_{TCSC}} - \pi \sin(2\alpha)X_C)}{X_C(\pi - 2\alpha)^2 - \pi^2 X_{L_{TCSC}}} \quad (4-27)$$

Equation (4-27) indicates that the effective reactance of the TCSC can be controlled, by the means of TCR firing delay angle, varying from minimum capacitive reactance ($X_{TCSCmin}$) of $(1/\omega C)$ to infinity which is coincident with parallel resonance occurrence where ($X_C = X_{L(\omega)}$). As the inductive reactance of the TCR ($X_{L(\omega)}$) further decreases, the effective TCSC reactance (X_{TCSC}) become inductive reaching its minimum value of X_{LTCSC} when the firing angle delay α equals zero, and the fixed capacitor is bypassed by the TCR. For this reason, the operation of TCSC is defined by two operating zones around its prohibited internal resonance as shown in Figure 4-13.

Figure 4-13 shows TCSC reactance versus firing delay angle α for a 75% series compensated tie-line in the kundur test system in figure 4-3. This curve is obtained using equation (4-27) assuming that 75% of the series inductive reactance of the tie-line in the figure 3-10 is compensated by the capacitive reactance of the TCSC.

The inductive operating region of the TCSC lies within the firing angle range of $0 \leq \alpha \leq \alpha_{Lim}$ (0° to 50°). This range of operation is rarely used during normal TCSC operation. However, the inductive operation mode of the TCSC can be effectively used during congestion to change the power flow, and also can be used to control power flow during system disturbance to damp power oscillation during system acceleration.

The prohibited firing delay angle zone is shown shaded, and is defined by the firing delay angle range of $L_{lim} \leq \alpha \leq \alpha_{Clim}$ (50° to 69°), which indicates the parallel resonance at $X_C = X_{L(\alpha)}$. The resonance occurs at the firing angle where the denominator in the equation (4-26) approaches zero, and can be calculated as

$$\alpha_{RES} = \frac{1}{2} \pi (1 + \omega_0 \sqrt{CL}) \quad (4-28)$$

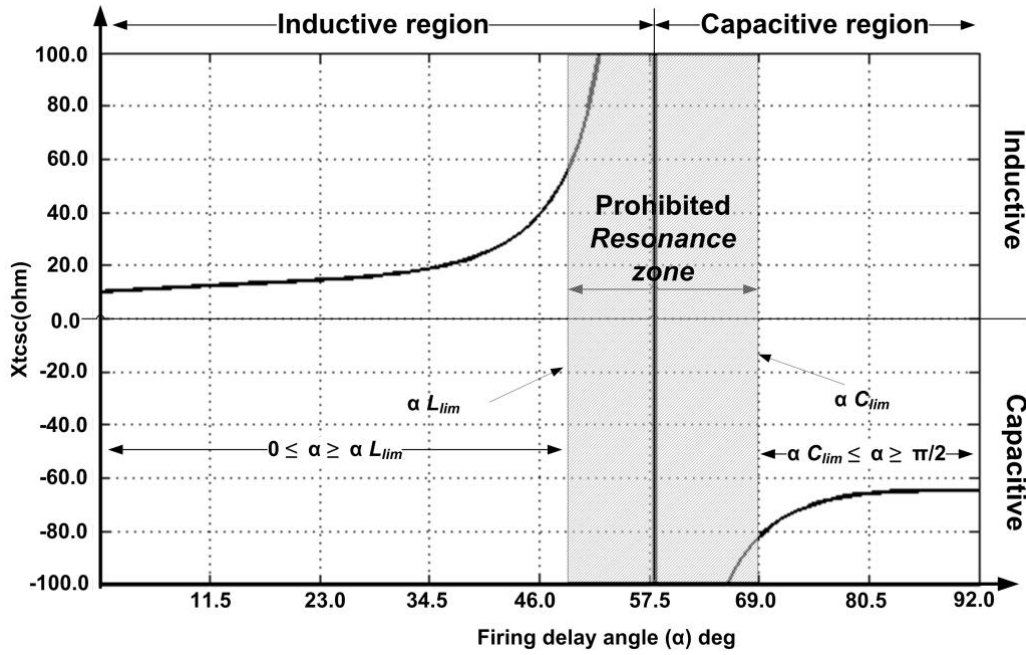


Figure 4-13: TCSC reactance versus firing angle delay α [$FC=40\mu\text{F}$, $L=22.8\text{mH}$]

With a reasonable L/C ratio (0.1333) for the $TCSC$, equation (4-28) indicates that parallel resonance occurs around a 57.5° firing delay angle for the 75% compensated tie-line in the test system. The $TCSC$ normally operates in a capacitive mode in order to achieve most of the desired aims and improvements. Figure 4-13 indicates that the capacitive operation zone of the $TCSC$ is defined within the range of $\alpha_{Clim} \leq \alpha \leq \frac{1}{2}\pi$ (70° to 90°).

4.6.2 $V-I$ characteristics of the $TCSC$

The capacitive and inductive region of the $TCSC$ is determined by the firing delay angle of the TCR as illustrated in the previous section. Therefore, $TCSC$ $V-I$ characteristics should be used to define the limits of firing delay angles α_{Clim} and α_{Llim} as shown in Figure 4-14. The minimum delay angle α_{Clim} in the capacitive region defines the maximum compensation voltage V_{Cmax} based on the line current. $TCSC$ operation is constrained by V_{Cmax} up to the minimum line current I_{min} . Beyond this operating point, the maximum line current I_{max} constrains $TCSC$ operation.

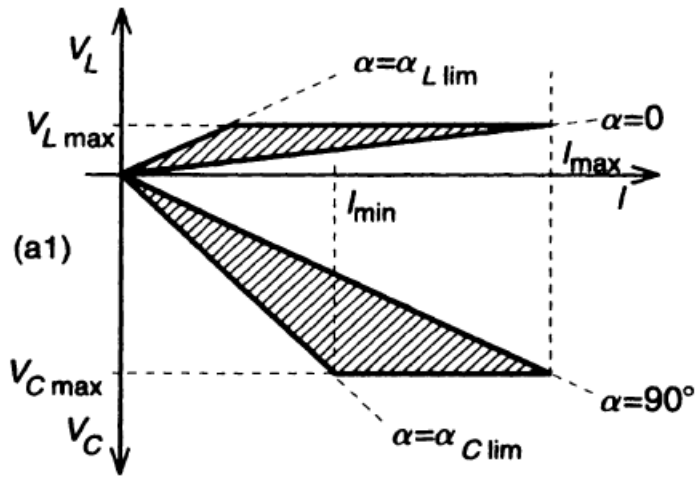


Figure 4-14: V - I characteristics of TCSC [3]

During inductive operation, the maximum delay angle α_{Lim} determines the boundary of the V - I characteristics. This means that α_{Lim} limits the maximum compensating voltage at the low line current and limits the maximum thyristor current at high line current. The V - I characteristic in Figure 4-14 can be translated into the relation between line current and compensation reactance, as shown in Figure 4-15.

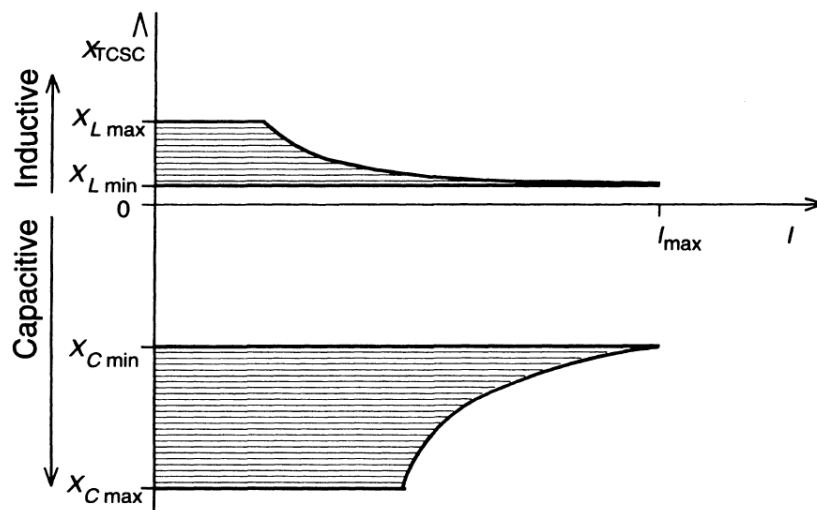


Figure 4-15: Reactance versus current characteristic of TCSC [3]

It can be concluded from this figure that in order to achieve constant compensation voltage (voltage compensation mode operation), the TCSC effective reactance has to be adjusted as the line current varies with the magnitude of transmitted power over the tie line. In contrast, the constant impedance operation mode of the TCSC requires variation of the compensation voltage in accordance with line current change.

The maximum voltage and current ratings of the TCSC are designed values that rate the TCSC components (reactor and capacitor banks and the thyristor valve) to meet the desired application requirements.

4.6.3 Natural resonance frequency with TCSC

As discussed, the effective reactance of the TCSC, as shown in Figure 4-10, determines the natural resonance frequency of the established LC circuit. Substituting X_C in equation (4-14) with the effective reactance of the TCSC given in equation (4-27) allows determination of natural resonance frequency as a function of TCSC firing delay angle α . Therefore the natural resonance frequency at any TCR TCSC firing angle delay can be estimated by:

$$F_R = f_0 \sqrt{\frac{X_C}{X_T} \times \frac{\left[\frac{\pi^2 X_{Lcsc}}{X_C} - \pi \sin(2\alpha) + 2\pi\alpha - 4\alpha^2 \right]}{\left[\frac{\pi^2 X_{Lcsc}}{X_C} - \pi^2 + 4\pi\alpha - 4\alpha^2 \right]}} \quad (4-29)$$

where $X_T = X_{Lsys1} + X_{Lsys2} + X_{Line}$

X_C in this equation can be represented by the compensation factor k and the inductive reactance of the compensated line as:

$$F_R = f_0 \sqrt{\frac{kX_{Line}}{X_T} \times \frac{\left[\frac{\pi^2 X_{Lcsc}}{k.X_{Line}} - \pi \sin(2\alpha) + 2\pi\alpha - 4\alpha^2 \right]}{\left[\frac{\pi^2 X_{Lcsc}}{kX_{Line}} - \pi^2 + 4\pi\alpha - 4\alpha^2 \right]}} \quad (4-30)$$

The significant of equation (4-30) is that it considers system parameters (system strengths on both sides), compensation factor k , and TCR firing delay angle, that may create an undesired natural resonance frequency.

4.6.4 TCSC control principles

The reversal of the capacitor voltage, which takes place at the instant of thyristor valve switch closure at firing delay angle α , defines the output voltage waveform of the TCSC. This gives accounts for the inductor size importance compared with the capacitor in the LC circuit of the TCSC. X_{Lcsc} is calculated as a fraction of X_C which should be chosen to be much smaller than the capacitive reactance of the fixed capacitor (typically 0.1 to 0.3) [3]. Practically, a small L/C ratio in the TCSC is

important to generate a secure voltage waveform that facilitates TCSC voltage and reactive power control. If $X_C \gg X_{L_{TCSC}}$, a well-defined reversal of the capacitor voltage is established producing a square wave across the capacitor. As a result, controlled and uncontrolled voltages together define the TCSC output voltage wave. The controlled square wave voltage V_{Ccr} in Figure 4-16b is added to the uncontrolled voltage V_{C0} in Figure 4-16a produced by the AC current flow, forming the relatively controllable output voltage shown in Figure 4-16-c. In other words, the output voltage includes a controlled square wave (V_{Ccr}), where the square wave voltage magnitude is controlled by the TCR reverse charge, and uncontrolled voltage component determined by the capacitor current flow.

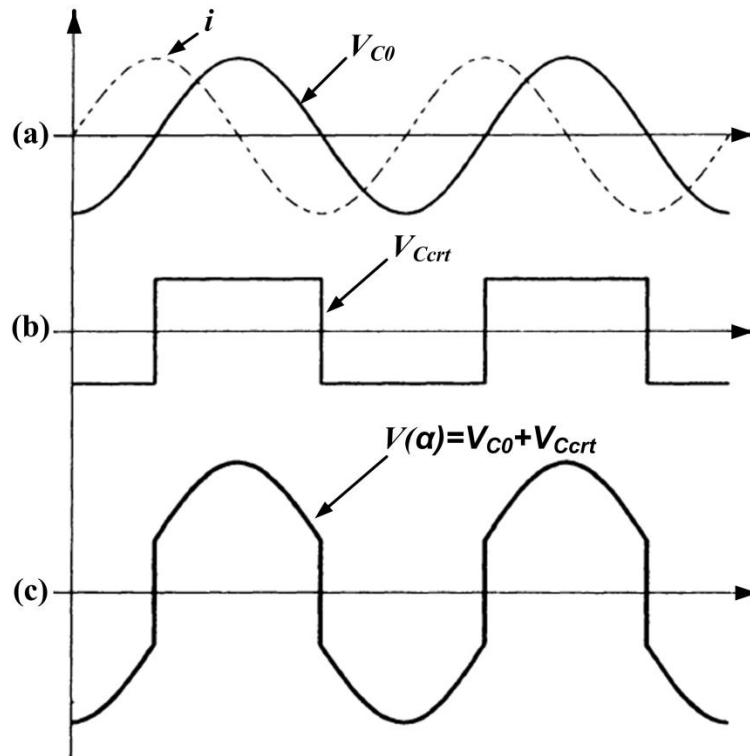


Figure 4-16: Ideal TCSC compensating voltage waveform ($V_c(a)$)

The TCSC control principle is inspired by the presented idea that allows controlling the output voltage in response to the system requirements by adjusting the TCR firing delay angle. The TCSC control system can be seen as an impedance amplifier, which adjusts its reactance in accordance with system requirements. The TCSC control structure is shown in Figure 4-17, and it includes external and internal controllers. The main objective of the external controller (system control) is to operate the controllable reactive power impedance to achieve the required level of

line compensation. From Figure 4-17, the external controller measurements can be line impedance, power, current or angle. According to the compensation objective, the measured signal, which can be actual capacitive reactance or compensation voltage, is compared with the input reference signal to achieve the desired system operation.

The operating reference is passed to the internal controller whose function is to define, in respect to the line current at the fundamental frequency, the conduction and blocking intervals of the TCR valve. As shown in the internal control in Figure 4-17, it requires simultaneous execution of three basic functions: synchronization with line current, firing angle computation and gating pattern generation within a specified interval. The internal control defines and generates the effective TCSC reactance at the fundamental frequency. The internal control has a protection system to protect the TCSC components during normal operation by current limiting or initiating a bypass path.

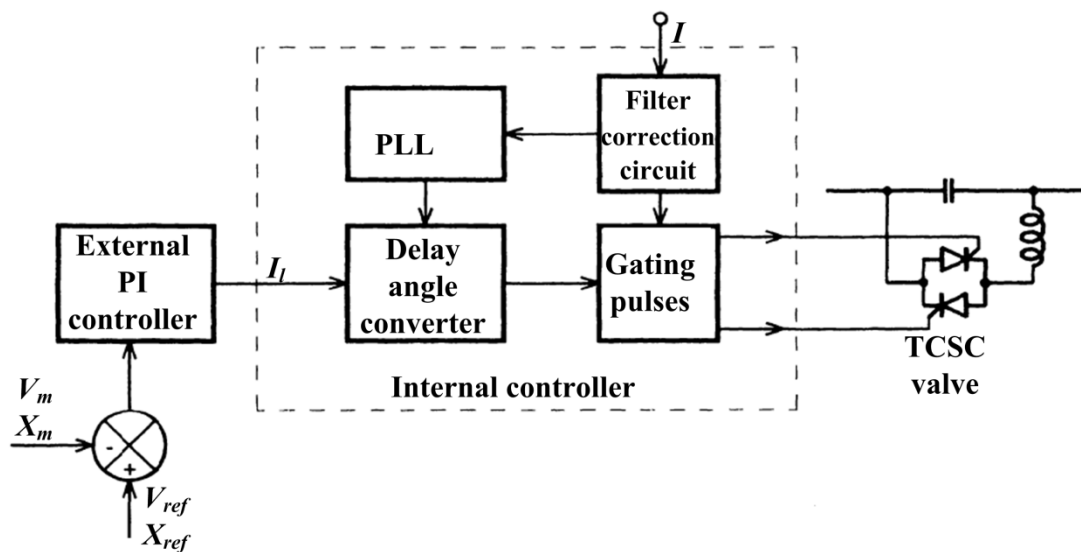


Figure 4-17: Simple control structure of the TCSC [3]

The TCSC internal control is designed to avoid sub-synchronous resonance. For this reason, as seen in the figure, the phase-locked-loop PLL system should include a filtering system to remove subsynchronous components from the line current which in turns provides correct phase information for successful synchronization.

4.7 Static synchronous series compensator (SSSC)

The static synchronous series compensator (SSSC) is a converter based series FACTS device. A self-commutated voltage source converter was proposed by Gyugyi in 1989 as a promising technique for shunt and series compensation. This type of converters provides controllable reactive power by circulating the alternating current among the phases [3]. The SSSC VSC technique provides an independently controllable output voltage in quadrature with the line current [19]. As in the variable impedance series FACTS devices (TCSC), the converter based series FACTS devices (SSSC) decrease the overall series inductive reactance of the line by compensating a portion of the voltage drop in the tie-line, which in turn improves dynamic behaviour, and also increase system utilization [20].

4.7.1 SSSC operation principles

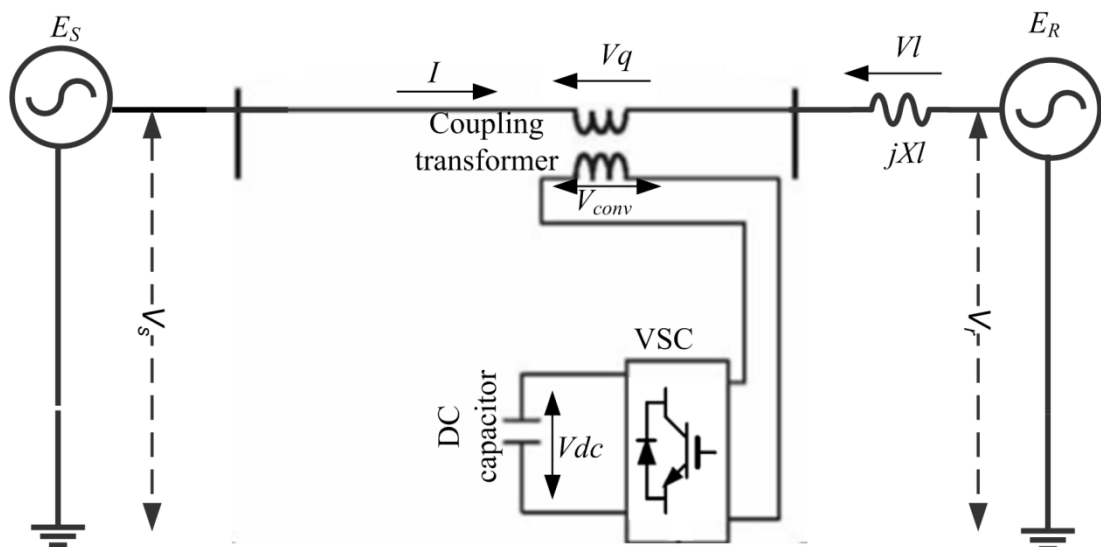


Figure 4-18: Two interconnected power systems with an SSSC compensated tie-line

Figure 4-18 shows an SSSC compensated tie-line in a two source interconnected power system. The general SSSC structure consists of a coupling transformer which couples the SSSC to the transmission line, a voltage source converter, and a DC capacitor [21].

SSSC produces voltage V_q in the series line which opposes the line reactance voltage at a given line current. The voltage drop across the series line reactance is increased by injected voltage from the series compensation V_q . Figure 4-19 shows the phasor diagram representation for Figure 4-18.

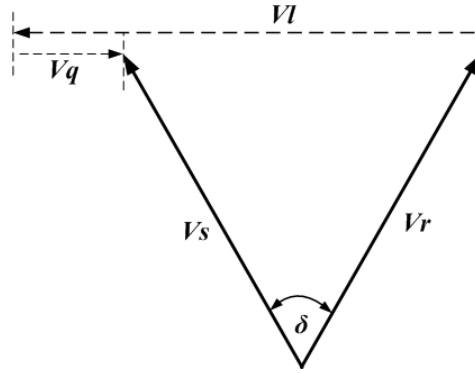


Figure 4-19: Phasor diagram for converter based series compensation (SSSC)

Theoretically, the voltage across the series capacitor V_C in the variable impedance based series FACTS shown in Figure 4-12, can be provided by a synchronous ac voltage source V_q whose output voltage is that same as the V_C , that is

$$V_q = V_C = -jX_C I = -jK X I \quad (4-31)$$

where V_C is the voltage across the series capacitor with reactance X_C , I is the line current and K is the compensation factor ($K=X_C/X$). Equation (4-31) indicates that the SSSC can accomplish the same voltage, as that provided across the series capacitor (V_C), by making the output voltage V_q of the synchronous voltage source a function of line current I .

The voltage generated at the terminals of the voltage source converter (V_{conv}) in Figure 4-18 is scaled by the conversion ratio. As considered in chapter 3 for the converter based FACTS, the three-phase ac voltage at the converter side (V_{conv}) is generated by the dc-ac converter. The charged capacitor of the SSSC provides a sustained DC voltage which is converted by the means of pulse-width modulation PWM to a set of controllable three-phase output voltage synchronised and coupled with the ac voltage through the coupling transformer leakage inductance.

For a constant DC capacitor voltage, the SSSC ac side voltage V_{conv} in Figure 4-18 is a function of modulation index M as given by equation 3-17. Therefore, being able to control the magnitude of V_{conv} allows control of the injected voltage V_q in quadrature to the line current. This provides the ability to control the total series inductive reactance of the tie-line.

Unlike the voltage across the series capacitor of the variable impedance based FACTS that depends on the line current, the SSSC compensating voltage can be

maintained constant or controlled independently of the amplitude of the line current. Being independently of the line current allows the SSSC to provide 90 degrees lead or lag output voltage. This means the SSSC can increase or decrease the line series inductive reactance which provides a further and controllable level of power transfer.

4.7.2 Power flow equation for an SSSC series compensated tie-line

The compensation factor usable by a SSSC series compensated transmission line depends on the injected compensating voltage V_q and the line current flow I . The level of series compensation, for a transmission line with series inductive reactance X , is maintained by adjusting the injected compensating voltage V_q at a given line current I . where the compensating voltage V_q required to maintain a certain level of series compensation is given by

$$X.k = \frac{V_q}{I} \quad (4-32)$$

Using equation(4-32), the power flow equation (4-6) can be written to include the effect the SSSC series injected voltage.

$$V_{pu} = \frac{A - \sqrt{3}VB.I \left(\sqrt{1 - pf^2} \cdot \left(x - \frac{V_q}{IVB^2} \right) + pf.r \right)}{F_C} \quad (4-33)$$

where

$$A = \sqrt{(VB.I)^2 \left(6\sqrt{1 - pf^2} \cdot pf.r \left(x - \frac{V_q}{IVB^2} \right) + 3 pf^2 .r^2 - 3 pf^2 \left(x - \frac{V_q}{IVB^2} \right)^2 - 3r^2 \right) + F_C}$$

The significance of new equation (4-33) is that it allows, at any line current I , calculation of the required SSSC output voltage to maintain the voltage at the receiving end of the SSSR, the line power flow (P), the power factor at the receiving end, and the X/R ratio of the transmission line. All these parameters can be controlled by the means of V_q which can be readily adjusted to meet certain compensation objectives using PWM control of the voltage source converter. Furthermore, being able to define the required compensating voltage at any level of power transfer, facilitates optimal sizing of the converter based FACTS.

Equation (4-33) is now used to determine to what extent an SSSC can improve the transfer capability of the tie-line in the test system in Figure 4-3.

Figure 4-20 parts a and b, obtained from equations (4-33) and (4-32) respectively, show normalized power versus voltage (P - V curve at bus 3) and its corresponding compensating voltage V_q provided by an SSSC to maintain $k = 25\%$ for the series compensated tie-line of the Kundur test system in figure 4-3.

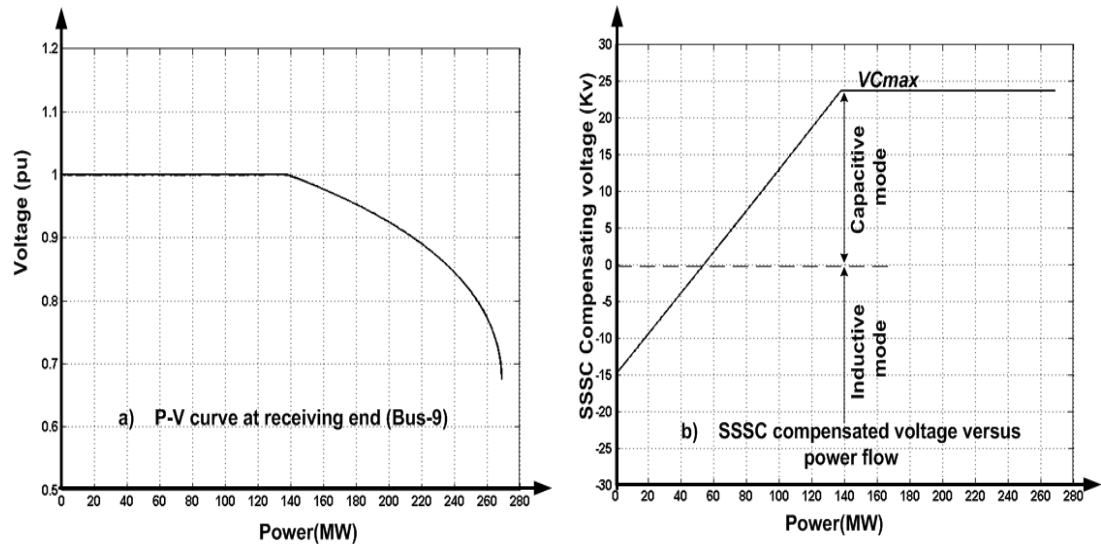


Figure 4-20: P - V curve at the receiving end in the case 25% SSSC compensated tie-line, and the compensating voltage provided by an SSSC at different line currents

The compensating voltage generated by the SSSC compensates 25% of the total series reactance of the tie-line which further increases the transfer capability of the line. Comparing Figure 4-20(a) with Figure 4-5 validates the proposed equation (4-33) as both establish almost the same VSL with a 25% compensation factor.

As the control objective is the voltage at bus-3, the SSSC maintains the voltage at its nominal value up to the maximum voltage VC_{max} , as shown in Figure 4-20(b). In order to achieve a 25% compensation factor of the line, Figure 4-20(b) shows that a 30MVA SSSC rating is required, with 25kV and 1200A ratings.

4.7.3 V - I characteristics of an SSSC

The static synchronous series compensator can operate in a voltage control mode or an impedance control mode, to achieve the desired compensation objective. It has been illustrated that the SSSC is able to provide capacitive and inductive compensating voltage independently of the line current. In the voltage compensation mode, the SSSC is controlled to maintain the voltage during line current variation from almost zero to maximum current rating as shown in Figure 4-21a. The 1 pu VA

rating of the SSSC covers a control range of a 2.0 pu VAR rating. The pu VA rating covers a control VAR range from -1.0 pu capacitive to +1.0 pu inductive [3].

In the impedance compensation mode, the SSSC is designed to provide maximum rated capacitive (X_{Cmax}) or inductive (X_{Lmax}) rating at any line current up its maximum rating, as illustrated in Figure 4-21b. Therefore, the rating of the SSSC VSC can be significantly reduced. Furthermore, SSSC can effectively serve a number of additional functions such as harmonic voltage compensation, dynamic damping.

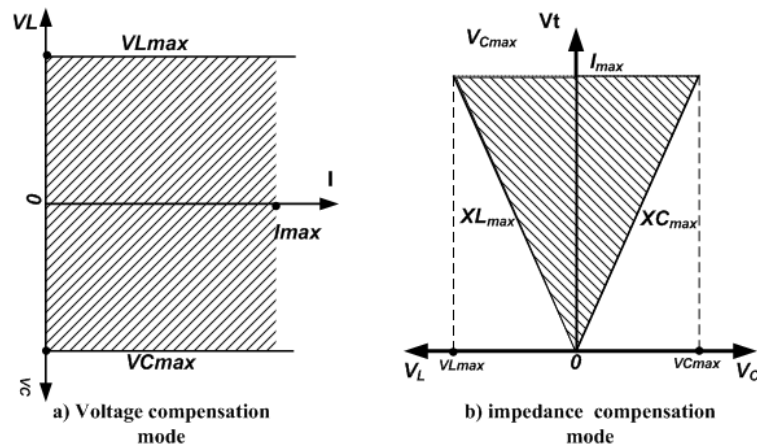


Figure 4-21: V-I Characteristic of SSSC [3]

As the inductive VAR requirement of the SSSC is minimal compared with a given line inductance. The SSSC can be accompanied with a fixed passive C. This adds series C, on the isolated side of the transformer, to compensate further line inductance. With proper control, the series C effect can be added to or subtract from the VSC across the C. The dynamic properties of the established VSC are sufficient to damp actively any resonant caused by the fixed C.

4.7.4 SSSC control principles

Similar to the TCSC structure control addressed in section 4.6.4, the converter based series compensation (SSSC) includes external and internal controllers. The SSSC operates based on the synchronous voltage source concept that employs the VSC to perform its reactive compensation functionality as discussed in chapter 3. The angle and magnitude of the VSC output voltage are controlled by manipulating the gating pattern of the VAR generator in order to achieve the desired control objective [3, 22].

As shown in Figure 4-21a, the V - I characteristics of VSC-based FACTS devices allow operation under capacitive and inductive modes. The general SSSC control structure in a capacitive operation mode is shown in Figure 4-22.

This diagram represents a reactance scheme-based controller that treats the input errors of the measured reactance (X_m) in the outer controller in response to the power flow change in the line. As a result, a proper output waveform voltage is generated to maintain power flow at a certain level.

The reactance error X_{err} is multiplied by the current amplitude $|I|$ which is passed after being phase-locked, to the voltage phase at the PCC. At this stage, the required compensating voltage reference V_{c_ref} is established with leading or lagging phase angle $\theta_i \pm \frac{1}{2}\pi$. As the VSC in the SSSC uses a fixed dc-ac gain conversion (in the case of 48-pulse $K = \sqrt[8]{6}/\pi$), the dc capacitor voltage reference V_{dc_ref} is established by multiplying the voltage reference V_{c_ref} by the gain K , as in the Figure 4-22. The capacitor dc voltage reference is processed in the internal controller to establish the desired phase angle β which is added $\theta_v \pm \frac{1}{2}\pi$ to obtain the desired magnitude and phase angle of output waveform voltage[21].

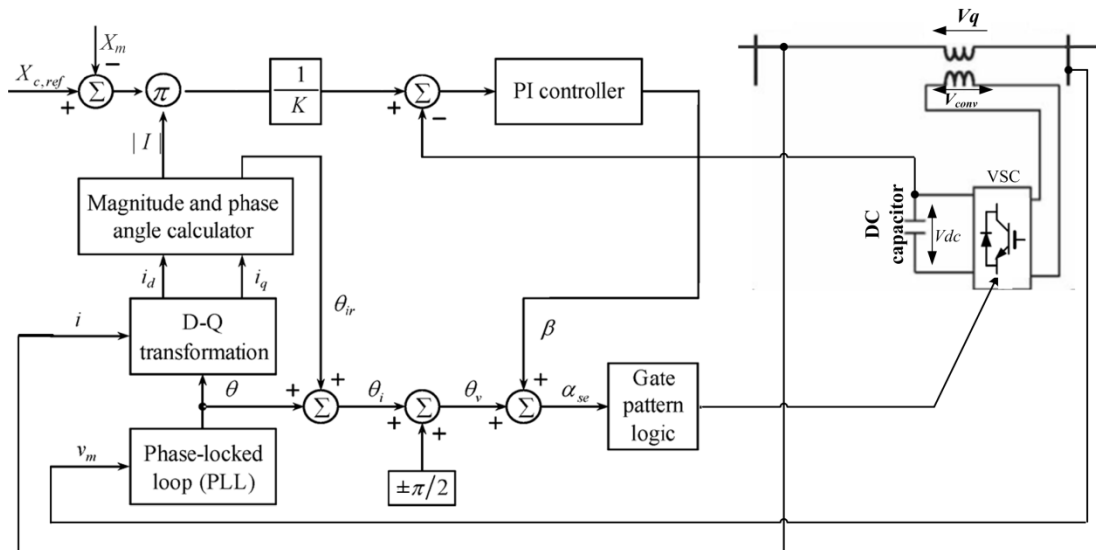


Figure 4-22: Control structure of the SSSC

4.8 Performance comparison between TCSC and SSSC

As addressed in the comparison between the VSC and the STATCOM in chapter 3, the difference in performance between the two types results from the nonsimilarity in; physical components, power circuits, and operating principles that characterize

the variable impedance and converter based FACTS. Both FACTS devices improve the power transfer capability of the tie-line. They can actively cancel a portion of the series inductive reactance of the tie-line which enhances voltage and angular stability limits of the tie-line. The main differences between the two mentioned types of the series compensators (TCSC and SSSC) are summarised are:

1. An SSSC can provide a symmetrical range for controllable capacitive or inductive compensating voltage, independent of the line current, whereas, a TCSC can only maintain the compensating voltage up to the TCR boosting current capability. Beyond this threshold, the maximum compensating voltage is determined by the TCSC $V-I$ characteristic at a given firing delay angle.
2. The voltage source converter based characteristics of the SSSC provide additional inherent power flow control capabilities not achievable with the variable impedance based characteristics of the TCSC. From a power system point of view, converter based FACTS that employ GTOs or IGBTs, operate as a synchronised voltage source. As discussed with the STATCOM, fast switching control techniques, such as PWM control provides fast response compared with that of line-commutated variable impedance types that need at least one fundamental cycle [3, 4]. Furthermore, the PWM allows the VSC based series SSSC with an external dc power source, to exchange active power with the line. This gives the ability to compensate the line resistance independent of the degree of series compensation. This feature of real power exchange is not possible for variable impedance VAR compensation types (TCSC).
3. The TCSC uses conventional thyristor which is robust and reliable semiconductors, with much higher voltage and current ratings than self-commutated devices such as IGBTs, which are employed in SSSC. Also, the TCSC is able to accommodate the necessary line fault protection requirements because of its high surge current capability.
4. The variable impedance series compensator TCSC is connected directly to the transmission line. For this reason, it is normally installed on a high voltage platform. Auxiliaries and control systems of the TCSC are located on

the ground which requires high voltage insulation. The SSSC, on the other hand, is connected to the transmission line through the coupling transformer, and this allows its installation in a building at ground possible. Therefore, the SSSC requires a relatively lower insulation voltage for the cooling and control systems[2, 3].

5. The reactance of series capacitor in the variable impedance based series FACTS (TCSC) is a function of system frequency. Therefore, at some subsynchronous frequencies, LC resonance can take place between the reactance of the series capacitor and the inductive reactance of the system as discussed in section 4.4. On the other hand, the SSSC is considered a synchronous voltage source that can supply voltage at the fundamental frequency, with the aid of the constant DC voltage. This means that the impedances of other frequencies are theoretically zero.

4.9 Summary

The level of Load-ability improvement in a series compensated transmission line depends on the compensation factor k . As the compensation factor increases, transfer capability of the line increases. However, a higher degree of series compensation is not desirable because of sub-synchronous resonance risk. As the series inductive reactance of the compensated line X_{line} increases compared with equivalent impedances, the resonance frequency F_R increases. This means that with increased system strength (the equivalent inductance decreases), the natural resonance frequency approaches the fundamental frequency f_0 as the degree of series compensation increases.

The $V-I$ characteristics of series compensation indicate that maintaining the series compensation voltage level during line load-ability change depends on the compensation technique. In the variable impedance type (TCSC) the compensation voltage is maintained by variation of the compensating reactance while it is maintained by the variation of line current in the case of converter based series FACTS (SSSC).

Load-ability improvement achieved by the series compensation is much higher than that achieved by the ideal midpoint shunt compensation for the given lossless tie-line with the same VAR rating. The proposed sizing and allocating approaches will be

examined on weak interconnection corridors in the Libyan network. As the linear operations of both types are almost the same, the analysis will focus on practical techniques available in the near term, mainly fixed capacitor and TCSC.

References

- [1] Y.-H. Song and A. Johns, *Flexible ac transmission systems (FACTS)*: IET, 1999.
- [2] X.-P. Zhang, *et al.*, *Flexible AC transmission systems: modelling and control*: Springer Science & Business Media, 2012.
- [3] N. G. Hingorani and L. Gyugyi, *Understanding FACTS: Concepts and Technology of Flexible AC Transmission Systems*: Wiley, 2000.
- [4] E. Acha, *et al.*, *FACTS: modelling and simulation in power networks*: John Wiley & Sons, 2004.
- [5] S. Gupta, *et al.*, "Voltage stability improvement in power systems using facts controllers: State-of-the-art review," in *Power, Control and Embedded Systems (ICPCES), 2010 International Conference on*, 2010, pp. 1-8.
- [6] R. Caldon, *et al.*, "An efficient modular model for static and dynamic analysis of FACTS performances on electric power systems," in *Electric Power Engineering, 1999. PowerTech Budapest 99. International Conference on*, 1999, p. 152.
- [7] A. M. Gole, *et al.*, "Guidelines for Modeling Power Electronics in Electric Power Engineering Applications," *Power Engineering Review, IEEE*, vol. 17, pp. 71-71, 1997.
- [8] B. T. Ooi, *et al.*, "Mid-point siting of FACTS devices in transmission lines," *Power Delivery, IEEE Transactions on*, vol. 12, pp. 1717-1722, 1997.
- [9] S. Purushothaman and F. de Leon, "Eliminating Subsynchronous Oscillations With an Induction Machine Damping Unit (IMDU)," *Power Systems, IEEE Transactions on*, vol. 26, pp. 225-232, 2011.
- [10] K. Padiyar, *Analysis of subsynchronous resonance in power systems*: Springer Science & Business Media, 2012.
- [11] C. E. J. Bowler, *et al.*, "Self Excited Torsional Frequency Oscillations with Series Capacitors," *Power Apparatus and Systems, IEEE Transactions on*, vol. PAS-92, pp. 1688-1695, 1973.
- [12] P. Kundur, *Power system stability and control*: Tata McGraw-Hill Education, 1994.
- [13] R. Thirumalaivasan, *et al.*, "Damping of SSR Using Subsynchronous Current Suppressor With SSSC," *Power Systems, IEEE Transactions on*, vol. 28, pp. 64-74, 2013.
- [14] A. R. Jordehi and M. Joorabian, "Optimal placement of multi-type FACTS devices in power systems using evolution strategies," in *Power Engineering and Optimization Conference (PEOCO), 2011 5th International*, 2011, pp. 352-357.
- [15] M. Gitizadeh and M. Kalantar, "A new approach for congestion management via optimal location of FACTS devices in deregulated power systems," in *Electric Utility Deregulation and Restructuring and Power Technologies, 2008. DRPT 2008. Third International Conference on*, 2008, pp. 1592-1597.

- [16] T. Masood, "Improvement of Voltage and Power Flow Control in the GCC Power Grid by using Coordinated FACTS Devices," University of Bath, 2012.
- [17] S. Shandilya, *Handbook of Research on Emerging Technologies for Electrical Power Planning, Analysis, and Optimization*, 2016.
- [18] L. Piyasinghe, *et al.*, "Impedance Model-Based SSR Analysis for TCSC Compensated Type-3 Wind Energy Delivery Systems," *Sustainable Energy, IEEE Transactions on*, vol. 6, pp. 179-187, 2015.
- [19] L. Gyugyi, *et al.*, "Static synchronous series compensator: a solid-state approach to the series compensation of transmission lines," *Power Delivery, IEEE Transactions on*, vol. 12, pp. 406-417, 1997.
- [20] H. F. Wang, "Design of SSSC damping controller to improve power system oscillation stability," in *Africon, 1999 IEEE*, 1999, pp. 495-500 vol.1.
- [21] W. Li and V. Quang-Son, "Power Flow Control and Stability Improvement of Connecting an Offshore Wind Farm to a One-Machine Infinite-Bus System Using a Static Synchronous Series Compensator," *Sustainable Energy, IEEE Transactions on*, vol. 4, pp. 358-369, 2013.
- [22] K. K. Sen and M. L. Sen, *Introduction to FACTS controllers: theory, modeling, and applications* vol. 54: John Wiley & Sons, 2009.

Chapter Five

Voltage source converter based HVDC transmission systems

5.1 Introduction

The power industry across the world has experienced significant developments in technologies related to generation, transmission and distribution systems. However, these developments are often at the expense of the environment such as harmful gases generated from the burning of fossil fuels and the impact of new infrastructure reinforcement of existing power transmission networks. This encourages energy companies to invest in the new renewable energy generation and power electronics-based technologies to improve the performance of the existing AC transmission systems to accommodate the increased penetration of the renewable energy [1, 2].

Power transfer using High Voltage Direct Current (HVDC) transmission systems remain non-competitive compared to High Voltage Alternating Current (HVAC) equivalents, at short and medium transmission distances. However, power transmission over long distances using HVAC systems has become a challenge due to line losses, charging current especially in the cables, and system instability, as discussed in chapter 2. With the emergence of semiconductors with higher voltage and current ratings, HVDC systems provide an attractive alternative for transmitting power reliably over long distances. Economic and technical considerations determine whether an HVDC system is a preferable choice compared with an HVAC system. The comparison can be made on the basis of; level of security required, fault level, line purpose, type of the transmission system (overhead line or power cable), and transmission distance[3].

Transmission distance and its investment related costs of both HVAC and HVDC transmission systems are shown in Figure 5-1. Economic comparison between AC and DC power transmission systems should include; transmission losses cost and the investment costs that include shunt reactive power requirements, AC or DC substations or terminals and the transmission lines.

For undersea power cables, the intersection between an AC system (blue line) and a DC system (red line) is a relatively short distance (about 50 km) which gives preference to the DC transmission systems [4]. This means that a DC system is more

economical than an AC system. For overhead lines, Figure 5-1 indicates that an HVAC system is favourable for distances up to 450km. At this distance, the HVDC alternative will always give the lowest cost, and is known as Break-even-distance. As the transmission distance exceeded 450km, HVDC system costs become less than those of an HVAC system; because of the required shunt compensation and higher transmission losses associated with HVAC systems [4].

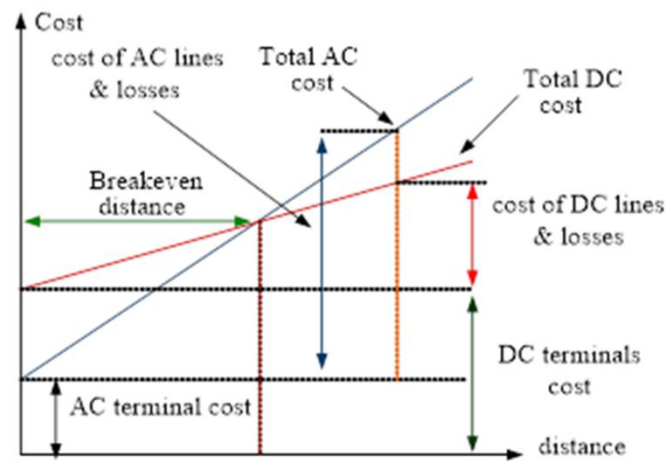


Figure 5-1: HVAC and HVDC transmission cost versus link distance [3]

In addition to the economic consideration, an HVDC system is preferable because [3, 5, 6]:

- HVDC transmission can efficiently transfer higher amounts of power over long distances, because of its relatively lower transmission losses.
- It can carry as high as 2.5 times more ampere rating than that of HVAC of the same voltage.
- Has the capability to connect asynchronous AC systems, with different frequencies.
- Offer controllable active and reactive power, which reflects positively on the system stability.
- Has less environmental impact than the HVAC system.

The first generation of HVDC transmission systems used the line-commuted converter (LCC) that controls power by delaying turning on of the thyristors relative to the natural commutating points (determined by the line voltages) [7-9].

Table 5-1: Summary of worldwide VSC-HVDC projects[10]

Project Name	Year of Commission	Power rating	Number of circuits	AC voltage	DC voltage	Length of DC cables	Comments and reasons for choosing VSC-HVDC	Topology	Semi-convertors
Hellsjön, Sweden	1997	3 MW ±3 MVar	1	10 kV (both ends)	± 10 kV	10 km Overhead lines	Test transmission. Synchronous AC grid.	2-level	IGBTs (series connected)
Gotland HVDC Light, Sweden	1999	50 MW -55 to +50 MVar	1	80 kV (both ends)	± 80 kV	2 × 70 km Submarine cables	Wind power (voltage support). Easy to get permission for underground cables.	2-level	IGBTs (series connected)
Eagle Pass, USA	2000	36MW ±36 MVar	1	138 kV (both sides)	± 15.9 kV	Back-to-back HVDC Light station	Controlled asynchronous connection for trading. Voltage control. Power exchange.	3-level NPC	IGBTs (series connected)
Tjereborg, Denmark	2000	8 MVA 7.2 MW -3 to +4 MVar	1	10.5 kV (both sides)	± 9 kV	2 × 4.3 km Submarine	Wind power. Demonstration project. Normally synchronous AC grid with variable frequency control.	2-level	IGBTs (series connected)
Terrenora Interconnection (Directlink), Australia	2000	180 MW -165 to +90 MVar	3	110 kV – Bangalore 132 kV – Mullumbimby	± 80 kV	6 × 59 km Underground cable	Energy trade. Asynchronous AC grid. Easy to get permission for underground cables.	2-level	IGBTs (series connected)
MurrayLink, Australia	2002	220 MW -150 to +140 MVar	1	132 kV – Berri 220 kV – Red Cliffs	± 150 kV	2 × 180 km Underground cable	Controlled asynchronous connection for trading. Easy to get permission for underground cables.	3-level ANPC	IGBTs (series connected)
CrossSound, USA	2002	330 MW ±150 MVar	1	345 kV – New- Heaven 138 kV – Shoreham	± 150 kV	2 × 40 km Submarine cables	Controlled synchronous connection for power exchange. Submarine cables.	3-level ANPC	IGBTs (series connected)
Troll A offshore, Norway	2005	84 MW -20 to +24 MVar	2	132 kV – Kollnesnes 56 kV - Troll	± 60 kV	4 × 70 km Submarine cables	Environment, CO ₂ tax. Long submarine cable distance. Compactness of converter on platform electrification.	2-level	IGBTs (series connected)
Estlink, Estonia-Finland	2006	350 MW ±125 MVar	1	330 kV – Estonia 400 kV – Finland	± 150 kV	2 × 31 km Underground 2 × 74 km Submarine	Length of land cable, sea crossing and non-synchronous AC systems.	2-level	IGBTs (series connected)
NORD E.ON 1, Germany	2009	400 MW	1	380 kV – Diele 170 kV – Borkum 2	± 150 kV	2 × 75 km Underground 2 × 128 km Submarine	Offshore wind farm to shore. Length of land and sea cables. Asynchronous system.	-----	IGBTs (series connected)
Caprivi Link, Namibia	2009	300 MW	1	330 kV – Zambezi 400 kV – Gerus	350 kV	970 km Overhead lines	Synchronous AC grids. Long distance, weak networks	-----	IGBTs (series connected)
Valhall offshore, Norway	2009	78 MW	1	300 kV – Lista 11 kV – Valhall	150 kV	292 km Submarine coaxial cable	Reduce cost and improve operation efficiency of the field. Minimize emission of green house gases.	2-level	IGBTs (series connected)

The performance of HVDC systems has improved with the emergence of the second generation of HVDC system that employs voltage source converter (VSC) technology which uses self-commutated IGBT switching devices. The first VSC based HVDC system with 3MW \pm 10kV PWM-controlled HVDC link of 10km was installed in March 1997 in Sweden [10]. In the context of using VSC-HVDC in renewable energy integration, BroWin1 in 2010 in Germany was the first commissioned project where a wind park of 400MW was integrated into the utility grid via \pm 150kV 75 km underground cable and 125km submarine cable[7]. Table 5-1 includes information about the installed VSC-HVDC projects worldwide.

Table 5-2: Technical comparison between VSC and LCC HVDC technologies

Cost and installation	LCC	VSC
Converter technology	Thyristor based	IGBT based
Voltage polarity	Changes with power direction	Does not changes with power direction
Current direction	Does not changes with power direction	Changes with power direction
Turn Off capability	uncontrollable	Controllable
Rating in operation (MW)	3000	350
Rating available (MW)	6400	1100
Voltage rating in operation (kV)	\pm 800	\pm 150
Voltage rating available (kV)	\pm 800	\pm 300
Operational experience	> 50 years	~ 15 years
Lifetime	30-40 years	30-40 years
losses	0.5-1.0 %	1-2.0%
investment cost	75-110 (k-Euro/MW) For \pm 350- \pm 500 1000-3000 MW	60-125 (k-Euro/MW) For \pm 150- \pm 350 350-1000 MW
System improvement		
TTC	strong	Good
Power flow control	strong	Strong
Transient stability	good	Strong
Voltage stability	limited	Good
Power oscillation damping	good	Strong
Reactive power requirements	High	Low
Reactive power support	no	Yes
Easy meshing	no	Yes
Cable line length limitation	no	No
Renewable integration ability	no	Yes

Being independently able to control active and reactive power on both sides, makes control of voltage and frequency in VSC-HVDC possible. Voltage source converter based HVDC systems have sophisticated control features compared with line commutated converter HVDC systems. For instance, independent control of active and reactive power allows feeding of passive networks, continuous control of voltage and frequency, black-starting and quick reversal of power flow[11]. On the other

hand, LCC-HVDC has higher power rating and lower power losses than VSC-HVDC [7, 12-14]. Table 5-2 summarises the main technical difference between LCC-HVDC and VSC-HVDC systems[15].

5.2 HVDC Transmission System Configurations

HVDC system configurations vary based on the desired function and converter station location. There are four common HVDC configurations that are applicable to both HVDC technologies (LCC and VSC) [10].

5.2.1 Monopolar HVDC configuration

In the monopolar configuration, the converters stations at each end of the DC link are connected through a single pole line which can be positive or negative with reference to ground. The monopole HVDC link can be configured as ground or metallic return, with ground return options offering a cost effective solution as it uses only one dc cable, see Figure 5-2(a) and (b). The metallic return also and the second terminal of the converters are connected to ground. However, the metallic return option is preferred for environmental reasons and is widely used because the metallic cable operates at ground potential; thus, low-cost insulated dc cable can be used.

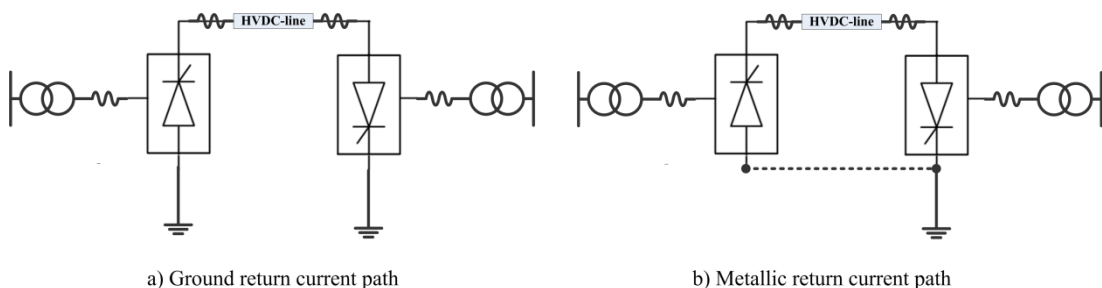


Figure 5-2: Monopolar HVDC configuration

5.2.2 Bipolar HVDC configuration

The bipolar configuration is the most commonly used topology in the line-commutated converter of HVDC. The converter station on each end of the DC link consists of two monopolar configurations. The converter valves are connected in series on the dc side. This connection provides positive and negative poles additional to an earthed midpoint as shown in Figure 5-3a. As the converters of both terminals have the same voltage rating, the currents in the positive and negative poles are equal, which results in a negligible ground current. The bipolar configuration is more

expensive than the monopolar because of additional components. However, the bipolar HVDC system is more reliable as it can operate at half a converter station rating in the case of failure of one pole, using the ground connection as the current return path Figure 5-3-b [16].

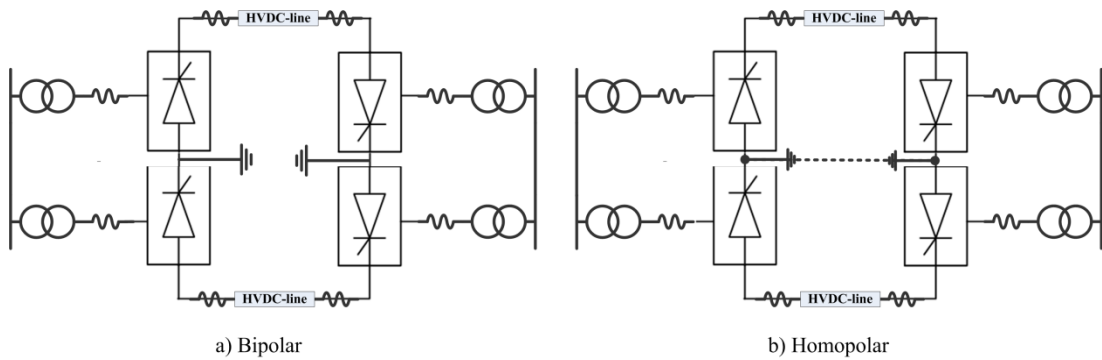


Figure 5-3: Bipolar HVDC configurations

5.2.3 Back-to-back (BTB) HVDC configuration

Figure 5-4 shows the typical back to back HVDC configuration. The two converter stations are located at the same site with an almost zero-meter-long link. Therefore, the BTB transmission losses are negligible, and is acceptable even in distribution systems with voltage levels as low as 66 or 132 kV. Furthermore, the control signals and the real-time measurements of voltage and current can be detected and treated in the unified digital controller. This feature adds more operation flexibility compared with HVDC involving a link, which requires reliable communication systems between the two remote ends of the link [17].

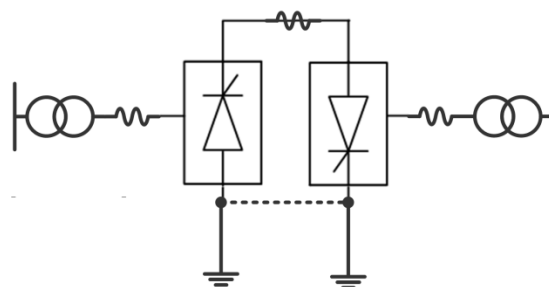


Figure 5-4: Back-to-back HVDC configuration[18]

5.2.4 Multi-terminal HVDC configuration

Both generations of HVDC transmission systems (LCC and VSC) can be configured as point-to-point HVDC link or as a multi-terminal dc network where the dc power

flows is governed by the magnitude of dc voltage at the terminals. Although most of the present HVDC projects are point-to-point configured, much research is focused on multi-terminal HVDC because of the sophisticated features of VSC technologies.

The main challenge in LCC multi-terminal is power flow control; in particular power flow reversal that requires changing the operating mode. That is, in order to change the power direction, the dc voltage polarity has to be changed by increasing the firing delay angle beyond 90° . The link current is unidirectional. This complexity is increased with multi-terminals LCC systems where power flow may continuously need to be reversed [19]. Due to this complexity only two multi-terminal HVDC systems (both LCC) have been installed worldwide:

- 1- Four multi-terminal HVDC network in Hydro Quebec-New England (USA/Canada). This project was started as point-to-point LCC HVDC with 690 MW between Des Cantons and Comerford, then extended to deliver 1800 MW and 2138 MW to other two dc terminals in Sandy Pond and Montreal [20].
- 2- Three terminal HVDC network in Italy, Italy–Corsica–Sardinia, was started as a point-to-point HVDC link that connects Corsica and Sardinia in 1965 and the third terminal was added in 1986 [21].

Unlike LCC HVDC systems, in VSC based HVDC power flow can be reversed by changing the dc current direction within the voltage source converters without the need to change the dc link voltage polarity and operating mode. As a result, faster and more flexibility of power flow control, between the dc nodes in the multi-terminal networks is provided by the VSC-HVDC than with LCC-HVDC. Furthermore, being able to control independently active and reactive power exchange at the dc terminals make it suitable for reducing the congestion in AC grids which reflects economically and technically on system performance. Moreover, the ability of VSC based multi-terminal HVDC to control active and reactive power injection in pilot nodes provides, along with a coordinated energy management system, an effective solution to the energy availability and economic dispatch of the generator units.

In multi-terminal HVDC, typically three to five terminals are connected either in series or in parallel as illustrated in Figure 5-5. In the parallel connection, the dc

voltage is controlled at one converter terminal station, and the power flow in the dc network is controlled by varying the current at other converter terminal stations. In contrast, with a series connection, the current is controlled by one converter in order to be the same in the whole system, and the power flow is controlled by varying the dc voltage at the other converters [17, 22]. Control systems, communication between different converter substations, varying dc link voltages, and fault isolation are amongst the challenges that retard the use of multi-terminal HVDC systems.

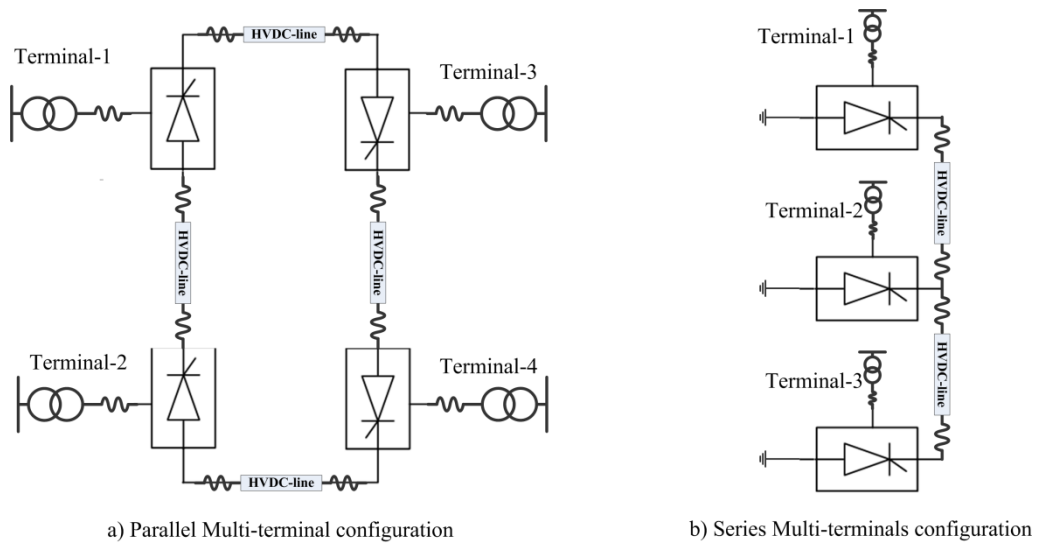


Figure 5-5: Multi-terminals HVDC configurations

5.3 VSC-HVDC transmission system components

A voltage source converter based HVDC system is typically configured as a symmetric monopole as shown in Figure 5-6. The main components of the VSC-HVDC system include; voltage source converters, coupling transformers, phase smoothing reactors, DC link (OHTL or power cable), DC link capacitor and the AC filters[13].

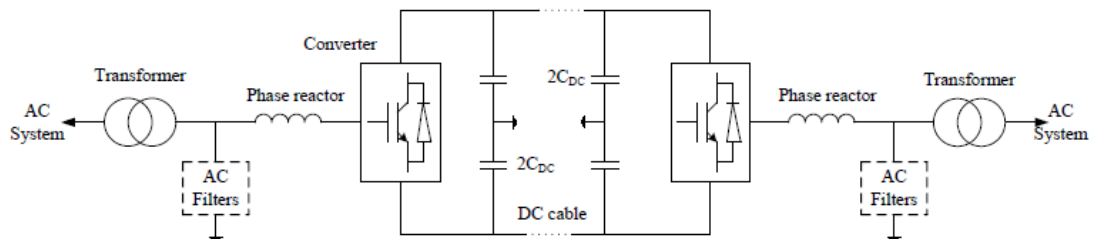


Figure 5-6: Typical voltage source converter based HVDC transmission system[13]

5.3.1 Voltage source converter

DC/AC and AC/DC conversion processes are performed by the rectifier/inverter at the two terminals of the VSC-HVDC system. The converter valve employs the Insulated-Gate Bipolar Transistor (IGBT) with turn on/off capability and freewheel diodes to facilitate current flow in both directions. The gating commands that determine the on and off intervals of the switches are generated by Pulse Width Modulation (PWM) techniques. As the voltage rating of IGBTs are relatively low (up to 6.5kV), a number of IGBTs are usually connected in series to form a single switch capable of operating at desired voltage levels for dc transmission systems (>80kV). Based on the arrangements of the switching valves in the bridge, there are three types of voltage source converters widely used:

- Two-level converter (Figure 5-7a);
- Three level diode-clamped converters such as the neutral-point-clamped (NPC) converter and its active version (Figure 5-7b); and
- Generic multilevel converters (modular and hybrid converters)- (Figure 5-8).

The two-level and three-level converters employ series connected IGBTs, while the generic multi-level converter can use or avoid the series connection of IGBTs. These types generate a large number of voltage levels per phase [13, 18]. Figure 5-7 (a and b) show the simple structure of two-level and three-level converters, and Figure 5-8 demonstrates the generic structure of the multilevel converter, which is comprised of cascaded H-bridges.

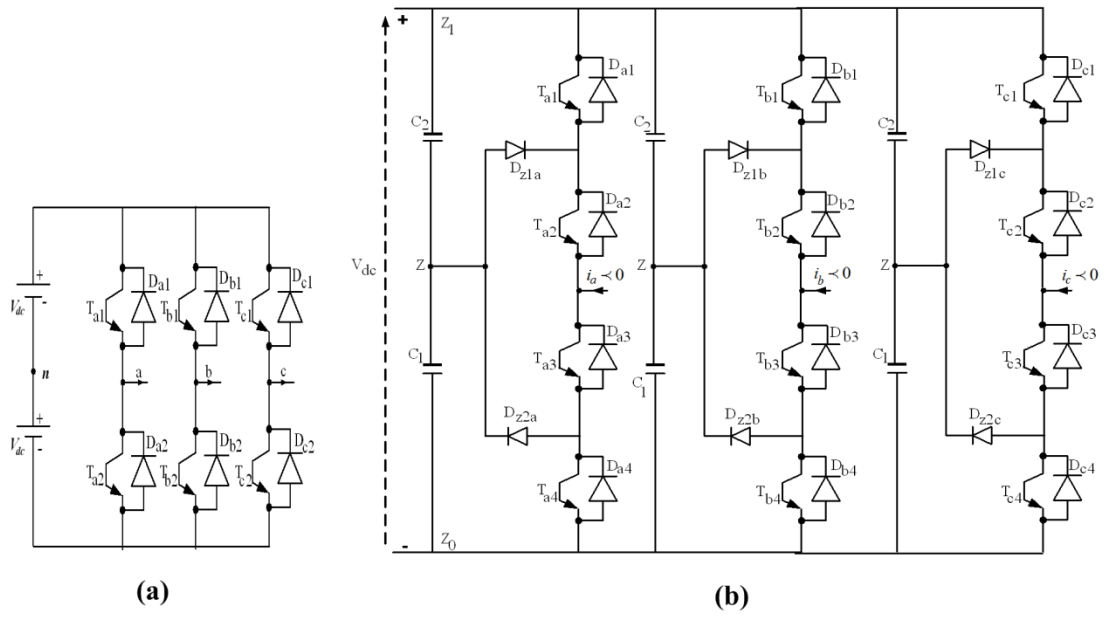


Figure 5-7: VSC-HVDC configurations[18]

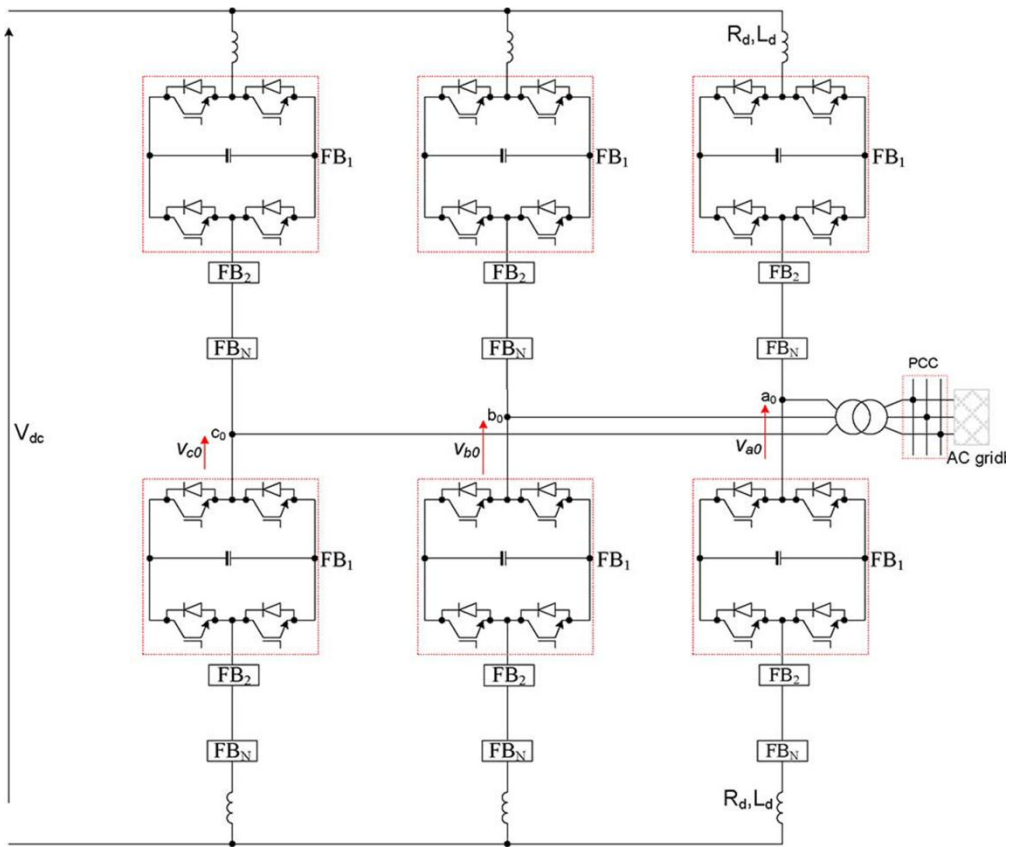


Figure 5-8: Generic multilevel converter [23]

5.3.2 Coupling transformers

The coupling transformer is normally located after the AC filter on the grid side, and its terminals are connected to the PCC as shown in Figure 5-6. The coupling transformer in a VSC-HVDC system normally has a small leakage inductance (10%-15%). This leakage operates in conjunction with the arm inductance, and the tie reactance between the HVDC link and the grid [8]. The transformer leakage inductance is important as it represents the means for reactive power exchange and active power control. Furthermore, coupling transformer is important to adapt the network grid voltage to be suitable for the dc link. Normally the transformer is equipped with a tap-changer that can help with voltage regulation[13].

5.3.3 Phase reactors

A phase reactor or converter reactor is an important component in the VSC-HVDC system because its leakage impedance (about 15%) is essential for independent control of active and reactive power. Moreover, the phase reactor functions as a low-pass filter, blocking the harmonic current components related to the high-frequency switching, thus reducing harmonic losses in the converter coupling transformer. The converter reactor with the coupling transformer defines the active and reactive power flow between ac grid and the DC link based on voltage magnitude and frequency. Furthermore, the leakage inductance and phase reactor limit fault currents [24].

5.3.4 AC filters

The AC filters are designed to eliminate undesired harmonics caused by the switching of the converter valves. A common application of VSC converters is machine drives that are relatively less sensitive to the harmonics generated in the DC link. In contrast, AC filters are essential for supplying quality sinusoidal voltage at the PCC, and fulfilling of transmission and distribution grid codes for renewable and HVDC systems integration. The filter configuration varies depending on the application and specified performance[24].

5.3.5 DC link capacitor

PWM creates a ripple in the voltage waveform of the converter generates. Therefore, the DC capacitor is essential to maintain a steady DC voltage during the switching of the valves. Furthermore, charging and discharging of the DC capacitor facilitates

maintaining the average DC voltage which can be affected by variation of the active power exchange between the DC link and the AC grid. The value of DC capacitance depends on system requirements, which should be in accordance with the switching frequency (ripple and dynamic performance)[25, 26]. Although large capacitance smoothes the ripple, it increases the response time during voltage changes. On the other hand, small DC capacitance allows faster converter response but at the expense of greater ripple. The dc capacitance is reflected in its dynamics that characterized a time constant τ . The time constant of the DC capacitor is the ratio between the stored energy at rated dc voltage and the nominal apparent power of the converter, which can be expressed by;

$$\tau = \frac{1/2 C V_{dc}^2}{S_n} \quad (5-1)$$

where V_{dc} is the nominal dc voltage, S_n is the nominal apparent power of the converter; C is the dc capacitance and τ is the time constant. The time constant represents the time needed to charge the capacitor from zero to rated DC voltage when the converter is supplied with active power corresponding to S_n . According to reference [26], the time constant τ can be selected to be less than 5ms to be consistent with small ripple and small dc over voltages.

5.3.6 DC line

Depending on the geographical topology, distance and application, DC lines can be cables or overhead lines. Unlike AC power cables where the current charging of the stray capacitance is a major concern, the use of dc in long distance HVDC transmission systems is not a barrier. For this reason, DC power cables are normally used for submarine transmission. Cross-Linked Poly-Ethylene (XLPE) cable is normally used in the HVDC link because its dc voltage resistance, low weight, mechanical strength and flexibility.

5.4 VSC-HVDC operating principle

The voltage source converter can be considered as a fast controllable synchronous machine connected to an AC system through tie inductance (X_T) that includes the phase reactor inductance and leakage inductance of the coupling transformer, as

shown in Figure 5-9. This system can be seen as controlled voltage source from the ac side and a controlled current source from the dc side [26].

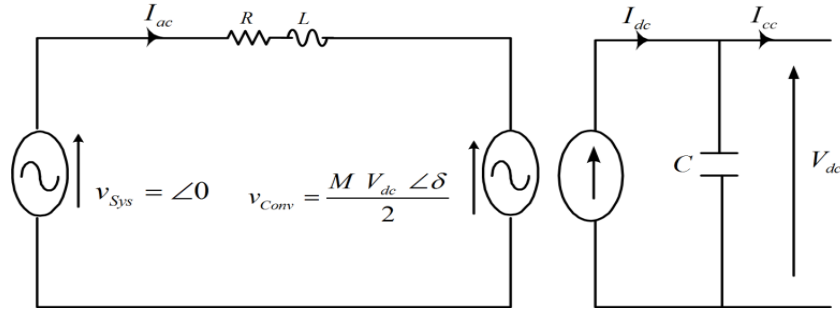


Figure 5-9: Simplified circuit diagram for VSC-HVDC terminal

The controllable voltage source is represented by the output voltage on the ac side of converter v_{Conv} which at the fundamental frequency is:

$$v_{Conv} = \frac{1}{2} M V_{dc} \sin(\omega t + \delta) \quad (5-2)$$

where M is the modulation index, ωt is the synchronous frequency, and δ is the phase shift of the converter side voltage.

The controlled current source I_{dc} from the dc side can be calculated from the dc side circuit in the Figure 5-9 as

$$I_{dc} = C \frac{dV_{dc}}{dt} + I_{cc} \quad (5-3)$$

Neglecting losses in the tie-inductance, active and reactive power at the converter side (P_{Conv} and Q_{Conv}) can be calculated in accordance with power flow theory in ac power systems.

$$P_{Conv} = \frac{V_{Conv} V_{Sys} \sin \delta}{X_T} \quad (5-4)$$

$$Q_{Conv} = \frac{V_{Conv}^2 - (V_{Conv} V_{Sys} \cos \delta)}{X_T} \quad (5-5)$$

The active and reactive power exchange between the dc link and the ac grid are functions of the magnitude and angle of the converter output voltage V_{Conv} . Hence, control of active and reactive power exchange can be achieved by adjusting the modulation index M and the phase shift δ in equation (5-2) to give any combination of active and reactive power flow [27]. Vector control methods with a synchronously

rotating dq reference frame are used with PWM to provide independent control of active and reactive power. This technique allows effective adjustment of currents i_d and i_q to obtain the required values of the magnitude and the phase shift of the converter output voltage.

In basic calculations, it is valid to neglect the resistive components of the coupling transformer and phase inductor, especially in small scale HVDC links. However, during high loading in large scale HVDC links, the losses of the tie-impedance can affect the accuracy of the power flow calculations which in turn can affect other steady-state based calculations (VSL and ASL). Inclusion of the resistive part of the coupling transformer for high power flow accuracy calculations is addressed in the next section

5.5 Power flow equation for a VSC-HVDC transmission system

Figure 5-10 shows an equivalent circuit for two ac power systems connected by VSC-HVDC link. As illustrated, two series impedances are considered for the calculation in both ac sides. The first impedance represents the tie-impedance between the PCC and the converter terminal ($Z = R+jX$), and the second impedance represents the equivalent impedance of the system seen from the PCC ($Z_n=R_n+jX_n$). The subscripts '1' and '2' represent the variable associated with the sending-end and receiving end stations, respectively. Power flow calculations in the dc side are based on the dc line resistance and inductance (R_{dc} and L_{dc}), additional to assuming fixed converter losses that are represented by R_c in Figure 5-10. The dc side model has been selected from WG B4-57 and WG B4-58 CIGRE, for the average model simulation [28].

The proposed algorithm for the power flow calculation of the system in Figure 5-10 is a cascade of three parts of the power flow calculations at the sending end, dc link and receiving end. The AC power flow parameters (P , Q , V and δ) can be mathematically calculated at points 1, 2, 5 and 6 at the AC sides while P_{dc} , V_{dc} and I_{dc} can be calculated for points 3 and 4 at the rectifier and inverter sides of the dc link.

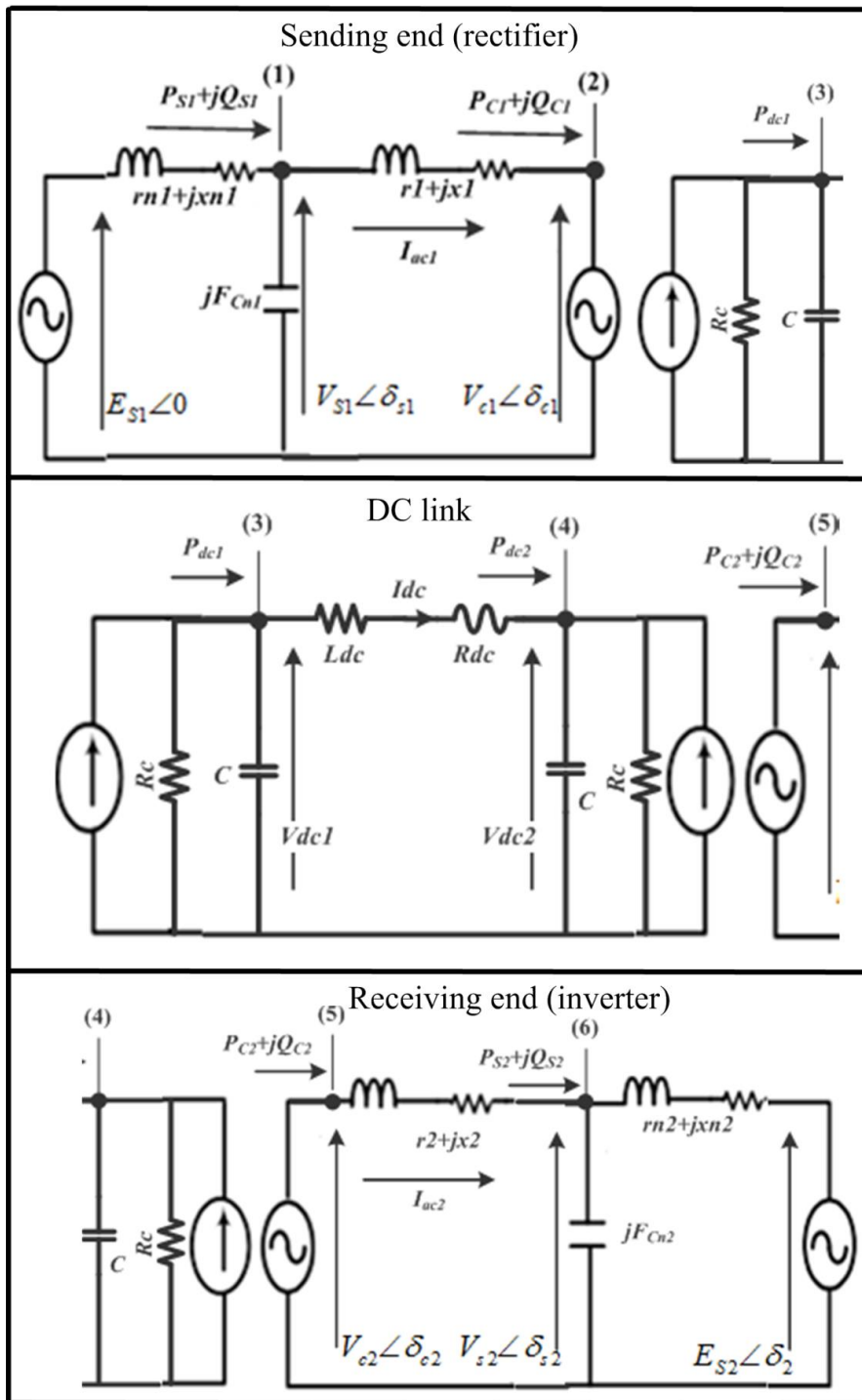


Figure 5-10: Equivalent circuit of a two power systems with a VSC-HVDC link.

5.5.1 Calculation of the power angle at the converter side

Power flow calculation for the VSC-HVDC requires determination of the power angle displacement between the PCC and the terminal voltage of the converter which facilitates calculating the required modulation indices Md and Mq . For this reason, this part introduces a mathematical approach to calculate the power angle difference between the sending and receiving ends of the coupling impedance.

Referring to the equivalent circuit in Figure 5-9, the relation between the voltage at the PCC (V_{Sys}) and at the converter side (V_{Conv}) can be defined by three angles, considering the resistive losses in the transformer, as shown in phasor diagram in Figure 5-11 [29]:

1. Power angle between V_{Sys} and V_{Conv} (δ).
2. Power factor between V_{Conv} and current I (ϕ).
3. The circuit tie impedance angle (θ) that includes the coupling transformer and phase reactor impedances ($Z=R+jX$).

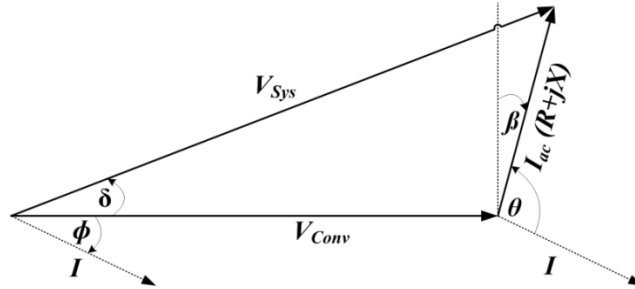


Figure 5-11: Angle relationship between the voltage at the PCC and at the converter terminal

The resistive losses of the tie impedance (R) and non-unity power factor of the load at the converter side establish a new angle β . This angle represents the angle by which the voltage drop in an ideal unity power factor load in the losses network (vertical dashed line) differs from the real network. Hence, β can be calculated from:

$$\beta = \frac{1}{2}\pi + \phi - \theta \quad (5-6)$$

Considering the established angle β in (5-6), the vertical component of the sending end voltage (V_{Sys}) in Figure 5-11 is given by:

$$V_{Sys} \sin \delta = I_{ac} [Z \sin(\phi - \theta)] \quad (5-7)$$

Since $\sin(\theta - \phi) = \sin\theta \cos\phi - \cos\theta \sin\phi$, multiplying both sides of equation (5-7) by V_{Conv} yields:

$$V_{Conv} (V_{Sys} \sin \delta) = V_{Conv} I [Z (\sin \theta \cos \phi - \cos \theta \sin \phi)] \quad (5-8)$$

Resistive and inductive components of the tie impedance (R and X), and the active and reactive power at the converter terminal (P_{Conv} and Q_{Conv}) can be calculated by from (5-9) and (5-10) respectively:

$$X = Z \sin \theta \quad \text{and} \quad R = Z \cos \theta \quad (5-9)$$

$$P_{Conv} = V_{Conv} I_{ac} \cos \phi, \quad \text{and} \quad Q_{Conv} = V_{Conv} I_{ac} \sin \phi \quad (5-10)$$

equations (5-8), can be rewritten using (5-9) and(5-10) as:

$$V_{Conv} (V_{Sys} \sin \delta) = X P - R Q \quad (5-11)$$

As simplified in chapter 2 for the generic power flow equation, assume $r = R/V_{Sys}^2$ and $x = X/V_{Sys}^2$. Both sides of equation (5-11) can be normalized by V_{Sys}^2 to establish the power angle equation as a function of active and reactive power (MW and MVar) and the pu converter voltage:

$$\sin \delta_{Conv} = \frac{x P - r Q}{V_{Conv}(pu)} \quad (5-12)$$

This equation will be used to calculate the power angle at the converter terminals and consequently the modulation indices Md and Mq .

5.5.2 Power flow calculations at the sending end VSC-HVDC

Normally, the power flow over the DC link is controlled at the sending end in addition to the ac voltage at the PCC. Thus, assume that the scheduled transmitted power on the dc link is P_{Sys1} , as calculated at PCC_1 in Figure 5-10. Also assume that the voltage at the PCC_1 is to be maintained fixed at V_{Sys1} .

From P_{Sys1} and V_{Sys1} , the reactive power at the PCC_1 can be calculated from the generic power flow equation 2-18 using the equivalent impedance of the system seen from PCC_1 (R_{n1}, X_{n1} and F_{Cn1}) and assuming maintained PCC voltage V_{Sys1} , which yields:

$$Q_{Sys1} = \frac{\sqrt{-F_{Cn1}^2 V_{Sys1}^4 r_{n1}^2 - (2 z_{n1}^2 V_{Sys1}^2 F_{Cn1}) (r_{n1} P_{Sys1} - 1/2) - P_{Sys1}^2 z_{n1}^4} - F_{Cn1} V_{Sys1}^2 x_{n1}}{z_{n1}^2} \quad (5-13)$$

where $z_{n1} = \sqrt{(r_{n1}^2 + x_{n1}^2)}$

The ac current in the sending end is:

$$I_{ac1} = \frac{1}{\sqrt{3}} \left(\frac{\sqrt{P_{Sys1}^2 + Q_{Sys1}^2}}{V_{Sys1}} \right) = \frac{1}{\sqrt{3}} \left(\frac{\sqrt{P_{Conv1}^2 + Q_{Conv1}^2}}{V_{Conv1}} \right) \quad (5-14)$$

Active and reactive power at the converter side can be calculated from equation (5-14) using the power balance formula $P_{Gen} = P_{load} + I^2 R$:

$$P_{Conv1} = \frac{P_{Sys1} \cdot V_{Sys1}^2 - (P_{Sys1}^2 + Q_{Sys1}^2) r1}{V_{Sys1}^2} \quad (5-15)$$

$$Q_{Conv1} = \frac{Q_{Sys1} \cdot V_{Sys1}^2 - (P_{Sys1}^2 + Q_{Sys1}^2) x1}{V_{Sys1}^2} \quad (5-16)$$

Where; $(r1 = R1/VB^2)$, $(x1 = X1/VB^2)$, V_{Sys} is in pu and P and Q are in MW and MVar (see section 2-3-4 in chapter 2 for more detail).

At this stage; active and reactive powers on both sides of the coupling transformer at the sending end are calculated (P_{Sys1} , Q_{Sys1} , P_{Conv1} and Q_{Conv1}). The only missing parameter at the sending end is the converter terminal voltage (V_{Conv1}), which can be calculated from the equation(5-14):

$$V_{Conv1} = V_{Sys1} \frac{\sqrt{P_{Conv1}^2 + Q_{Conv1}^2}}{\sqrt{P_{Sys1}^2 + Q_{Sys1}^2}} \quad (5-17)$$

Taking the sending end voltage angle as reference ($E_S \angle 0$), the PCC1 voltage angle (δ_{Sys1}) and at the converter terminal (δ_{Conv1}), with respect to the reference voltage angle, are calculated on the basis of equation(5-12):

$$\delta_{Sys1} = \frac{(P_{Sys1} x_{n1} - Q_{Sys1} r_{n1})}{V_{Sys1}} \quad (5-18)$$

$$\delta_{Conv1} = \frac{(P_{Conv1} x_1 - Q_{Conv1} r_1)}{V_{Conv1}} + \delta_{Sys1} \quad (5-19)$$

The voltage components at the converter side V_{d1} and V_{q1} , that define id and iq and consequently Md and Mq are calculated from δ_{Conv1} as:

$$V_{Cd1} = V_{Conv1} \cdot \cos \delta_{Conv1}, \text{ and } V_{Cq1} = V_{Conv1} \cdot \sin \delta_{Conv1} \quad (5-20)$$

5.5.3 Power flow equations in the dc link

Assuming constant converter losses (R_C) shown in Figure 5-10 and based on power balance theory at the ac and dc sides, the dc power in the sending end of the dc line is given by:

$$P_{dc1} = P_{Conv1} - \frac{V_{dc1}^2}{R_C} \quad (5-21)$$

The steady state dc voltage at the sending end (V_{dc1}) can be calculated from the dc circuit calculations in(5-22);

$$P_{dc1} = \frac{V_{dc1}}{I_{dc}} \cdot P_{dc1}, \quad P_{dc1} = P_{dc2} + I_{dc}^2 \left(\frac{V_{dc1} - V_{dc2}}{I_{dc}} \right) \text{ and } R_{dc} = \frac{V_{dc1} - V_{dc2}}{I_{dc}} \quad (5-22)$$

R_{dc} and the receiving end dc voltage V_{dc2} are known, then, the dc voltage at the sending end (V_{dc1}) and the dc current (I_{dc}) can be calculated from equations (5-21) and (5-22) respectively:

$$V_{dc1} = \frac{1}{2} \left(V_{dc2} + \sqrt{4P_{dc1} \cdot R_{dc} + V_{dc2}^2} \right) \quad (5-23)$$

$$I_{dc} = \frac{2 \cdot P_{dc1}}{\sqrt{4P_{dc1} \cdot R_{dc} + V_{dc2}^2} + V_{dc2}} \quad (5-24)$$

DC power at the receiving end can be calculated from equation(5-22):

$$P_{dc2} = P_{dc1} - I_{dc}^2 \left(\frac{V_{dc1} - V_{dc2}}{I_{dc}} \right) \quad (5-25)$$

Using V_{dc1} from(5-23), the modulation indices M_d and M_q that allow generation of required terminal waveform voltage V_{Conv1} at the terminal of the sending end converter can be calculated from:

$$V_{cd1} = \frac{1}{2} M_d \cdot V_{dc1} \quad (5-26)$$

$$V_{cq1} = \frac{1}{2} M_q \cdot V_{dc1} \quad (5-27)$$

5.5.4 Power flow calculations at the receiving end VSC-HVDC

On the basis of the power balance theory described for the rectifier side and assuming fixed rate converter losses, the ac power (P_{Conv2}) injected into the ac system through the receiving end converter is:

$$P_{Conv2} = P_{dc2} - \frac{V_{dc2}^2}{R_C} \quad (5-28)$$

Although both ac terminals of the dc link are ruled by same power flow theories, the power flow equations of the inverter side are more complicated than those of the rectifier side because of different unknown parameters.

As mentioned for the rectifier side, three of six parameters are available (P_{Sys1} , V_{Sys1} are known and Q_{Sys1} can be calculated), and the other three parameters (V_{Conv1} , P_{Conv1} , and Q_{Conv1}) are evaluated from the introduced equations.

In contrast, active power in the converter side P_{Conv2} and P_{CC2} voltage (V_{Sys2}) are the only known parameters on the inverter side. The reactive power requirements (Q_{Sys2}) to maintain the voltage V_{Sys2} at $PCC2$ is a function of unknown parameter P_{Sys2} , which involves simultaneous equations. P_{Sys2} is calculated from the generic power flow equation that considers system series impedance from the terminal of the receiving end E_{S2} to the converter terminal including the points (5 and 6) at in Figure 5-10 ($R_{n2}+R_2+j(X_{n2}+X_2)$). The formula for P_{Sys2} is derived in the appendix B-8.

The other ac receiving end unknown parameters can be calculated using the same methodology used at the sending end side considering system parameters R_{n2} , X_{n2} and F_{Cn2} , and the coupling transformer tie-impedance (r_2 and x_2).

5.5.5 Validation of power flow equations

The Kundur test system in figure 4-3 is used to validate the equations established in subsections 5.5.2 and 5.5.4. One of the tie-lines (line-2) in the test system is replaced by a ± 200 kV VSC-HVDC link of length 110 km (DCS1 section in Cigre B4 HVDC test system)[30] [28]. The test system is modelled using a commercial power system analysis tool (NEPLAN) to verify the steady state results obtained from the derived mathematical equations [31]. The comparison presented in Table 5-3 shows that the derived mathematical equations produce results which are in line with those obtained from NEPLAN, with negligible error; this confirms the validity of the proposed calculation method. Table 5-3 compares power flow results of the proposed mathematical approach and the numerical analysis method of NEPLAN. These discussions show that the derived equations provide an analytical means to perform steady-state analysis of a VSC-HVDC link with sufficient accuracy, without the need for time-consuming simulations.

Table 5-3: Summary of power flow comparison between NEPLAN and mathematical approach

	parameter	NEPLAN	equations	Error (%)
Sending end side	Voltage V_{s1} (pu)	1	1	0.00
	Voltage V_{c1} (pu)	1.002	1.002	0.03
	Active Power P_{c1} (MW)	399.5	399.5	0.00
	Reactive Power Q_{c2} (MVar)	33.35	33.37	0.06
	Power angle δ_{c1} (deg)	4.77	4.76	0.21
	MD1	0.995	0.991	0.40
	MQ1	0.081	0.083	3.61
Receiving end side	Voltage V_{s2} (pu)	1	1	0.00
	Voltage V_{c2} (pu)	1.008	1.007	0.10
	Active Power P_{c2} (MW)	398.1	398.1	0.00
	Reactive Power Q_{c2} (MVar)	66.5	68.5	2.92
	Power angle δ_{c2} (deg)	30.4	31.1	2.25
	Md2	0.87	0.86	0.70
	Mq2	0.51	0.52	2.11
DC link	Voltage dc (V_{dc1})	401.46	401.45	0.00
	Voltage dc (V_{dc2})	400	400	0.00
	dc Power (P_{dc1})	399.5	399.5	0.00
	dc Power (P_{dc2})	398.1	398.1	0.00

5.6 VSC capability chart

Independent control of active and reactive power in a VSC-HVDC facilitates theoretically operation of a VSC at any operating point (P - Q) in all four quadrants of the P - Q capability chart. The VSC capability chart is typically a circle with a radius determined by the converter maximum MVA rating as shown in Figure 5-12. However, in practice there are three technical limitations that restrict VSC capability [32, 33]:

1. The maximum continuous current of the converter switching devices can tolerate during normal operation. This current and the AC voltage imposed by the coupling transformer at converter terminal determine

the maximum MVA rating of the converter. Hence, for the same IGBTs current rating, the higher the AC voltage imposed at converter terminal by the coupling transformer, the higher the converter MVA rating. This limit is depicted by the green boundary in the Figure 5-12.

2. The reactive power flow through the coupling transformer depends on the voltage difference between the two terminals of the transformer. This means, in order to keep the level of the reactive power negligible compared with the level of the active power, the difference between the AC voltages at the both sides of the coupling transformer has to be small. On the other hand, the AC voltage terminal at the converter side is also a function of the DC voltage ($V_{ac} = \frac{1}{2} M V_{dc}$). Thus, as the level of the AC voltage increases, the dc voltage must be increased to maintain sufficient margin to perform other functions. The DC voltage limit of the VSC-converter is determined by the lower red curve which is defined by higher ac voltage in Figure 5-12.
3. The third limit is the maximum permissible current through the DC cable.

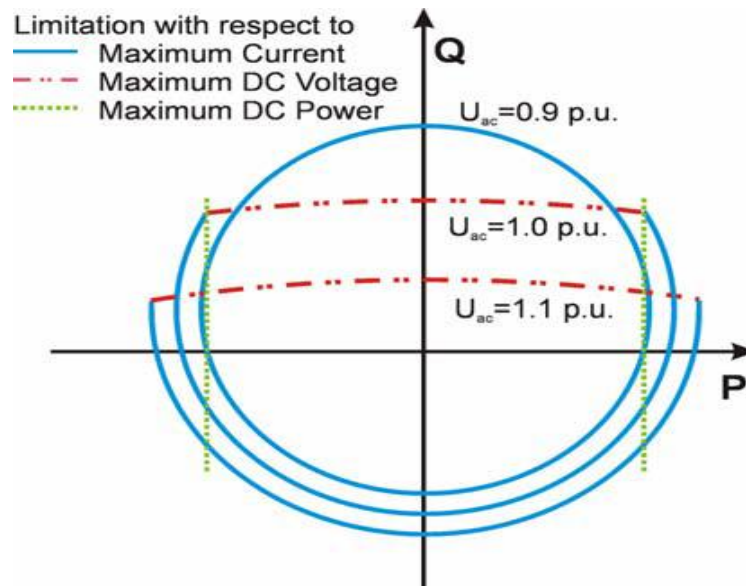


Figure 5-12: Typical P-Q capability characteristics of VSC-HVDC [33]

From Figure 5-12, the VSC P - Q capability is similar to a typical synchronous generator capability curve, except it encompasses four quadrants instead of two.

Maximum IGBT current in the VSC corresponds to the maximum armature current of the synchronous generator, whereas maximum DC voltage represents the maximum field current in the rotor. The inner circle in Figure 5-12, which represents the P-Q capability chart during the low voltage ($V=0.9$ pu), indicates VSC capability is determined by the maximum IGBT current as the maximum dc voltage limit vanished. On the other hand, as the ac voltage increases, the maximum DC voltage limit shrinks the P-Q capability, as represented by the upper red line ($V=1.1$ pu) [33].

5.6.1 Current limiter

Converter valves are designed to operate within a maximum current rating, and increase beyond the limit may lead to converter damage. Converter output current at any operating point (I_{OP}) is calculated from equation (5-29) that incorporates the reactive current component (i_q) and the active current component (i_d).

$$I_{OP} = \sqrt{id^2 + iq^2} \quad (5-29)$$

I_{OP} is continuously monitored and compared with the maximum reference current imposed by the current limiter. When the reference current is exceeded, the current limiter limits the VSC current. Based on system strength and VSC objective, there are three possible strategies to limit the VSC current. The strategy defines which of the current components (i_d or i_q) should be reduced in order to maintain the component of higher priority, and respect the maximum current rating, as shown in Figure 5-13.

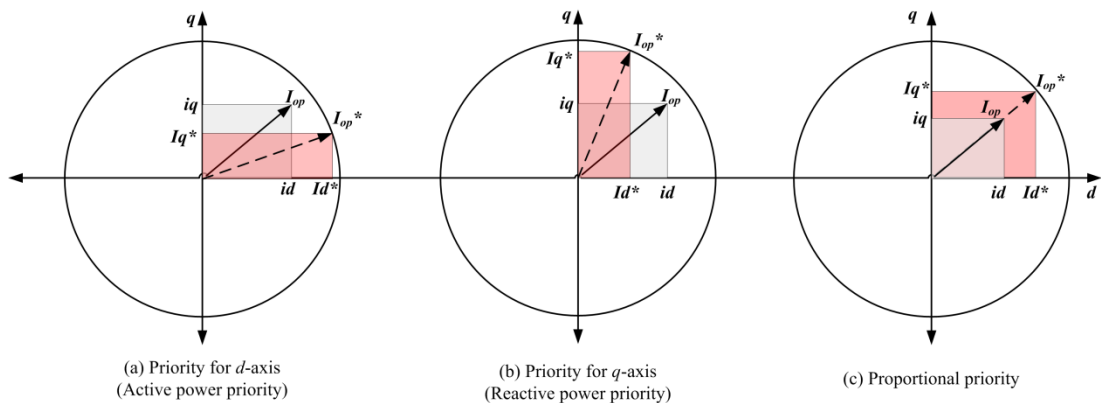


Figure 5-13: Current limiting strategies

In weak ac networks, priority is normally given to the q -axis current (i_q) where maintaining reactive power support is more important than the level of active power

on the dc link, as seen in Figure 5-13-b. In contrast, in strong systems, priority is given to the d -axis current which can be increased on demand up to its maximum (from i_d to i_d^*) at the expense of a slight change in the q -axis current (from i_q to i_q^*), as illustrated in Figure 5-13a. The third strategy is to limit both current components proportionally in order to maintain the power factor, as illustrated in Figure 5-13c.

5.7 VSC-HVDC control

There are different control strategies that allow active and reactive power control on both sides of the VSC-HVDC link. The vector control method is a widely used in VSC-HVDC transmission systems. PWM is used along with vector control, where the three-phase stationary coordinate system is transformed into the d - q rotating coordinate system, facilitating independent control of active and reactive power [27].

5.7.1 d - q transformation

Vector control is based on a d - q representation of the three phase system. The three-phase stationary coordinates are converted into two-phase stationary coordinate which is then transformed into a d - q rotating coordinate system. The transformation from three-phase into two-phase stationary frames is performed using Clark and inverse-Clark transformations where the variables (voltage and current) are dropped in α - β stationary reference form. The two-phase α - β stationary references are converted to d - q rotating references using Park transformation and inverse-Park for vice versa transformations, as shown in Figure 5-14.

For simplicity, the α -axis of the α - β stationary reference frame is aligned with the phase a -axis in the three-phase. The established d - q reference frame rotates at synchronous speed ω with respect to the stationary α - β frame. The displacement of the d -axis from the α -axis at any instant t is given by θ .

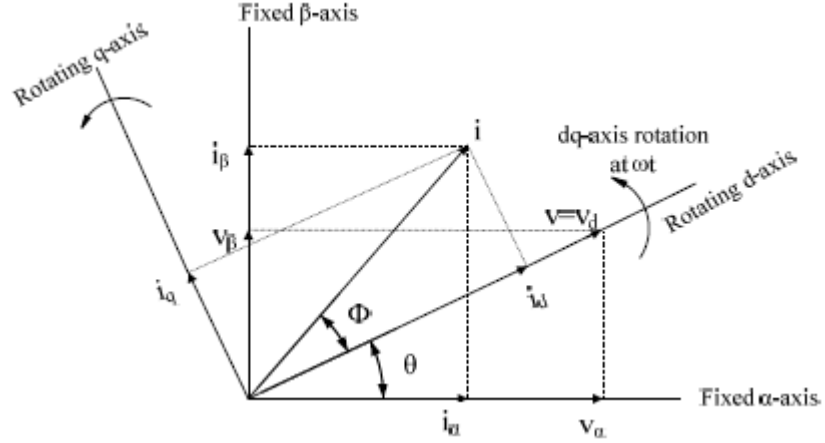


Figure 5-14: Axis transformation between three stationary coordinates to d - q rotating coordinates [27]

5.7.2 Vector control

Considering the VSC-HVDC equivalent circuit in Figure 5-9, the three phase voltage at the converter terminal $V_{Conv(abc)}$ is given by [34]:

$$V_{Conv(abc)} = V_{Sys(abc)} - \left[L \frac{di_{(abc)}}{dt} + Ri_{(abc)} \right] \quad (5-30)$$

Using a - b - c to d - q transformations, the three-phase voltage and current in equation (5-30) can be expressed in the d - q reference frame, and rotating at the synchronous speed ω :

$$\begin{bmatrix} Vd_{Sys} \\ Vq_{Sys} \end{bmatrix} = R \begin{bmatrix} i_d \\ i_q \end{bmatrix} + L \frac{d}{dt} \begin{bmatrix} i_d \\ i_q \end{bmatrix} + L \begin{bmatrix} 0 & -\omega \\ \omega & 0 \end{bmatrix} \begin{bmatrix} i_d \\ i_q \end{bmatrix} + \begin{bmatrix} Vd_{Conv} \\ Vq_{Conv} \end{bmatrix} \quad (5-31)$$

Solving of (5-31) yields:

$$\begin{aligned} L \left(\frac{di_d}{dt} \right) &= Vd_{Sys} - Vd_{Conv} - Ri_d + \omega Li_q \\ L \left(\frac{di_q}{dt} \right) &= Vq_{Sys} - Vq_{Conv} - Ri_q - \omega Li_d \end{aligned} \quad (5-32)$$

The dc current is calculated as:

$$I_{dc} = I_{cc} + C \frac{dV_{dc}}{dt} \quad (5-33)$$

Based on power balance theory, the ac power at the converter terminal must equal the dc power, assuming lossless converter.

$$P_{Conv(ac)} = \sqrt{3} V_{Conv} I_{ac} \cos \theta = V_{dc} I_{dc} \quad (5-34)$$

where; θ is the power factor at the converter side.

It is assumed that the voltage vector of the grid lies along the d -axis, which means that its associated virtual flux vector acts along the q -axis. With this alignment, $V_q=0$ and the active and reactive power outputs are:

$$\begin{aligned} P_{Conv} &= \frac{3}{2}(Vd_{Conv} i_d) \\ Q_{Conv} &= -\frac{3}{2}(Vd_{Conv} i_q) \end{aligned} \quad (5-35)$$

From Figure 5-14, the angle between the α -axis on the α - β frame and the d - q rotating frame is given by:

$$\theta = \tan^{-1}\left(\frac{V\beta}{V\alpha}\right) \quad (5-36)$$

where $V\beta$ and $V\alpha$ are the voltage components in the α - β two axis stationary reference frame.

In practice, the angle θ is computed using a phase locked loop (PLL) synchronization technique. The PLL synchronizes the gating on/off of the valve. The orientation of the rotating d - q coordinate system with respect to the voltage vector splits the current into two independent id and iq components. This allows independent control of active and reactive power in the both terminals of the VSC-HVDC transmission system. The importance of decoupled control of active and reactive power, by the means of vector control, is that it allows a cascade control structure with outer and inner PI control loops.

Reference control values are hierarchically passed from the outer controller into the faster acting inner current control loop. VSC-HVDC links are typically designed to control active power in the sending end converter, and the dc voltage is controlled at the receiving end converter. Reactive power on both sides is controlled in order to maintain the AC voltage and reactive power at desired levels [35].

5.7.3 Inner current controller

The inner current control loop is composed of four blocks, as depicted in Figure 5-15. This control system can be implemented in the d - q frame as discussed when considering vector control [27, 35].

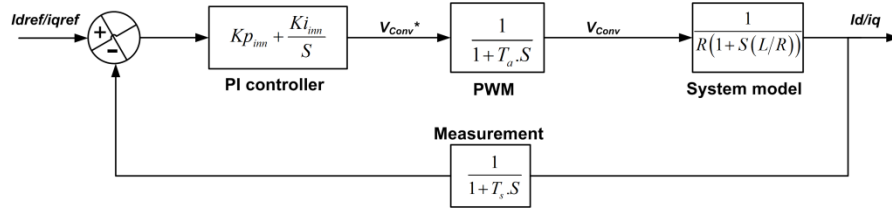


Figure 5-15: Block diagram of inner control loop in dq axes

i. PI compensator

The basic transfer function for the PI of the inner current controller is:

$$G1_{inn}(s) = kp_{inn} + \frac{ki_{inn}}{s} \quad (5-37)$$

where Kp_{inn} and Ki_{inn} are the proportional and integral gains. Hence, the PI controller output in Figure 5-15 can be calculated in s domain as:

$$V_{Conv}^*(s) = \left(kp_{inn} + ki_{inn} \frac{1}{s} \right) (I_{ref}(s) - I(s)) \quad (5-38)$$

ii. PWM converter

The converter is considered an ideal power transformer from the control point of view. However, due to VSC switching, an average time delay (T_a) of half the switching cycle ($T_a = 1/2 T_s$) is applied to the converter output voltage. Hence, the transfer function of PWM converter is

$$G2_{inn}(s) = \frac{1}{1 + T_a s} \quad (5-39)$$

From equation(5-39), the PWM output is:

$$V_{Conv}^* \left(\frac{1}{1 + T_a s} \right) = V_{Conv}(s) \quad (5-40)$$

iii. System model

As indicated in equation (5-32) in section 5.7.2, the ac current is a function of a number of variables. Therefore, the VSC model in the synchronous frame includes strongly coupled nonlinear system with multi-inputs multi-outputs. The Vd and Vq solutions of the equation (5-32) must include the terms $\omega L.Id$ and $\omega L.Iq$, which represents the system frequency/speed. These terms result in cross-coupling between the two axes. Each axis is influenced by the other, resulting in the disturbance. For

this reason, a dual-close-loop direct current controller with decoupled current compensation and voltage feed-forward compensation is required [36].

With two separate inner current loop controllers, $V_{Conv}^*(s)$ in equation (5-40) can be represented by the two voltage reference signals from(5-38):

$$\begin{aligned} (I_{d_{ref}}(s) - Id(s)) \cdot \left(kp_{inn} + \frac{ki_{inn}}{s} \right) \cdot \left(\frac{1}{1 + T_a \cdot s} \right) &= Vd_{Conv}(s) \\ (I_{q_{ref}}(s) - Iq(s)) \cdot \left(kp_{inn} + \frac{ki_{inn}}{s} \right) \cdot \left(\frac{1}{1 + T_a \cdot s} \right) &= Vq_{Conv}(s) \end{aligned} \quad (5-41)$$

As the d and q components are cross-coupled by $\omega L \cdot Id$ and $\omega L \cdot Iq$, two references inputs are used. The first is obtained from the converter and the second is a feed-forward term to cancel the cross-coupling of d and q . Hence, the system input for the converter can be determined using the equation (5-32)

$$\begin{aligned} Vd_{Sys} - (I_{d_{ref}}(s) - Id(s)) \cdot \left(kp_{inn} + \frac{ki_{inn}}{s} \right) \cdot \left(\frac{1}{1 + T_a \cdot s} \right) + \omega \cdot Li_q &= Vd_{Conv}^*(s) \\ Vq_{Sys} - (I_{q_{ref}}(s) - Iq(s)) \cdot \left(kp_{inn} + \frac{ki_{inn}}{s} \right) \cdot \left(\frac{1}{1 + T_a \cdot s} \right) - \omega \cdot Li_d &= Vq_{Conv}^*(s) \end{aligned} \quad (5-42)$$

The system equations can be rewritten from(5-32), (5-41) and (5-42) as:

$$\begin{aligned} L \left(\frac{di_d}{dt} \right) + Ri_d &= Vc_d \\ L \left(\frac{di_q}{dt} \right) + Ri_q &= Vc_q \end{aligned} \quad (5-43)$$

The cross-coupled terms are cancelled in the established system equation (5-43) which allows independent control of active and reactive power as previously discussed.

The system transfer function in the equation (5-43) can be determined from Laplace transformation as:

$$G_{3_{inn}}(s) = \frac{1}{R} \cdot \frac{1}{1 + s(L/R)} \quad (5-44)$$

The term L/R represents the time constant of the system impedance (τ).

iv. Measurement circuit

Measurements time delay of the inner current controller is expressed by:

$$G_{i_{in}}(s) = \frac{1}{1 + T_s \cdot s} \quad (5-45)$$

where T_s is the sampling time of the inner controller [35].

The block diagram of the entire inner current controller is shown in Figure 5-16

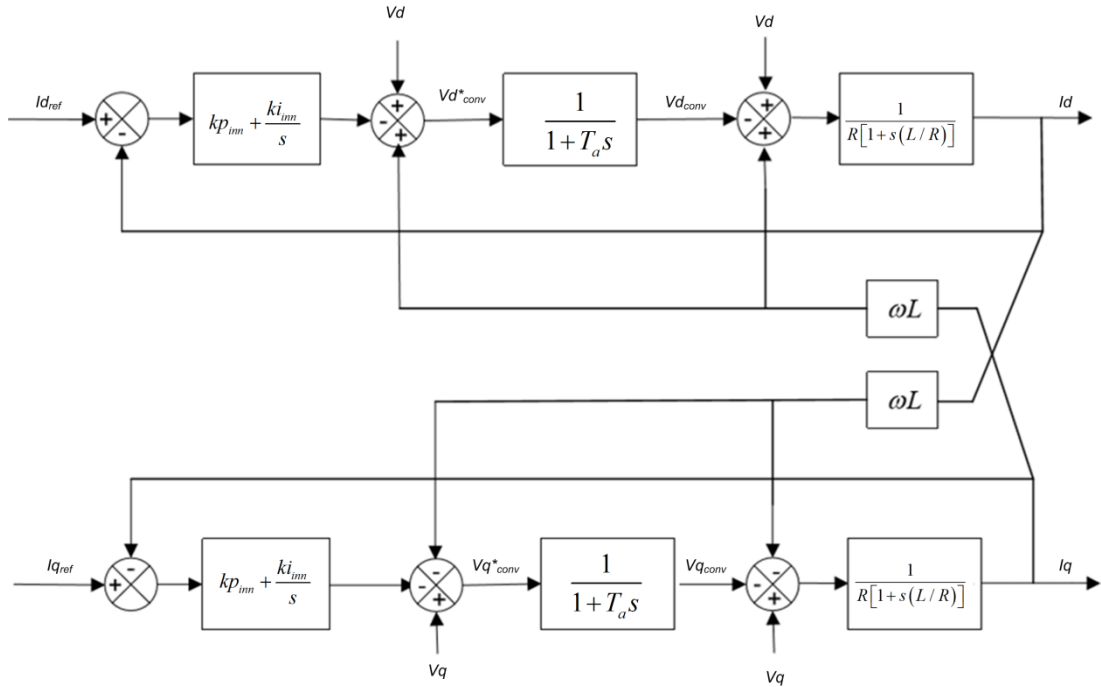


Figure 5-16: Block diagram of the inner controller [36]

5.7.4 DC voltage outer controller

The main objective of the dc voltage controller is to maintain the dc voltage level at an acceptable level. Vector control makes this object achievable, by adjusting the active current component (i_d), facilitating the control of the dc power in response to the dc voltage reference.

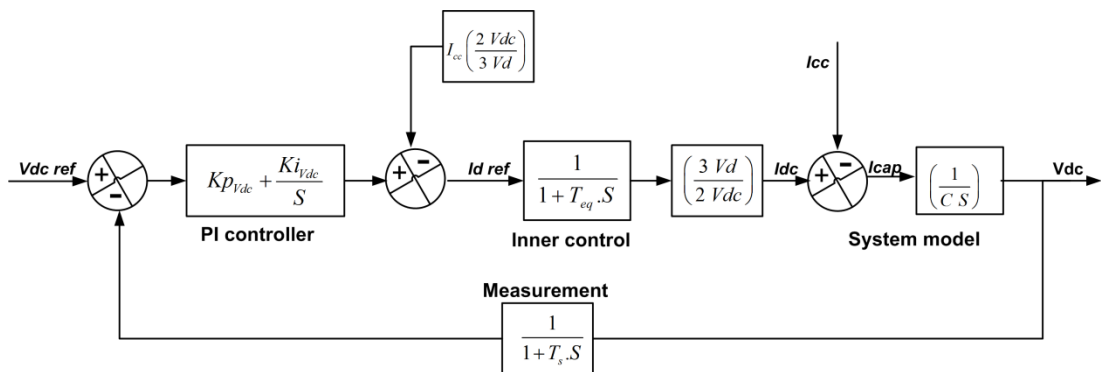


Figure 5-17: DC voltage control loop in d - q axis

DC voltage control in VSC-HVDC is performed by inner and outer control loops in an integrated operation. The DC voltage control system is formed of four parts in addition to the measurement circuits, as shown in Figure 5-17 [35].

i. PI regulator

The main function of the PI regulator in the dc voltage control is the calculation of the current reference I_{dref} in response to dc voltage error. The transfer function of the PI regulator of the dc voltage control system is:

$$G1_{vdc}(s) = kp_{vdc} + \frac{ki_{vdc}}{s} \quad (5-46)$$

ii. Inner current controller

The relation between the references current (I_{dref}), which is passed to the inner current controller from the PI regulator, and the VSC id output current is given by:

$$G2_{vdc}(s) = \frac{1}{1 + T_{eq} \cdot s} \quad (5-47)$$

where $T_{eq} = 2 T_a$ (see [27] for more detail).

iii. System model

Referring to the balance equation (5-34), and the alignment of voltage vector in the d - q reference frame where V_q is assumed zero, the dc current can be expressed as a function of id , V_d and V_{dc} as:

$$I_{dc} = \frac{3}{2} \cdot \frac{V_d}{V_{dc}} \cdot i_d \quad (5-48)$$

Substituting I_{dc} in the power balance equation (5-34), (with Taylor series based linearization around steady-state point and neglecting the I_{cc} disturbance affect), provides the dc voltage control loop transfer function for the system model, equation (5-49):

$$G3_{vdc}(s) = \left(\frac{3 V_d}{2 V_{dc}} \right) \left(\frac{1}{C s} \right) \quad (5-49)$$

iv. The feed-forward

The main objective of the feed-forward signal is to improve the slow dynamic response of the cascade control. With feed-forward, the load variation can be

reduced, and a large voltage controller gain is also avoided, achieving better performance of the dc voltage control [37].

As the dc voltage controls the capacitor current to maintain power balance, during balanced conditions the capacitor current is zero and I_{dc} theoretically equals I_{cc} .

Thus, the i_d reference value which represents feed-forward term in the figure can be calculated assuming $I_{dc}=I_{cc}$ during balanced conditions.

$$i_d = I_{cc} \left(\frac{2 V_{dc}}{3 V_d} \right) \quad (5-50)$$

5.7.5 Active and reactive power outer controllers

The structure and transfer functions of active and reactive power control are similar to those of dc voltage control. The system consists of an active and reactive power PI controller, the equivalent of the inner current controller, power transmission relationship and measurement circuits as shown in Figure 5-18 and Figure 5-19.

The transmission system model for active and reactive power control in per-unit are established using $d-q$ transformation, assuming $V_q=0$. This relation is given by:

$$\begin{aligned} P_{pu} &= v d_{pu} i d_{pu} \\ Q_{pu} &= -v d_{pu} i q_{pu} \end{aligned} \quad (5-51)$$

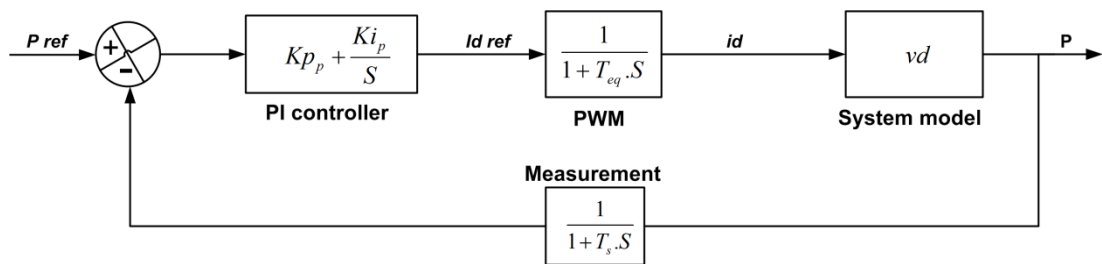


Figure 5-18: Active power control loop in $d-q$ axes

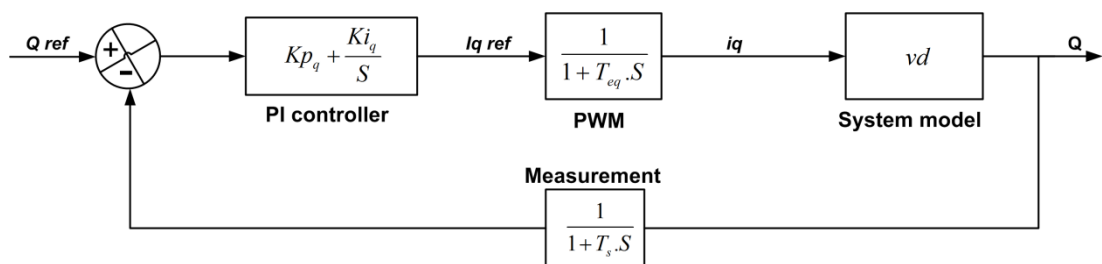


Figure 5-19: Reactive power control loop in $d-q$ axes

5.8 Total transfer capability of VSC-HVDC transmission system

An important feature of the VSC-HVDC transmission system is the ability to provide leading or lagging reactive power independent of the active power direction. This allows reactive power support during normal and emergency conditions. However, system strength at both sides can limit the transfer capability of the VSC-HVDC system. During converter current control saturation, the voltage stability limit at the PCC may be exceeded due to a load-ability increase as a result of insufficient in-feed of the reactive power from the converter. This phenomenon can take place in weak and remote networks connected to VSC-HVDC links. The *VSL* in such a case is determined by the tie impedance between the PCC and the converter terminal and the system impedance equivalent seen from the PCC.

5.9 Black start capability of VSC-HVDC

Electrical power systems are designed to operate within strict limits of voltage and frequency. During severe frequency disturbances, the grid may split into a number of islands. In severely affected islands, a blackout can take place, and the entire system de-energizes, tripping all the generators in the island. After clearing the cause of the blackout, the system has to be re-energized or black started. System restoration may be started from the system itself if it is equipped with black start diesel generators or hydro pumped storage plants. Another option is to re-energize the system through the tie-lines. As the voltage and frequency should be within the acceptable limits during restoration, the nearest power plant should be re-energized first in order to take the voltage and frequency control responsibility on the island. The main concern of this traditional ac restoration is that the initially re-energized synchronous generators may not be able to cope with the step-like increase of active and reactive power during load energization. Furthermore, re-energizing of long lines can cause temporary over-voltages which can further complicate restoration, due to limited control sources.

With the emerge of VSC-HVDC systems, a new concept of black-start has been introduced [38]. Black start capability of the new HVDC generation has facilitated re-energizing of the affected side of the dc link without harm to the other side of the dc link. In other words, the possibility of generating voltage with appropriate magnitude and phase shift, at one end of the dc link during normal operation of the

other side, is achievable. Independent active and reactive control capability of VSC-HVDC allows simultaneous control of voltage and frequency.

As the dc line is energized from the in-service side of the dc link, the ac voltage at the converter terminal of the dead side is ramped up in a controlled manner to re-energize the coupling transformer and auxiliaries, and gradually re-energizes the nearby area according to the restoration plan. Upon re-energized assistance in the dead network, the converter automatically takes responsibility of balancing the active and reactive power demand during load variation. Active and reactive powers are controlled almost instantaneously, within the operating range of P - Q chart, in response to voltage and frequency.

5.10 Frequency control capability of VSC-HVDC

AC systems are designed to operate within a strict frequency range. During disturbances, the system frequency may change due to active power mismatch between generation and demand. Primary, secondary and tertiary frequency control measures are adopted in the power industry to maintain the frequency within its nominal values.

In non-synchronous connected systems, the dc link can allow sharing of frequency regulation between the systems by adjusting the power flow on the dc link. This allows sharing of perturbation handling in addition to mitigation of undesired local perturbation handling.

The principle of frequency control in VSC-HVDC depends on changing converter active power set point in order to change the dc power based on the frequency. This can be achieved by including a frequency control loop either in the active power controller or the dc voltage controller.

Based on the system configuration, strength and nature of the load (industrial or domestic) at the dc link terminals, three frequency control strategies are described in [12]:

- 1- Fixed frequency control.
- 2- DC voltage based frequency control.
- 3- Active power based frequency control.

5.10.1 Dynamics of system frequency in AC systems

The system frequency depends on the amount of rotating inertia which determines the power-frequency characteristics of the system during and after a disturbance. The rotating inertia of the system is given by [39]:

$$2H \frac{d\omega_t}{dt} = T_m - T_e \quad (5-52)$$

where ω_t is angular speed, T_m and T_e are mechanical and electromagnetic torques and H is system inertia. Equation (5-52) can be expressed as a relationship between frequency deviation, and electrical and mechanical powers (P_e and P_m) as:

$$2H \frac{df}{dt} = P_m - P_e \quad (5-53)$$

This equation can be expressed as a steady state power-frequency characteristic droop (R) given by:

$$f - f_0 = -R(P - P_0) \quad (5-54)$$

where $f - f_0$ is the deviation from the nominal frequency and is caused by $P - P_0$, the change in power ΔP .

The effect of the VSC-HVDC link on system inertia and the power-frequency characteristics can be understood from the relationship between the rate of change of frequency (RoCoF) at the AC terminal and the variation of dc power (P_{dc}). The desired change in dc power to re-balance the system is given by:

$$P_{dc} = P_{des} - K_{dc} \frac{df}{dt} \quad (5-55)$$

where K_{dc} is dc power-frequency droop and P_{des} is the desired power ordered by the HVDC controller.

From (5-53) and (5-55), the general equation of the frequency dynamics, including the contribution of HVDC power, yields:

$$2(H + \frac{1}{2}K_{dc}) \frac{df}{dt} = P_m - P_e + \Delta P_{dc} \quad (5-56)$$

Where, $\Delta P_{dc} = (P_{dc} - P_{des})$

Equation (5-56) indicates that the change in dc power influences system frequency and the RoCoF which is proportionally changes with the change of dc power.

5.10.2 Fixed frequency control strategy

Fixed frequency control is performed by the HVDC converter to maintain the frequency at its nominal value (f_0) in isolated systems that do not include any frequency control measures. In this control strategy, the frequency control is performed only by the HVDC link. Fixed frequency control is achieved using dual vector controller that facilitates supplying of the output voltage with a fixed frequency f_0 . Any change in power demand is reflected as an error, and processed in the frequency controller in response to f_0 [12].

5.10.3 DC voltage based frequency control strategy in VSC-HVDC

The theory of frequency control by the means of V_{dc} depends on the relationship between the change of V_{dc} and energy stored in the dc capacitor (W_{dc}). In steady state the energy stored in the dc capacitor is given by [12]:

$$W_{dc} = \frac{1}{2} C_{dc} \cdot V_{dc}^2 \quad (5-57)$$

During system disturbances, the imbalance between ac and dc powers causes a change in dc voltage which in turn temporary changes the stored energy in the dc capacitor. Neglecting converter losses, the change in the dc power (ΔP) can be written as a function of instantaneous change of dc capacitor energy:

$$\Delta P = \frac{d}{dt} W_{dc} = \frac{1}{2} C_{dc} \cdot \frac{d}{dt} V_{dc}^2 \quad (5-58)$$

Considering the energy balance theory, for the power exchange between the ac and the dc systems ($\Delta P_{cd} = \Delta P_{ac}$), and using the power-frequency droop characteristic given in (5-54), equation (5-58) can be written to include the frequency droop:

$$f - f_0 = -R \frac{1}{2} C_{dc} \cdot \frac{V_{0_{dc}}^2 - V_{1_{dc}}^2}{T} \quad (5-59)$$

where $V_{0_{dc}}$, $V_{1_{dc}}$ are the dc capacitor voltage change from V_0 to V_1 over time T . The term $-R \cdot C_{dc} / 2T$ represents the V_{dc} -frequency droop characteristic of the system (R_{dc}). Hence, the V_{dc} -frequency droop characteristic is given by

$$f - f_0 = -R_{dc} (V_{0_{dc}}^2 - V_{1_{dc}}^2) \quad (5-60)$$

The relation between V_{dc} and the frequency is a proportional type, with a gain of $R_{dc} = -R \cdot C_{dc} / 2T$, which can be introduced as a gain in the V_{dc} outer controller as shown in Figure 5-20.

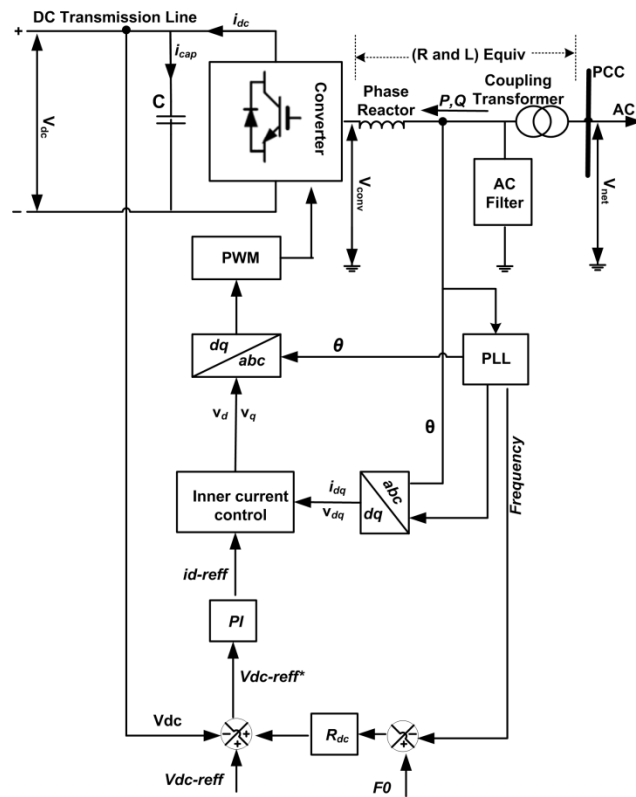


Figure 5-20: DC voltage based control strategy

5.10.4 Active Power based frequency control strategy

The third strategy for VSC-HVDC frequency control is based on the power frequency droop characteristics described in section 5.10.1. This controller may include a proportional control with steady state frequency droop or proportional-integral (PI) control to eliminate steady state error. The frequency at the PCC is treated in the PLL before it is compared with the nominal frequency to establish the frequency error signal. The error signal is then passed to the frequency controller which establishes the required power error signal in response to the change in system frequency. This signal, along with the scheduled power reference, defines the new power reference of the outer power controller, as shown in Figure 5-21.

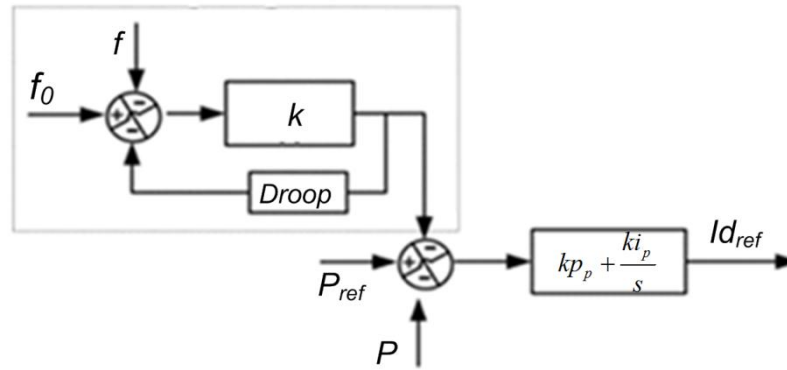


Figure 5-21: Active power based frequency control structure

5.11 Summary

This chapter reviewed the VSC-HVDC transmission system, including its main attributes, components, configuration, applications and control. A steady state mathematical model of the rectifier side, dc link and the inverter side were introduced, including the resistive losses of the tie-impedance. Validation of the presented VSC-HVDC link mathematical model showed its results converged with that of a numerical approach. Moreover, this chapter proposed a new approach for sizing of the VSC-HVDC link, considering steady state voltage and angular stability limits. System load-ability improvement with the VSC-HVDC was investigated, and results show robust system performance with VSC-HVDC. Additionally, the VSC-converter station control systems were investigated. Black start and frequency control capability method for the VSC-HVDC were addressed. The introduced steady state mathematical model along with the numerical dynamic model will be used to investigate the potential of VSC-HVDC to increase total transfer capability of the Libyan tie-line and mitigate stability concerns.

5.12 References

- [1] D. Jinxu and A. Somani, "Reduction of green house gas emission by clean power trading," in *Energy Conversion Congress and Exposition (ECCE), 2010 IEEE*, 2010, pp. 4588-4592.
- [2] G. Kalcon, *et al.*, "HVDC network: Wind power integration and creation of super grid," in *Environment and Electrical Engineering (EEEIC), 2011 10th International Conference on*, 2011, pp. 1-4.
- [3] D. M. Larruskain, "Transmission and Distribution Networks: AC versus DC," *IEEE Power Engineering Society General Meeting, 24-28 June 2007*, pp. 1-5.
- [4] C.-K. Kim, *et al.*, HVDC transmission: power conversion applications in power systems: John Wiley & Sons, 2009.
- [5] P. Jiuping, *et al.*, "AC Grid with Embedded VSC-HVDC for Secure and Efficient Power Delivery," in *Energy 2030 Conference, 2008. ENERGY 2008. IEEE*, 2008, pp. 1-6.
- [6] K. R. Padiyar, *HVDC power transmission systems: technology and system interactions*. New Delhi: New Age International (P) Limited, Publishers, 2005.
- [7] E. Prieto-Araujo, *et al.*, "Methodology for Droop Control Dynamic Analysis of Multiterminal VSC-HVDC Grids for Offshore Wind Farms," *Power Delivery, IEEE Transactions on*, vol. 26, pp. 2476-2485, 2011.
- [8] N. G. Hingorani and L. Gyugyi, *Understanding FACTS: Concepts and Technology of Flexible AC Transmission Systems*: Wiley, 2000.
- [9] M. R. Hasan, *et al.*, "Generic high level VSC-HVDC grid controls and test systems for offline and real time simulation," in *Electric Power Quality and Supply Reliability Conference (PQ), 2014*, 2014, pp. 57-64.
- [10] N. Flourentzou, *et al.*, "VSC-Based HVDC Power Transmission Systems: An Overview," *IEEE Trans on Power Electronics*, vol. 24, pp. 592-602, 2009.
- [11] Z. Xiao-Ping, "Multiterminal voltage-sourced converter-based HVDC models for power flow analysis," *IEEE Transactions on Power Systems*, vol. 19, pp. 1877-1884, 2004.
- [12] C. Du, *et al.*, "Comparison of Different Frequency Controllers for a VSC-HVDC Supplied System," *Power Delivery, IEEE Transactions on*, vol. 23, pp. 2224-2232, 2008.
- [13] C. Du, *et al.*, "A New Control Strategy of a VSC-HVDC System for High-Quality Supply of Industrial Plants," *Power Delivery, IEEE Transactions on*, vol. 22, pp. 2386-2394, 2007.
- [14] C. Du and M. H. J. Bollen, "Power-frequency control for VSC-HVDC during island operation," in *AC and DC Power Transmission, 2006. ACDC 2006. The 8th IEE International Conference on*, 2006, pp. 177-181.
- [15] A. L'Abbate, *et al.*, "The role of facts and HVDC in the future paneuropean transmission system development," in *AC and DC Power Transmission, 2010. ACDC. 9th IET International Conference on*, 2010, pp. 1-8.

- [16] M. P. Bahrman and B. K. Johnson, "The ABCs of HVDC transmission technologies," *Power and Energy Magazine, IEEE*, vol. 5, pp. 32-44, 2007.
- [17] K. Sekiguchi, *et al.*, "A Grid-Level High-Power BTB (Back-To-Back) System Using Modular Multilevel Cascade Converters Without Common DC-Link Capacitor," *Industry Applications, IEEE Transactions on*, vol. 50, pp. 2648-2659, 2014.
- [18] G. O. A. Kalcon, "Control design and stability assessment of VSC-HVDC networks for large-scale offshore wind integration," Ph.D, Electronic and Electrical Engineering, University of Strathclyde, Glasgow-UK, 2011.
- [19] W. F. Long, *et al.*, "Application aspects of multiterminal DC power transmission," *Power Delivery, IEEE Transactions on*, vol. 5, pp. 2084-2098, 1990.
- [20] G. Morin, *et al.*, "Modeling of the Hydro-Quebec-New England HVDC system and digital controls with EMTP," *Power Delivery, IEEE Transactions on*, vol. 8, pp. 559-566, 1993.
- [21] V. K. S. Chan-Ki Kim, Gil-Soo Jang, Seong-Joo Lim, Seok-Jin Lee *HVDC Transmission: Power Conversion Application in Power System*: John Wiley & Sons (Asia), Publication, 2009, Singapore.
- [22] G. P. Adam, *et al.*, "Multi-terminal DC transmission system based on modular multilevel converter," in *Universities Power Engineering Conference (UPEC), 2009 Proceedings of the 44th International*, pp. 1-5.
- [23] G. P. Adam and I. E. Davidson, "Robust and Generic Control of Full-Bridge Modular Multilevel Converter High-Voltage DC Transmission Systems," *Power Delivery, IEEE Transactions on*, vol. 30, pp. 2468-2476, 2015.
- [24] P. Haugland, "It's time to connect- Technical description of HVDC Light® technology," *ABB HVDC Light® on the Interne*, 2008.
- [25] C. Du, "The control of VSC-HVDC and its use for large industrial power systems," Department of Energy and Environment, Chalmers University of Technology, Gothenburg, 2003.
- [26] D. Van Hertem, *et al.*, *HVDC Grids: For Offshore and Supergrid of the Future*: Hoboken, New Jersey: Wiley, 2016.print.
- [27] C. Bajracharya, *et al.*, "Understanding of tuning techniques of converter controllers for VSC-HVDC," in *Nordic Workshop on Power and Industrial Electronics (NORPIE/2008), June 9-11, 2008, Espoo, Finland*, 2008.
- [28] Vrana, Til Kristian, Yongtao Yang, Dragan Jovcic, Sebastien Denetiere, Jose Jardini, and Hani Saad. "The CIGRE B4 DC grid test system." *Electra* 270 (2013): 10-19.
- [29] A. B. Morton, "A Guide to 'Steady-State' Voltage Stability Analysis," November 2007 ed: Senergy/Econnect, 2007, pp. 1-23.
- [30] P. Kundur, *Power system stability and control*: Tata McGraw-Hill Education, 1994.
- [31] C. P. A. B. Busarello. *NEPLAN, power system analysis software*. Available: www.neplan.ch

- [32] H. Latorre S.. "Modeling and Control of VSC-HVDC Transmissions." Royal Institute of Technology, Stockholm, Sweden, Thesis ISBN (2011): 978-91.
- [33] S. G. Johansson, *et al.*, "Power system stability benefits with VSC DC-transmission systems," in *CIGRE Conference, Paris, France*, 2004.
- [34] R. Song, *et al.*, "VSCs based HVDC and its control strategy," in *Transmission and Distribution Conference and Exhibition: Asia and Pacific*, 2005 IEEE/PES, 2005, pp. 1-6.
- [35] W. Liying and N. Ertugrul, "Selection of PI compensator parameters for VSC-HVDC system using decoupled control strategy," in *Universities Power Engineering Conference (AUPEC), 2010 20th Australasian*, 2010, pp. 1-7.
- [36] M. Davari and Y. A. R. I. Mohamed, "Robust Multi-Objective Control of VSC-Based DC-Voltage Power Port in Hybrid AC/DC Multi-Terminal Micro-Grids," *Smart Grid, IEEE Transactions on*, vol. 4, pp. 1597-1612, 2013.
- [37] B. Van Eeckhout, "The economic value of VSC HVDC compared to HVAC for offshore wind farms," *Offshore (Conroe, TX)*, 2008.
- [38] Z. Chengyong, *et al.*, "A novel coordinated control strategy for improving the stability of frequency and voltage based on VSC-HVDC," in *Electric Utility Deregulation and Restructuring and Power Technologies, 2008. DRPT 2008. Third International Conference on*, 2008, pp. 2202-2206.

Chapter Six

Strengthening the Libyan internal tie-line with FACTS technologies

6.1 Introduction

Discussion in chapters 4 and 5 both concluded that the main reason for the poor performance of medium and long transmission tie-lines is the lack of adequate reactive power support. It was also concluded that FACTS devices have become a viable solution to reactive power associated problems. However, the level of performance improvement depends on the choice of the technology, the size and the location of the FACTS device. The optimal choice should be based on technical and economic consideration studies that include: voltage stability analysis, steady state and dynamic stability, and risk of sub-synchronous resonance with the nearby conventional power plant.

This chapter investigates the potential of shunt and series reactive power compensation to improve the Libyan internal tie-line, and to what extent the transfer capability of the existing tie-line can be improved.

Steady state and dynamic analysis are undertaken to evaluate the performance of the tie-line when incorporating FACTS devices. Available types of shunt and series FACTS devices (SVC, STATCOM and TCSC) are used and adjusted to conform to the present system Libyan network.

For FACTS types, optimal sizing and allocating approaches explored earlier are used to find out the optimal place and size of the FACTS devices that ensure maximum utilization of the Libyan internal tie-line, and to confirm the validity of these approaches in real networks.

The first part of this chapter addresses shunt FACTS devices in steady state and during credible network disturbances, with a focus on tie-line performance in terms of total transfer capability.

Series compensation and its effect on the Libyan internal tie-line is investigated in the second part of the chapter. As both sides of the tie-line include combined cycle power plants, sub-synchronous resonance may be introduced into the system during system disturbances. Therefore, TCSC sizing is performed in order to achieve

maximum tie-line utilization factor while avoiding operation close to the SSR risk range.

6.2 Present performance of West-East Libyan internal tie-line

The Libyan transmission grid is divided into four geographical regions; east, west, south-west, and south-east. The east and west transmission networks are connected via a 500km tie line that includes a 220kV double circuit overhead transmission line (OHTL) and a single circuit 400kV OHTL [1, 2].

The present load demand of the Libyan power system is about 7500MW. Normal power flow is from the eastern side of the country, where the vast majority of the generation capacity is installed, to western network area where about 70% of the load demand is concentrated. Geographical distribution of load centers and power generation has affected the transmission system performance, as they limit the TTC due to voltage instability and power oscillations which coincide with a certain level of power exchange over the internal tie-line. This poor performance has added operational and economic challenges, forcing the ties to be operated at considerably lower than their designed thermal capacity. Figure 6-1 shows the present distribution of load demand and power generation in the two operating regions (east and west), and load-ability of the internal Libyan tie line [3].

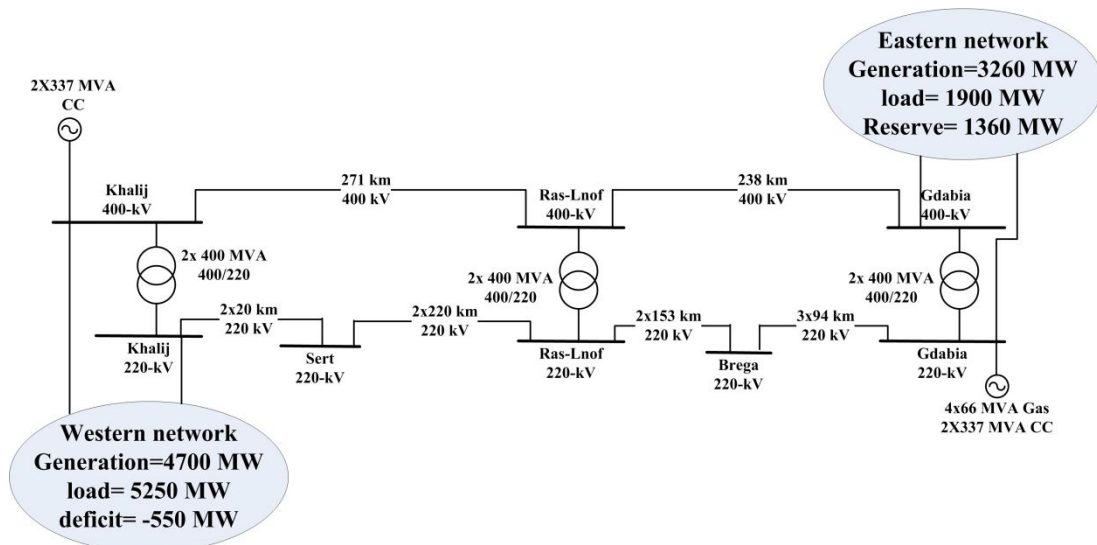


Figure 6-1: West-East internal Libyan tie-line

The internal tie line is thermally rated to carry a total of 3.75kA (1.25kA on the 400kV single circuit and 2.5kA on the 220kV double-circuit), in either direction.

Theoretically, this present rating should allow the exchange of about 1800MW without any thermal limit violation. However, reliability requirements have reduced the transfer capability of the tie-line to about 1345MW, as a precaution against a potential *N-1* scenario. Therefore, 1325MW of power exchange between the east and west Libyan networks should be used as a target in any future reinforcement of the Libyan transmission network to ensure efficient use of this corridor.

6.2.1 Present load-ability of East and West Libyan tie-line

Referring to General Electricity Company of Libya GECOL grid code, all nodal voltages during normal operating conditions should be within $\pm 5\%$ of the nominal voltage of the transmission level (220 and 400 kV). During post-fault operating conditions, the nodal voltage should remain within the recommended operational voltage limit of $\pm 10\%$ of the nominal voltage [4]. Adhering to this voltage restriction imposed by the grid code, the maximum power transfer limit from east to west should not exceed 500MW during *N-1* operating conditions. This level of power transfer is defined according to the minimum accepted voltage level during an emergency (-10 %). The present level of the power exchange accounts for less than 47% of the efficient level of power exchange which substantially affects system utilization.

Optimal utilization of the west-east tie-line requires measures that allow increased transfer capability from the existing level of power exchange (500MW) to 1345MW. Reinforcing this tie-line with a new transmission line can improve the performance of the existing line. However, this option may not be competitive with solutions that use advanced FACTS and HVDC technologies [5].

6.2.2 Reduced model of the west-east tie-line

In order to avoid any unrelated problems that can affect the analysis and cause a misleading judgment of west-east tie-line performance (such as load-flow divergence due to voltage violations or overloading of some distribution transformers), the detailed Libyan network is reduced to include only the west-east tie-line and the related nearby areas, as shown in Figure 6-1. Thevenin equivalents are calculated at the tie-line's terminals (Gdabia in the east and Kahlije in the west). Table 6-1 summarises the parameters of the equivalent system impedances at both sides of the tie-line.

Table 6-1: Equivalent of east and west system impedances at the terminals of the tie-line

Reduced network	Terminal station	$R(\Omega)$	$X(\Omega)$	$B(\mu\text{S})$	r	x	FC
East	Gdabia-400 kV	0.268	5.639	-	$0.1674e^{-5}$	$0.325e^{-4}$	1
West	Khaliq-400 kV	0.536	11.278	-	$0.334e^{-5}$	$0.704e^{-4}$	1
Tie-line (N)	-	10.46	99.51	1814.9	$0.645e^{-4}$	$0.565e^{-3}$	0.827
Tie-line (N-1)	-	23.28	192.61	580.43	$0.143e^{-3}$	$0.113e^{-2}$.8913

Figure 6-2a and Figure 6-2b show the impedance representation of the west- east tie-line during normal and N-1 conditions (loss of one circuit between Sert and Ras-Lanuf).

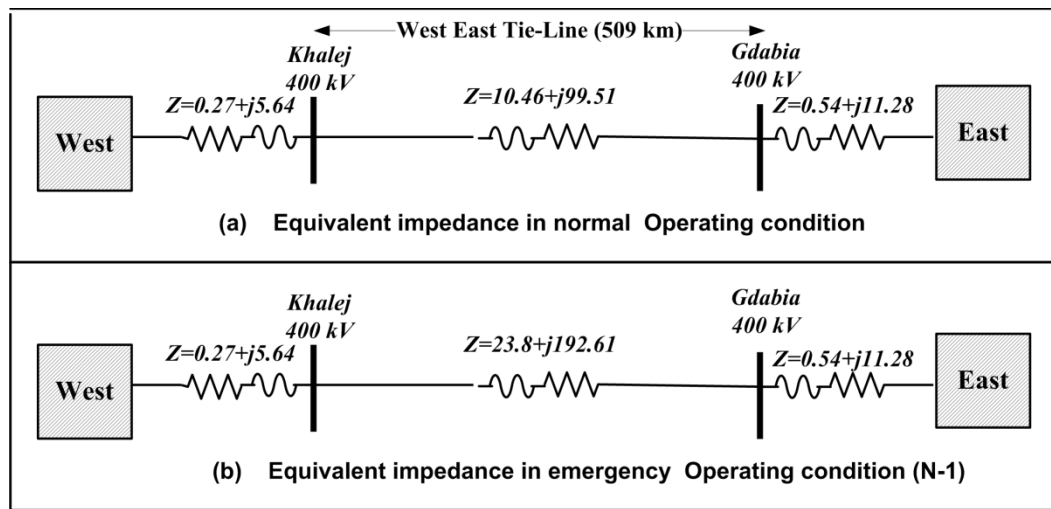


Figure 6-2: Impedance representation of the Libyan internal west-east tie-line

In steady-state studies, these equivalents are considered sufficient basically to assess the transmission power performance of the tie-line, as discussed in chapter 2. Voltage and angular stability limits (VSL and ASL), and reactive power requirements at any load-ability level can also be calculated from the system impedance equivalent. However, in complicated meshed systems that include a variety of voltage regulators, other additional and detailed verification steps are required.

6.2.3 Validation of reduced model of the west-east tie-line

The reduced model is validated under steady state conditions to ensure that the results are consistent with the real results from the detailed model of the entire Libyan grid. A power flow case study of 600MW power transfer from east to west is performed using the reduced model and a detailed model of Libyan network. Detailed Power flow results for both models are in appendixes E-1 and E-2.

Summary of the results comparison of nodal voltages and active and reactive powers in the branches are in Table 6-2 and Table 6-3.

Table 6-2: Validation of reduced west-east tie-line reduced model (buses voltages)

Station	Voltage level (kV)	Reduced model V (%)	Detailed model V (%)	Error (%)
Gdabia	400	96.84	96.91	0.07
	220	97.36	97.61	0.26
Ras-Lanuf	400	97.3	97.56	0.27
	220	97.4	97.6	0.20
Khalej	400	98.57	98.83	0.26
	220	97.39	98.47	1.10
Sert	220	98.73	98.43	0.30
Brega	220	96.9	97.0	0.10

Table 6-3: Validation of reduced west-east tie-line reduced model (active and reactive powers)

Branch	P(MW)		Error (%)	Q(MVAr)		Error (%)
	Reduced model	Detailed model		Reduced model	Detailed model	
271 km	340	347	2.0	93	96	3.1
20 km	228	231	1.3	43	41	4.9
240 km	255	259	1.5	61	58	5.2
238 km	342	348	1.7	82	80	2.5
153 km	268	274	2.2	65	63	3.2
94 km	281	287	2.1	45	42	7.1
9 km	657	657	0.0	59	55	7.3

From Table 6-2, the reduced model of the east-west tie-line and nearby areas produces similar results as those obtained from the detailed model of the entire Libyan network, with a maximum error of less than 7.5%. Therefore, the reduced model is deemed an acceptable representation of the east-west tie line being studied. Thus, it will be used in subsequent sections to generate an initial idea of the feasibility of future reinforcement possibilities for the Libyan network. Findings from this model will be validated on a detailed model of the Libyan network.

6.2.4 Voltage stability limit (VSL) of west-east Libyan tie-line

Voltage instability is one challenge that affects utilization of the Libyan transmission network, especially east-west tie-line. Many of the reported instability cases in the Libyan grid are associated with poor performance of this line. The problem would be exacerbated by the loss of a 400kV line between Ras-Lanufe and Khaleej substations, which further weakens the connection between the eastern and western power networks, as it is indicated in Figure 6-2b. As a result, total transfer capability

of west-east tie-line will be determined to assume the worst case scenario: losing that line.

Voltage stability limit of this transmission corridor can be estimated analytically using equation 2-29, considering the impedance representation shown in Figure 6-2b. However, for more accurate results and for ease of presentation analysis, a time domain simulations is used. Load demand is gradually increased in the western area simultaneously with balanced generation increase in the eastern network forcing the power to flow towards the western network. As discussed, as the load-ability increases, the voltage starts to decrease, reaching the critical voltage at the point of collapse (*PoC*) as shown in Figure 6-3.

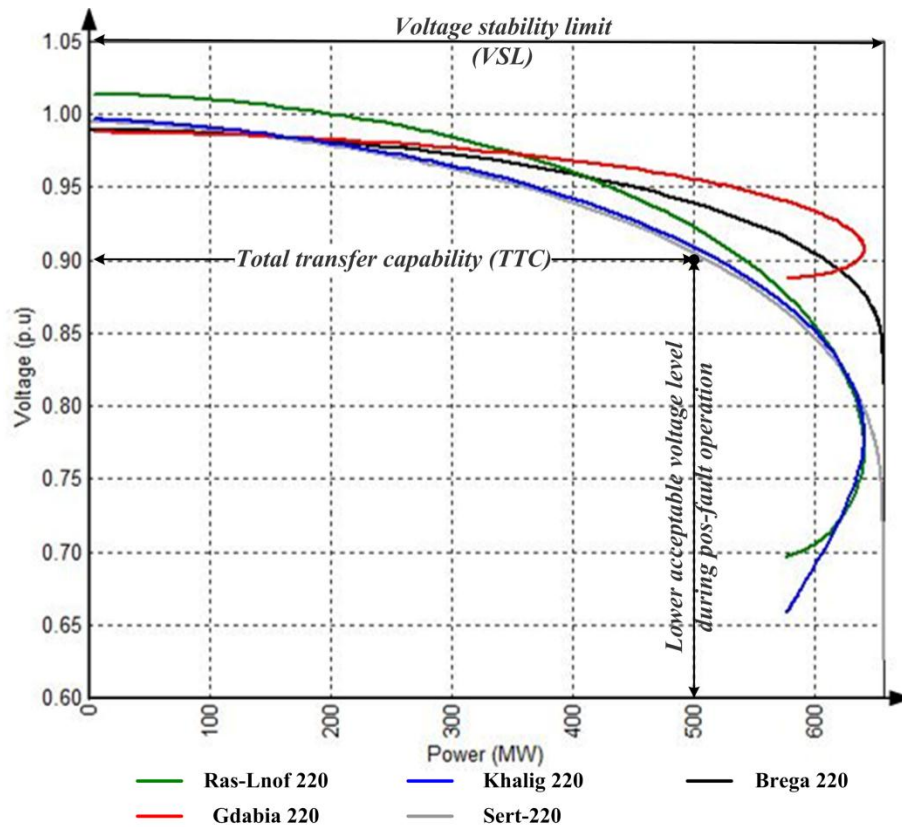


Figure 6-3: Power versus voltage at 400kV stations along the west-east Libyan tie-line

From *P-V* curves displayed in Figure 6-3, two load-ability limits are established:

- 1- Maximum load-ability of the tie-line (TTC=500 MW) that defines the loading point at which the voltage of a given bus reaches its minimum emergency level of 90%. In some special circumstances, the Libyan Grid Code allows operation at this voltage level for a limited period of time. However, this limit should be respected, and TTC should be defined upon this load-ability level [6].

- 2- The second limit is voltage stability limit (VSL=630 MW). This limit is important as it affects system security if exceeded. Therefore, sufficient stability margin should be considered to avoid slipping into unacceptable operating zones as discussed in chapter 2

6.2.5 Angular stability limit (ASL) of west-east Libyan tie-line

Steady state angular stability limit (*ASL*) for a given transmission corridor can be estimated from equation 2-35, which was derived in chapter 2. The *ASL* corresponds to the load-ability level where the voltage vectors at the both sides of the transmission corridor are displaced from each other by 90° . Equation 2-35 indicates that theoretically this level of power transfer can only be achieved by raising the voltage level (V) or reducing the total series impedance of the tie-line (but this will increase *PoC*). However, increasing *PoC* is not desirable from a system security point of view as discussed in chapter 3. This level can be considered as the maximum load-ability improvement that can be achieved by shunt injected reactive power with the risk of a higher *PoC*.

By contrast, the angular stability limit equation indicates that reducing the series impedance is an effective approach to increase *ASL* of a given corridor.

Using equation 2-35, assuming the series impedance shown in Figure 6-2b, transmitted power from the east network to west network is about 800MW.

Time domain simulation using a detailed model of entire Libyan network can accurately determine the *ASL* of the west-east Libyan internal tie-line. Figure 6-4 shows time domain simulation results obtained using NEPLAN. From Figure 6-4-a, the relative power angle between Gdabia at the east and Khalej at the west diverges with increasing power transfer from east to west. Figure 6-4b shows that at the *ASL* of about 620MW, the two areas have lost synchronism when the power angle approaches 90° . The lost synchronism phenomenon is accompanied by the occurrence of what is called electrical centre phenomenon, where theoretically the voltage drops to zero at the tie line midpoint. This is shown by the blue curve in Figure 6-4d that refers to the voltage level close to the midpoint of the tie-line (Ras-Lanuf substation). As addressed, the presence of substations close to the midpoint exposes them to the electrical centre risks, more than other locations. Accordingly,

reactive power support measures must be placed in the vicinity of the midpoint region to improve the performance and effectiveness of the tie-lines.

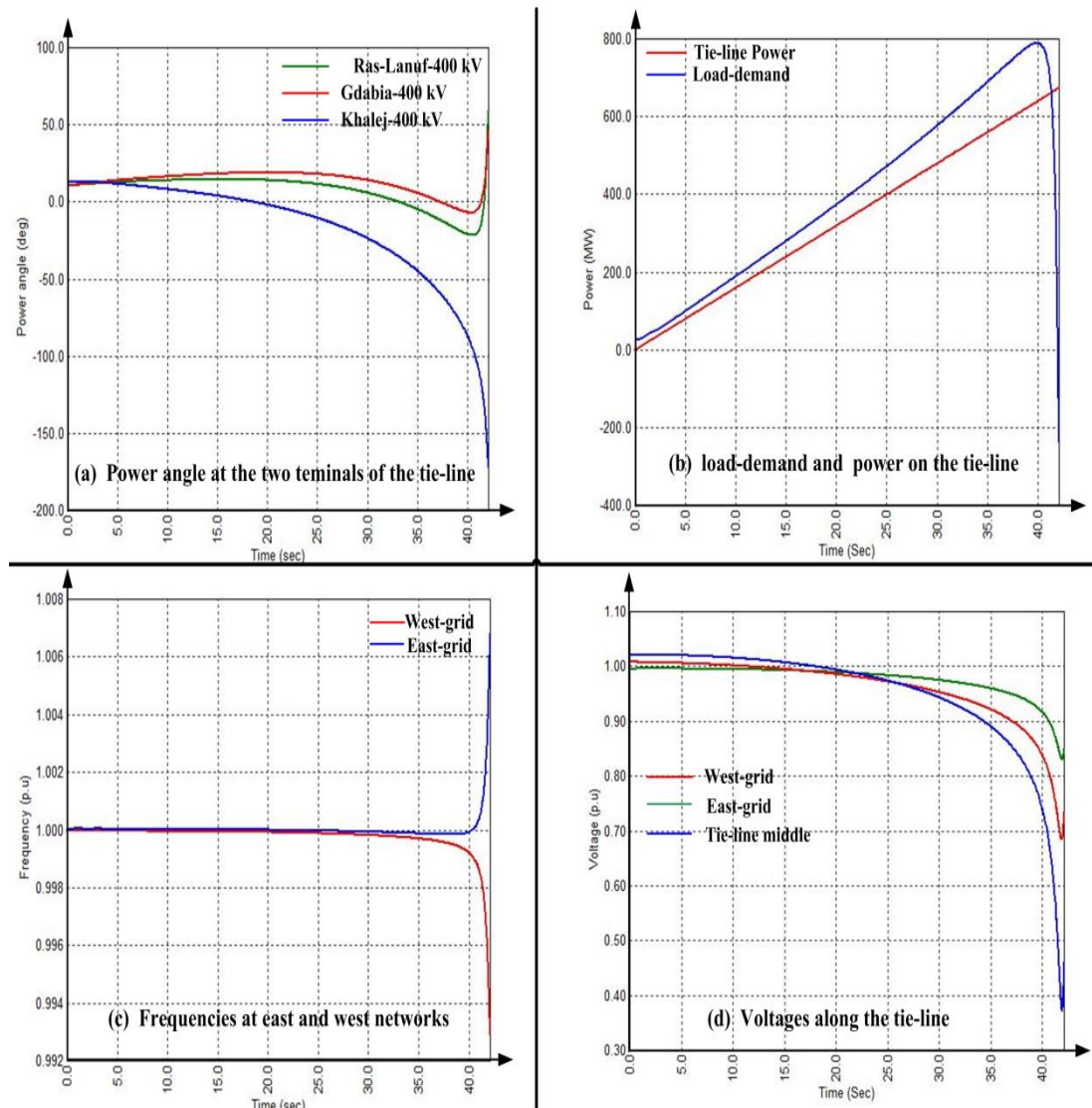


Figure 6-4: Calculation of ASL for west-east Libyan internal tie line using time domain simulation

6.2.6 Summary of West-East tie-line performance and requirements

West-east Libyan internal transmission corridor is a relatively long tie-line. As expected in long transmission lines, power transfer over this corridor is firstly limited by the voltage stability limit and secondly by the steady state angular stability limit. Although the line's thermal limit allows transfer as high as 1345MW during emergency ($N-1$) operating conditions, adhering to reliability and security requirements reduces this limit to 500 MW. Present performance of the tie-line is summarized in Table 6-4, which was obtained in accordance with the voltage and steady state angular stability studies performed in sections 6.2.4 and 6.2.5.

Table 6-4: Power transfer limitation of west-east Libyan internal tie-line

Voltage (kV)	Thermal Capacity(MW)	Tie-line thermal capacity(MW)		(N-1) Voltage restrictions limits (MW)		Angular stability Limit(MW)	Utilization (%)
		Normal	(N-1)	V<90%	VSL		
220	2x480	1830	1345	500	630	800	37
400	870						

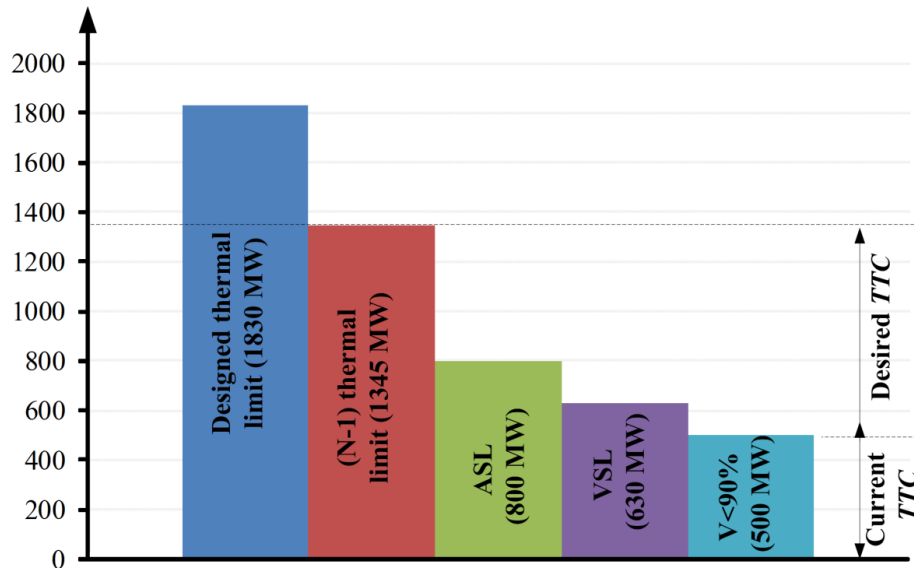


Figure 6-5: Summary performance of west-east Libyan internal tie-line

For further clarification, the performance of the west-east internal Libyan tie-line in Table 6-4 is transformed into the histogram shown in Figure 6-5, which can be summarized by the following points:

- Designed thermal limit of the transmission corridor is 1830MW (blue bar). However, adhering to the reliability requirements reduces this capability to 1345MW as a precaution against an *N-1* condition (loss of the 400kV line between Ras-lanuf and Kahlej).
- The present level of power exchange is about 500 MW, which satisfies operational voltage emergency requirements which stated that the voltage should not be lower than 90% during post-fault operating conditions (*N-1*).
- Optimal utilization of the tie-line requires interconnector reinforcement to increase its total transfer capability by 140% from present level or to be able to exchange securely 1200MW out of 1345MW (when 10% is withheld as a stability margin).

6.3 Discussion of the proposed solutions to improve west-east tie-line performance

Many reactive power related problems of a tie-line can be improved by the means of FACTS and HVDC technologies. However, judgement of the effectiveness of these technologies should be based on technical and economic considerations.

Midpoint shunt compensation can be cost effective compared with series compensation and HVDC technologies. However, the maximum power transfer improvement that can be achieved, even with ideal midpoint shunt compensation, is the steady state angular stability limit (*ASL*) where theoretically the voltage angles at both sides of the tie-line are 90° displaced with respect to each other. Accordingly, TTC of the Libyan internal tie-line can be improved up to its ASL (800MW), and this is the maximum achievable *TTC* with the existing series impedance of the tie-line. Furthermore, to transfer this power level along the tie-line will require the installation of a large size shunt compensator, which is not cost-effective and may increase the risk of voltage instability due to higher *PoC*, as discussed in chapter 3.

Series compensation is one of the practical alternatives to improve tie-line load-ability as it reduces the series impedance of the tie-line, as discussed. However, considerable load-ability improvement may require a higher compensation factor, which increases the risk of sub-synchronous resonance, especially with two multi-shafts CCP power plants at each end of the tie-line.

Although an HVDC solution is more expensive than FACTS solutions, a voltage source converter based HVDC link provides an attractive solution for reinforcement of the internal tie-line in the future [7] for the following reasons:

- 1- The possibility of converting an existing AC OHTL to DC OHTL.
- 2- STATCOM and black start capability.

HVDC increases the level of power exchange between the exciting energy markets, and it is considered the backbone for the future integration of renewable energy with Europe.

6.4 Allocating and sizing of shunt FACTS to maximize TTC in the Libyan internal tie-line

Variable impedance and converter based shunt FACTS devices can be used efficiently to maintain the voltage either at the remote end or at the midpoint along the tie-line. This improves overall tie-line performance as it: improves tie-line utilization, improves transient stability, and provides oscillation damping [8-10]. However, the effectiveness of the SVC, in terms of tie-line utilization improvement, depends on its location and size of the FACTS devices [11].

6.4.1 Allocating shunt FACTS on the basis of *TVCI*

It was established in section 3.5 that the transfer capability of a tie-line is doubled with the presence of sufficient reactive power support provided by ideal midpoint compensation. This finding is consistent with the allocating approach that uses total voltage change index (*TVCI*) to allocate shunt FACTS (section 3.6.1).

TVCI is used in this section to allocate shunt reactive VAR sources in the most suitable substation along the Libyan internal tie-line shown in Figure 6-6.

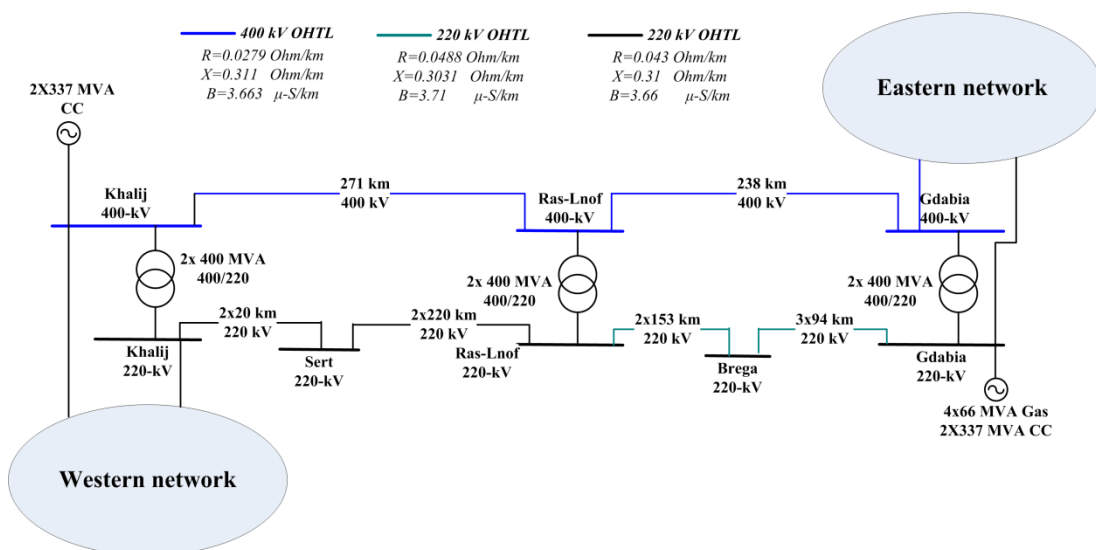


Figure 6-6: Single line diagram of West-East Libyan internal tie line of about 510 km long

Model analysis is performed to determine the node with the highest *TVCI* amongst the candidate nodes. The entire Libyan network is considered in this analysis in order to include all the influential factors and controllers that might affect shunt FACTS allocation.

Table 6-5 shows TVCI calculation results for each candidate substation along the Libyan internal tie-line in Figure 6-6. From the last row of this table, Ras-Lanuf 220kV has the highest TVCI (0.0631 V%/MVA_r) amongst the candidates substations which nominates it as the most suitable location to install a shunt reactive power source (SVC and STATCOM).

Table 6-5: TVCI calculation for shunt VAr source allocation amongst the substations in Figure 6-6

Candidate substation	Self and mutual sensitivity $\Delta V(\%)/\Delta Q(\text{MVA}_r)$							
	Gdabia 400	Gdabia 220	Brega 220	Ras-Lanuf 400	Ras-Lanuf 220	Sert 220	Khalij 400	Khalij 220
Gdabia 400	0.0054	0.0034	0.0032	0.0027	0.0025	0.0007	0.0002	0.0005
Gdabia 220	0.0034	0.0088	0.0072	0.003	0.0035	0.0009	0.0003	0.0007
Brega 220	0.0032	0.0072	0.0227	0.0066	0.0093	0.0023	0.0006	0.0017
Ras-Lanuf 400	0.0027	0.003	0.0068	0.0191	0.0148	0.004	0.0014	0.0031
Ras-Lanuf 220	0.0028	0.0036	0.0095	0.0148	0.0222	0.0054	0.0014	0.004
Sert 220	0.0007	0.0009	0.0023	0.004	0.0054	0.0178	0.0026	0.0125
Khalij 400	0.0002	0.0003	0.0006	0.0014	0.0014	0.0025	0.0028	0.0026
Khalij 220	0.0005	0.0007	0.0017	0.0031	0.004	0.0125	0.0026	0.0132
TVCI	0.0189	0.0279	0.054	0.0547	0.0631	0.0461	0.0119	0.0383

Allocating shunt FACTS on the basis of TVCI in Table 6-5 is supported by the fact that the exciting configuration of the internal tie-line shown in figure 6-1 shows that Ras-Lanuf substation lies geographically in the middle of the tie-line and a little closer to the eastern end. Furthermore, Ras-lanuf substation is connected with important branches in the corridor, which nominate it for any reactive power support as precautions against losing of any of those branches. Moreover, the TVCI results in Table 6-5 agree with the other FACTS allocating approaches that use module analysis and short circuit level to estimate voltage sensitivity to reactive power change at a given node FACTS [12].

6.4.2 Technical constraints for shunt FACTS sizing

Tie-line load-ability is increased by reactive injection at the PCC, which displaces the knee point of the $P-V$ curve further along the horizontal power axis and up along the vertical voltage axis, as addressed in chapter 3. In principle, this means that the

higher the VAR source rating, the more tie-line load-ability can be increased. However, in addition to the cost of higher reactive power rating of FACTS devices, there are other two important technical constraints that limit the amount of shunt injected reactive power at the PCC:

- The first technical limitation for the permissible amount of reactive power injection into the PCC is undesired displacement of PoC on the $P-V$ curve. As discussed in chapter 3, as the PoC raises the safety margin between the maximum loadability and the voltage stability limit (VSL) shrinks and vanishes when the critical voltage become closest to 1 pu [13]. Unless the system is equipped with a sophisticated protection scheme, any small disturbance with such a high PoC can results in the system being unstable.
- The second important factor that limits the injected reactive power is the required voltage difference to force the reactive power to flow from or towards the grid to maintain the PCC voltage. The reactive power on both sides of the coupling transformer are:

$$Q_{term} = \frac{E_{term}^2 - E_{term}E_{PCC} \cos \delta}{X_T}, \quad Q_{PCC} = \frac{E_{term}E_{PCC} \cos \delta - E_{PCC}^2}{X_T} \quad (6-1)$$

where Q_{term} , Q_{PCC} , E_{term} , and E_{PCC} refer to the reactive powers and the voltages on both side of the coupling transformer with X_T leakage reactance.

This equation indicates, in the capacitive mode the terminal voltage (E_{term}) is greater than the PPC voltage (E_{PCC}) and vice versa in the inductive mode.

As coupling transformer resistance is considered negligible compared with its inductive reactance, the power angle between the two ends of the coupling transformer is zero. Hence, the reactive powers at the FACTS terminal (Q_{term}) and at the PCC (Q_{PCC}) are determined by the voltages on both sides:

$$Q_{term} = \frac{E_{term}^2 - E_{term}E_{PCC}}{X_T}, \quad Q_{PCC} = \frac{E_{term}E_{PCC} - E_{PCC}^2}{X_T} \quad (6-2)$$

The line currents on both sides of the transformer are the same (with different sign) and can be calculated as:

$$I_q = \frac{(E_{term} - E_{PCC})}{\sqrt{3} X_T} \quad (6-3)$$

Since the PCC voltage should be maintained within specific operating levels (normally 1 pu) [14], equation (6-3) indicates that the amount of injected or absorbed reactive current to maintain the PCC voltage changes with the voltage level at the FACTS device terminal. Apart from voltage insulation requirements and associated cost, a general conclusion can be drawn for all types of shunt reactive power compensation the higher the voltage level at the VAR source terminal, the lower the FACTS device (*STATCOM*, *SVC*) current rating to satisfy the PCC reactive power requirements.

6.4.3 Sizing of shunt FACTS on the basis of device terminal voltage

For the proposed shunt FACTS at the middle of the Libyan internal tie-line, the choice of the sizing criteria (PoC or terminal voltage of the FACTS) should be determined by the nature and strength of the Libyan grid around the tie-line connection. As the power systems at each tie-line end are relatively strong, the risk of undesired displacement of the *PoC* are low and can be neglected in the FACTS sizing. In contrast, *FACTS* terminal voltage changes in response to power flow change on the tie-line should be considered as the sizing criteria basis. In the same context, the operating voltage level is introduced in [15] as external voltage constraints in the power flow problem to define the acceptable voltage range during the *STATCOM* control modes.

The idea of this sizing criterion is to maintain the PCC voltage at a certain level (specified in the PCC grid requirements) and accordingly the terminal voltage of the FACTS device can vary within its permissible voltage range ($\pm 5\%$). According to standard ‘Std 1031-2011 Guide for the Functional Specification of Transmission Static VAR Compensators’ [16], the voltage during normal and emergency operating conditions should be maintained within specific overvoltage limits for a specific duration, as shown in Figure 6-7. Therefore, the maximum capacitive size of the VAR source is defined at $V=1.05$ pu. Based on the capacitive size, the required inductive size is determined depending on the FACTS type. In the *SVC*, the inductive rating is determined to be slightly higher than the size of a single *TSC*, while in the *STATCOM* capacitive and inductive rating are normally similar.

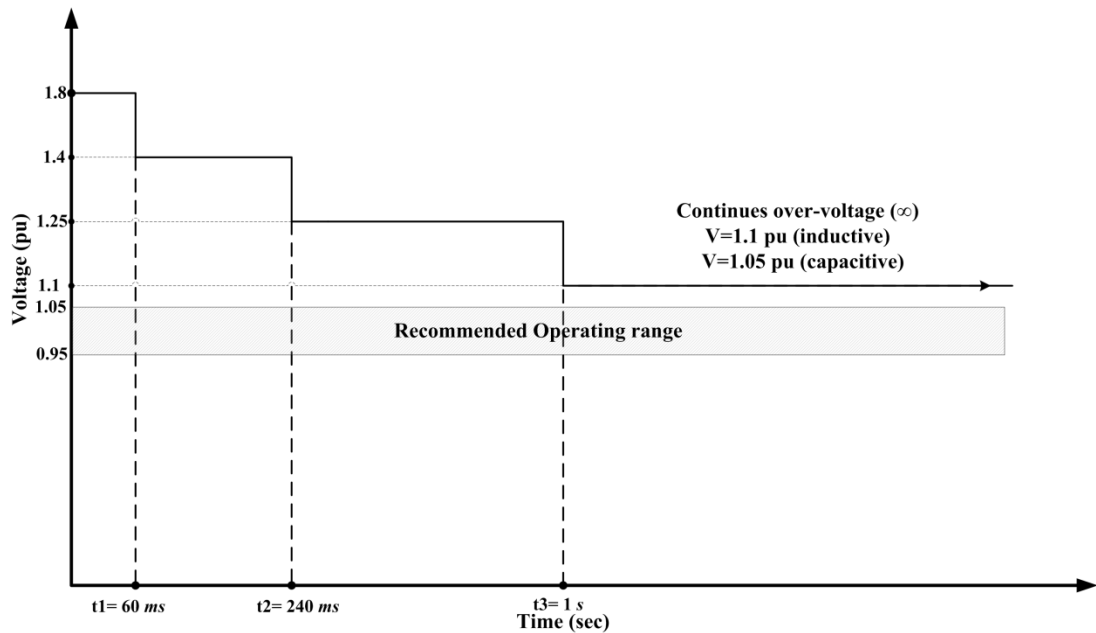


Figure 6-7: Acceptable operational voltage levels for temporary operation [16]

This sizing criterion is used to determine the optimal size of the shunt FACTS device that ensures maximizing of TTC of the Libyan internal tie-line while respecting *PCC* grid code requirements.

In order to determine a reasonable transformer ratio for the coupling transformer, three voltage levels (15kV, 20kV, and 25kV) are evaluated to choose the nominal voltage of the coupling transformer at the FACTS device side. Based on the terminal voltage of the FACTS devices, the optimal size (maximum current rating) of the shunt FACTS, and accordingly TTC of the tie-line are determined.

Reactive current output and the terminal voltage of the VAR source are continuously monitored during the gradual increase of tie-line power transfer from east to west in Figure 6-6. As mentioned, the maximum current rating of devices is determined at the level when the terminal voltage reaches 1.05 pu. Simulation results for this sizing criterion are shown in Figure 6-8.

Point C in the figure defines the maximum operating point on the terminal voltage curve ($v=1.05$ pu) which in turns determines the FACTS device size based on its nominal voltage. The required current rating of the VAR source at each nominal voltage is established as 7.3kA, 5.5kA, and 4.35kA. The optimal FACTS size is an inverse relationship with the FACTS designed nominal voltage, as discussed. The VAR source size for a 15kV nominal voltage is about 68% larger than for 25kV.

However, the choice of FACTS nominal voltage involves other aspects such as insulation level, cost, and FACTS device type.

FACTS device size is normally defined by its MVA rating. It follows that regardless of terminal voltage and FACTS type, the same reactive power is required to maintain the PCC voltage at a certain level of power transfer over the tie-line. Figure 6-8 indicates that the total transfer capability of the Libyan internal tie-line can be improved to 610MW with a 200MVA capacitive rating FACTS device installed in the Ras-Lanuf substation.

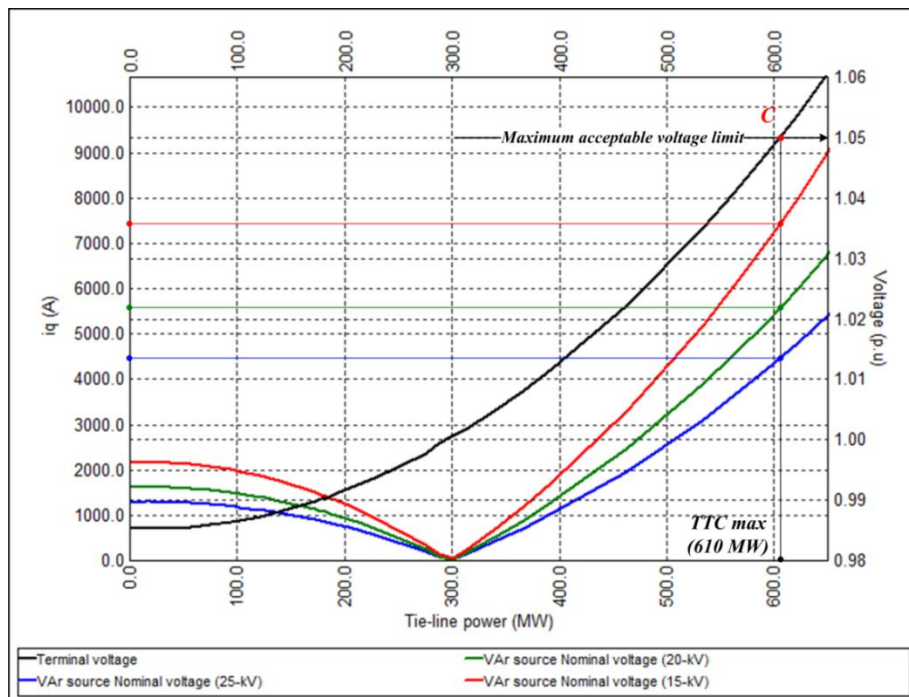


Figure 6-8: Sizing of shunt VAr sources on the basis of terminal voltage

6.5 Libyan internal tie-line with a midpoint SVC

The SVC is classified as variable impedance shunt compensator that employs reactive power bank storage to release the controllable reactive power that facilitates voltage control at the PCC. Based on terminal sizing criteria, the proposed size of the SVC is about 200MVA capacitive rating at 20kV nominal voltage. The SVC is connected to the grid through 220 MVA coupling transformer with 10.5 % short circuit impedance. This size can be divided into three TSCs each rated at 65MVar. Accordingly, the TCR size is assumed to be about 72MVar. The TCR can be employed along with the existing switchable reactors to maintain the voltage during light loading conditions.

6.5.1 Dynamic performance of the SVC during TSC switching

A gradual increase in tie-line loading is simulated in order to investigate the system response during TSC switch in and system strength adequacy to accommodating SVC switching dynamics. An SVC performs its control tasks through a set of TSCs that injects the reactive power in a step-like change while a TCR smoothly absorbs the surplus capacitive reactive power.

The time domain simulation in Figure 6-9 indicates that the Libyan grid is relatively strong to absorbing SVC switching transients. Apart from small dips at the instant of a TSC switching, Figure 6-9a demonstrates that net reactive power output from the SVC is smoothed by the TCR firing delay angle. The TSCs step-like change with the TCR smoothing effect is shown in Figure 6-9b.

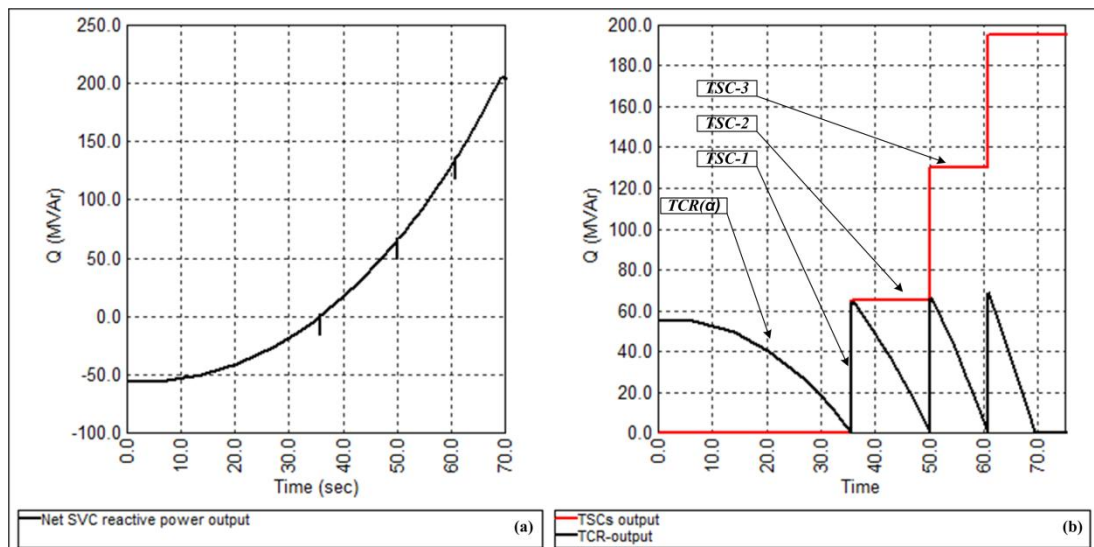


Figure 6-9: Dynamic of SVC during TSC switching

6.5.2 Dynamic behaviour of the tie-line during three phase short circuit

Figure 6-10 shows the reduced model of the Libyan internal tie-line, modelled in NEPLAN, with a (-200+72) MVAr SVC installed in the middle of the tie-line (in Ras-Lanuf substation). A severe 3-phase short circuit at the middle of the 400kV line, which is cleared after 150ms by opening the line at both sides as shown in the figure, is simulated. The operating scenario where the tie-line is transmitting its peak power, 600MW (TCC of the line with 205MVAr SVC), is considered in this for dynamic analysis.

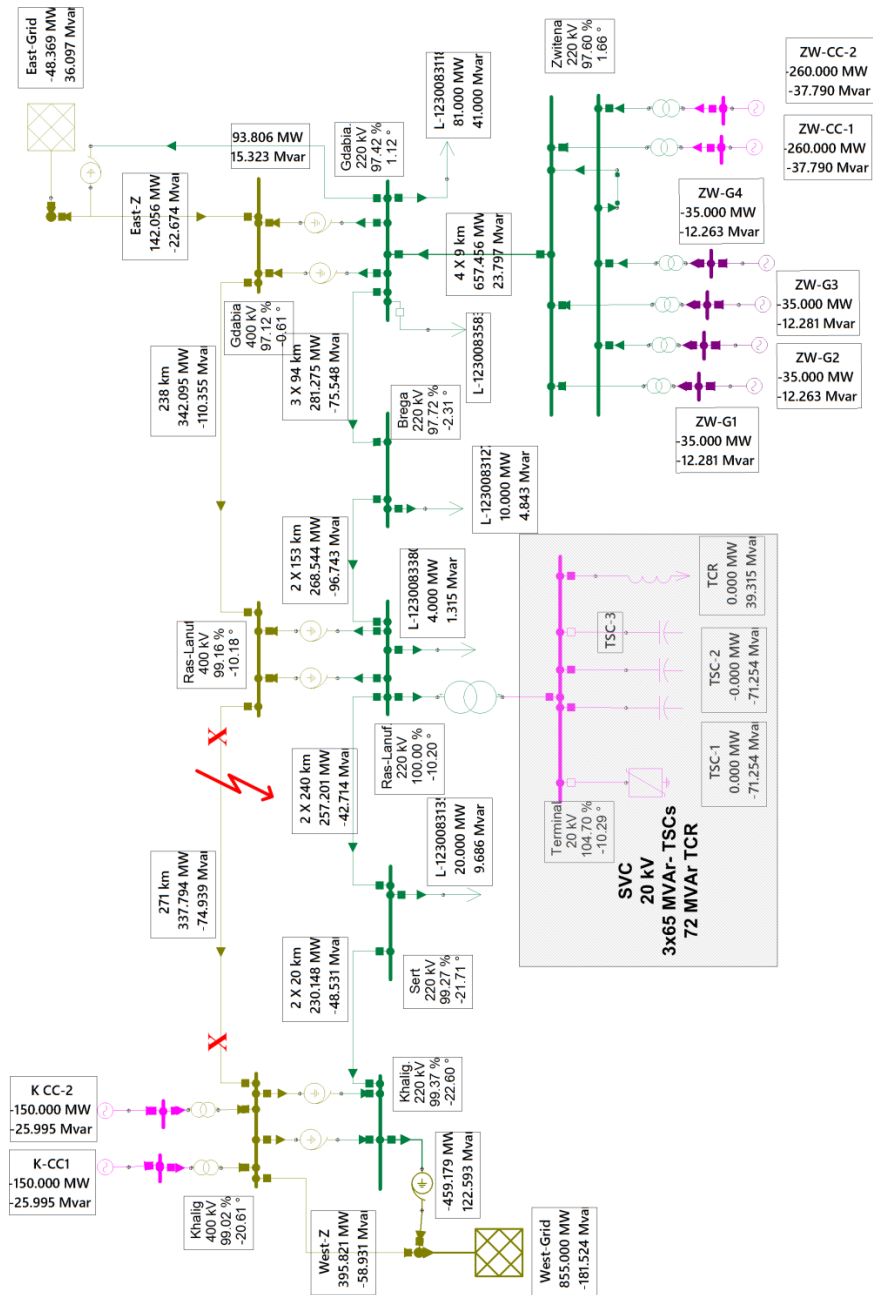


Figure 6-10: Reduced model of the Libyan internal tie-line with a (-200,+72)MVar SVC installed in Ras-Lanouf

Figure 6-11 presents the results (30s of simulation time) where entire Libyan transmission network is modelled. From Figure 6-11b, the SVC responds to the fault when its control system switches in the TSCs in response to the voltage dip during the fault, as shown in Figure 6-11a. The first TSC-1 is switched-in to control the PCC voltage in accordance with the tie-line reactive power requirements at the *TTC* (610MW). The black curve in Figure 6-11b, which refers to the *TCR* output, indicates that the TCR efficiently performs its task pre and post-fault. Initially, the

TCR absorbs about 2MVar to cancel the surplus reactive power from TSC-1, while during and post-fault it operates with a firing delay angle of 90°, eliminating any inductive energy absorbed, as shown in Figure 6-11c and Figure 6-11d.

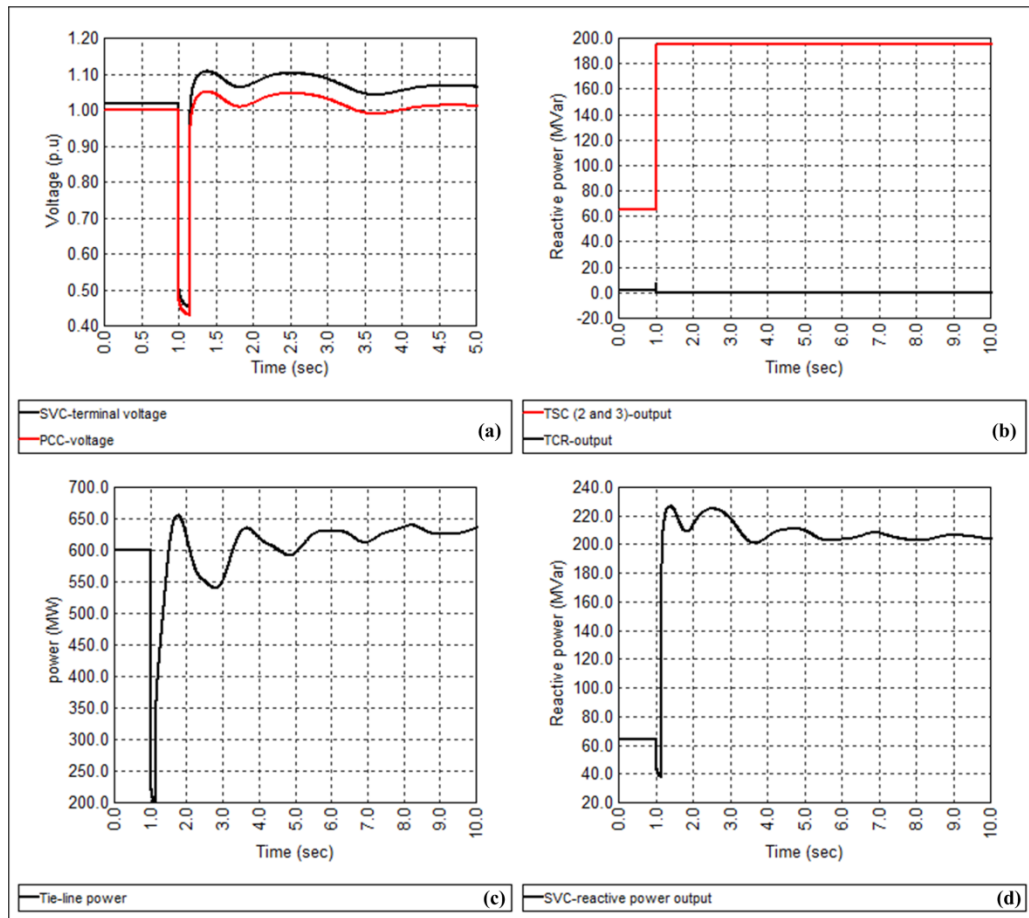


Figure 6-11: SVC response for a 3-ph fault on the middle of 400kV line

6.6 Libyan internal tie-line with midpoint STATCOM

A STATCOM with a rating of ± 200 MVA is used to investigate the system dynamics under stressed operating conditions. With the same nominal voltage as the SVC case, 20kV, the current rating of the STATCOM is about 5.92kA. For practical and reasonable current rating (less than 1kA), the total 200MVA is modelled as a group of 8 parallel STATCOMs, each 26MVA (current rating is 0.98kA) installed in 220 kV Ras-Lanouf substation.

6.6.1 Dynamic behaviour of the tie-line during a three phase short circuit

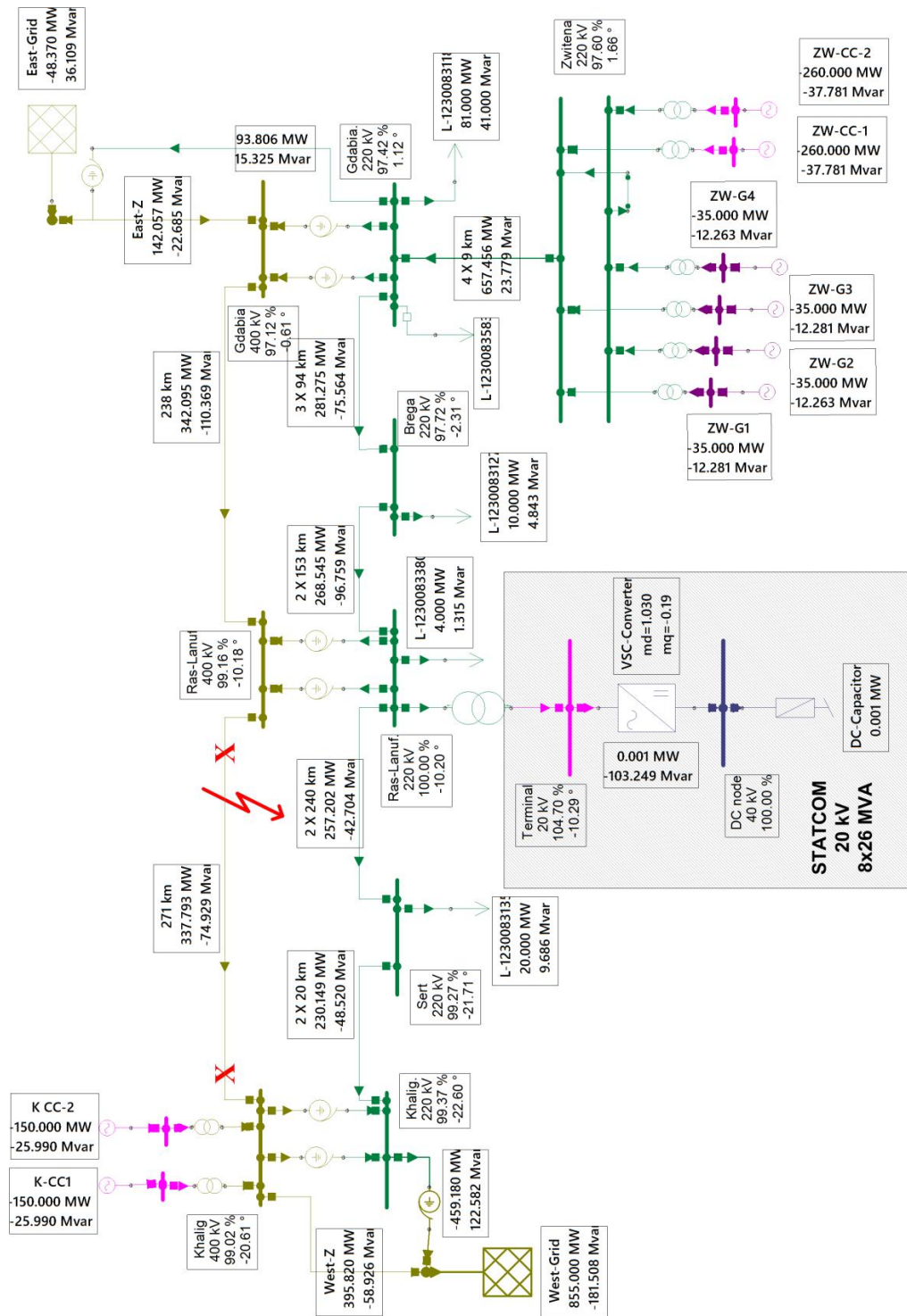


Figure 6-12: Reduced model of the Libyan internal tie-line with 200 MVA STATCOM installed in Ras-Lanouf

For the time domain analysis, single line diagram of the Libyan internal-tie line with STATCOM installed in the middle of the tie-line is illustrated in Figure 6-12. Dynamic simulation is performed to investigate the tie-line performance with a

STATCOM. A solid three phase short circuit at the middle of the 400kV line is simulated. The operating scenario when the tie-line is transmitting 600MW (TTC) is considered in the simulation (as with the SVC).

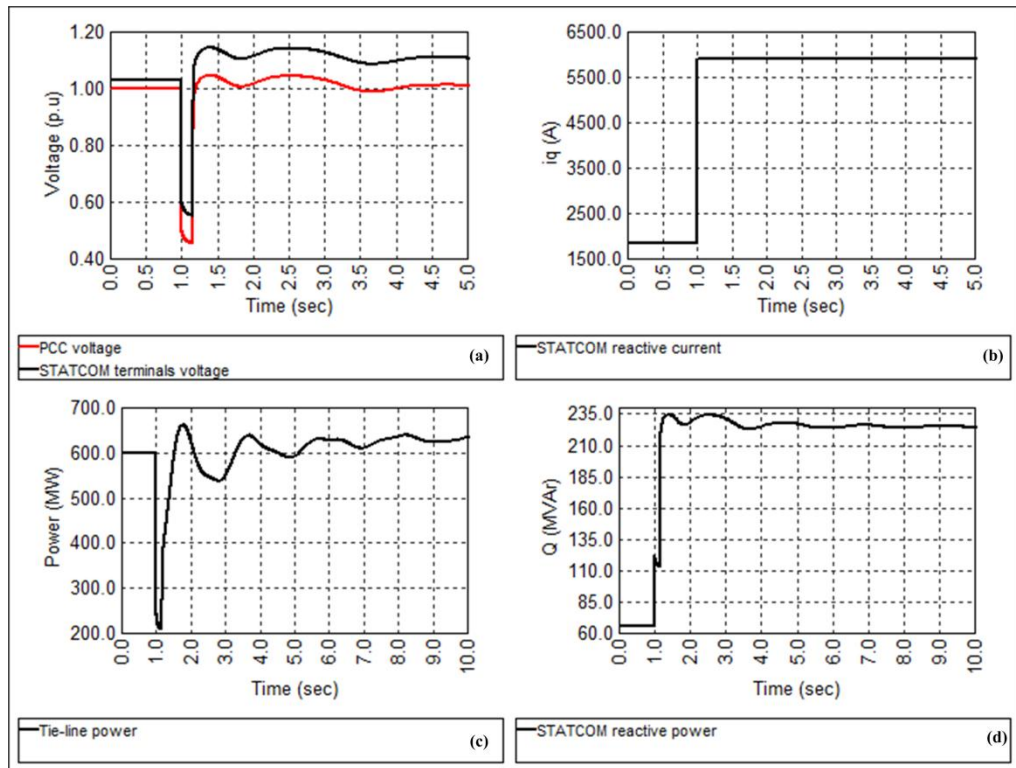


Figure 6-13: STATCOM response for a 3-ph fault on the middle of 400kV line

Figure 6-13 shows simulation results that illustrate the STATCOM response to a 3-phase fault that trips the 400kV line in Figure 6-6. As expected for a converter based FACTS with constant current characteristic, the STATCOM provides its full current rating to support the system during the voltage dip, as it is indicated in Figure 6-13b. Simulation results in Figure 6-13a illustrate that the $V-I$ characteristics of the STATCOM provide better voltage support than that provided by the SVC in Figure 6-11a. (The voltage dip during the fault in the STATCOM case is about 0.58 pu while the drop is to 0.44 pu in the SVC case.) The difference between the two FACTS types can also be observed from the reactive power output during the fault which is increased in the STATCOM case (Figure 6-13d) while it reduces with the voltage dip in the SVC case in Figure 6-11d.

Despite the mentioned behavioural differences of the STATCOM and SVC during the fault, both types provide the required reactive power support to maintain system stability. However, Figure 6-11c and Figure 6-13c demonstrate damped

electromechanical oscillations on the tie-line which is difficult to be improved with the proposed FACTS rating.

6.7 Libyan internal tie-line with series compensation

Series compensation can improve tie-line load-ability, and provides an effective solution for power flow control over tie-lines in interconnected power systems. As discussed in chapter 4, the controllable series impedance (capacitive or inductive) of series FACTS devices allows cancellation or addition of a portion of the series inductive reactance of the tie-line in accordance with system requirements [17]. The main technical challenge in the series compensation is the possible risk of the sub-synchronous resonance SSR especially in fixed capacitor based series compensation technologies such as FC and TSSC.

6.7.1 Potential subsynchronous resonance around the Libyan internal tie-line

As studied in section 4.4 in chapter 4, the rotating inertia of the mechanically coupled masses in conventional power plants can introduce SSR into a system. In such conditions, the LC resonant circuit of the compensated line can establish natural resonance frequencies close to the torsional oscillation during system disturbances [18, 19].

As both tie-line ends involve combined cycle turbines with multi-mass shafts, small signal stability is carried out to establish possible oscillatory modes that can interact with TCSC possible natural resonance frequencies in the tie-line. Results of this analysis will then be used to determine a suitable compensation factor for the TCSC that ensures TTC maximizing, well away from any SSR risks.

Small signal stability results for the area around the internal tie-line indicates that all the eigenvalues have negative real parts which indicate a stable system around the studied operating condition (peak scenario). The results also show that the dominant mode is non-oscillatory with a real part of -0.15 with an acceptable damping factor (0.242Hz), and the major contributors to this mode are states related to generating unit controllers (speed governor in Homs GT) which can be improved with better tuning.

Table 6-6 shows the system eigenvalues results around the internal tie-line with the oscillatory mode that can introduce system SSR. Although the presented eigenvalues

indicate sufficient damping factor and negative real parts, at least two modes can cause sub-synchronous torsion interaction. Therefore, these modes (39 and 27) should be addressed as they can excite their 50Hz complementary natural resonance frequencies (11 and 23) which can introduce system SSR.

Table 6-6: Torsional oscillatory modes of the generating units around the internal tie-line

Eigenvalue	damping ratio (ζ)	Frequency (Hz)	State variable
-87.6±j245	0.33	39	d-ang-GOV-Zwitina
-11.5±j132	0.086	27	d-wr-GOV-Zwitina
-7.72±j52.3	0.146	8.3	dvt2-AVR-Hosm steam-1
-7.68±j52.3	0.145	8.3	dvt2-AVR-Hosm steam-3

6.7.2 Allocating series compensation to maximize TTC of the Libyan tie-line

In the course of FACTS allocating, the tie-line middle normally experiences the largest voltage sag, as it represents the weakest point where the electrical centre can be established. For this reason, the series FACTS device should be as close as possible to the middle of the line. More precisely, it should be closer to the electrical centre of the interconnection, which is slightly biased to the vulnerable end of the interconnection link, as established in chapter 4. This location provides the required midpoint voltage support and represents the point of the lowest short circuit level which reduces the fault current through the FACTS valves, considerably.

Figure 6-14 illustrates the equivalent circuit of the effective series impedances of the transmission line around the tie-line.

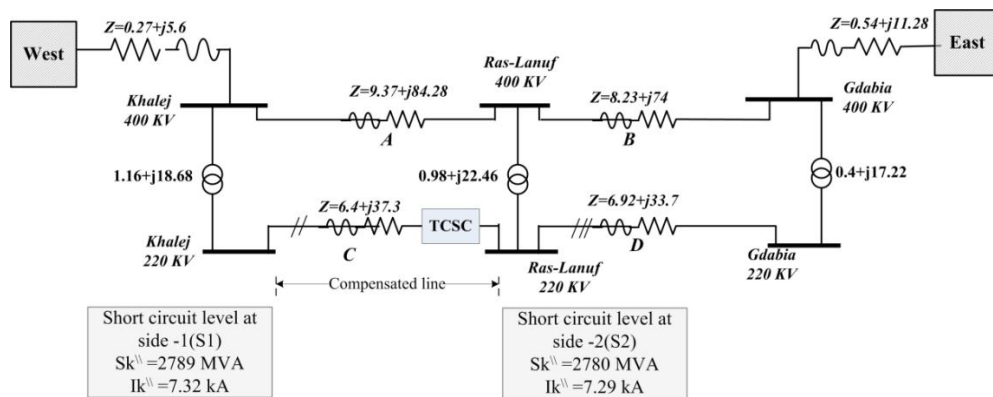


Figure 6-14: Effective series impedance around the internal tie-line

220kV line-C in the figure represents the longest and the less influential line in the corridor. Furthermore, the east side end of the line is connected to the Ras-Lanuf 220kV substation in the midpoint of the tie-line which represents a pilot node in terms of voltage support along the tie-line.

Based on these considerations, the optimal placing of the series compensation along the Libyan tie-line should be around this substation, especially being an easily accessed substation, and with expansion possibilities.

6.7.3 Technical considerations for series compensation sizing in the Libyan tie - line

A suitable series compensation size should be determined considering the full current rating of the compensated line. Furthermore, the series capacitor size has to be determined to avoid participating and exuberating in system SSR.

The full current rating of the 240km 220kV double circuit line-C in Figure 6-14 is about 2x1250 A. This allows about 2x476 MVA in total, at the operating voltage (220 kV). Therefore, the series compensation device must be able to carry the full line current especially during any emergency where the compensated line is designed to operate normally at its current rating [20]. Based on the technical specifications of the 220kV line-C, the voltage drop at full current is about 90kV. Simply compensation of about 30% of this voltage drop (90 kV) requires a capacitive rating of about 68MVAR per phase (C rating= 0.3 x 90 x 2500) that is, 202MVA 3 phase rating. The voltage across the compensation equipment at full current rating is about 30kV. This MVA rating accounts for about 20% of the line rating which reveals the effectiveness of the series compensation. However, as discussed in chapter 4, any series-connected equipment has to be able to carry 100% current loading during an emergency.

Subsynchronous resonance concerns also have to be considered in the sizing of series capacitors. The natural resonance frequency of the established LC circuit can be estimated from the short circuit levels at the both sides of the compensated line as described section 4.4.1.

Figure 6-14 illustrates that the equivalent Thevenin impedances at both sides of the compensated line are 17.35 Ω and 17.4 Ω . These values are used with the series

impedances of the compensated Line-C ($Z=6.4+j37.3 \Omega$) in equation 4-15 to estimate the natural resonance frequency at different compensation factors, as shown in Figure 6-15.

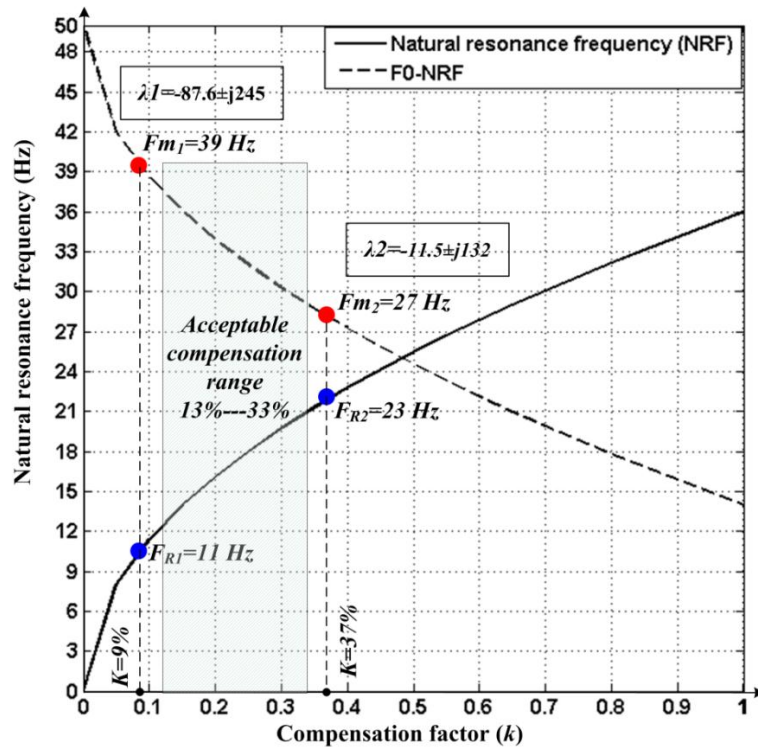


Figure 6-15: Natural resonance frequency versus the tie-line compensation factor

As expected, the black curve in the figure indicates that the natural resonance frequency (NRF), of the established LC circuit, increases with the increased compensation factor. In the same figure, the dashed line represents the 50Hz NRF complementary frequency ($f_m=f_0-NRF$). If the complementary series resonance frequency f_m of the compensated line coincides with poorly damped torsional modes of the turbo-generator shaft, an increased mechanical stresses can be induced in the turbine shafts due to the SSR. At 9% and at 37% of compensation factor, two natural resonance frequencies (11 or 23 Hz) coincide with the poorly damped torsional modes ($f_m=27$ and 39 Hz) associated with Zwitina CCP turbine which can introduce system SSR. Therefore, this risk should be a taken in a consideration when a fixed capacitor (FC) or thyristor switched series capacitor ($TSSC$) is used to compensate the Libyan internal tie-line. Based on this discussion, the compensation factor for the Libyan internal tie-line can be chosen within a reasonable range of between 15% and 35%, as indicated in Figure 6-15.

6.8 Thyristor controlled series compensation (TCSC) in the Libyan tie-line

The thyristor controlled series compensator (TCSC) is an effective and widely used series FACTS device. As addressed in chapter 3, the TCSC is efficiently used to improve transfer capability of a tie-line, enhance voltage and transient system stability, control the power flow in the parallel lines, and provides power oscillation damping [21]. Unlike FC and TSSC, TCSC can be used for effective SSR mitigation as it can eliminate since its series capacitor acts inductively in the subsynchronous frequency band. This allows further compensation of the tie-line and consequently further TTC improvement [21].

6.8.1 TCSC operating ranges

The suitable range for the series compensation in the Libyan tie-line is from 15% to 35% as determined in section 6.7.3. However, a compensation factor of 30% is used in this analysis to maintain a reasonable margin from the SSR risk. Then the fixed capacitor size of the TCSC is about 22.4Ω , accordingly the suitable TCR size (typically L/C ratio is about 0.1333[20]) is about 3Ω .

The capacitive and inductive sizes define the firing delay angle range which ensures a proper inductive and capacitive operation while avoiding the prohibited firing delay range associated with parallel LC resonance [22]. Equation 4-25 is used to establish TCSC effective series impedance (X_{tcsc}) versus firing delay angle α for the given capacitor and inductor sizes. Based on the firing delay angle, three zones are defined in Figure 6-16. The TCSC inductive operation mode is defined by the firing delay angle from $0 \leq \alpha \leq \alpha_{L_{lim}}$ (0° to 53°). The prohibited firing delay angle zone is shown shaded, and is defined by the firing delay angle range of $\alpha_{L_{lim}} \leq \alpha \leq \alpha_{C_{lim}}$ (54° to 64°), which indicates parallel resonance at $X_C = X_{L(\alpha)}$. The normal TCS operating mode is capacitive which is within the range $\alpha_{C_{lim}} \leq \alpha \leq \frac{1}{2}\pi$ (65° to 90°).

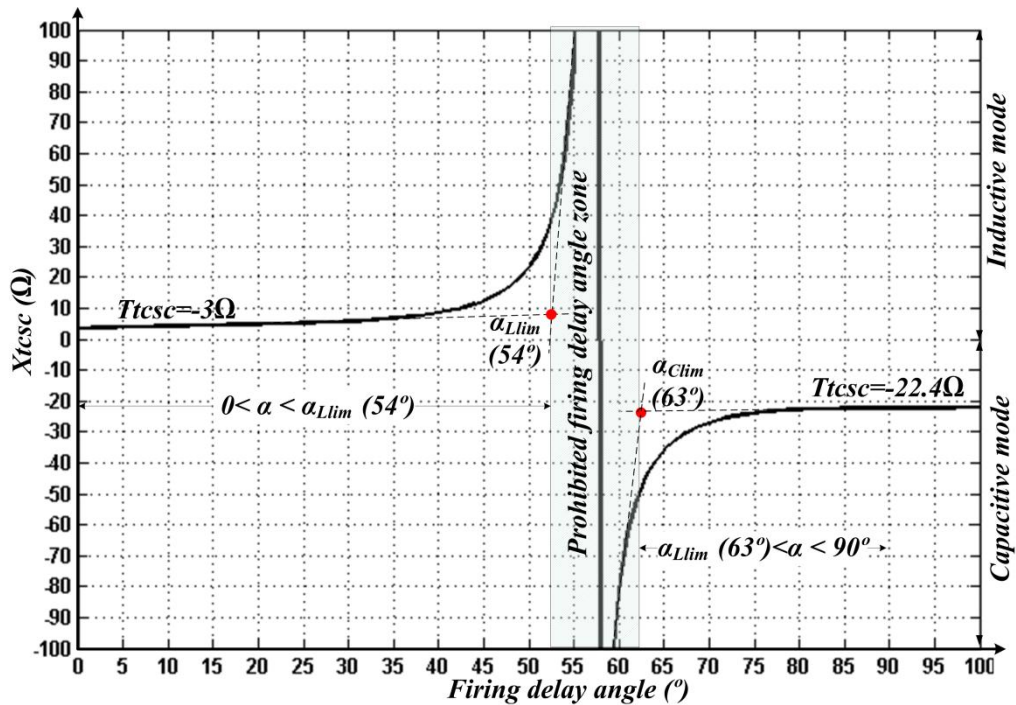


Figure 6-16: Effective impedance versus firing delay angle for the TCSC in the Libyan tie-line

6.8.2 Total transfer capability of the Libyan internal tie-line with TCSC

The extent of *VSL* and *TTC* improvement in the Libyan tie-line with the TCSC can be assessed using *P-V* curve analysis, where the power demand is gradually increased in the western area in order to force the power energy to flow from the eastern network through the tie-line. As discussed, tie-line performance should be assessed based on an *N-1* operating scenario. Hence, the analysis includes evaluation of tie-line performance during an emergency operating condition where the 400kV branch (Line-A) is out of service. Four case studies (with the TCSC installed in Line-C) with different series compensation factors are investigated ($k=0\%$, $k=25\%$, $k=30\%$ and $k=35\%$). Voltage stability limit (*VSL*) corresponds to line loading at the knee point of the *P-V* curve while total transfer capability (*TTC*) of the tie-line is determined at the first voltage violation ($\pm 5\%$ in normal operating and $\pm 10\%$ during an emergency).

Figure 6-17 shows midpoint voltage changes, at Ras-Lanuf substation, with the change of power transmission over the tie-line. As the level of series compensation increases both indices of power transfer increase (*TTC* and *VSL*).

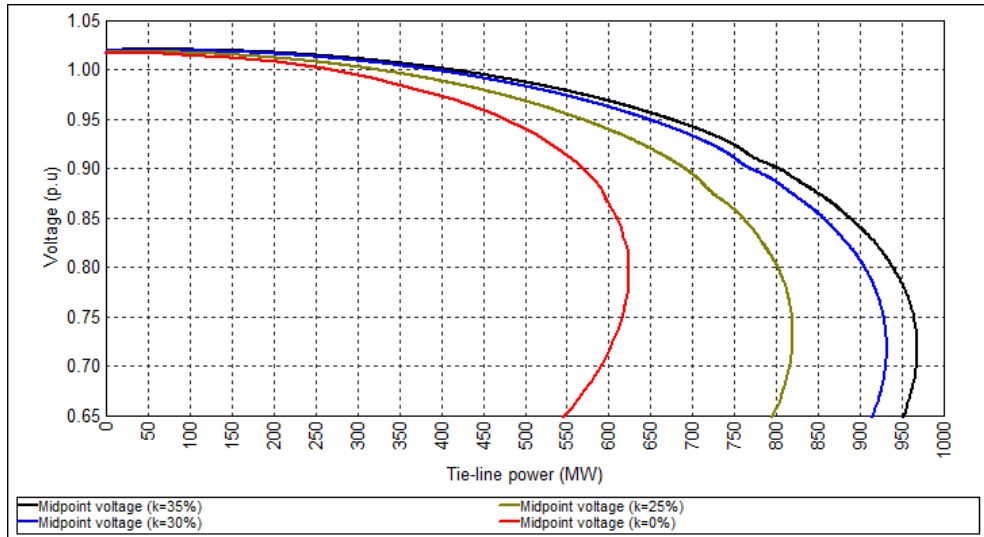


Figure 6-17: Tie-line load-ability at different series compensation factors (*P-V* curves)

The black curve ($k=35\%$) shows that the voltage stability limit is dramatically increased with this compensation factor, by about 60% while TTC is increased by 39%, compared with the improvement with a 25% compensation factor (40% for TTC and 31% for VSL). Table 6-7 summarizes tie-line performance results for different series compensation levels.

Table 6-7: summary of tie-line performance with TCSC with different compensation factors

Compensation Factor (%)	TTC (MW)	VSL (MW)	TCSC size			Voltage across TCSC (kV)	Improvement Indicator (%)	
			(MVA)	FC (F)	TCR (H)		TTC	VSL
0	500	624	-	-	-	-	-	-
25	700	819	101	1.7×10^{-4}	0.0079	47	40	31
30	775	931	119	1.42×10^{-4}	0.0095	55	55	49
35	800	986	138	1.22×10^{-4}	0.0111	64	60	58

In addition to the considerable *TTC* improvement, *VSL* improvement indicator in Table 6-7 illustrates that the voltage stability margin ($VSM=VSL-TTC$) in the tie-line improves as the compensation factor increase which reflects on system security. However, this preference aspect may be at the expense of other aspects such as size, voltage insulation requirements and consequently the cost. The MVA rating of the TCSC, which is calculated at a full current rating of the compensated line (1250A), in the case of 25% compensation factor, is about a third that required for a 35% compensation factor, at the same line current rating.

6.8.3 Dynamic performance of the TCSC during a severe fault

Steady-state based analysis shows that the Libyan internal tie-line with TCSC ($k=30\%$) improves the tie-line performance in terms of load-ability and voltage profile under normal and emergency operating conditions. In this section, dynamic analysis using time domain simulation is performed to investigate tie-line performance with a severe fault at peak load. Figure 6-18 shows the pre-fault configuration and power flow around the compensated tie-line. The TCSC controller structure shown in the figure along with network generating unit controllers are phasor models. In order to show the importance of the TSCS in terms of transient stability improvement, the same disturbance is simulated for an uncompensated tie-line under the same loading condition.

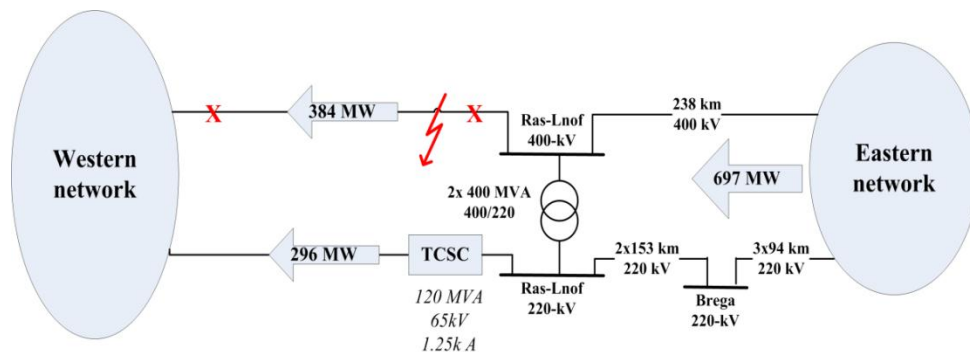


Figure 6-18: Pre-fault condition around the compensated tie-line

From Figure 6-19, the dynamic performance of the compensated line is improved compared with that of the uncompensated tie-line which faces loss of synchronism between the two operating areas. As the fault is applied at the middle of the line, the voltage drops to just above 0.4 at the midpoint of the tie-line (Ras-Lanuf) before recovering after fault clearance, as shown in Figure 6-19a. In the compensated line case, the voltage settles around the steady state value while when uncompensated, the voltage starts to decline due to the prolong loss of synchronism dynamics that occur after 10s, as shown in Figure 6-19c. As indicated in Figure 6-19d, the TCSC manages to modify its effective inductance which further strengthens the handling tie-line impedance. Proper TCSC action allows power flow unbalance handling during the fault and after the losses of the crucial 400kV line. On the other hand, the loss of synchronism in the uncompensated tie-line case is mainly due loss of the

400kV which reduces the angular stability limit of the tie-line below its operating load-ability.

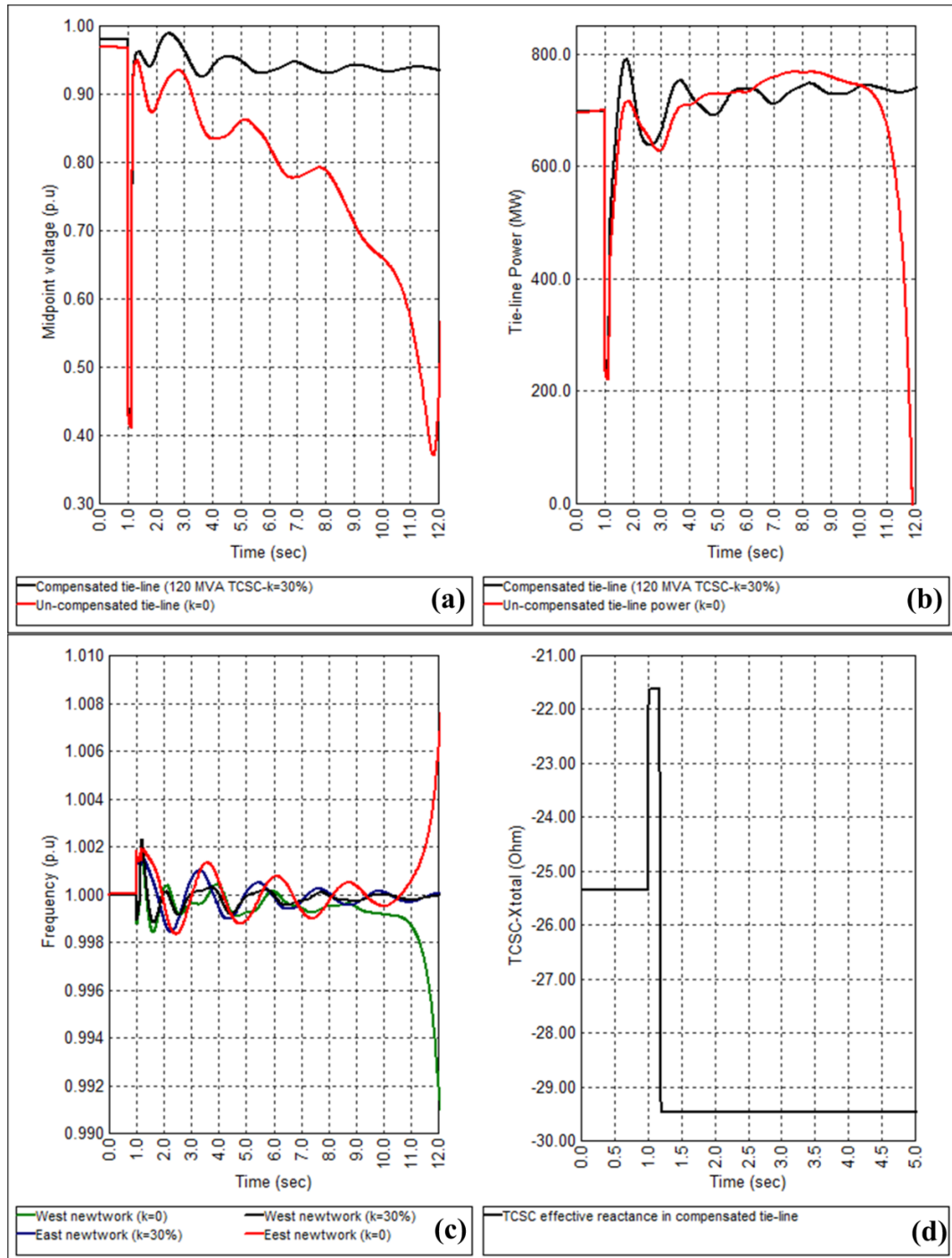


Figure 6-19: Dynamic performance for compensated tie-line during 3-phase fault

6.9 Summary

The performance of the Libyan internal tie-line in terms of its power transfer capability was investigated. Analysis showed that shunt and series FACTS can improve the total transfer capability of the tie-line, though series compensation offers better TTC improvement. Total transfer capability of the Libyan internal tie-line can be increased by the means of shunt FACTS up to 610MW beyond which the terminal voltage at the FACTS terminal exceeds the acceptable level. This level of power transfer requires a FACTS installation of 200MVar capacitive rating in Ras-Lanuf substation.

Steady state and dynamic analysis of the Libyan internal tie-line with TCSC results in significant improvement in the tie-line performance. A 30% compensation factor is sufficient to achieve 55% TTC improvement while maintaining enough safety margin to prevent the risk of sub-synchronous resonance.

References

- [1] C. E. a. A. S. G.Vukojevic "CONSULTANCY FOR UPDATING LIBYAN TRANSMISSION NETWORK EXPANSION STUDIES 2010-2030 " 15.00/PP01:63713A/151010., 2010.
- [2] A. S. Elansari, *et al.*, "Improve transient frequency response by adjusting generators' over frequency relays," in *Power and Energy (PECon), 2012 IEEE International Conference on*, 2012, pp. 458-463.
- [3] G. C. C. Bruno, "Consultancy services about Optimal Operation Schemes for the Libyan 400 kV and 220 kV Networks " CESI, Milan, Italy2011.
- [4] P. F. Cignatta Massimiliano, "Consultancy Services for update of Libyan network defence plans " CESI, Milan,Italy2009.
- [5] G. Uhlen, *et al.*, "Application of small signal stability analysis to the Nordel power system," *VII SEPOPE, Curitiba, Brazil*, 2000.
- [6] T. T. C. T. Force, "Available transfer capability definitions and determination," *North American Electric Reliability Council, Princeton, New Jersey*, 1996.
- [7] R. d. S. Les Brand , Errol Bebbington and Kalyan Chilukuri, "Grid West Project HVDC Technology Review," JA4846, 17th December 2014 2014.
- [8] U. P. Mhaskar and A. M. Kulkarni, "Power oscillation damping using FACTS devices: modal controllability, observability in local signals, and location of transfer function zeros," *Power Systems, IEEE Transactions on*, vol. 21, pp. 285-294, 2006.
- [9] J. F. Gronquist, *et al.*, "Power oscillation damping control strategies for FACTS devices using locally measurable quantities," *Power Systems, IEEE Transactions on*, vol. 10, pp. 1598-1605, 1995.
- [10] M. J. Gibbard, *et al.*, "Interactions between, and effectiveness of, power system stabilizers and FACTS device stabilizers in multimachine systems," *Power Systems, IEEE Transactions on*, vol. 15, pp. 748-755, 2000.

- [11] B. K. Kumar, *et al.*, "Placement of FACTS controllers using modal controllability indices to damp out power system oscillations," *Generation, Transmission & Distribution, IET*, vol. 1, pp. 209-217, 2007.
- [12] T. T. Lie, "Method of identifying the strategic placement for compensation devices," *Power Systems, IEEE Transactions on*, vol. 10, pp. 1448-1453, 1995.
- [13] T. Van Cutsem, "Voltage instability: phenomena, countermeasures, and analysis methods," *Proceedings of the IEEE*, vol. 88, pp. 208-227, 2000.
- [14] E. Date, "PJM Manual 03: Transmission Operations."
- [15] X.-P. Zhang, *et al.*, *Flexible AC transmission systems: modelling and control*: Springer Science & Business Media, 2012.
- [16] "IEEE Guide for the Functional Specification of Transmission Static Var Compensators - Redline," *IEEE Std 1031-2011 (Revision of IEEE Std 1031-2000) - Redline*, pp. 1-106, 2011.
- [17] T. Orfanogianni and R. Bacher, "Steady-state optimization in power systems with series FACTS devices," *Power Systems, IEEE Transactions on*, vol. 18, pp. 19-26, 2003.
- [18] K. Padiyar, *Analysis of subsynchronous resonance in power systems*: Springer Science & Business Media, 2012.
- [19] C. E. J. Bowler, *et al.*, "Self Excited Torsional Frequency Oscillations with Series Capacitors," *Power Apparatus and Systems, IEEE Transactions on*, vol. PAS-92, pp. 1688-1695, 1973.
- [20] N. G. Hingorani and L. Gyugyi, *Understanding FACTS: Concepts and Technology of Flexible AC Transmission Systems*: Wiley, 2000.
- [21] ABB, "TCSC Thyristor Controlled Series Compensation Keeping grids together," ABB, Västerås,- SWEDEN2010.
- [22] P. K. Dash, *et al.*, "Damping multimodal power system oscillation using a hybrid fuzzy controller for series connected FACTS devices," *Power Systems, IEEE Transactions on*, vol. 15, pp. 1360-1366, 2000.

Chapter Seven

Strengthening the Libyan internal tie-line with VSC-HVDC Transmission

7.1 Introduction

This chapter addresses the potential use of a VSC-HVDC system to improve power transfer capability of the Libyan internal tie-line. Although the length of the targeted line may not be long enough to justify the project from the economical point of view, in the long run, congestion cost reduction and system security may outweigh the cost of VSC-HVDC. Steady state and dynamic evaluation, for the reinforced tie-line, are carried out using a detailed model of the Libyan network [1]. The optimal AC line to be converted to a dc line is determined along with the optimal size converters stations. The performance of the tie-line during normal and emergency conditions is evaluated including; STATCOM operation, frequency control capability during unsynchronized connection, and power management during of the hybrid AC/DC tie-line.

7.2 Rationale for converting an existing AC line to a DC transmission systems

Upgrading of the existing ac line to dc line with relatively fewer facilities change and lower cost is a challenge [2, 3]. Only limited work has been carried out to determine the suitable AC line to be converted to DC line and to evaluate feasible topologies [4, 5]. In order to reduce the implementation time and cost of the project, one of the existing AC lines could be converted into DC line. Theoretically, the less influential AC line, in the transmission corridor, is the suitable choice for conversion to DC. This ensures maximum benefits from the reinforced east-west internal interconnectors. The extent of the AC line influence on the system can be established from the computation participation factor matrix which is extractable from modal analysis of the tie-line being studied. In this analysis, all the branches in the transmission corridor are ranked in ascending order based on their participation factor with respect to the lowest eigenvalue that represents the dominant mode.

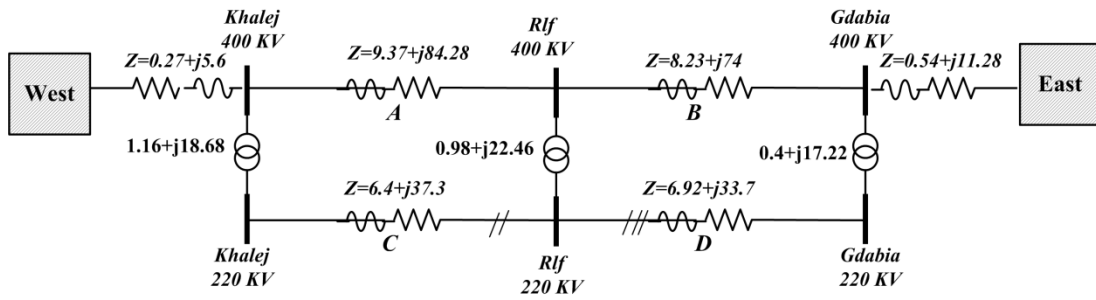


Figure 7-1: Impedance representation of the Libyan internal tie-line

Table 7-1 shows the ascending branch participation factor ranking for the branches in Figure 7-1. These results show that the 220kV line between Khalej and Ras-lanuf (C) has the lowest participation factor. This indicates that the loss of this branch has the lowest effect on voltage stability compared with a loss of any other branch in the corridor. Therefore, from power system points of view, this branch is a suitable candidate for conversion to a DC line.

Table 7-1: Branch participation factor analysis

Branch	Lowest eigenvalue	Branch participation Factor (%)
A	8.7	81
B		100
C		47
D		70

Impedance representation of west-east tie-line after VSC-HVDC reinforcement is shown in Figure 7-2.

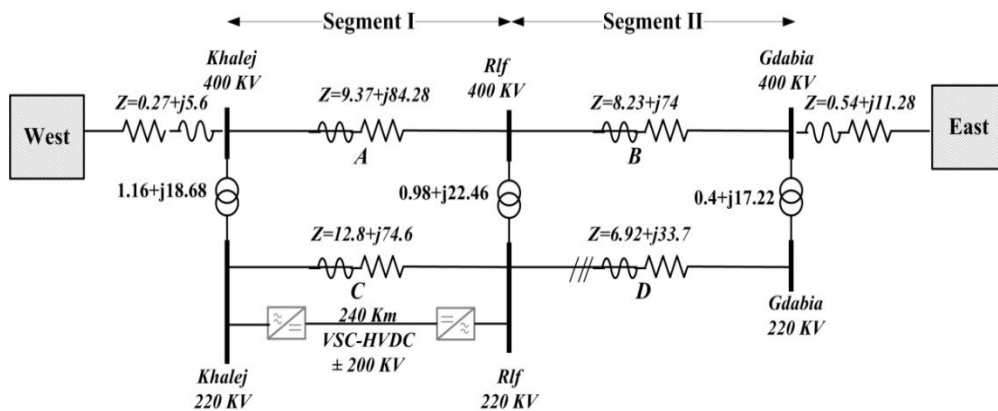


Figure 7-2: west-east internal tie-line after VSC-HVDC reinforcement

The proposed VSC-HVDC link is connected in parallel with single 220 kV circuit and single 400kV AC circuits (A and C), and can transmit real power while maintaining the voltage at both ends. Theoretically, this means that the electrical distance from the source to the load demand can be changed by controlling active and reactive power at both sides of VSC-HVDC link.

7.3 Sizing of the VSC-HVDC links based on *ASL*

The voltages at the two terminals of the west-east interconnector in Figure 7-2 are maintained by the relatively strong utility grids (at Jdabia in the east and Khalij in the west), and the proposed HVDC link maintains the voltage at the middle bus at Ras-Lanuf. This, in theory, means that the voltage is maintained along the west-east Libyan internal tie-line, which enhances the voltage stability limit of this corridor. It follows that the transfer capability of the tie-line is further improved, including its steady state angular stability limit (*ASL*). This transfer limit (*ASL*) should be used as a guide to define the maximum converter size for any proposed HVDC project.

Based on this discussion, the corridor from Ras-Lanuf to Jdabia substations (line-B and line-D in addition to the power transformers in Figure 7-8) represents the sole power path between the border of the eastern grid and Ras-Lanuf terminal of the HVDC link. Hence, maximum power exchange between the eastern HVDC link side and the eastern grid from Ras-Lanuf to Gdabia (lines B and D in Figure 7-1) should be defined by *ASL* at the weakest AC terminal.

7.4 Sizing of VSC-HVDC converter base on terminal voltage

From chapter 5, the AC voltage at the PCC (V_S) is a function of; the controllable terminal voltage of the converter (V_C), power flow in the dc link, coupling transformer impedance, and the system impedance equivalent at the PCC[6]. From section 5.5.2:

$$V_{conv} = \sqrt{\frac{(r_T^2 + x_T^2)P_{PCC}^2 - 2P_{PCC} \cdot V_{PCC}^2 \cdot r_T + (r_T^2 + x_T^2)Q_{PCC}^2 - 2Q_{PCC} \cdot V_{PCC}^2 \cdot x_T + V_{PCC}^2}{V_{PCC}^2}} \quad (7-1)$$

where V_{conv} and V_{PCC} are per unit voltages at the converter terminal and at the PCC, P_{PCC} and Q_{PCC} are active and reactive power at the PCC, r_T and x_T are resistance and inductance of the coupling transformers and are given by $r_T=R(\Omega)/VB^2$ and $x_T=X(\Omega)/VB^2$.

In order to maintain the PCC voltage V_{PCC} within the permissible limits specified by the grid code, the controllable converter terminal voltage V_{conv} has to change, within a defined range (normally between 0.95 and 1.05), in response to the level of active and reactive power flow in the coupling transformer (P_{PCC} and Q_{PCC}) to maintain the PCC voltage.

From this discussion, a variation of the converter terminal voltage within tight limits stated can be used as a guide to estimate the maximum active and reactive power that can maintain stable operation, including the provision of AC voltage support at the PCC. Additionally, dc overvoltage limitation related to higher AC voltage operating conditions as discussed in VSC capability chart in chapter 5 must be taken into account or at least not violated.

This approach is used to estimate the converter size for the proposed west-east VSC-HVDC link. Considering the equivalent of system impedances, seen from the PCCs at both dc link sides in Table 7-2, equation (7-1) is used to plot the converter terminal voltages at both sides of the dc link (Ras-Lanuf and Khalij) when the dc power flow steadily changes within the range ± 1 GW).

Table 7-2: System impedances at the AC terminals of the proposed HVDC link

PCC terminal	Terminal station	Normal operation			(N-1) operation		
		R(Ω)	X(Ω)	B(μS)	R(Ω)	X(Ω)	B(μS)
East	Res-Lanuf 220 kV	1.55	13.99	2611	2.27	18.95	3374
West	Khalij 220 kV	0.707	13.22	1363	0.742	18.7	-453

Figure 7-3 shows the generated curves at both sides of the HVDC link. The red curve represents Kahlij AC terminal voltage while the eastern AC terminal curve at Ras-Lanuf is black. A red horizontal line in Figure 7-3 defines the boundary of maximum AC voltage (1.05 pu) beyond which, any increase in the dc power theoretically pushes the terminal voltage over the acceptable boundary.

The coupling transformers are identical on both sides, and the two power systems have virtually the same short circuit levels. This gives a logical explanation for the similarity of the voltage behaviour at both converter terminals. The AC terminal voltages of both converters rise with increasing dc power regardless of its direction. This is because both the sending and receiving converters try to increase their

terminal voltages to generate the capacitive reactive power needed to support their PCC AC voltages.

As discussed, maximum dc power is defined at the dc power level where the first upper voltage threshold at any converter terminal is violated. Accordingly, Figure 7-3 indicates that the red curve (Ras-Lanuf terminal) intersects the maximum acceptable voltage level (1.05 pu). This point corresponds to about 850MW on the dc power axis (X -axis) and defines the theoretically maximum acceptable level of transmitted dc power.

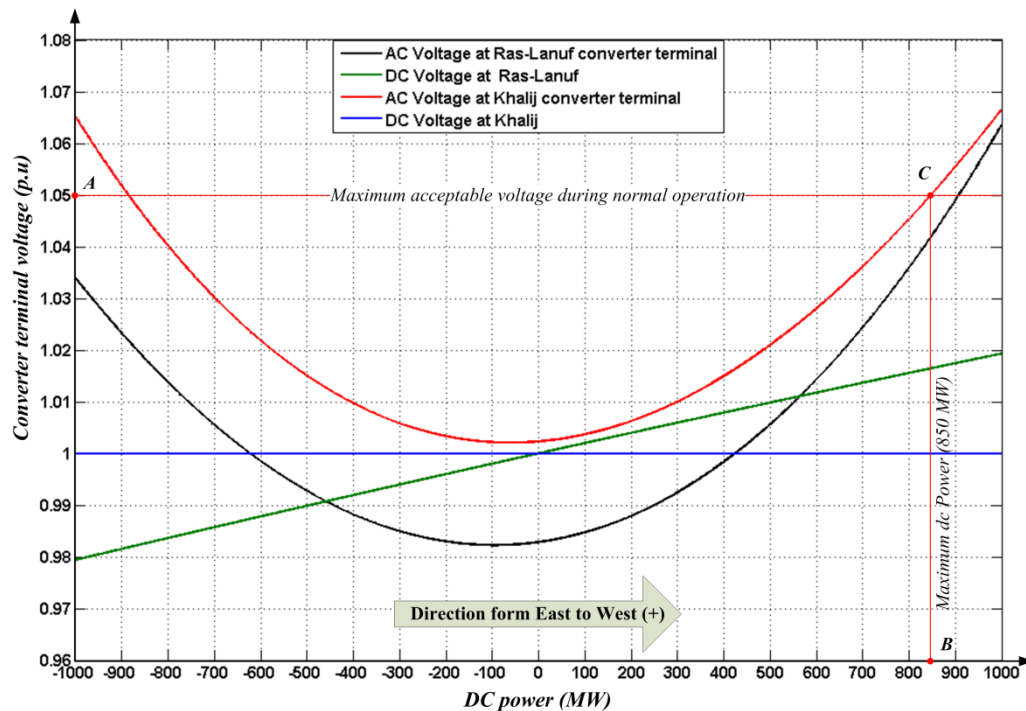


Figure 7-3: Sizing of HVDC converters on the basis of the AC voltage at the converter terminals

The converter operating point P - Q at this level of dc power transfer (850MW) should define the radius of the P - Q chart for a suitable converter size. Therefore, in order to determine the converter operating point, it is necessary to determine the reactive power at the converter terminal, ignoring transformer power losses.

In the course of reactive power estimation, the blue horizontal line in Figure 7-3 that refers to the PCC voltages can be used to estimate the converter operation mode on each side. That is, all the operating points above the blue line refer to a converter capacitive operating mode ($V_{PCC} < V_{conv}$ then Q towards the grid) and below the line for an inductive operating mode. Hence, the converter at Khalije (red curve) normally operates in a capacitive mode regardless of dc power direction, while Ras-

Lanuf converter station operates in an inductive mode for a wide range of dc power (-600MW to 400MW).

Converter reactive power output changes with dc power flow, to satisfy the PCC voltage requirements, in accordance with equation (7-2).

$$Q_{conv} = \left(\frac{S_{PCC}}{V_{PCC}} \right)^2 x_T + Q_{PCC} \quad (7-2)$$

Using this equation, assuming 1 pu PCC voltage, and with the simultaneous calculation of Q_{PCC} and S_{PCC} (Q_{PCC} is Q_{CI} in equation 5.17), a P versus Q curve at the voltage terminal is established as in Figure 7-4.

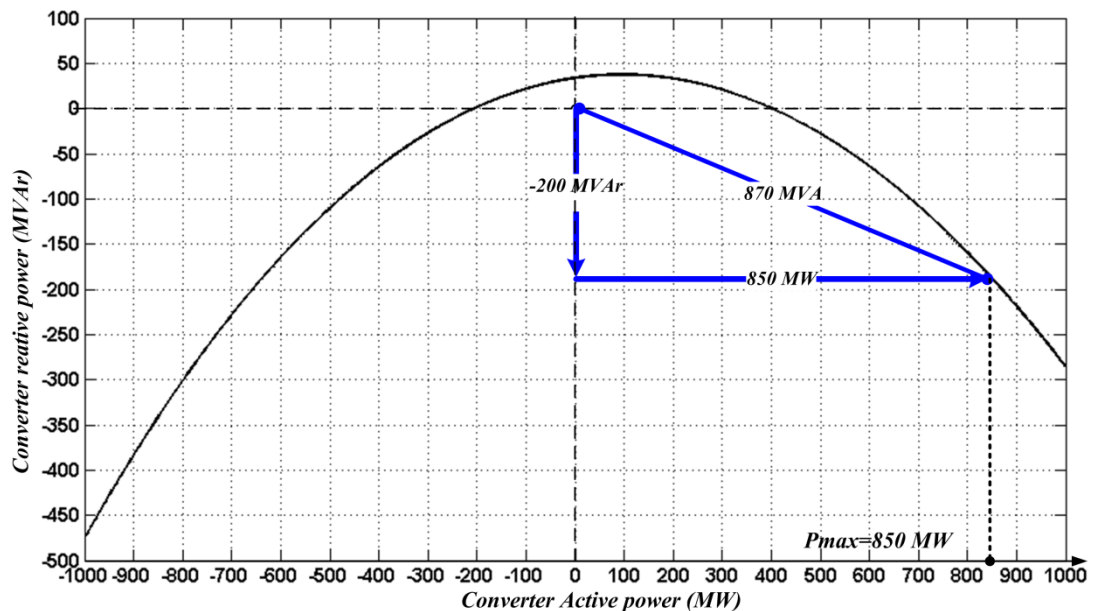


Figure 7-4: P - Q curve for Ras-Lanuf and Khalij converter stations

About -200MVar is required to maintain the PCC voltage at 1pu while transferring 850MW in the dc link. This P - Q operating point is used to calculate an MVA rating of about 870MVA, which sets the radius of the P - Q capability chart of the converter.

This discussion concludes that a reasonable HVDC converter size is 1GVA when allowing a 10% reserve capacity. However, the maximum power transfer level on the proposed dc link should not exceed 850MW to maintain PCC voltages and terminal voltages at 1 pu and 1.05 pu respectively.

7.5 Power transfer capability of the strengthened west-east Libyan tie-line

The VSC-HVDC based reinforcement proposal indicates higher power transfer capability than that of the existing AC tie-line. Figure 7-2 shows that the HVDC link establishes a midpoint and maintains the voltage at Ras-Lanuf substation that lies in the middle of the east-west tie-line. However, there is a scenario where loss of any of the circuits that form the first segment from Khalij to Ras-Lanuf may create a bottleneck that may limit the transfer capability of the hybrid AC/DC transmission tie-line. Therefore, the secure level for power transfer of the hybrid AC/DC transmission tie-line must be determined considering the mentioned worst case scenario.

Under the worst operating scenario, normal and emergency operational voltage levels and converter ratings are the main factors that define the steady state transfer capability of the reinforced tie-line. Total transfer capability of the tie-line is estimated using offline steady state analysis (power flow or voltage stability), where the exchange power level over the tie-line is gradually increased to the loading level until the voltage or loading thresholds are violated. The improvement achieved in tie-line TTC with HVDC reinforcement is compared to that without HVDC reinforcement. Therefore, the analysis includes steady state performance of the current tie-line.

7.5.1 Existing configuration of the tie-line (no HVDC link)

As voltage instability is the main concern that restricts transfer capability of the tie line as being discussed, a $P-V$ curve based voltage stability analysis is carried out to assess system voltage stability during normal and emergency operating conditions. An outage of one line of three lines of the first segment in Figure 7-2 is assumed, to evaluate the tie-line performance during a contingency. The outcomes of the steady state analysis of the existing tie line under these contingencies are summarised in Table 7-3.

It can be observed from the table that the existing Libyan internal tie-line can transmit up to 980MW without any voltage violation. However, as mentioned in chapter 2, $N-1$ precautions reduce the power transfer capability of the tie line to about 500MW (-49%)[7]. The loss of the 400kV circuit represents the worst emergency scenario for TTC determination. The loss of the 220kV circuit is less

significant than the loss of the 400kV, and this confirms the validity of the proposed approach of HVDC allocating on the basis of branch participation factor, discussed in section 7.2.

Table 7-3: Summary of existing west-east Libyan tie-line (without HVDC reinforcement)

Operating scenario	TTC (MW)	Voltage Violation		Emergency reduction factor (%)
		(%)	Node	
Normal	980	< 95%	Ras-Lanuf	-
N-1 (220 kV trip)	864	< 90%	Ras-Lanuf	11.8
N-1 (400 kV trip)	500	< 90%	Ras-Lanuf	48.9

7.5.2 Steady state transfer capability of the reinforced west-east Libyan tie-line

Steady state assessment of the west-east hybrid AC/DC transmission tie-line includes voltage level monitoring as well as the power flow through converters during normal and emergency operating conditions. In order to clearly establish the expected TTC improvement and the most critical contingency that may significantly affect the performance of the reinforced tie-line, six emergency cases in addition to the normal operation of the tie-line with the HVDC link, are included in the analysis.

Table 7-4 summarise the main results of the steady state based analysis, where the total transfer capability of the tie-line in each case is determined. This table also includes the violation correspondence to the TTC in each operating scenario, and the emergency reduction factor which evaluates the negative impact of the contingency in terms of TTC reduction.

Table 7-4: performance Summary of strengthened west-east Libyan internal tie-line

Operating scenario	TTC (MW)	Violation				Emergency reduction factor (%)
		voltage		overloading		
		(%)	Node	(%)	converter	
Case 0-0	1610	-	-	>100	Ras-Lanuf	
Case 1-1	1403	-	-	>100	Ras-Lanuf	13
Case 1-2	1000	< 90	Ras-Lanuf	-	-	38
Case 1-3	1370	-	-	>100	Ras-Lanuf	15
Case 1-4	1410	-	-	>100	Ras-Lanuf	12
Case 1-5	1107	-	-	>100	Ras-Lanuf	31

- Case 0-0: normal operation for west-east tie-line with HVDC link
- Case 1-1: west-east tie-line in STATCOM mode at both sides (dc line out).
- Case 1-2: west-east tie-line in STATCOM mode at Khalij.
- Case 1-3: west-east tie-line in STATCOM mode at Ras-Lanuf.
- Case 1-4: west-east tie-line with 220kV AC circuit out of service.
- Case 1-5: west-east tie-line with 400kV AC circuit out of service.

Comparison between the tie-line performance with HVDC in Table 7-4 and with that of the present performance in Table 7-3 indicates that total transfer capability of the Libyan internal tie-line is doubled, from 500MW (in Table 7-3) to about 1000MW with the proposed VSC-HVDC link. Table 7-4 indicates that case 1-2, which represents the emergency operating scenario for loss of the remote converter in Ras-Lanuf, is the most critical scenario as it has the highest contingency reduction factor (38%). Therefore, 1000MW is the maximum transfer capability of the hybrid AC/DC Libyan internal tie-line.

The importance of Ras-Lanuf converter terminal lies in it being the main source of reactive power support at the middle of the tie-line. The study indicates that the importance of Ras-Lanuf converter to be in-service (STATCOM mode) is sometimes more important than the dc line itself. This highlights the importance of midpoint shunt compensation as a competitive alternative to increase the TTC. However, being operating at VSC-HVDC link with higher AC terminal voltage gives a preference for the VSC-HVDC than the shunt compensation. This is because of the risk of high PoC, and the narrow voltage operating range associated with the low terminal voltage of present shunt FACTS.

7.6 Dynamic performance of the VSC-HVDC link

Time domain analysis in this section investigates the dynamic behaviour of the AC/DC west-east hybrid tie-line. A detailed model of the entire Libyan network along with an average VSC-HVDC model with typical controllers parameters are used in the analysis. Technical specifications of the proposed west-east HVDC link are from the two-terminal symmetric monopole ($\pm 200\text{kV}$) VSC-HVDC link of the CIGRE B4 DC Grid Test System [8].

Time domain analysis investigates the response of the system and the HVDC link to a number of disturbances during transmission of 1GW from east to west (maximum TTC based on steady state analysis).

7.6.1 Step response of the dc Power controller

Step response analysis is used to evaluate the system performance when subjected to disturbances that require fast response action from the active or reactive power controllers of the VSC-HVDC link. Controller response should be with an acceptable overshoot and response time. In general, the overshoot should stay within a tolerance of $\pm 10\%$ after the first peak which should not exceed 30% of the power ordered [9].

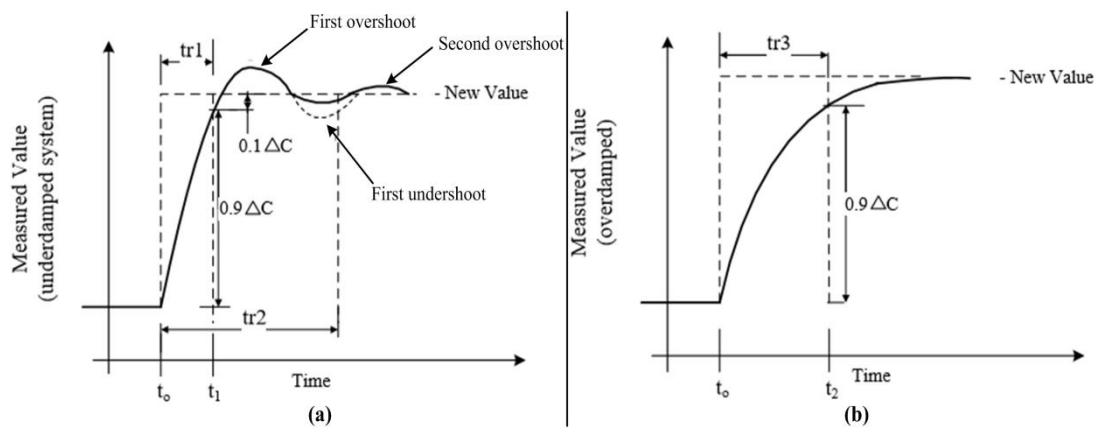


Figure 7-5: Definition of step response

Depending on the transient damping and overshoot, three time responses are defined, as shown in Figure 7-5.

- 1- In the underdamped case in Figure 7-5a, if the first overshoot is within $\pm 10\%$ of the final value, the time response (or rise time) is measured from the instant when the step change is initiated to the instant when the quantity being controlled reaches 90% of its final steady-state set point (tr_1).
- 2- After the first overshooting, if the next overshoot exceeds the tolerance of $\pm 10\%$ of the ordered change, the time response is defined from the instant of the ordered change to the time when the measured value returns to the range of $\pm 10\%$ of the ordered change (tr_2).
- 3- In an over-damped system, Figure 7-5b, the time response is defined as the time from the instant of the ordered change to the time when 90% of the new steady-state set point is reached (tr_3).

These response definitions are used as a guide to evaluate the step response of the active and reactive HVDC controllers.

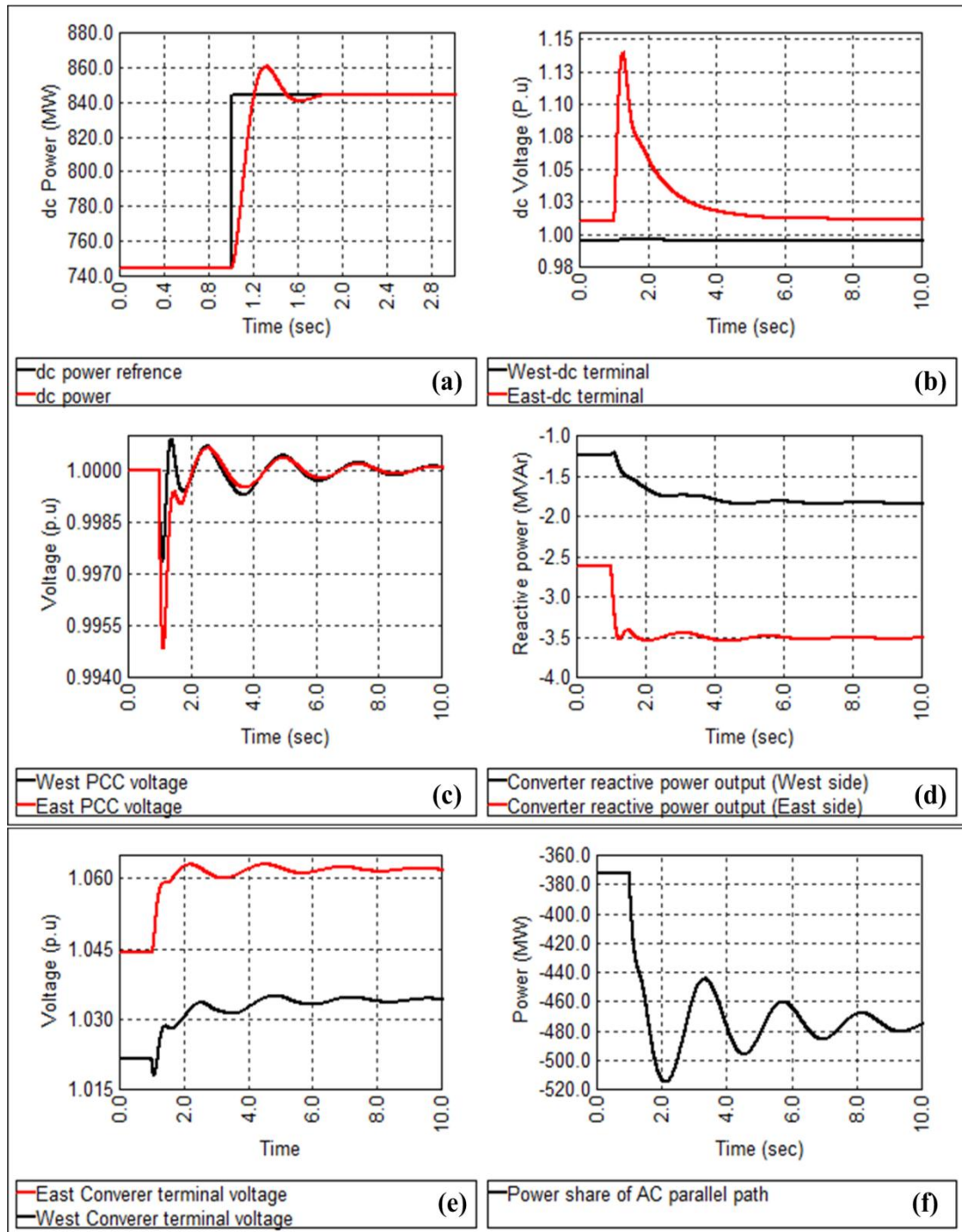


Figure 7-6: Simulation results for a step change of 100MW in the dc power

Figure 7-6 shows simulation results for the power controller response at the eastern side of the HVDC link. A step change of a 13.4% (100MW) in the dc power reference is ordered during a peak load scenario when 1000MW is being transmitted from east to west (loading scenario with TTC of 1GW on the tie-line). In the Figure

7-6a, the first dc power overshoot is about 2.6% of the ordered change of 100MW. Accordingly the time response measured in accordance to tr_1 in Figure 7-5a is about 175ms. The dc voltage transient is also within an acceptable limit of 10%. Generally, the ac systems on both sides of the dc link are strongly enough to accommodate this order dc power step change, as shown in Figure 7-6 parts c to f.

7.6.2 Step response of reactive Power and AC voltage controllers

In order to evaluate the performance of the outer reactive power and voltage controllers under a maximum transfer condition, a step change of -123MVar is applied to the reactive power output (123MVar to zero) at western converter station. Based on the overshoot and rise time definitions given, the reactive power controller exhibits satisfactory behaviour, see Figure 7-7.

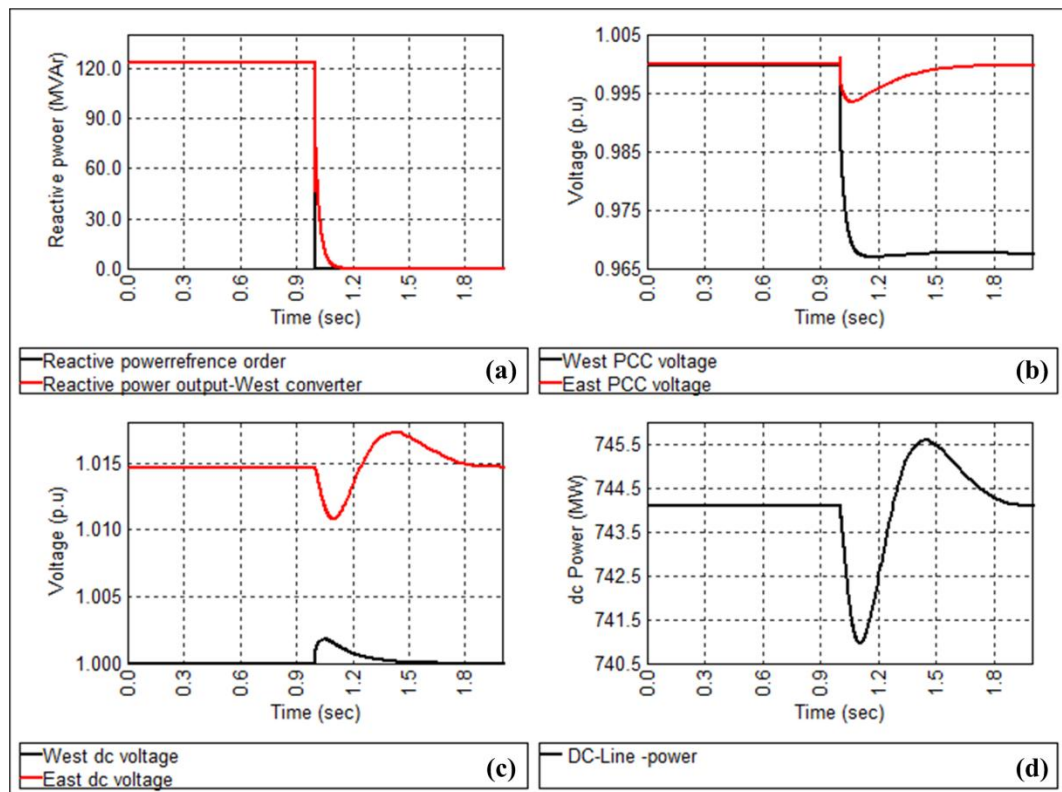


Figure 7-7: Simulation for a step change of -123MVar in the reactive power output at the Khalij converter station

In Figure 7-7a, the controller represents an over-damped system (tr_3) with a rise time of 90ms. The voltage at the converter station levels off, in response to the new reactive power order (Mq), at an acceptable level (0.97%) and within an acceptable settling time as shown in Figure 7-7b. The AC voltage change at Kahlj terminal

reflects on the AC voltage controller at the other side of the HVDC link, which conversely, increases its reactive power output to maintain the voltage at 1 pu (red curve in Figure 7-7b). Importantly, the noticeable disturbance in the AC voltage is handled by the dc capacitors, which minimally impact on the dc voltages and dc power, as shown in Figure 7-7c and Figure 7-7d respectively.

7.6.3 System response to a 3-phase short circuit at the receiving end terminal

A three phase short circuit faults at the receiving end is a critical disturbance that can affect VSC performance. For this reason, a 150ms three phase short circuit is applied at the western converter terminal (Khalij-220kV in Figure 7-2) to investigate the performance of the hybrid AC/DC west-east tie-line. Maximum load-ability of the tie-line (TTC =1000MW east to west) is considered in this simulation. The results of this simulation are shown in Figure 7-8.

Figure 7-8a shows the phase currents which rise to about 3kA during the fault, before falling back to the initial level. In Figure 7-8c, the active power at the AC receiving terminal drops to zero which causes energy imbalance between the DC and AC sides. The energy imbalance reflects on the dc voltages on both sides which are increased due to the trapped energy in the dc system during the fault, as shown in Figure 7-8d. The stored energy in the dc system is released just after fault clearance, causing large power flow at the receiving terminal and on the dc line, as depicted in Figure 7-8c.

As the fault, at $t=0.5s$, the voltage at the receiving terminal drops to zero before fault clearance at $t=0.65 s$. On the other hand, the sending end drops to about 80%, due to the long distance of the AC parallel path and the fault ride-through capability of the VSC-HVDC converter, see Figure 7-8e. Both AC voltage controllers inject the required reactive power to bring the voltage back to the nominal values within an acceptable recovery time, despite the severity of the fault at Khalije converter station terminal, Figure 7-8f.

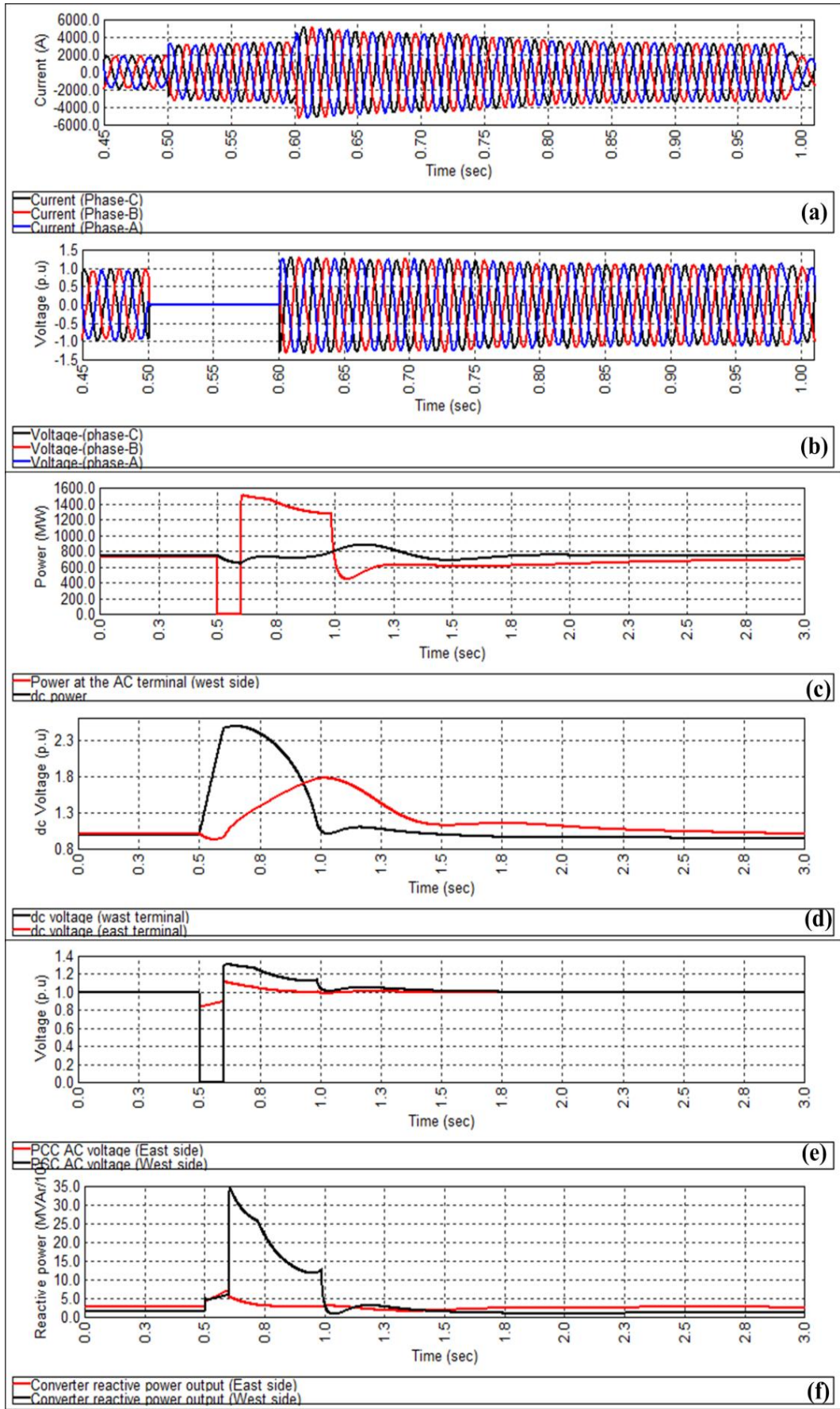


Figure 7-8: Results for 3-phase short circuit at the receiving terminal

7.7 DC power ramping in the hybrid AC/DC Libyan internal tie-line

Steady state and dynamic analyses indicate that the total transfer capability (TTC) of the proposed hybrid AC/DC Libyan internal tie-line is 1GW in either direction. However the ability of this line to accomplish the tasks entrusted to it requires specific operation rules. Among the important rules in HVDC operation is the ramping rate of the dc power command (MW/s) which should be defined to be accommodated smoothly by the AC system. Another important operation rule is how to distribute the transmitted power between the parallel lines to ensure efficient usage of the tie line during normal and emergency operating conditions.

7.7.1 AC system time constant (inertia) and its influence on dc power ramping

In strong AC terminals of any VSC-HVDC (high SCR), fast ramping of dc power is normally accommodated by the system inertia and does not cause system disturbance. But in weak systems, fast power dc ramping can be reflected onto the system dynamics, especially in synchronized power systems where the AC parallel path has to change its loading to maintain system balance. This sudden power flow change can cause undesired power oscillations. Therefore, the HVDC active power reference demand ramp rate has to be controlled to be compatible with the AC system strength.

AC/DC energy balance theory governs the energy exchange between DC and AC systems. Any unbalances in the energy exchange between the DC and AC systems are reflected as a dc voltage change within dc systems and as frequency change in ac systems. Figure 7-9 illustrates the change of dc voltage, at Ras-Lanuf converter station, with dc power command change for different ramping rates.

In Figure 7-9a, the dc voltage overshoot differs with dc power ramp rate due to load rejection, and as a result, the dc capacitors have to act as temporary energy storage to accommodate energy trapped in the dc link. Another factor that influences the dc

power ramp rate is the dc link dynamics ($C \frac{dV_{dc}}{dt} = I_{dc} - I_i \rightarrow \frac{d}{dt} (\frac{1}{2} CV_{dc}) = P_{dc} - P_{ac} \rightarrow \frac{dE}{dt} = P_{dc} - P_{ac}$), and a 0 to rated value active or dc power change corresponds to a

converter change of the dc voltage that regulates active power according to $V_{dc} = V_{dc0} - 2R_{dc}I_{dc}$. At zero power $V_{dc} = V_{dc0}$, and at rated power V_{dc} can be less or greater than V_{dc0} by $2R_{dc}I_{dc}$, depending on the dc power direction. The dc voltage change of the

active power controller will be associated with an energy level change of its dc capacitor, ($\Delta E = \frac{1}{2}C(V_{dc0}^2 - V_{dc}^2)$). The stored energy in the dc system (under the curve areas in Figure 7-9a) are similar, though at different dc voltages

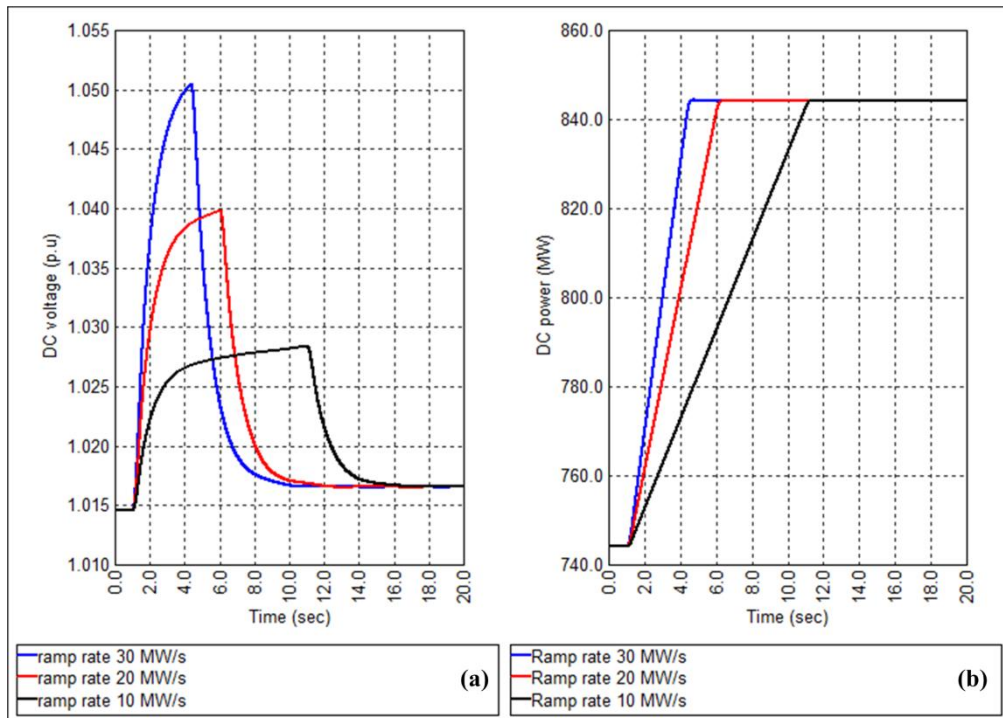


Figure 7-9: Change of the dc voltage with dc power ramp rate at the Ras-Lanufe converter station

Thus, the dc power ramp rate must be set taking into account AC system strength and converter inertia (energy storage per converter). From these observations, the ramp rate of 10MW/s is compatible with the dynamics of the Libyan grid, and will be used in the HVDC system simulations.

7.7.2 Simulation of DC power ramping during load demand increase

In this section, time domain analysis is used to investigate the dynamic response of Libyan east-west ties during a step change in dc power demand. This case simulates a gradual increase in the western network load demand, which is met with an increase in the dc power reference at Ras-Lanufe converter station. Figure 7-10(a) shows the reference dc power which is changed from 750MW to 850MW, with a step-up rate of 10MW/s. As the dc reference power starts to raise, the dc voltage at the sending end increases to allow increased dc link power, the new load demand. The steady state dc voltage can be calculated at the new desired dc power using the equation (7-3) as shown in section 5.5.3:

$$V_{dc1} = \frac{V_{dc2}R_c + \sqrt{(4P_{C1}R_{dc} + V_{dc2}^2)R_c^2 + 4P_{C1}R_{dc}^2R_c}}{2(R_c + R_{dc})} \quad (7-3)$$

Where; V_{dc1} and V_{dc2} are dc voltages at the sending and receiving ends, P_{C1} is the reference power order, R_C represents the converter resistive loss and R_{dc} is the dc line resistance. From CIGRE B4 DC Grid Test System specification: $R_C=20000\Omega$, $V_{dc2}=400\text{kV}$, and $R_{dc}=3.192\Omega$. From equation(7-3), the dc voltage at the sending end increases from 1.0149 pu at the initial dc power (750MW) to 1.0168 pu after the dc power levels off at the new reference dc power (850MW), as shown in Figure 7-10b. In Figure 7-10c, the dc power change causes slight AC voltage variation on both sides. Also, the AC voltage controller brings the voltages back to nominal values by adjusting the reactive power output of the converters, as shown in Figure 7-10d.

These results further validate the proposed converter sizing methodology in section 7.4, and the mathematical equations for AC/DC calculations in section 5.5. Table 7-5 compares the results in Figure 7-10 with those obtained from the mathematical approach described in chapter 5. At 850MW dc power transfer, the terminal voltage of the Ras-Lanuf converter just exceeds the acceptable voltage limit (1.05 pu) which confirms the sizing method.

Table 7-5: Comparison between the mathematical equation and time domain analysis using NEPLAN

DC Terminal	dc power reference (MW)	DC V (pu)		Term AC V (pu)		Q (MVar)	
		Figure	Equation	Figure	Equation	Figure	Equation
		6.11b	(7-3)	6.11e	(7-1)	6.11d	(6.3)
Ras-Lanuf	$t=0\text{s}$ (750)	1.0146	1.0149	1.0433	1.0443	262	261
Kahlij		1	1	1.0216	1.0214	124	123
Ras-Lanuf	$t=20\text{s}$ (850)	1.0166	1.0164	1.0619	1.0605	352	345
Kahlij		1	1	1.0340	1.0314	184	174

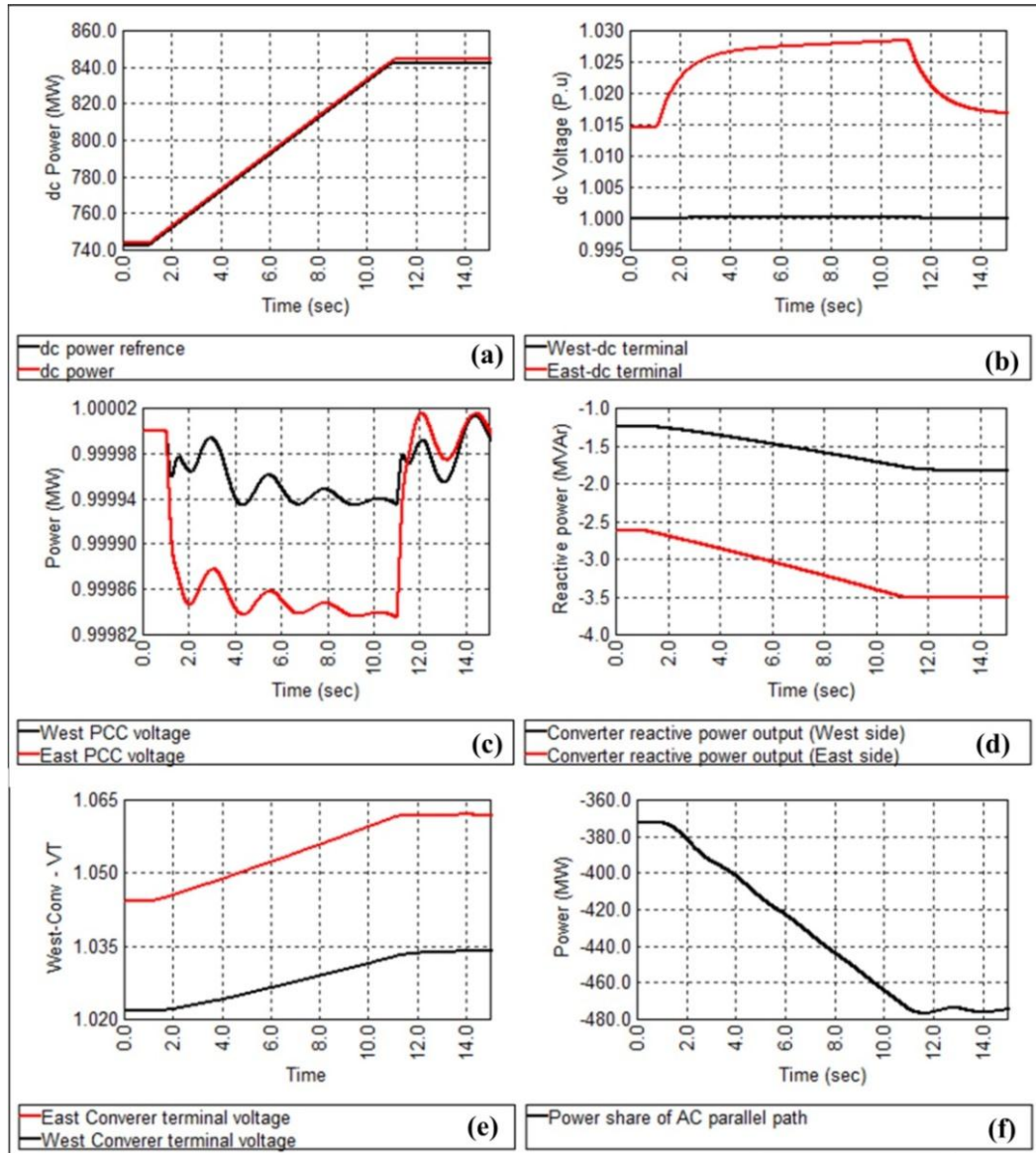


Figure 7-10: Steady state dc power change

7.7.3 Operating strategy of the hybrid AC/DC tie-line during N-1 scenario

The steady-state evaluation of the hybrid AC/DC tie-line, in section 7.5.2, indicates that the total transfer capability of the reinforced tie-line is 1GW in either direction. However, secure operation of this tie-line at this TTC requires an operating strategy that ensures efficient and reliable operation of the line during normal and emergency operating conditions. This means finding a strategy to control the power flow on the AC parallel path during normal and emergency operating conditions. The ability of the dc link to change the dc power demand and direction makes the use of this strategy possible[10]. That is, dc link power flow can be changed on demand to decrease the loading of the AC parallel path should system security be violated.

This strategy can be applied, for the hybrid AC/DC tie-line in Figure 7-2, in accordance with the flowchart in Figure 7-11 which can be summarised by the following methodology:

- A- Total Power (P_{TOTAL}) in the AC parallel path (line-a and line-d in Figure 7-2) is continuously monitored and compared with the most respective ASL of the 220kV line (ASL_{220}).
- B- If the total power in the AC parallel path (P_{TOTAL}) exceeds the ASL of the 220kV line (ASL_{220}), the new dc power set point is established ,only if the 400 kV line is out of service, ($P_{dc_ref}^* = P_{dc0} + (P_{TOTAL} - ASL_{220})$).

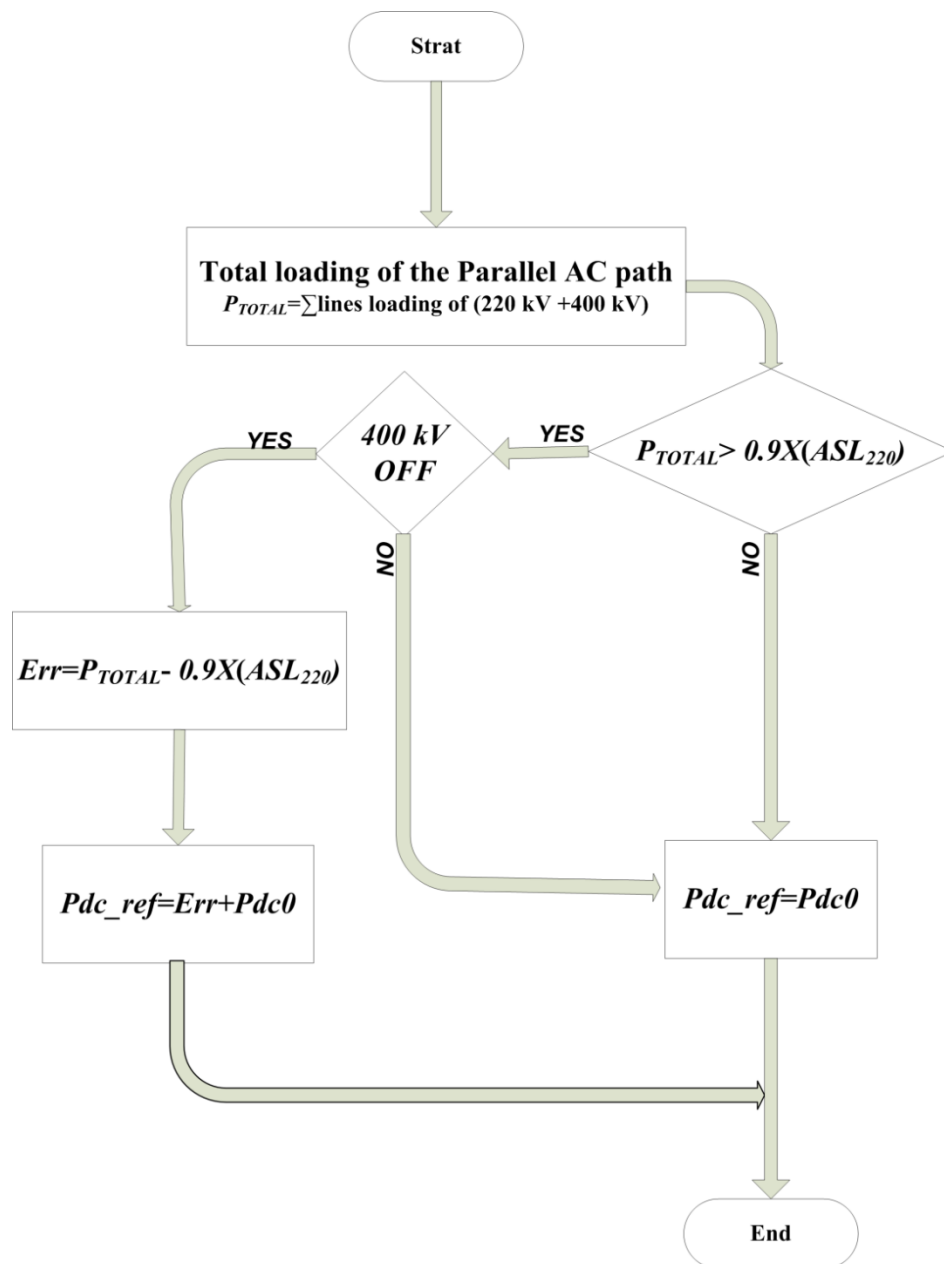


Figure 7-11: Power flow control strategy in the HVDC link and the AC parallel path

In the proposed flow chart logic in Figure 7-11, the new error signal (*Err*) from an external control loop is fed into the outer HVDC power controller. If secure load-ability of the tie-line is exceeded, a new power set point is established by the outer power controller.

Equation 2-35 indicates that steady state angular stability limits for the 220kV are 550 MW and for the 400kV line is 1700MW respectively (the lines are from Khalej to Ras-lanuf in Figure 7-2). Accordingly, the maximum transfer power on the AC parallel path should not exceed 550MW ($ASL_{220}=550$).

With this assumption ($ASL_{220}=550$), loss of the 400kV AC line during peak load the corresponded to transfer of 1000MW from east to west (TTC at the base-case) is simulated to assess the efficiency of the proposed power flow control strategy.

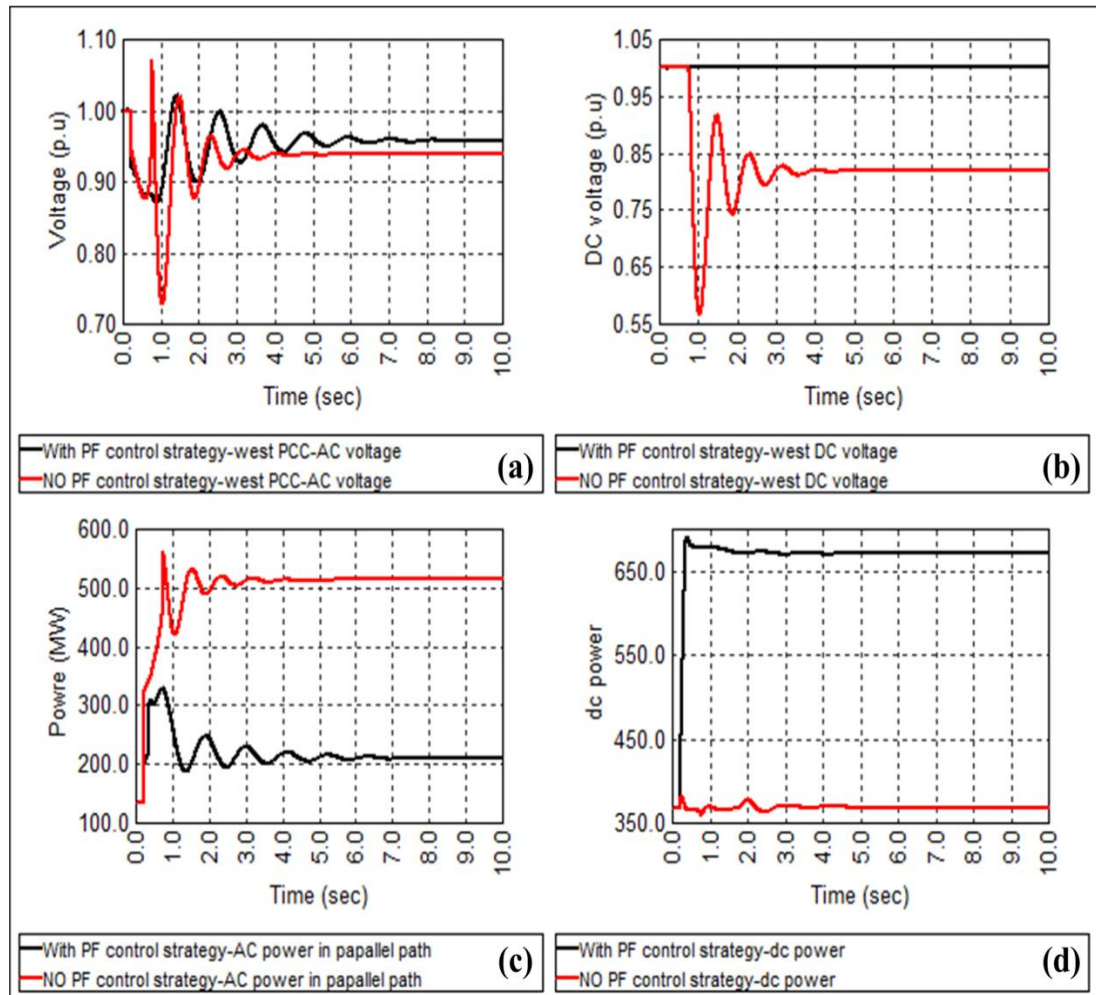


Figure 7-12: Libyan internal tie-line with power flow control strategy

Figure 7-12 shows the simulation results with and without the proposed power flow control strategy. From Figure 7-12d, the power flow in the dc link is increased in response to the power flow change in the AC parallel path. Then the power flow on the remaining 220kV AC line decreases to the secure limit, as in Figure 7-12c. The significance of this strategy is reflected in the AC and DC voltages which are within acceptable AC and DC voltage levels, with the implementation of the power flow control strategy (continuous line).

7.8 STATCOM operation

Steady state analysis in section 7.5.2 (case 1-1) indicates that both HVDC terminals can provide reactive power support which improves tie-line performance. Reactive power can be injected or absorbed either during transmitting of dc power over the dc link or during the STATCOM operation mode (sleep mode) of the VSC-HVDC. The STATCOM operation mode can be executed with or without the dc line connected.

The switchover from the normal operating mode to the STATCOM operation mode (sleep mode) requires ramping of the dc power down to zero at a suitable ramp rate. If the dc line is in-service during STATCOM operation, the dc voltage continues to be controlled at one side of the VSC-HVDC link. During dc faults or whenever the dc line is not in service, each converter terminal controls its own DC voltage and full current capacity is available for reactive power support.

Figure 7-13 shows simulation results for an operating condition where 550MW (*ASL* of 220kV AC line) is transmitted over the AC path while the converter stations at both sides (Ras-Lanuf and Khalij) are changed-over to the STATCOM mode. A 200ms 3-phase fault at the middle of the 400kV line (line-A in figure 7-8) is simulated to evaluate the dynamic performance of the VSC converters during the fault. Also, the stressed post-fault condition, where the in-service 220kV line has to take responsibility for transmitting the power at its *ASL*, is evaluated.

As demonstrated in Figure 7-13a, the fault causes a voltage drop at both converter terminals. The voltage drop is more severe at the Ras-Lanuf converter station than at the Khalije terminals because of the difference in the short circuit levels. Thus, each converter behaves based on the voltage drop severity and injects the required reactive current to compensate the voltage depression, as in Figure 7-13b and Figure

7-13c. As discussed in chapter 3, Ras-Lanuf supplies its full reactive current (2.625kA) even with low AC voltage, as in Figure 7-13b.

Importantly, the STATCOM in the Ras-Lanuf terminal responds consistently to the sudden increase in the power flow in the 220kV AC line and gradually dampens the power oscillation, as shown in Figure 7-13d.

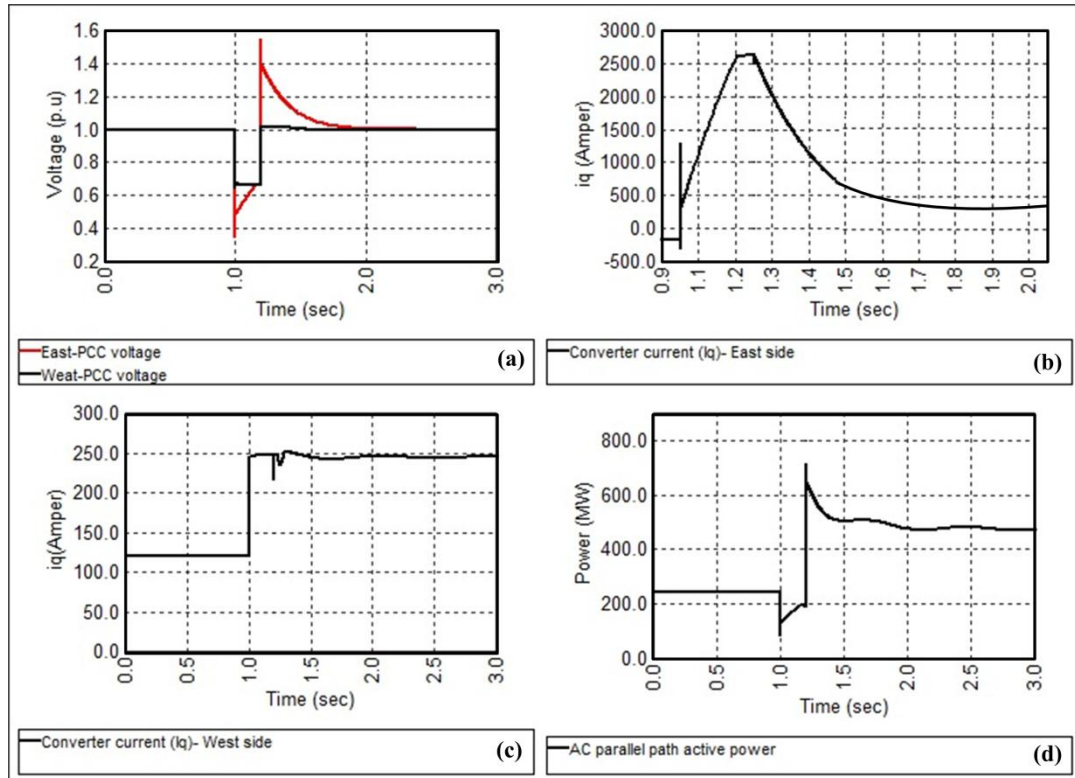


Figure 7-13: STATCOM operation mode during dc line disconnection

7.9 Frequency control capability of the reinforced Libyan internal tie-line

As discussed in chapter 5, a voltage source converter based HVDC system provides frequency control, for unsynchronized power systems. However, the efficiency of the HVDC transmission system to control frequency depends on the power frequency characteristics of the system (rotating inertia and the available reserve) at the AC terminals. The proposed frequency control strategy of the VSC-HVDC link is examined to evaluate its ability to support the eastern network frequency, in terms of power frequency characteristics; during unsynchronized operation of the tie-line (only dc link is connected).

A network fault that causes disconnection of the loaded AC parallel path is simulated. This fault forms a critical post-fault operating condition that includes two

unsynchronized AC networks with unbalanced load demand and generation. According to the pre-fault condition, where the power flows towards the western network, after splitting, the eastern network is left with excessive generation while the western network faces a generation deficit. Therefore, the VSC-HVDC, as part of the tie-line, can handle such a severe contingency by adjusting its dc link power flow. Active power based frequency control structure shown in figure 5-21 is included in the outer power controller of the HVDC eastern terminal in Figure 7-2 to contribute to frequency control during contingencies.

Figure 7-14 shows time domain simulation results for this contingency. Frequency behaviour of the eastern network after being supported by the HVDC link is compared with the frequency behaviour without HVDC support.

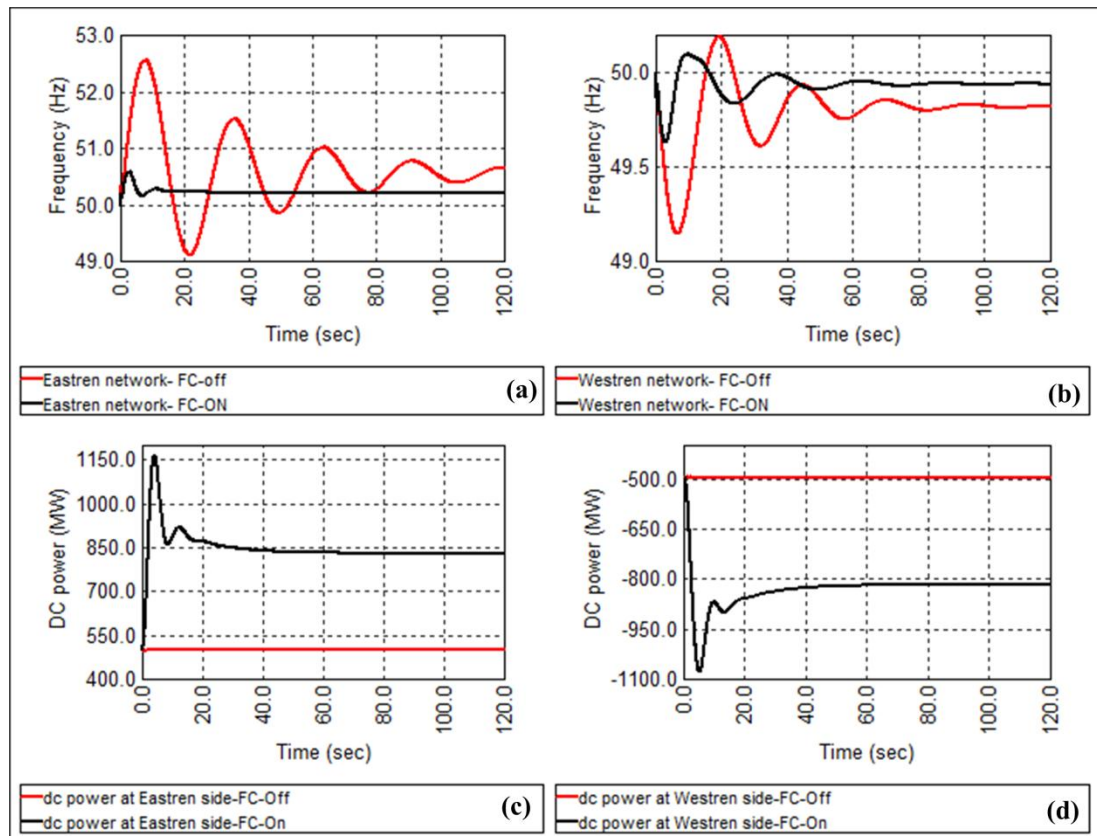


Figure 7-14: Performance of tie-line with and without frequency control at the eastern terminal

The red curve in Figure 7-14a refers to the frequency behaviour without the HVDC control strategy in the eastern network. Isolation of eastern network with initially higher generation than load demand ($\Delta P = +500\text{MW}$) leads to frequency overshoot when splitting, reaching about 52.5Hz which is about 2% higher than the generating units over frequency thresholds (51.5Hz). In contrast, the black curve in the figure

represents the frequency behaviour with HVDC frequency control which effectively returns the frequency closest to its nominal value (droop of 1%) by increasing the exported power via the HVDC link, as shown in Figure 7-14c. The intervention of the frequency control strategy also improves the electromechanical oscillation by controlling the energy exchange between the decoupled AC systems in accordance with their instantaneous energy requirements.

7.10 Comparison between shunt FACTS, series FACTS, and VSC-HVDC in the Libyan internal tie-line

Total transfer capability of the Libyan internal tie-line can be improved, the extent to which is dependent on the technology use. As the reactive power support along the tie-line is a key in terms of tie-line load-ability improvement, FACTS devices and SVC-HVDC can play an important role in providing reactive power support. However, each technology has its own characteristics that define its operating principles and steady state and dynamic behaviour [11, 12].

The strength of the Libyan internal interconnection plays a major role in assessing the amount of reactive power required, and consequently, the rating of the equipment assets to be installed for the purpose of load-ability improvement. Steady-state based analysis has shown that the MVA rating of the generating device, whether FACTS or HVDC, is the main determinant of the level of tie-line TTC improvement. Apart from the economic aspects, the general conclusion that can be drawn is: as the MVA rating increases, the tie-line transfer capability increases. However, each of the three technologies has its own criteria to define its maximum rating and accordingly the TTC improvement. In terms of the maximum rating of the three VAR generating devices, two general aspects arose during steady state analysis of the Libyan internal tie line;

1. The terminal voltage of the VAR generator rises with an increase of tie-line load-ability. This is because of the tendency of the VAR generator to maintain the PCC voltage at the expense of its terminal voltage. This problem is experienced in SVC-HVDC sizing at Ras-Lanuf and, it affects the sizing of the shunt compensation in the midpoint of the tie-line.
2. The likelihood of sub-synchronous resonance and the voltage drop developed across the series compensator at full line current are both affect TCSC sizing.

Being part of a tie-line that is directly connected with power plants on both sides, increases the risk of SSR and reduces the level of the accepted compensation factor.

In comparing FACTS devices, series FACTS compensation gives a better improvement in terms of TTC of the Libyan tie-line than shunt FACTS compensation. Moreover, MW improvement to MVA rating of series FACTS is much better than that with shunt compensation.

From a transient stability point of view, voltage source converter based VAR generators (STATCOM and VSC-HVDC) show better dynamic performance during disturbances. The transport lag time delay of a converter is considerably smaller than that of current source converters, thus has better frequency bandwidth, smaller voltage regulator time constant, and better overall dynamic performance.

A voltage source converter based HVDC system offers the greatest transfer capability improvement, at the expense of a larger converter rating than with FACTS devices. HVDC provides additional features not be provided by the passive reactive power compensators, such as; frequency control , black start and STATCOM capability and also can provide power flow management. Table 7.6 is a technical comparison between shunt FACTS, series FACTS and VSC-HVDC systems, in the Libyan internal tie-line.

Table 7-6: Technical performance comparison between FACTS and VSC-HVDC

	Shunt compensation	Series Compensation (30%)	VSC-HVDC
TTC (MW) 500MW base	620	775	1000
TTC improvement (%)	24	55	100
Rating (MVA)	200	138	800
Improvement MW/MVA	0.6	1.99	0.62
Violation at TTC	Terminal voltage	Line current rating	Terminal voltage
Power flow control	no	good	very good
Transient stability enhancement	limited	good	very good
Voltage control	yes	limited	very good
Oscillation damping	limited	good	very good
Load sharing	no	fast	fast
Power quality mitigation	yes	-	-

7.11 Summary

The weak interconnection between eastern and western Libyan networks considerably limits power exchange between the two operating areas, which presents operational and economic challenges, since operating levels are considerably lower than the designed thermal capacity of the tie line. The lack of reactive power support along the tie-line is the main factor limiting the utilization factor of the internal Libyan tie-line. Optimal utilization of the tie-line requires interconnector reinforcement that increases the total transfer capability by 140% to be able to exchange 1200MW securely.

A voltage source converter based HVDC transmission system is a solution to increase total transfer capability of the tie-line. Steady state and dynamic analysis have shown that the total transfer capability of the Libyan internal tie-line is doubled after being reinforced by a 1GW VSC-HVDC link. The results showed that this rating can not be increased due to the converter terminal voltage limits which are proportionally increased with dc power transfer increase. However, apart from the dynamic performance which is in favour of the VSC-HVDC alternative, steady state analysis has shown that series compensation can be a competitive alternative and can play a role in TTC improvement.

References

- [1] G. C. C. Bruno, "Consultancy services about Optimal Operation Schemes for the Libyan 400 kV and 220 kV Networks " CESI, Milan, Italy 2011.
- [2] G. O. A. Kalcon, "Control design and stability assessment of VSC-HVDC networks for large-scale offshore wind integration," Ph.D, Electronic and Electrical Engineering, University of Strathclyde, Glasgow-UK, 2011.
- [3] B. Liu, *et al.*, "Feasibility study and design of hybrid AC/DC high power transmission considering unbalanced line impedances," in *Applied Power Electronics Conference and Exposition (APEC), 2014 Twenty-Ninth Annual IEEE*, 2014, pp. 350-357.
- [4] K. P. Basu and H. Rahman, "Feasibility Study of Conversion of Double Circuit ac Transmission Line for Simultaneous ac-dc Power Transmission," in *Power Electronics and Drives Systems, 2005. PEDS 2005. International Conference on*, 2005, pp. 972-976.
- [5] H. Rahman and B. H. Khan, "Power upgrading by simultaneous AC-DC power transfer in a double circuit AC line," in *Power India Conference, 2006 IEEE*, 2006, p. 7 pp.
- [6] J. Arrillaga, *et al.*, *Flexible Power Transmission Systems-The HVDC Options*: John Wiley & Sons, Publication, 2007.

- [7] P. F. Cignatta Massimiliano, "Consultancy Services for update of Libyan network defence plans " CESI, Milan,Italy2009.
- [8] T. K. Vrana, *et al.*, "The CIGRE B4 DC grid test system," *System*, vol. 500, p. D1, 2013.
- [9] A. O'Dwyer, *Handbook of PI and PID controller tuning rules* vol. 57: World Scientific, 2009.
- [10] M. M. Alamuti, *et al.*, "A novel VSC HVDC active power control strategy to improve AC system stability," in *PES General Meeting | Conference & Exposition, 2014 IEEE*, 2014, pp. 1-5.
- [11] A. L'Abbate, *et al.*, "The role of facts and HVDC in the future paneuropean transmission system development," in *AC and DC Power Transmission, 2010. ACDC. 9th IET International Conference on*, 2010, pp. 1-8.
- [12] X.-P. Zhang, *et al.*, *Flexible AC transmission systems: modelling and control*: Springer Science & Business Media, 2012.

Chapter 8

Conclusion

8.1 General conclusions

Chapter one reviewed interconnected power systems in terms of their ability to provide a secure, reliable and efficient level of power exchange which are necessary and fit for 21st century integrated power systems. It has been shown that the full utilization of the tie-lines power transfer capacity is a major challenge in the interconnected power systems. Therefore, flexible AC transmission system (FACTS) devices and high voltage direct current HVDC systems were introduced as potential solutions that could be used to maximize power transfer capacity of individual tie lines that resemble interconnected power systems.

Discussion of the fundamentals of active and reactive power flow in chapter two showed that the voltage stability limit (*VSL*) and angular stability limit (*ASL*) are the main restrictions that prevent better utilization of medium and long tie lines in favour of security and reliability of the power supply. Additionally, the lack of reactive power support along tie-lines is the main cause of the voltage instability phenomenon. This normally starts at the weakest point (in the middle of specific tie line in the weakest part of the network) and then spreads to affect the entire system if not properly mitigated. Mathematical formulations and analysis are introduced in this chapter established the link between power and voltage stability and active and reactive power flow in interconnected systems, including necessary simplifications for ease of understanding. Validation of the presented mathematical formulations and analysis against NEPLAN results confirmed their accuracy and applicability to basic and complex steady state calculations. The analytical solution presented show that TTC improvement can be achieved either by shunt or series FACTS devices (the former by maintaining the voltage at a pilot point or the latter by reducing the series impedance of the tie line).

Chapters 2 and 3 discussed shunt and series type FACTS devices and their operating principals, control systems and their roles for enhancement of the power systems performance and utilization, considering both line and self-commutated devices.

In quest for optimal location and sizing of the FACTS devices, this thesis has indicated that the efficiency of FACTS devices depends on the correct choice of the

installation location and the size of the equipment. Apart from economic aspects, three stability constraints were taken into account in the sizing of FACTS devices:

- 1- Undesired displacement of the point of collapse (PoC) on the P-V curve due to increased shunt injected reactive power.
- 2- Respecting the recommended range of $\pm 5\%$ for voltage deviation in transmission systems as FACTS devices vary their terminal voltages to maintain a constant voltage at the PCC. Transformer secondary voltage and dc link voltage are selected such that maximum capacitive and inductive reactive power, which are defined by dc voltage and current limits in the $P-Q$ chart, coincide with the maximum and minimum voltage of 1.05pu and 0.95pu respectively.
- 3- Sizing of series compensators must take into consideration the risk of sub-synchronous resonance that may arise.

Total voltage change index ($TVCI$) was introduced as an effective approach to allocating shunt FACTS devices. This index confirmed that the optimal location for the shunt compensator in radial systems is at the receiving end. On the other hand, the midpoint of tie-line is the optimal compensation point in a relatively strong interconnected power system. Regarding series FACTS allocation, a two identical line segments approach was introduced to find the closest point to the electrical centre between the two systems. This ensures maximum load-ability improvement with lower short-circuit current rating of the series FACTS device.

Chapter Five presented a review of HVDC transmission systems and focused on the potential use of the voltage source converter type as an alternative for typical FACTS devices; especially for addressing problems in interconnected power systems, particularly the cases when extra power transfer capacity is needed. Its steady state mathematical model was introduced to facilitate power flow calculations of the entire VSC-HVDC link. Validation of the presented model against NEPLAN shows that it produces accurate results for both AC and DC power flows. To illustrate the transient stability improvement that VSC-HVDC link could offer, a multi-tasking controller was designed and incorporated into VSC-HVDC systems that include frequency and power management controllers in addition to the basic controllers such as AC and DC voltages, and active and reactive powers.

Chapters 6 and 7 investigated the performance of the present Libyan internal tie-line, and its future performance if its backbone tie line (East-West) is reinforced by line

and self-commutated FACTS devices and an HVDC link. Analysis of the present tie-line performance showed that only about 40% of the designed thermal capacity of the line is utilized, due to voltage instability. Therefore, steady-state and transient performance of the Libyan transmission system were examined, considering SVC, STATCOM, TCSC, and VSC-HVDC; in an attempt to establish to what extent these devices could extend its steady-state and dynamic ratings to the design values.

Steady-state based analysis showed that correct sizing of the FACTS devices or HVDC link are important as the transfer capability of the tie-line improves with the power ratings of these devices. It was shown that series FACTS devices offer the largest improvement of the Libyan tie-line TTC than from shunt FACTS devices, where series FACTS devices could achieve a 55% improvement compared to 24% with shunt equivalents. That is, MW improvement per MVAR rating of the series FACTS is much better than that of a shunt counterpart; viz., 1.99 MW/MVAR for the series compensator compared to 0.6 MW/MVA for the shunt compensator. This fact confirms the superiority of series compensators over shunt counterparts, in spite of their higher cost, which can be justified by the congestion cost at this important power corridor.

Regarding the improvement that can be achieved by a VSC-HVDC link, this research indicates that the TTC of the internal tie-line could be doubled, allowing 1000 MW to be transferred over the dc link, should one of the existing 220kV AC lines be converted to a dc link.

In Chapter 7 it was also concluded that secure operation of the hybrid tie-line requires a strategy that ensures efficient and reliable operation of the line during abnormal conditions. The ability of the dc link to change the dc power and its direction makes use of this strategy possible. Power flow in the dc link can be changed on demand to decrease the loading of the AC parallel path should system security be violated. Results of this scenario show that the loss of synchronism between the western and eastern networks could be avoided by adopting such a strategy.

Given the many advantages that characterize a VSC-HVDC system, which offset its high cost compared with typical line and self-commutated FACTS devices, a VSC-HVDC transmission may be the best option for improving the Libyan internal tie-line; especially, in the near future when a more secure and reliable interconnected power system is needed.

8.2 Suggestions for future research

Suggestions for further investigation to improve the efficiency of the Libyan power industry by exploiting the possibilities power-electronic systems can offer, are summarised as follows:

- Investigate the possibility of reinforcing the southern part of the Libyan power network by using FACTS devices and HVDC links to improve its utilization.
- Investigate the possibility of using a UPFC system to improve the steady-state and dynamic performance of the transmission systems.
- Investigate the use of a multi-terminal VSC-HVDC system to connect the proposed renewable energies projects with the existing AC Libyan transmission system.
- Investigate the feasibility of establishing an HVDC backbone to further increase the energy exchange between the Mediterranean Sea interconnected power systems.
- Investigate the possibility of using high capacity undersea cables to connect the Libyan grid with Italy in the course of energy exchange between southern Mediterranean (and other European countries), viz., desert-tech.

Appendix- A

Long mathematical formulas

A-1 Angular stability limit (ASL) derivation

The comprehensive power flow equation is;

$$V = \sqrt{\frac{1-2(rP+xQ) + \sqrt{1-4(rP+xQ+(Px-Qr)^2)}}{2F_C}} \quad (A-1)$$

$$Q = \sqrt{3} I V \sin[\cos^{-1}(pf)] \quad (A-2)$$

Reactive power (Q) in (A-1) can be substituted by that in (A-2) that yields;

$$V = \sqrt{\frac{1-2(rP+xVVB I \sqrt{3(1-pf^2)}) + \sqrt{1-4(rP-xVVB I \sqrt{3(1-pf^2)}) + (Px-VVB I \sqrt{3(1-pf^2)})^2}}{2FC}} \quad (A-3)$$

Extract the current I from(A-3);

$$I = (1/3) * (FC * \sqrt{-pf^2+1}) * \sqrt{3} * V^2 * x + \sqrt{3} * \sqrt{(pf-1) * (pf+1) * (2*FC*P*V^2*r^3+P^2*r^4 + (FC^2*V^4+2*P^2*x^2-FC*V^2)*r^2+2*FC*P*V^2*r*x^2+P^2*x^4-FC*V^2*x^2))} / ((pf-1) * (pf+1) * (r^2+x^2) * VB * V) \quad (A-4)$$

ASL correspond to the condition when the under root in (A-4) is zero. That is;

$$\sqrt{(pf-1) * (pf+1) * (2*FC*P*V^2*r^3+P^2*r^4 + (FC^2*V^4+2*P^2*x^2-FC*V^2)*r^2+2*FC*P*V^2*r*x^2+P^2*x^4-FC*V^2*x^2))} = 0 \quad (A-5)$$

Equation (A-5) can be simplified as;

$$\sqrt{3} \sqrt{(pf^2-1)(F_C^2 r^2 v^4 + 2F_C P r^3 v^2 + 2F_C P r v^2 x^2 + P^2 r^4 + 2P^2 r^2 x^2 + P^2 x^4 - F_C r^2 v^2 - F_C v^2 x^2)} = 0 \quad (A-6)$$

The angular stability limit ASL in MW at a given receiving end voltage V in p.u is calculated by extracting the power (P) from (A-6)

$$ASL = \left[\frac{(\sqrt{F_C (r^2 + x^2)} - F_C \cdot r V) V}{r^2 + x^2} \right] \sin \delta \quad \text{when } \delta=90^\circ \quad (A-7)$$

A-2 Active power formula at the PCC of receiving end in VSC-HVDC link

$$\begin{aligned} PS2 = & 1/8 * (-2 * FCn2 * (-4 * (r2^2 * VS2^4 * FCn2^4 + (-2 * VS2^4 * r2 * rn2 - \\ & 2 * VS2^2 * r2^2) * FCn2^3 + ((- \\ & 2 * PC2 * VS2^2 * r2 + VS2^4) * rn2^2 + 2 * r2 * VS2^2 * rn2 + r2 * (- \\ & 2 * PC2 * VS2^2 * xn2^2 + r2)) * FCn2^2 - 2 * (- \\ & PC2 * VS2^2 * rn2 + r2 * PC2 + 1/2 * VS2^2) * (rn2^2 + xn2^2) * FCn2 + PC2^2 * (rn2^2 + xn2^ \\ & 2) ^2) * (r2 * rn2 * FCn2 - 1/2 * rn2^2 - 1/2 * xn2^2) ^2) ^{(1/2)} * r2 * xn2 - 4 * (- \\ & 1/2 * PC2 * rn2^4 + r2 * PC2 * rn2^3 * FCn2 + (-PC2 * xn2^2 - \\ & 1/2 * FCn2^2 * VS2^2 * r2 + 1/2 * FCn2 * r2) * rn2^2 + r2 * FCn2 * (FCn2^2 * VS2^2 * r2 + PC2 * \\ & xn2^2 - FCn2 * r2) * rn2 + 1/2 * xn2^2 * (FCn2^2 * VS2^2 * r2 - \\ & PC2 * xn2^2 + FCn2 * r2)) * (r2 * rn2 * FCn2 - 1/2 * rn2^2 - 1/2 * xn2^2)) / (FCn2^2 * r2^2 - \\ & r2 * rn2 * FCn2 + 1/4 * rn2^2 + 1/4 * xn2^2) / (rn2^2 + xn2^2) / (r2 * rn2 * FCn2 - \\ & 1/2 * rn2^2 - 1/2 * xn2^2) \end{aligned}$$

Appendix- B

Matlab script codes

B-1 P-V and P- δ curves for detailed and lossless tie-line (Fig 2-5 and Fig 2-8)

Typical parameter of 230KV transmission line

$R(\Omega)/Km$	$X(\Omega)/Km$	$B(\mu\bar{O})/Km$	r	x	F_C
0.05	0.488	3.371	0.940027e-4	0.914833e-3	.983682703

```
clear all
clc
FC = .983682703, r = 0.940027e-4, x = 0.914833e-3, pf = .95, VB =
230, v = 1
values = [0:1:1200];
for i = 1:length(values)
if i<=180
delta=values(i)
FC = .983682703, r = 0.940027e-4, x = 0.914833e-3,
ASL0=(-FC*r*v+sqrt(FC*r^2+FC*x^2))*v*sin((1/180)*delta*pi)/(r^2+x^2)
FC = 1 ,r=0
ASL1=(-FC*r*v+sqrt(FC*r^2+FC*x^2))*v*sin((1/180)*delta*pi)/(r^2+x^2)
resultvec(i,2)=ASL0;
resultvec(i,3)=ASL1;
end
P=values(i)
FC = 1, r = 0, x = 0.914833e-3,
v0 = (1/2)*sqrt(2)*sqrt(1-2*x*P*sqrt(-pf^2+1)/pf+sqrt(-4*x^2*P^2-
4*x*P*sqrt(-pf^2+1)/pf+1))
FC = 1, r = 0.940027e-4, x = 0.914833e-3
v1 = (1/2)*sqrt(2)*sqrt((-2*r*P+1-2*x*P*sqrt(-pf^2+1)/pf+sqrt(-
4*r*P+1-4*x*P*sqrt(-pf^2+1)/pf-4*(-r*P*sqrt(-pf^2+1)/pf+x*P)^2))/FC)
FC = .983682703, r = 0.940027e-4, x = 0.914833e-3,
v2 = (1/2)*sqrt(2)*sqrt((-2*r*P+1-2*x*P*sqrt(-pf^2+1)/pf+sqrt(-
4*r*P+1-4*x*P*sqrt(-pf^2+1)/pf-4*(-r*P*sqrt(-pf^2+1)/pf+x*P)^2))/FC)
resultvec(i,1)=i;
resultvec(i,4)=v0;
resultvec(i,5)=v1;
resultvec(i,6)=v2;
end
```

B-2 Impact of the midpoint compensation on TTC (Fig 3-18)

impact of the midpoint compensation on the transfer capability of the tie-line in the Kundur test system.

```
clear all
clc
x=91.7,V=230
values = [0:1:180];
for i = 1:length(values)
d = values(i)*pi/180
P=(V^2/x)*sin(d)
Pcomp=(2*V^2/x)*sin(d/2)
Qcomp=(4*V^2/x)*(1-cos(d/2))
resultvec(i,1)=d;
resultvec(i,2)=P;
```

```

resultvec(i,3)=Pcomp;
resultvec(i,4)=Qcomp;
end

```

B-3 level of shunt compensation versus critical voltage (Fig 3-25)

Equivalent system impedances for emergency operating conditions (line-3 out of service) in Kundur test system.

Node	$r (R/E_s^2)$	$x (X/E_s^2)$	FC
Bus-2 (Meddle)	0.000053	0.000627	0.967214
Bus-3 (receiving)	0.000159	0.001631	0.91483

```

clear all
clc
FC = .91483, r = 0.159e-3, x = 0.1631e-2, pf = .95
values = [170:-1:-280];
for i = 1:length(values)
pf=0.95
Qgen=0
Qsh=values(i)
Vc_SVC = 1/2*2^(1/2)*(-2*((Qsh*r^2+Qsh*x^2+FC*x)*(-
pf^2+1)^(1/2)+r*FC*pf)*(-(-FC*r*(-
pf^2+1)^(1/2)*Qgen*pf+(pf^2*x*Qgen-
1/4)*FC+Qsh*pf^2*Qgen*(r^2+x^2))*(FC^2+2*Qsh*x*FC+Qsh^2*(r^2+x^2)
)*FC*(r^2+x^2))^(1/2)-
1/2*FC*(x^2*Qsh+x*FC+r^2*(2*FC*Qgen+Qsh))* (Qsh*r^2+Qsh*x^2+FC*x)*
(-pf^2+1)-
FC*r*pf*Qgen*(r^2+x^2)*(Qsh^2*r^2+Qsh^2*x^2+2*FC*Qsh*x+FC^2)*(-
pf^2+1)^(1/2)+(-
1/2*FC+FC*x*Qgen+Qsh*r^2*Qgen+Qsh*x^2*Qgen)*(x^4*Qsh^2*pf^2+2*x^3
*Qsh*FC*pf^2+(2*Qsh^2*pf^2*r^2+FC^2*pf^2)*x^2+2*x*Qsh*FC*r^2*pf^2
+Qsh^2*r^4*pf^2+FC^2*r^2))/(-2*pf*r*FC*(Qsh*r^2+Qsh*x^2+FC*x)*(-
pf^2+1)^(1/2)+x^4*Qsh^2*pf^2+2*x^3*Qsh*FC*pf^2+(2*Qsh^2*pf^2*r^2+
FC^2*pf^2)*x^2+2*x*Qsh*FC*r^2*pf^2+(Qsh^2*r^2*pf^2+(-
pf^2+1)*FC^2)*r^2)/(Qsh^2*r^2+Qsh^2*x^2+2*FC*Qsh*x+FC^2))^(1/2)
resultvec(i,1)=Qsh;
resultvec(i,2)=Vc_SVC;
end

```

B-4 Series compensation (k) versus VSL and ASL (Fig 4-4 and Fig 4-6)

```

clear all
clc
FC = .91483, r = 0.159e-3, x = 0.1631e-2, pf = .95, v = 1
values = [0:0.1:1];
for i = 1:length(values)
k=values(i)
VSL=(-(1/2)*(-sqrt(-pf^2+1))*x*(1-k)-pf*r+sqrt(r^2+x^2*(1-
k)^2))*pf/(2*sqrt(-pf^2+1)*pf*r*x*(1-k)+pf^2*r^2-pf^2*x^2*(1-
k)^2-r^2)
ASL = (-FC*r*v+sqrt(FC*r^2+FC*x^2*(1-k)^2))*v/(r^2+x^2*(1-k)^2)
resultvec(i,1)=k;
resultvec(i,2)=VSL;
resultvec(i,3)=ASL;
end

```

B-5 Sizing of series compensation on the bases of the SSR (Fig 4-10)

```
clear all
clc
FC = .91483, r = 0.159e-3, x = 0.1631e-2, pf = .95
VB=230,S1=4577.9,S2=4577.9,f0=60,XLine=87.285,f0=60,k=0.3
Lsys1=(VB^2/S1)/(2*pi*f0),Lsys2=(VB^2/S2)/(2*pi*f0),XC=k*XLine,C=1/(
2*pi*f0*XC)
XLsys1=Lsys1*2*pi*f0,XLsys2=Lsys2*2*pi*f0
Xltotal=XLine+XLsys1+XLsys2
m1=XLine/Xltotal
values = [0:0.1:1];
for i = 1:length(values)
k= values(i)
FR = 1/(pi*sqrt((XLsys1+XLsys2+XLine)/(k*XLine*pi^2*f0^2)))
Feff=f0-FR
resultvec(i,1)= k;
resultvec(i,2)= FR;
resultvec(i,3)= Feff;
end
```

B-6 Firing delay angle-VS-effective TCSC impedance (Fig 4-13)

```
clear all
clc
FC = .91483, r = 0.159e-3, x = 0.1631e-2, pf = .95
VB=230,S1=4577.9,S2=4577.9,f0=60,XLine=87.285,f0=60,k=0.75
Lsys1=(VB^2/S1)/(2*pi*f0),Lsys2=(VB^2/S2)/(2*pi*f0),XC=k*XLine,C=1/(
2*pi*f0*XC)
XLsys1=Lsys1*2*pi*f0,XLsys2=Lsys2*2*pi*f0
Xltotal=XLine+XLsys1+XLsys2
values = [0:1:180];
a=0.1333
for i = 1:length(values)
alpha= values(i)*pi/180
XLtcsc=a*k*XLine
Xtcsc = -(pi^2*XLtcsc/XC-pi*sin(2*alpha)+2*pi*alpha-
4*alpha^2)*XC/(pi^2*XLtcsc/XC-pi^2+4*pi*alpha-4*alpha^2)
resultvec(i,1)= alpha;
resultvec(i,2)= Xtcsc;
end
```

B-7 P-V curve and compensated voltage with 25% compensation factor SSSC (Fig 4-20 a -b)

P-V curve at the receiving end in the case 25% SSSC compensated tie-line, and the compensating voltage provided by SSSC at different line current.

```
% method 1 on calculation on the basis of current (amp) SSSC
calculation
clear all
clc
FC = .91483, r = 0.159e-3, x = 0.1631e-2, pf =
.95,VB=230,k=0.25,Vref=1,c=0
values = [0.001:0.001:5];
for i = 1:length(values)
amp= values(i)
```

```

if c<1
VSSSC = ((1/3)*FC*sqrt(3)*sqrt(-(pf-1)*(pf+1))*Vref+amp*x*VB-
(1/3)*sqrt(-6*FC*sqrt(3)*VB*amp*pf*r*Vref-3*FC^2*pf^2*Vref^2-
9*VB^2*amp^2*r^2+3*FC))*VB
end
%-----
% Step 2 calculation of the injected X_TCSC
if VSSSC>=25
c=1
end
%-----
% P-V calculation based on X_TCSC
V= -1/2*2^(1/2)*(-(12*r*VB^2*pf*amp*(VB^2*amp*x-VSSSC)*(-(pf-
1)*(pf+1))^(1/2)+6*amp^2*((r^2-x^2)*pf^2-
r^2)*VB^4+(12*VSSSC*amp*pf^2*x+2*FC)*VB^2-
6*VSSSC^2*pf^2)^(1/2)+3^(1/2)*2^(1/2)*((VB^2*amp*x-VSSSC)*(-(pf-
1)*(pf+1))^(1/2)+r*VB^2*pf*amp))/VB/FC
P=sqrt(3)*V*VB*amp*pf
resultvec(i,1)= P;
resultvec(i,2)= V;
resultvec(i,3)= VSSSC;
resultvec(i,4)= Vdroop;
resultvec(i,5)= amp;
resultvec(i,6)= sqrt(3)*amp*VSSSC*sin(acos(pf));% reactive powre
injected by SSSC
end

```

B-8 VSC-HVDC power flow calculation and sizing

```

clear all
clc
%% Side -1 P and Vac control
VS1=1, rn1=0.00002475876239, xn1=0.2425416558e-
3, FCn1=.9666918477, r1=0.602/220^2, x1=15.4275/220^2,
PS1=750
QS1 = (sqrt(-FCn1^2*VS1^4*rn1^2-(2*(rn1^2+xn1^2))*VS1^2*(rn1*PS1-
1/2)*FCn1-PS1^2*(rn1^2+xn1^2)^2)-FCn1*VS1^2*xn1)/(rn1^2+xn1^2);
PC1 = -((( -PS1^2-QS1^2)*r1+PS1*VS1^2)/VS1^2);
QC1 = -((( -PS1^2-QS1^2)*x1+QS1*VS1^2)/VS1^2);
VC1 = sqrt(PC1^2+QC1^2)*VS1/sqrt(PS1^2+QS1^2);
d1 = ((PS1*xn1-QS1*rn1)/(sqrt(2)*FCn1^2))*180/pi
dC1 = (PC1*x1-QC1*r1)/(VC1)*(180/pi)+d1
Vd1=VC1*cos(dC1*pi/180)
Vq1=VC1*sin(dC1*pi/180)
%% DC calculations at the sending end
% power balance theory
Vdc2=400 % Vdc2 is maintained at the reciving end
Rdc=0.0133*240 ,VdcBase=400,Rc=200000
Vdc1 =
(1/2)*(Vdc2*Rc+sqrt(Rc*(4*PC1*Rc*Rdc+4*PC1*Rdc^2+Rc*Vdc2^2)))/(Rc
+Rdc)
Vdc1_pu=Vdc1/Vdc2
Pdc1=PC1-Vdc1^2/Rc
Mdl=Vd1/(Vdc1/VdcBase)
Mq1=Vq1/(Vdc1/VdcBase)
Idc = 2*Pdc1/(sqrt(4*Pdc1*Rdc+Vdc2^2)+Vdc2)
Pdc2 = Idc*Vdc2
%% reciving End
FCn2 = 1.008492278, rn2 = 0.8812556865e-5, xn2 =0.3880071575e-
3, r2=0.602/220^2, x2=15.4275/220^2,
FCn2 = 0.9877954771, rn2 = 0.1434461646e-4, xn2 = 0.1783704575e-3

```

```

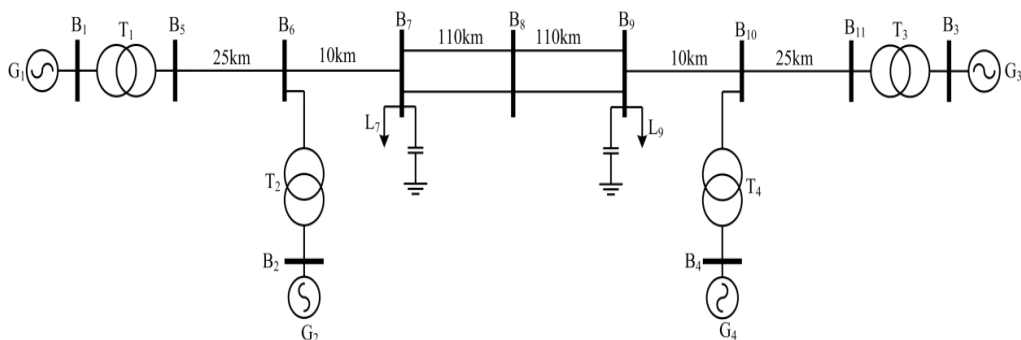
VS2=1
PC2=Pdc2-(Vdc2^2/Rc)
PS2 = 1/8*(-2*FCn2*(-4*(r2^2*VS2^4*FCn2^4+(-2*VS2^4*r2*rn2-
2*VS2^2*r2^2)*FCn2^3+((-
2*PC2*VS2^2*r2+VS2^4)*rn2^2+2*r2*VS2^2*rn2+r2*(-
2*PC2*VS2^2*xn2^2+r2))*FCn2^2-2*(-
PC2*VS2^2*rn2+r2*PC2+1/2*VS2^2)* (rn2^2+xn2^2)*FCn2+PC2^2*(rn2^2+x
n2^2)^2)*(r2*rn2*FCn2-1/2*rn2^2-1/2*xn2^2)^2)^(1/2)*r2*xn2-4*(-
1/2*PC2*rn2^4+r2*PC2*rn2^3*FCn2+(-PC2*xn2^2-
1/2*FCn2^2*VS2^2*r2+1/2*FCn2*r2)*rn2^2+r2*FCn2*(FCn2^2*VS2^2*r2+P
C2*xn2^2-FCn2*r2)*rn2+1/2*xn2^2*(FCn2^2*VS2^2*r2-
PC2*xn2^2+FCn2*r2))* (r2*rn2*FCn2-1/2*rn2^2-
1/2*xn2^2))/(FCn2^2*r2^2-
r2*rn2*FCn2+1/4*rn2^2+1/4*xn2^2)/(rn2^2+xn2^2)/(r2*rn2*FCn2-
1/2*rn2^2-1/2*xn2^2)
PS2=-PS2
QS2 = (sqrt(-FCn2^2*VS2^4*rn2^2-(2*(rn2^2+xn2^2))*VS2^2*(rn2*PS2-
1/2)*FCn2-PS2^2*(rn2^2+xn2^2)^2)-FCn2*VS2^2*xn2)/(rn2^2+xn2^2)
QC2 = ((-PS2^2-QS2^2)*x2+QS2*VS2^2)/VS2^2
VC2 = sqrt(PC2^2+QC2^2)*VS2/sqrt(PS2^2+QS2^2);
d2 = ((-PS2*xn2-QS2*rn2)/(sqrt(2)*FCn2^2))*180/pi
dC2 = (PC2*x2-QC2*r2)/(VC2)*(180/pi)+d2
Vd2=VC2*cos(dC2*pi/180)
Vq2=VC2*sin(dC2*pi/180)
Md2=Vd2/(Vdc2/VdcBase)
Mq2=Vq2/(Vdc2/VdcBase)

```

Appendix- C

Two areas Kundur test system technical data

C-1 Single line diagram of two areas Kundur test system



C-2 Network data

Table C2-1: Synchronous generator data

Machine	Gen 1,2	Gen 3,4
S (MVA)	900	900
V (KV)	20	20
F (Hz)	60	60
X _d (%)	1.8	1.8
X _q (%)	1.7	1.7
X' _d (%)	0.3	0.3
X' _q (%)	0.55	0.55
X'' _d (%)	0.25	0.25
X'' _q (%)	0.25	0.25
X _l (%)	0.2	0.2
R _a (pu)	0.0025	0.0025
T' _{do} (s)	8	8
T' _{qo} (s)	0.4	0.4
T'' _{do} (s)	0.03	0.03
T'' _{qo} (s)	0.05	0.05
H (s)	6.5	6.175

Table C2-2: Transmission line data

Name	L (Km)	R(pu/km)	X(pu/km)	B(pu/km)
Lines 5-6 and 10-11	25	0.0001	0.001	0.00175
Lines 6-7 and 9-11	10	0.0001	0.001	0.00175
Lines 7-8 and 8-9	110	0.0001	0.001	0.00175

Table C2-3: Power transformers data

Name	S (MVA)	V1 (KV)	V2 (KV)	U _k %
T1,T2,T3 and T4	900	230	20	15

C-3 Generator excitation control system

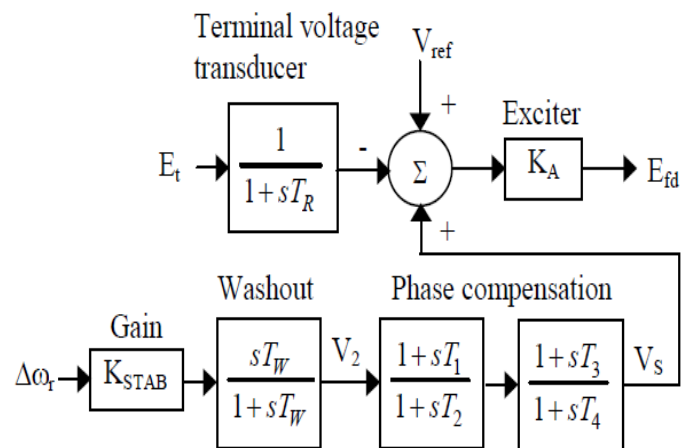


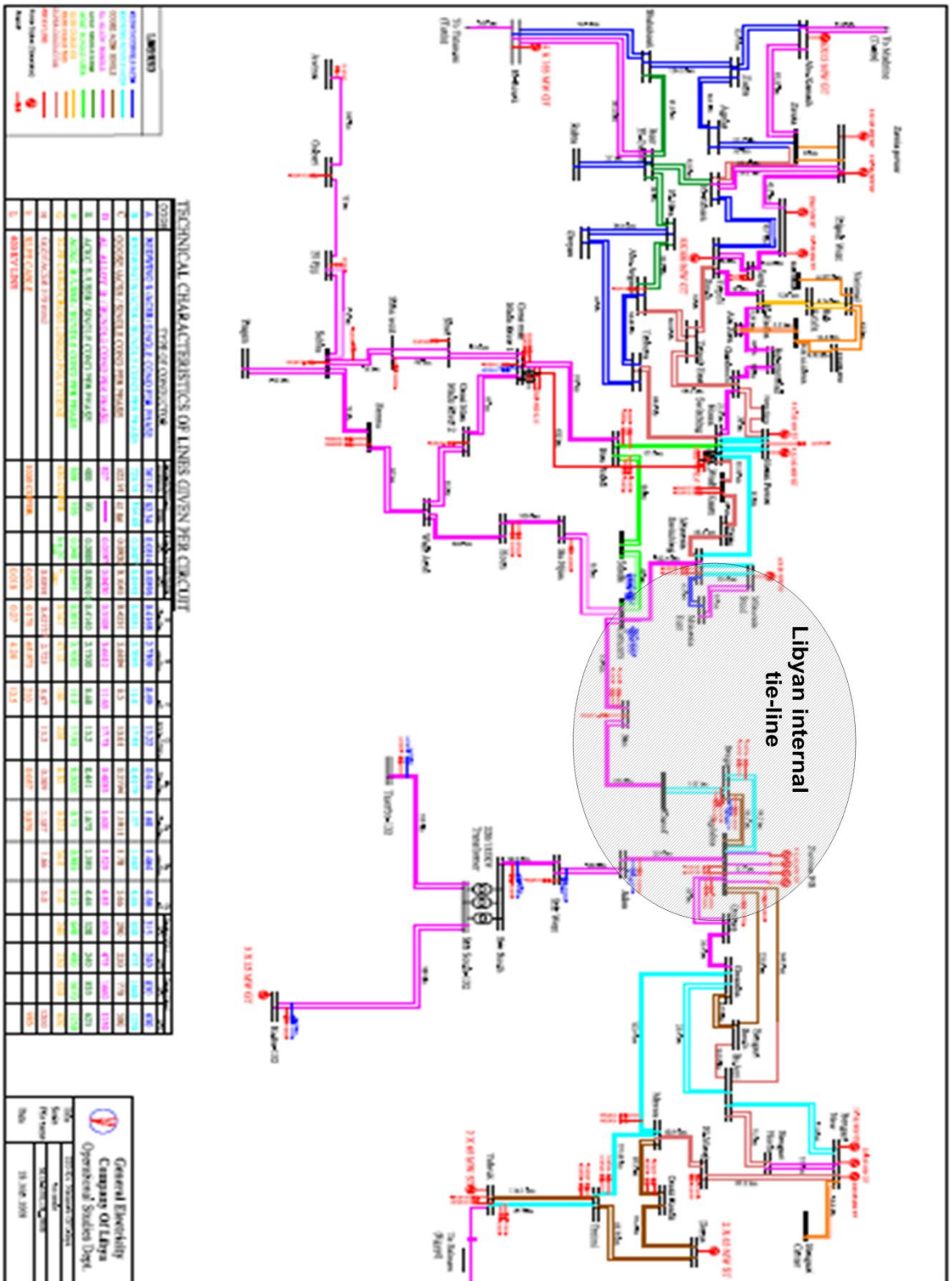
Figure C3-1: Thyristor exciter with high transient gain with PSS

Table C2-3: Power transformers data

Type	K _A	T _R	K _{STAB}	T _W	T ₂	T ₃	T ₁
Thyr_Exciter With PSS	200	0.01	20	10	0.02	3	0.05

Appendix- D

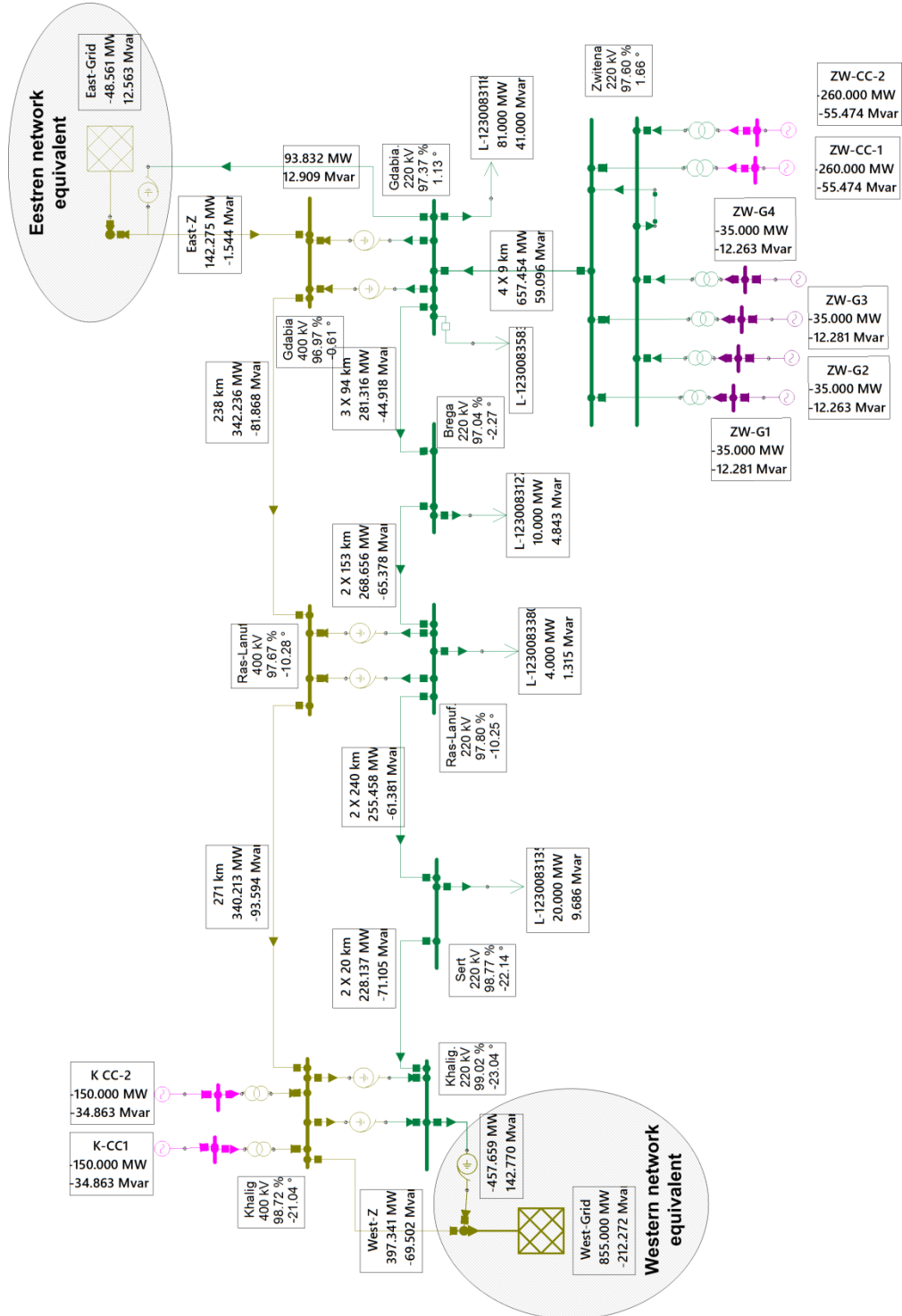
Single line diagram of the Libyan national grid



Appendix- E

NEPLAN power flow calculation

E-1 Power flow results for the Libyan internal tie-line (reduced model)



E-2 Power flow results for the Libyan internal tie-line (detailed model)

